frontiers | Research Topics

New molecular pathways in thyroid biology: role of coding and noncoding genes in thyroid pathophysiology, volume II

Edited by
Cesar Seigi Fuziwara and Juan Pablo Nicola

Published in
Frontiers in Endocrinology
Frontiers in Oncology

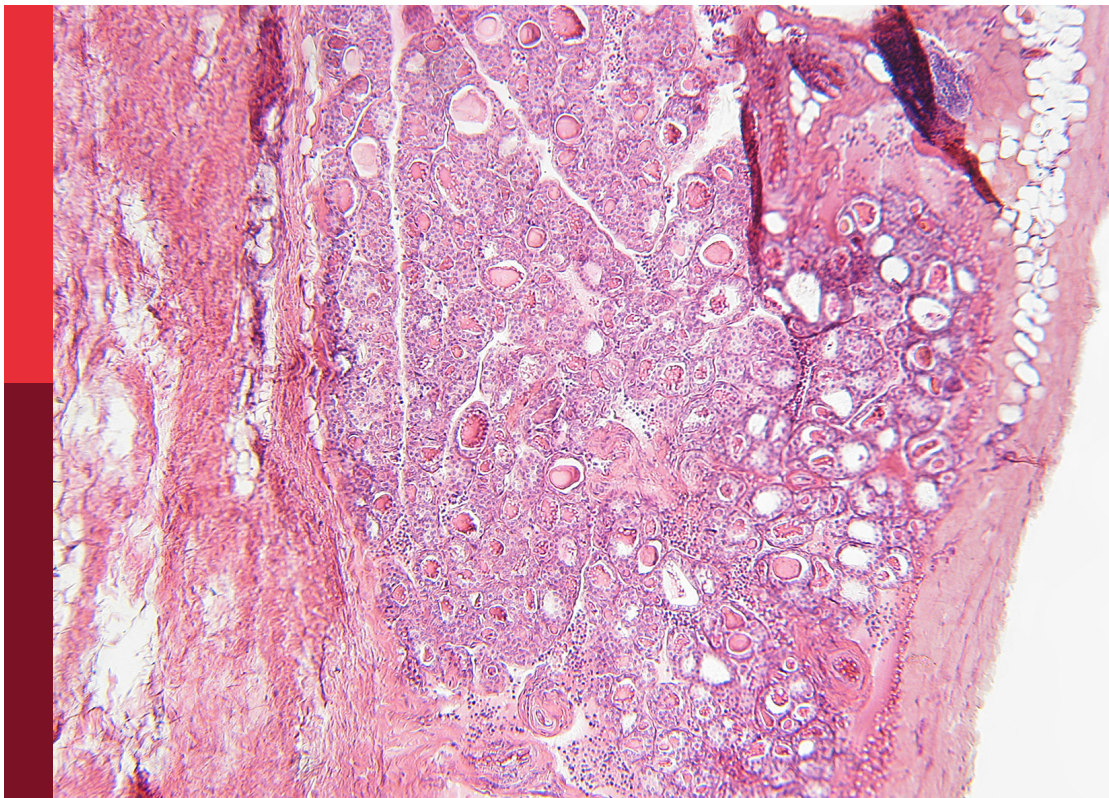

ISSN 1664-8714
ISBN 978-2-8325-7144-6
DOI 10.3389/978-2-8325-7144-6

Generative AI statement
Any alternative text (Alt text) provided alongside figures in the articles in this ebook has been generated by Frontiers with the support of artificial intelligence and reasonable efforts have been made to ensure accuracy, including review by the authors wherever possible. If you identify any issues, please contact us.

About Frontiers

Frontiers is more than just an open access publisher of scholarly articles: it is a pioneering approach to the world of academia, radically improving the way scholarly research is managed. The grand vision of Frontiers is a world where all people have an equal opportunity to seek, share and generate knowledge. Frontiers provides immediate and permanent online open access to all its publications, but this alone is not enough to realize our grand goals.

Frontiers journal series

The Frontiers journal series is a multi-tier and interdisciplinary set of open-access, online journals, promising a paradigm shift from the current review, selection and dissemination processes in academic publishing. All Frontiers journals are driven by researchers for researchers; therefore, they constitute a service to the scholarly community. At the same time, the *Frontiers journal series* operates on a revolutionary invention, the tiered publishing system, initially addressing specific communities of scholars, and gradually climbing up to broader public understanding, thus serving the interests of the lay society, too.

Dedication to quality

Each Frontiers article is a landmark of the highest quality, thanks to genuinely collaborative interactions between authors and review editors, who include some of the world's best academicians. Research must be certified by peers before entering a stream of knowledge that may eventually reach the public - and shape society; therefore, Frontiers only applies the most rigorous and unbiased reviews. Frontiers revolutionizes research publishing by freely delivering the most outstanding research, evaluated with no bias from both the academic and social point of view. By applying the most advanced information technologies, Frontiers is catapulting scholarly publishing into a new generation.

What are Frontiers Research Topics?

Frontiers Research Topics are very popular trademarks of the *Frontiers journals series*: they are collections of at least ten articles, all centered on a particular subject. With their unique mix of varied contributions from Original Research to Review Articles, Frontiers Research Topics unify the most influential researchers, the latest key findings and historical advances in a hot research area.

Find out more on how to host your own Frontiers Research Topic or contribute to one as an author by contacting the Frontiers editorial office: frontiersin.org/about/contact

New molecular pathways in thyroid biology: role of coding and noncoding genes in thyroid pathophysiology, volume II

Topic editors

Cesar Seigi Fuziwara — University of São Paulo, Brazil

Juan Pablo Nicola — National University of Cordoba, Argentina

Citation

Fuziwara, C. S., Nicola, J. P., eds. (2025). *New molecular pathways in thyroid biology: role of coding and noncoding genes in thyroid pathophysiology, volume II*. Lausanne: Frontiers Media SA. doi: 10.3389/978-2-8325-7144-6

Table of contents

frontiers | Frontiers in Endocrinology

TYPE Editorial
PUBLISHED 30 October 2025
DOI 10.3389/fendo.2025.1729485

OPEN ACCESS

EDITED AND REVIEWED BY
Claire Perks,
University of Bristol, United Kingdom

*CORRESPONDENCE
Cesar Seigi Fuziwara
cesar.fuziwara@usp.br

RECEIVED 21 October 2025
ACCEPTED 23 October 2025
PUBLISHED 30 October 2025

CITATION
Fuziwara CS and Nicola JP (2025) Editorial: New molecular pathways in thyroid biology: role of coding and noncoding genes in thyroid pathophysiology, volume II. *Front. Endocrinol.* 16:1729485. doi: 10.3389/fendo.2025.1729485

Editorial: New molecular pathways in thyroid biology: role of coding and noncoding genes in thyroid pathophysiology, volume II

Cesar Seigi Fuziwara[1,2]* and Juan Pablo Nicola[3,4]

[1]Department of Cell and Developmental Biology, Institute of Biomedical Sciences, University of São Paulo, São Paulo, Brazil, [2]Department of Biochemistry, Federal University of Sao Paulo, Sao Paulo, Brazil, [3]Department of Clinical Biochemistry (CIBICI-CONICET), Faculty of Chemical Sciences, National University of Córdoba, Córdoba, Argentina, [4]Clinical Biochemistry and Immunology Research Center, National Scientific and Technical Research Council (CIBICI-CONICET), Córdoba, Argentina

KEYWORDS

thyroid cancer (THCA), tumor microenvironment - TME, metastasis, circRNA, PANoptosis, FNA (fine needle aspiration), molecular analyses

Editorial on the Research Topic
New molecular pathways in thyroid biology: role of coding and non-coding genes in thyroid pathophysiology, volume II

In Volume II of the Research Topic "*New molecular pathways in thyroid cancer and pathophysiology: Role of coding and noncoding genes*," we continued to explore recent advances in the understanding of thyroid biology, especially those involved in thyroid oncogenesis and progression.

Thyroid cancer is often a curable disease detected predominantly as papillary thyroid cancer (PTC), the most common variant: it is classified as a well-differentiated tumor (DTC) that maintains a certain similarity to a normal thyroid gland, mainly the ability to concentrate iodine. However, a small fraction of PTC cases may exhibit more aggressive behavior and an enhanced probability of recurrence, often resulting in poor outcomes. In this context, Liu et al. investigated how the molecular genetic background of DTC could help predict the risk of recurrence and reported that high-risk DTC often exhibits late-hit genetic alteration. Moreover, Liu et al. analyzed the differential expression of high- and low-risk dedifferentiation PTC and found that, besides the thyroid differentiation score (TDS), the signatures of 17 differentially expressed genes (DEGs) were associated with dedifferentiation and that the complement pathway was a key component, with CD55 being overactivated in the high-risk group and tall-cell PTC.

In the process of cancer progression, metastasis dissemination is an indicator of recurrence and poor prognosis, as tumor cells escape from primary sites and acquire more migratory and invasive characteristics. Hu et al. investigated the differential expression of metastatic papillary microcarcinoma by RNAseq and identified the increase in thrombospondin 4 (THBS4) as a potential new biomarker for predicting lymph node

metastasis dissemination, which correlates with the presence of PDGFRA+ inflammatory cancer-associated fibroblasts in the tumor. Additionally, Wang et al. showed PMAIP1/NOXA is a new player in follicular thyroid cancer (FTC) progression and metastasis by inducing the transcription factor FOSL3 via the Wnt signaling pathway and contributing to cell migration and invasion of FTC.

Using an extensive strategy irrespective of genetic background or variant, Zou et al. investigated a common intersection in the transcriptome among different variants of metastatic thyroid cancer derived from transgenic mouse models and found a signature that points to immune cell microenvironment modulation. In this environment, the metastatic cells produce more inflammatory cytokines and chemokines, such as IL6 and IL6R, and express the immunomodulatory PDL1. Additionally, Ma et al. investigated the impact of Hashimoto thyroiditis (HT) on the PTC microenvironment using single-cell RNA sequencing analysis and identified a tumor microenvironment where immune and stromal cells are different from non-HT, creating a TSH-inhibiting environment for PTC growth.

Meanwhile, Li et al. investigated the expression of genes related to PANoptosis, a new type of cell death that combines key features of pyroptosis, apoptosis, and necroptosis, and identified the signatures of eight key genes, including the tumor necrosis factor receptor superfamily (TNFRSF) and PMAIP1 cited previously, linking inflammatory cell death to immune microenvironment dysregulation in thyroid cancer.

To identify new vulnerabilities for thyroid cancer cells, Ma et al. bring new aspects of thyroid cancer biology linked to the deregulation of circular RNAs (circRNAs), a class of noncoding RNAs with a covalent continuous closed loop. CircRNAs may act as competing endogenous RNAs (CeRNAs) that displace miRNA-mediated regulation at target genes, acting as miRNA sponges, thus modulating signaling pathways involved in tumorigenesis and cancer progression. Another interesting context of the role of noncoding RNA deregulation is shown by Chen et al., who reported a case report and literature review of thyroblastoma, a singular disease that presents distinctive primitive characteristics and shows prevalent mutations in *DICER1*, a key nuclease in the microRNA biogenesis pathway. Finally, correct diagnosis of thyroid cancer is essential for the assessment of prognosis and clinical practice. Wu et al. built a risk stratification model based on the FNA washout DNA copy number variation using low-coverage whole-genome sequencing to identify high-risk lymph node metastasis.

In sum, we hope the Research Topic "*New molecular pathways in thyroid cancer and pathophysiology: Role of coding and noncoding genes, Volume II*," has contributed to accelerating the understanding of this thrilling field of thyroid biology and that further studies can bring fruitful applications for thyroid pathology treatment.

Author contributions

CF: Writing – original draft, Writing – review & editing. JN: Writing – original draft, Writing – review & editing.

Conflict of interest

The authors declare that the research was conducted in the absence of any commercial or financial relationships that could be construed as a potential conflict of interest.

The author(s) declared that they were an editorial board member of Frontiers, at the time of submission. This had no impact on the peer review process and the final decision.

Generative AI statement

The author(s) declare that no Generative AI was used in the creation of this manuscript.

Any alternative text (alt text) provided alongside figures in this article has been generated by Frontiers with the support of artificial intelligence and reasonable efforts have been made to ensure accuracy, including review by the authors wherever possible. If you identify any issues, please contact us.

Publisher's note

frontiers | Frontiers in Endocrinology

TYPE Original Research
PUBLISHED 14 October 2022
DOI 10.3389/fendo.2022.888072

OPEN ACCESS

EDITED BY
Terry Francis Davies,
Icahn School of Medicine at Mount Sinai, United States

REVIEWED BY
Hongcui Diao,
Jinan Central Hospital, Shandong University, China
Yun Canhua,
Department of Nuclear Medicine, Shandong University, China

*CORRESPONDENCE
Shu-rong Shen
zxyzlkzyy@163.com

SPECIALTY SECTION
This article was submitted to Thyroid Endocrinology, a section of the journal Frontiers in Endocrinology

RECEIVED 02 March 2022
ACCEPTED 13 September 2022
PUBLISHED 14 October 2022

CITATION
Wu L, Zhou Y, Guan Y, Xiao R, Cai J, Chen W, Zheng M, Sun K, Chen C, Huang G, Zhang X, Zhai L, Qian Z and Shen S-r (2022) Washout DNA copy number analysis by low-coverage whole genome sequencing for assessment of thyroid FNAs. *Front. Endocrinol.* 13:888072. doi: 10.3389/fendo.2022.888072

Washout DNA copy number analysis by low-coverage whole genome sequencing for assessment of thyroid FNAs

Linfeng Wu[1], Yuying Zhou[1], Yaoyao Guan[2], Rongyao Xiao[1], Jiaohao Cai[1], Weike Chen[1], Mengmeng Zheng[1], Kaiting Sun[1], Chao Chen[1], Guanli Huang[3], Xiaogang Zhang[4,5], Lijuan Zhai[4,5], Ziliang Qian[5,6] and Shu-rong Shen[1]*

[1]Oncology and Hematology, Wenzhou Hospital of Integrated Traditional Chinese and Western Medicine, Wenzhou, China, [2]Department of Plastic Surgery, Sir Run-Run Shaw Hospital, Zhejiang University School of Medicine, Hangzhou, China, [3]Thyroid Surgery, The First Affiliated Hospital of Wenzhou Medical University, Wenzhou, China, [4]Hangzhou Catcher Bio Inc., Hangzhou, China, [5]Hongyuan Biotech Inc., Suzhou, China, [6]Prophet Genomics Inc., San Jose, CA, United States

Background: Papillary thyroid microcarcinoma (PTMC) is defined as a papillary carcinoma measuring ≤ 10 mm. The current management of PTMC has become more conservative; however, there are high-risk tumor features that can be revealed only postoperatively. For thyroid cancer, *BRAF* mutations and somatic copy number variation (CNV) are the most common genetic events. Molecular testing may contribute to clinical decision-making by molecular risk stratification, for example predicting lymph node (LN) metastasis. Here, we build a risk stratification model based on molecular profiling of thyroid fine needle aspiration (FNA) washout DNA (wDNA) for the differential diagnosis of thyroid nodules.

Methods: Fifty-eight patients were recruited, FNA wDNA samples were analyzed using CNV profiling through low-coverage whole genome sequencing (LC-WGS) and *BRAF* mutation was analyzed using quantitative PCR. FNA pathology was reported as a Bethesda System for Reporting Thyroid Cytopathology (BSRTC) score. Ultrasound examination produced a Thyroid Imaging Reporting and Data System (TIRADS) score.

Results: In total, 37 (63.8%) patients with a TIRADS score of 4A, 13 (22.4%) patients with a TIRADS score of 4B, and 8 (13.8%) patients with a TIRADS score of 4C were recruited after ultrasound examination. All patients underwent FNA with wDNA profiling. CNVs were identified in 17 (29.3%) patients. CNVs were frequent in patients with a BSRTC score of V or VI, including eight (47.1%) patients with a score of VI and five (29.4%) with a score of V, but not in patients with a score of III, II, or I (0%). *BRAF* mutation was not significantly correlated with BSRTC score. LN metastasis was found more frequently in CNV-positive (CNV+) than in CNV-negative (CNV−) patients (85.7% vs. 34.6%, odds ratio = 11.33, p = 0.002). In total, three molecular subtypes of thyroid nodules were identified in this study: 1) CNV+, 2) CNV− and *BRAF* positive

(*BRAF*+), and 3) CNV− and *BRAF* negative (*BRAF*−). For the CNV+ subtype, 10 (83.3%) lesions with LN metastasis were found, including four (100%) small lesions (i.e. ≤ 5 mm). For the CNV− and *BRAF*+ nodules, LN metastases were detected in only seven (60.0%) larger tumors (i.e. > 5 mm). For CNV− and *BRAF*− tumors, LN metastasis was also frequently found in larger tumors only.

Conclusions: It is feasible to identify high-risk LN metastasis thyroid cancer from FNA washout samples preoperatively using wDNA CNV profiling using LC-WGS.

KEYWORDS

thyroid cancer, genome sequencing, washout-DNA, chromosome instability, LC-WGS

Introduction

Thyroid cancer is the most common malignant tumor in the endocrine system and in head and neck tumors (1). In recent years, the incidence of thyroid cancer has increased rapidly throughout the world, and the percentage of papillary thyroid microcarcinoma (PTMC) has presented the most growth and the fastest increase, but its mortality rate has remain stable (2). PTMC is defined by the WHO as papillary carcinoma of the thyroid measuring ≤ 10 mm (3). Most PTMCs are indolent and rarely develop into clinically significant thyroid cancer, and some are even asymptomatic for life; however, a small proportion of PTMCs are associated with highly aggressive features, and local invasion, lymph node (LN) metastasis, or distant metastases may occur at an early stage (4). Currently, treatment of PTMC can be controversial, focusing mainly on the necessity and scope of surgery. In accordance with guidelines issued by the American Thyroid Association in 2015, patients with low-risk PTMC are recommended to choose active surveillance (AS) rather than surgical treatment (5). The consensus statement on PTMC (2016) formulated by the Chinese Association of Thyroid Oncology (CATO) recommended that the need for surgical treatment of PTMC should be based on a preoperative risk assessment. For patients with low levels of psychological stress and no obvious risk factors (e.g. LN metastasis, high-risk molecular subtypes, family history, radiation exposure history, pathological high-risk subtypes), timely follow-up can replace surgery (6). However, the description of high-risk molecular subtypes in the statement remains unclear.

Fine needle aspiration (FNA) guided by ultrasonography has been used to obtain samples of thyroid neoplasms to prepare cytology smears for several decades (7, 8). FNA is the most accurate examination method for preoperative diagnosis of thyroid cancer and has been routinely used in clinical practice (9). However, by comparison with histopathology, about 10%–40% of thyroid cancer remains indeterminate using FNA (10). In the past 5–10 years, as the understanding of the molecular mechanisms underlying thyroid cancer has increased, several biomarkers have been developed for the diagnosis of thyroid cancer, including *RET*/*PTC*, *RAS*, and *BRAF* mutations (11). For example, since the early 2000s the *BRAF* gene mutation has been widely used as a hot diagnostic and prognostic marker for thyroid cancer in clinical practice, and the *BRAF* mutation test has been shown to improve diagnostic sensitivity to thyroid cancer (12). However, the $BRAF^{V600E}$ mutation occurs in only 50%–70% of papillary thyroid carcinomas (PTCs), and *BRAF* mutations can distinguish between only benign neoplasm and malignant thyroid tumors at present, but there is a lack of evidence supporting the correlation between the *BRAF* mutation and the malignancy of thyroid cancer (13). In addition, most of the studies involved in the current literature used postoperatively histological specimens for gene testing, which could not provide appropriate guidance for the surgical management of patients.

Chromosomal instability (CIN), which was first proposed by Boveri nearly a century ago, refers to changes in chromosome number and structural aberrations caused by errors in chromosome separation in tumor cells during mitosis and was considered a hallmark of cancer (14). CIN is prevalent in various tumor types and is a manifestation of heterogeneity within tumors. In addition, CIN has been associated with metastasis, drug resistance, and poor prognosis in a wide range of cancers (15). Studies have shown that CIN is also common in thyroid cancer, including chromosomal rearrangement, copy number variations, and focal amplifications. Recent studies have shown that different types of thyroid cancer have chromosome copy number abnormalities, manifested as loss of heterozygosity (LOH), and chromosome 9p, 13p, and 22q LOH frequently occurs in thyroid tumor tissues, accounting for approximately 40% of cases (16). Patients with poorly differentiated thyroid cancer mostly have chromosomal abnormalities and loss of chromosome 9 copy number, and the 2-year survival rate is< 30% (17). In recent years, next-generation sequencing and analysis methods have greatly promoted the identification and cataloging of somatic cell copy number variations (CNVs), providing new possibilities to better detect dynamic changes of CIN (18). Scheinin et al. developed a low-

coverage whole genome sequencing (LC-WGS) assay, which is a simple, economical, and reliable CNV identification technique (19).

The present study investigated the incidence of CIN in FNA washout samples from thyroid nodules. In addition, we investigated the significance of CIN in washout samples for the diagnosis of thyroid carcinoma.

Methods

Patient characteristics and ethics statement

A cohort study was conducted involving 58 patients with thyroid nodules (Table 1), with the approval of an ethics committee (approval number 2021-K006) and the informed consent of all patients. Informed consent was obtained from every patient prior to clinical trial participation. All patients underwent fine needle aspiration biopsy (FNAB) sampling at admission to identify aberrations and cytology of the chromosomes.

DNA extraction

The washout samples were centrifuged at a g-force of 300g for 10 min, and the washout DNA (wDNA) was isolated using a QIAGEN (Hilden, Germany) circulating nucleic acid kit.

Low-coverage whole genome sequencing

LC-WGS was carried out as previously described (20). Libraries were prepared using the KAPA HyperPrep Kit

TABLE 1 Patient characteristics.

Parameter	Subtype	Frequency	Percentage
Gender	Male	11	19.0
	Female	47	81.0
Age (years)	≤ 45	28	48.3
	> 45	30	51.7
CNV	Negative	41	70.7
	Positive	17	29.3
*BRAFV600E*_washout	Negative	26	44.8
	Positive	32	55.2
*BRAFV600E*_tissue	Negative	24	41.4
	Positive	34	58.6
Clinical Pathology	Benign	15	25.9
	PTC	40	69.0
	Udx	3	5.2
Lymph node	Negative	19	47.5
	Metastasis	21	52.5
TIRADS	4a	37	63.8
	4b	13	22.4
	4c	8	13.8
Thyroid nodule size (mm) (ultrasound)	< 5	5	8.6
	5–10	31	53.4
	> 10	22	37.9
BSRTC	VI	15	25.9
	V	19	32.8
	III	6	10.3
	II/I	18	31.0
Multi_foci	1	29	72.5
	> 1	11	27.5
Tumor size (mm)	≤ 5	14	35.0
	> 5	26	65.0
ETE	Negative	37	92.5
	Positive	3	7.5

CNV, copy number variation; PTC, papillary thyroid cancer; Udx, undiagnostic; TIRADS, Thyroid Imaging Reporting and Data System; BSRTC, Bethesda System for Reporting Thyroid Cytopathology; ETE, extrathyroidal extension.

(Roche, Basil, Switzerland) with custom adapters [Integrated DNA Technologies (IDT) and Broad Institute], starting with 3–20 ng of cell-free DNA input (median 5 ng), or approximately 1,000–7,000 haploid genome equivalents, for low-pass whole genome sequencing. Up to 22 libraries were pooled and sequenced using 150-bp pair-end runs over 1 × lane on a HiSeq X Ten (Illumina Inc., San Diego, CA, USA). Segment copy numbers were derived using a customized workflow ultrasensitive chromosomal aneuploidy detector (UCAD). The sample was excluded if the median absolute deviation of copy ratios ($\log_2$ ratio) between adjacent bins, genome-wide, was 0.38, suggesting poor-quality sequence data.

$BRAF^{V600E}$ amplification refractory mutation system assay

Analysis of the $BRAF^{V600E}$ mutation was performed using an amplification refractory mutation system, that is, using a BRAF Gene V600E Diagnostic kit (AmoyDx, Xiamen, China) on a real-time PCR system in accordance with the manufacturer's instructions.

Statistical analyses and data visualization

The wDNA was isolated and sequenced using a HiSeq X Ten. At least 10 paired-end reads were collected per sample. The sequences were then aligned to the human reference genome hg19. The genomic coverage and depth were calculated using the Samtools software package (20). The average coverage was calculated for each 200k bin. Data were normalized by *z*-score transformation using the following formula:

$$\text{Coverage}_{\text{normalized}} = \frac{\text{coverage}_{\text{raw}} - \text{mean}\left(\text{coverage}_{\text{controls, raw}}\right)}{\text{stdev}\left(\text{coverage}_{\text{controls, raw}}\right)} \quad \text{(Formula 1)}$$

Significant genomic breakpoints and CNVs were identified using the circula binary segmentation algorithm in the R package "DNACopy" (21). A *p*-value of< 0.05 was considered statistically significant. The chi-squared test was used to analyze categorical variables. All statistical analyses were performed by SPSS software (version 17.0). The proportional trend test was used to analyze the correlation between positive UCAD screening and clinicopathological parameters. Data were presented as mean and standard deviations, median and quartile ranges, and hazard ratios or odds ratios (ORs) with 95% CIs. Missing data were deleted from the analysis. All analyses were performed using R software, version 3.4.3. The anonymized data and the R code used for statistical analysis can be provided on request.

Results

Patient characteristics

At the time of manuscript preparation, 58 patients with potentially malignant tumors according to an ultrasound examination Thyroid Imaging Reporting and Data System (TIRADS) score of 4 (i.e. 4A, 4B, 4C), and who had a clinician's recommendation for and whom had consented to FNAB, were recruited. Among the 58 patients, 47 (81.0%) were women and 11 (19.0%) were men; 37 (63.8%) had a TIRADS score of 4A, 13 (22.4%) a TIRADS score of 4B, and eight (13.8%) a TIRADS score of 4C. The numbers of patients with thyroid nodule sizes measuring < 5 mm, 5 mm–10 mm, and > 10 mm were five (8.6%), 31 (53.4%), and 22 (37.9%), respectively. The specific malignant indications of recruited patients evaluated by ultrasound as shown in sTable 1, including hypoechogenicity, irregular margins, calcifications and taller-than-wider shape. Furthermore, 11 (19.0%) patients with multiple lesions were identified. The tumor size was also measured in patients who underwent surgery. The STARD (Standards for the Reporting of Diagnostic Accuracy Studies) flow diagram is shown in Figure 1.

Cytology reports of fine needle aspirations

All patients were further investigated using fine needle investigations. Fifteen (25.9%) patients were reported as having a Bethesda System for Reporting Thyroid Cytopathology (BSRTC) score of VI, 19 (32.8%) patients with a BSRTC score of V, and six (10.3%) patients with a BSRTC score of III. The remaining 18 (31.0%) patients were reported as having a BSRTC score of I/II (Table 1).

Pathological reports

As shown in Table 2, 40 patients underwent surgical treatment, including all 15 (100%) patients who had a BSRTC score of VI, 17 out of the 19 (89.5%) patients who had a BSRTC score of V, and three out of the six (50%) patients who had a BSRTC score of III (Table 2). All patients were confirmed with malignancy after pathological examinations. Five out of the 18 (27.8%) patients who had a BSRTC score of I/II also underwent surgical treatment. In addition, three out of 40 (7.5%) patients were confirmed with extrathyroidal extension (ETE): two patients with a BSRTC score of VI and one patient with a BSRTC score of III.

10.3389/fendo.2022.888072

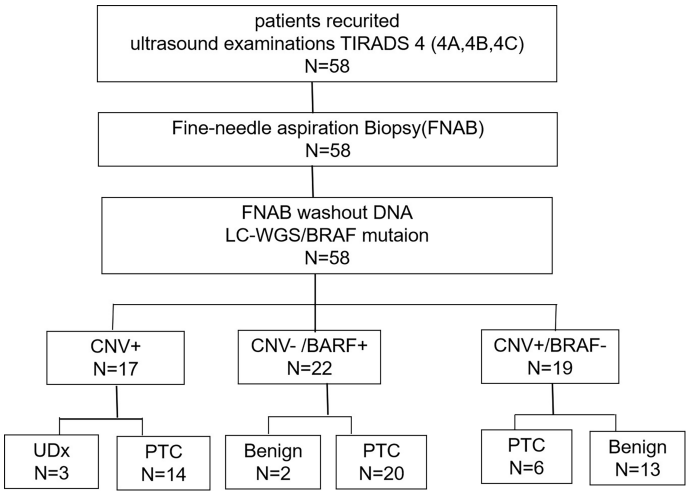

FIGURE 1
The STARD flowchart for participant recruitment.

Washout cells showed high-consistency BRAF^{V600E} mutations status with matched tissue

As shown in Table 3, of the 54 samples with wDNA and tissue DNA matching available, high levels of consistency of *BRAF* mutations were found. The FNA washout predicted 31 out of 34 (91.2%) *BRAF* mutations. Furthermore, wDNA revealed one additional *BRAF* mutation. The overall consistency between washout and matched tissue was 93.1%.

Washout cells showed copy number variations

Chromosomal aberrations were frequently identified on chromosomes 22 and 17. Chr22q deletions were present in 11 (19.0%) samples. Chromosome 17 gains were identified in three (5.2%) samples. In patients who underwent surgery, all patients with deletion of chr22q were diagnosed with PTC. All chromosome 17 gains were among patients with a BSRTC score of II. In patients with chromosome 17 gains, gains continued to be observed during the follow-up period. No pathological examinations were reported.

Frequent CNVs were found in patients with a higher BSRTC score, including eight (53.3%) patients with a score of VI and five (26.3%) patients with a score of V. Fewer chromosomal copy number changes were identified in patients with a score of III (0/6 = 0%) or I/II (3/18 = 16.7%). The results indicate that chromosomal instabilities may be associated with tumor aggressiveness (Figure 2).

The adding of washout copy number variations profiling increased detection sensitivity

As shown in Table 4, *BRAF*^{V600E} mutations were found in 55.2% and 58.0% of the samples in our dataset and The Cancer Genome Atlas (TCGA) dataset, respectively. Somatic copy number alterations (SCNAs) were found in 29.3% and 16.1% samples in our dataset and of the TCGA PTC dataset, respectively. The addition of SCNA increases the detection positive rate to 62.1% and 65.1% for our dataset and the TGCA PTC dataset, respectively.

TABLE 2 Pathology findings for different BSRTC score patient groups.

		BSRTC, *n* (%)				Total, *n* (%)
		VI	V	III	II/I	
Clinical pathology	PTC	15 (100)	17 (89.5)	3 (50)	5 (27.8)	40 (69.0)
No Surgery	0 (0)	2 (10.5)	3 (50)	13 (72.2)	18 (31.0)	

10.3389/fendo.2022.888072

TABLE 3 Comparison between washout and matched tumor tissues.

		$BRAF^{V600E}$_washout		Percentage
		Mutated	Wild type	
$BRAF^{V600E}$_tissue	Mutated	31	3	91.2
	Wild type	1	23	95.8
Overall percentage				93.1

Variations in copy number and tumor size correlated with lymph node metastasis in papillary thyroid carcinoma

It is difficult to determine preoperative LN metastasis of PTC in clinical practice. As shown in Table 5, we found that the CNV was statistically correlated with LN metastasis [p = 0.002, OR = 11.33 (95% CI 2.07 to 62.11]). The tumor size was also correlated with LN metastasis [p = 0.026, OR = 4.72 (95% CI 1.15 to 19.41]). However, there was no significant correlation between the *BRAF* mutation, ETE, and LN metastasis [p = 0.689, OR = 1.6 (95% CI 0.31 to 8.30) and p = 0.614, OR = 1.90 (95% CI 0.16 to 22.75), respectively].

The receiver operating characteristic curves were plotted to identify the diagnostic value of the three variables to predict LN metastases. As shown in Figure 3, CNV gave the best performance for the prediction of LN metastasis. The order of these three variables to predict LN metastasis was CNV followed by tumor size followed by *BRAF*. The area under the curve (AUC) of CNV was 0.733 (95% CI 0.574 to 0.892), which was higher than that of tumor size (AUC 0.668, 95% CI 0.496 to 0.840) and *BRAF* (AUC 0.534, 95% CI 0.352 to 0.715) for all patients In addition, as shown in Table 6, the prediction performance is significantly higher than that of BRAF (p=0.015).

A binary logistic regression model was established to evaluate the effects of CNV, *BRAF* mutation, and tumor size on LN metastasis in patients with PTC. As shown in Table 7, the final logistic model was statistically significant. The model could correctly classify 72.5% of the subjects. Sensitivity and specificity were 57.1% and 89.5%, respectively. The positive predictive value and negative predictive value were 85.7% and 65.4%, respectively. Among the three independent variables included in the model, CNV and tumor size were statistically significant, and their ORs were 14.122 (95% CI 2.099 to 95.35) and 6.624 (95% CI 1.088 to 36.073), respectively.

Variations in copy number correlated with lymph node metastasis in papillary thyroid microcarcinoma

We further classified PTC into three molecular subtypes based on the mutation of CNV and *BRAF*: 1) CNV positive (CNV+), 2) CNV negative (CNV–) and *BRAF* positive (*BRAF*+), and 3) CNV– and *BRAF* negative (*BRAF*–).

As shown in Table 8, for PTMC with a tumor size< 5 mm, LN metastasis was identified in four (100%) CNV+ patients but was not identified in CNV– patients (OR > 10, p = 0.001). For PTMC with a tumor size > 5 mm, LN metastasis was found in eight (80.0%) CNV+ patients and in seven (63.6%) CNV– and *BRAF*+ patients (OR 2.283, p = 0.635).

In summary, copy number variations and a tumor size > 5 mm could predict high-risk PTC with LN metastasis risk, whereas *BRAF* mutation showed no prediction value for LN metastases.

Discussion

Thyroid nodules have become a common clinical problem, and differentiated thyroid cancer is becoming more and more prevalent (5). The differential diagnosis of thyroid nodules and the risk stratification of malignancy require multidisciplinary expertise, including local ultrasound practice and specific FNA cytology (22). Even in this multidisciplinary setting, some of the

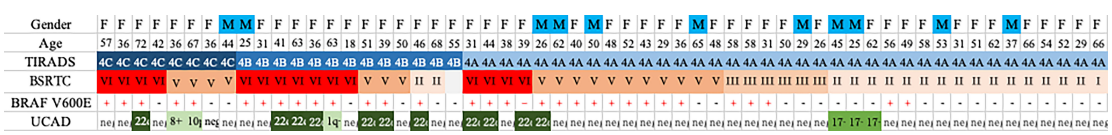

FIGURE 2
Overview of genetics changes and patient characterizations.

TABLE 4 The addition of washout copy number profiling increases cancer detection sensitivity.

Group	Event	Frequency (%)
This study	$BRAF^{V600E}$ or SCNA	62.1
	$BRAF^{V600E}$	55.2
	Washout SCNA	29.3
TCGA	$BRAF^{V600E}$ or SCNA	65.1
	$BRAF^{V600E}$	58.0
	Washout SCNA	16.1

cytopathological results of FNA are still undetermined as benign or malignant (23). However, there is growing evidence that this limitation can be overcome by using molecular diagnostic methods through comprehensive genomic analysis (11). There is, however, no suitable biomarker to indicate the malignant degree of thyroid cancer and so it is of great clinical significance to find biomarkers with high specificity and sensitivity to establish a rapid, economic and reliable detection technology.

Molecular diagnosis of FNA is an important complement to FNA cytology; it can significantly reduce unnecessary surgery and help to better determine whether or not surgery is required for thyroid nodules in patients with uncertain FNA cytology. For example, the greatest benefit has come from the use of *BRAF* mutations in the diagnosis of malignancies, as *BRAF* mutations are highly specific for malignancies when detected using well-validated techniques (24). However, more than 10% of thyroid cancers are wild-type *BRAF*, and these tumors may be more aggressive, as they have been reported to harbor chromosomal aberrations (25).

In this study, 58 thyroid FNA biopsy samples were analyzed using LC-WGS, and chromosomal changes and $BRAF^{V600E}$ mutations were identified. We found a coincidence rate of 93.1% between *BRAF* mutations detected in wDNA using this technique and the results of routine clinical tests. Furthermore, we found that an additional three (5.1%) patients were identified as wild-type *BRAF* in routine tests, but $BRAF^{V600E}$ mutations were identified using LC-WGS profiling. Combination genetic testing can improve the detection rate of *BRAF* mutations.

The treatment of low-risk PMTC (T1aN0M0) has become a major clinical problem in recent years. Although many AS clinical trials for low-risk PTMC have reported favorable outcomes, not all PTMCs are suitable for AS (26). According to the current AS guidelines for PTMC, indications include the presence of LN metastases or distant metastases, aggressive subtypes, and suspected invasion of important structures in the neck (recurrent laryngeal nerve or trachea). Tumors located near these structures should be treated immediately with surgery. Among these tumors, cervical LN metastasis is a risk factor for an increased rate of recurrence in patients with PTMC (27). There are many factors for central LN metastasis of PTMC, including age, tumor diameter, and thyroid capsule invasion (28). Potential central LN metastases have been found to occur in the early stage of PTMC, especially in the central region (29). Central LN dissection may increase the risk of recurrent laryngeal nerve and parathyroid gland injury, and these complications are often the main factors in medical disputes (30, 31). Furthermore, this discomfort can have a huge impact on the patient's subsequent quality of life and mental health. Hence, a correct preoperative evaluation is important in deciding whether or not to perform prophylactic central LN dissection (32). So far, there is no effective biomarker for the preoperative evaluation of LN metastases.

In this study, we determined that CNV was significantly associated with LN metastasis in PTC, but *BRAF* was not, especially for PTMC ≤ 5 mm. As shown in Table 8, LN metastases were confirmed after surgery in all four patients with positive CNV. Among these patients, a patient with a TIRADS score of 4B and a BSRTC score of II who did not receive timely surgical intervention was, on subsequent surgery, confirmed to have PTMC with LN metastasis. Among CNV– patients, none underwent surgery or developed LN metastasis. In addition, we followed up two patients who were CNV– and *BRAF*+ without surgery for 14 and 18 months, respectively, and

TABLE 5 The correlation between CNV, *BRAF* and tumor size with LN metastasis of PTC.

		N stage, *n* (%)		Total (*n*)	OR (95% CI)	*p*-value
		N0	N1			
CNV	CNV–	17	9 (34.6)	26	11.33 (2.07 to 62.11)	0.002
	CNV+	2	12 (85.7)	14		
BRAF (mutation)	*BRAF*–	4	3 (42.9)	7	1.6 (0.31 to 8.30)	0.689
	BRAF+	15	18 (54.8)	33		
Size (mm)	≤ 5	10	4 (28.6)	14	4.72 (1.15 to 19.41)	0.026
	> 5	9	17 (65.)	26		
ETE	Negative	18	19 (51.4)	37	1.90 (0.16 to 22.75)	0.614
	Positive	1	2 (66.7)	3		

CNV, copy number variation; ETE, extrathyroidal extension.

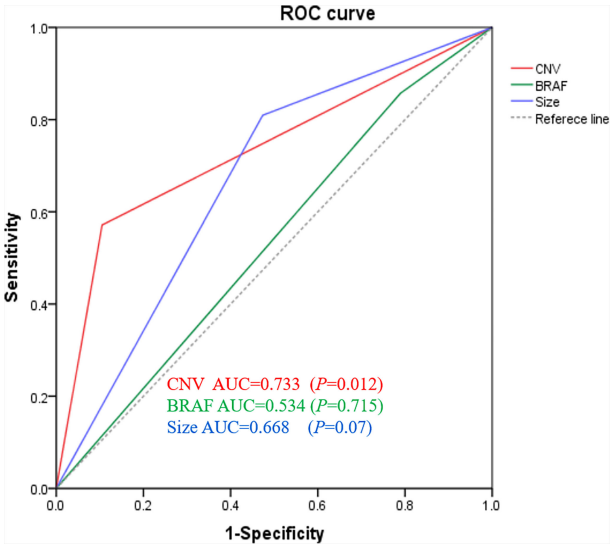

FIGURE 3
Genomic classifier to predict lymph node metastasis risk. ROC of CNV, *BRAF*, and tumor size of lymph node prediction in all surgical patients (*n* = 40). ROC, receiver operating characteristic; AUC, area under curve.

found no abnormalities. These findings suggest that patients with PTMC< 5 mm are at a higher risk of LN metastasis if CNV is positive, whereas CNV– patients belong to a low-risk subtype and AS can be used instead of surgery.

Furthermore, in this study, tumor size was found to be a risk factor for LN metastasis in PTC (OR = 4.72). For PTMC ≤ 5 mm, the incidence of LN metastasis was 28.6%. In the absence of CNV+, there is no evidence of LN metastasis. However, in our study, when the tumor size was > 5 mm, the proportion of LN metastasis increased significantly (65.3%). LN metastasis tended to occur independently of CNV (Table 5). These results were consistent with previous reports on the relationship between tumor size and LN metastasis. For example, in a retrospective cohort study, central LN metastases were found to be associated with tumor size (> 5 mm) but not with the *BRAF* mutation (33).

Genomic instability, generally considered to be a promoter of solid tumor progression, usually occurs in three forms: microsatellite instability, aneuploidy, or intrachromosome instability (34). Although much is known about the underlying mechanisms of microsatellite instability and aneuploidy, less is known about the molecular basis of intrachromosome instability (35). In fact, it now appears that intrachromosomal instability can be subdivided into several independent forms, each of which may have its own molecular origin, which is evident when different analytical methods are used (36). In this study, we clarified features of genomic instabilities described in thyroid carcinomas. As shown in Figure 2, 14 out of 58 (24.1%) cases presented chromosome instability detected by LC-WGS, including chromosome 22q loss, chromosome 17p loss, and chromosome 1q gain. Most patients with positive CIN underwent surgery and were confirmed as having thyroid cancer by postoperative pathology.

Frequent allelic deletions of, for example, chromosome 22q could suggest genetic areas to be evaluated to detect the presence of suppressor genes associated with follicular thyroid cancer (37). The consistency of the Ch22q deletion pattern in PTC suggests that this genetic lesion may represent a distinct subgroup of these tumors. The consistency of the chromosome 22q deletion pattern in PTC suggests that the genetic lesion may represent a unique subtype of these tumors.

In this context, it should be noted that a large number of Chr22q deletions are associated with tumor aggressiveness and a distinct subtype of malignant follicular carcinoma and,

TABLE 6 CNV, *BRAF*, and tumor size in predicting lymph node metastasis.

	AUC (95% CI)	TN	TP	FN	FP	PPV (%)	NPV (%)	Sensitivity (%)	Specificity (%)	Accuracy (%)
CNV	0.733 (0.574 to 0.892)	17	12	9	2	85.7	65.3	57.1	89.5	72.5
BRAF	0.534 (0.352 to 0.715)	4	18	3	15	54.5	57.1	85.7	21.1	55
Size	0.668 (0.496 to 0.840)	10	17	4	9	65.4	71.4	81	52.6	67.5

AUC, area under curve; TN, true negative; TP, true positive; FN, false negative; FP, false positive; PPV, positive prediction value; NPV, negative prediction value. CNV vs. BRAF, p=0.015.

TABLE 7 Binary logistic regression model for LN metastasis in PTC.

				N stage predicted		Percentage correct
				N0	N1	
N stage observed			N0	17	2	89.5
N1	9	12	57.1			
Overall percentage						72.5
Variables in the equation.						
	B	SE	Wald	df	Sig.	OR (95% CI)
CNV	2.648	0.973	7.41	1	0.006	14.122 (2.099 to 95.035)
Size	1.835	0.893	4.22	1	0.040	6.264 (1.088 to 36.073)
Constant	−1.908	0.825	5.345	1	0.021	0.148

Binary logistic regression model for LN metastasis.
B, regression coefficient beta; SE, standard error; Wald, Wald chi-square value; df, degree of freedom; Sig., significance, p value.

TABLE 8 Association of three molecular subtypes with LN metastasis of PTC.

LN size	CNV+	CNV− and *BRAF*+	CNV− and *BRAF*−	OR (95% CI)	*p*-value
≤ 5 mm					
N0	0	9	1	a	0.001
N1	4	0	0	(CNV+ vs. CNV− and *BRAF*+)	0.001
> 5 mm					
N0	2	4	3	2.283 (0.316 to 16.393)	0.366
N1	8	7	2	(CNV+ vs. CNV− and *BRAF*+)	0.635
All sizes					
N0	2	13	4	11.1 (1.92 to 66.67)	0.006
N1	12	7	2	(CNV+ vs. CNV− and *BRAF*+)	0.003

therefore, may indicate a precursor lesion. However, we were unable to associate any clinical or pathological parameters with specific CNV populations, other than the statistically significant association between chromosome 22q deletion groups and young age. It is worth noting that these two wild-type *BRAF* PTCs support the notion that PTCs can broadly belong to follicular or papillary neoplasms, each with different molecular and clinical characteristics.

Taken together, in the study, LC-WGS detected CNV and *BRAF* mutation status of FNA wDNA. We found that the detection of the CNV and *BRAF* mutation increased the sensitivity of FNA. In addition, CNV has a significant correlation with LN metastasis of PTC, especially for PTMC< 5 mm, which is of clinical significance. We also found that tumor size was a risk factor for LN metastasis. Therefore, we conclude that CNV and a larger tumor (i.e. > 5 mm) are risk factors for PTC LN metastases. CNV detection can be used for the preoperative risk stratification of PTC.

Data availability statement

The datasets presented in this study can be found in online repositories. The names of the repository/repositories and accession number(s) can be found in the article/Supplementary Material. The raw sequence and processed data fles are available through the National Omics Data Encyclopedia database (https://www.biosino.org/node/search) with accession number OEP003680.

Ethics statement

The studies involving human participants were reviewed and approved by the Institutional Ethics Committee of Wenzhou Hospital of Integrated Traditional Chinese and West Medicine of Zhejiang Province. The patients/participants provided their written informed consent to participate in this study. Written informed consent was obtained from the individual(s), and minor(s)' legal guardian/next of kin, for the publication of any potentially identifiable images or data included in this article.

Author contributions

LW, YZ, YG, RX, JC, WC, MZ, KS, CC, GH, XZ, and LZ participated in the design of the study and performed the statistical analysis; LW, YZ, ZQ, and S-rS drafted the manuscript. All authors read and approved the final manuscript.

Funding

Major science and technology projects of Wenzhou science and Technology Bureau grant number: ZY2021008.

Conflict of interest

Authors LZ and XZ were employed by Suzhou Hongyuan Biotech Inc. and Hangzhou Catcher Bio Inc. Author ZQ was employed by Suzhou Hongyuan Biotech Inc. and Prophet Genomics Inc.

The remaining authors declare that the research was conducted in the absence of any commercial or financial relationships that could be construed as a potential conflict of interest.

Publisher's note

Supplementary Material

The Supplementary Material for this article can be found online at: https://www.frontiersin.org/articles/10.3389/fendo.2022.888072/full#supplementary-material

References

1. Siegel RL, Miller KD, Fuchs HE, Jemal A. Cancer statistics, 2021. *CA Cancer J Clin* (2021) 71(1):7–33. doi: 10.3322/caac.21654

2. Sutherland R, Tsang V, Clifton-Bligh RJ, Gild ML. Papillary thyroid microcarcinoma: Is active surveillance always enough? *Clin Endocrinol* (2021) 95 (6):811–7. doi: 10.1111/cen.14529

3. Ito Y, Miyauchi A, Oda H. Low-risk papillary microcarcinoma of the thyroid: A review of active surveillance trials. *Eur J Surg Oncol J Eur Soc Surg Oncol Br Assoc Surg Oncol* (2018) 44(3):307–15. doi: 10.1016/j.ejso.2017.03.004

4. Baloch ZW, LiVolsi VA. Pathologic diagnosis of papillary thyroid carcinoma: today and tomorrow. *Expert Rev Mol Diagn* (2005) 5(4):573–84. doi: 10.1586/14737159.5.4.573

5. Haugen BR, Alexander EK, Bible KC, Doherty GM, Mandel SJ, Nikiforov YE, et al. American Thyroid association management guidelines for adult patients with thyroid nodules and differentiated thyroid cancer: The American thyroid association guidelines task force on thyroid nodules and differentiated thyroid cancer. *Thyroid Off J Am Thyroid Assoc* (2015) 26(1):1–133. doi: 10.1089/thy.2015.0020

6. Chinese Association for Thyroid Cancer(CATO). Chinese Consensus statement on diagnosis and treatment of papillary thyroid microcarcinoma (2016 version). *Chin J Clin Oncol* (2016) 43(10):405–11. doi: CNKI:SUN:ZGZL.0.2016-10-001

7. Gharib H, Goellner JR. Fine-needle aspiration biopsy of the thyroid: an appraisal. *Ann Internal Med* (1993) 118(4):282–9. doi: 10.7326/0003-4819-118-4-199302150-00007

8. Lin JD, Huang BY, Weng HF, Jeng LB, Hsueh C. Thyroid ultrasonography with fine-needle aspiration cytology for the diagnosis of thyroid cancer. *J Clin Ultrasound JCU* (1997) 25(3):111–8. doi: 10.1002/(SICI)1097-0096(199703)25:3<111::AID-JCU3>3.0.CO;2-J

9. Kim DW, Park AW, Lee EJ, Choo HJ, Kim SH, Lee SH, et al. Ultrasound-guided fine-needle aspiration biopsy of thyroid nodules smaller than 5 mm in the maximum diameter: assessment of efficacy and pathological findings. *Korean J Radiol* (2009) 10(5):435–40. doi: 10.3348/kjr.2009.10.5.435

10. Bongiovanni M, Spitale A, Faquin WC, Mazzucchelli L, Baloch ZW. The Bethesda system for reporting thyroid cytopathology: a meta-analysis. *Acta Cytol* (2012) 56(4):333–9. doi: 10.1159/000339959

11. Xing M, Haugen BR, Schlumberger M. Progress in molecular-based management of differentiated thyroid cancer. *Lancet* (2013) 381(9871):1058–69. doi: 10.1016/S0140-6736(13)60109-9

12. Rashid FA, Munkhdelger J, Fukuoka J, Bychkov A. Prevalence of BRAF (V600E) mutation in Asian series of papillary thyroid carcinoma-a contemporary systematic review. *Gland Surg* (2020) 9(5):1878–900. doi: 10.21037/gs-20-430

13. Xing M, Clark D, Guan H, Ji M, Dackiw A, Carson KA, et al. BRAF mutation testing of thyroid fine-needle aspiration biopsy specimens for preoperative risk stratification in papillary thyroid cancer. *J Clin Oncol Off J Am Soc Clin Oncol* (2009) 27(18):2977–82. doi: 10.1200/JCO.2008.20.1426

14. Bakhoum SF, Cantley LC. The multifaceted role of chromosomal instability in cancer and its microenvironment. *Cell* (2018) 174(6):1347–60. doi: 10.1016/j.cell.2018.08.027

15. Heng HH, Bremer SW, Stevens JB, Horne SD, Liu G, Abdallah BY, et al. Chromosomal instability (CIN): what it is and why it is crucial to cancer evolution. *Cancer Metastasis Rev* (2013) 32(3-4):325–40. doi: 10.1007/s10555-013-9427-7

16. Kunstman JW, Juhlin CC, Goh G, Brown TC, Stenman A, Healy JM, et al. Characterization of the mutational landscape of anaplastic thyroid cancer *via* whole-exome sequencing. *Hum Mol Genet* (2015) 24(8):2318–29. doi: 10.1093/hmg/ddu749

17. Yoo SK, Song YS, Lee EK, Hwang J, Kim HH, Jung G, et al. Integrative analysis of genomic and transcriptomic characteristics associated with progression of aggressive thyroid cancer. *Nat Commun* (2019) 10(1):2764. doi: 10.1038/s41467-019-10680-5

18. Greene SB, Dago AE, Leitz LJ, Wang Y, Lee J, Werner SL, et al. Chromosomal instability estimation based on next generation sequencing and single cell genome wide copy number variation analysis. *PloS One* (2016) 11(11): e0165089. doi: 10.1371/journal.pone.0165089

19. Scheinin I, Sie D, Bengtsson H, van de Wiel MA, Olshen AB, van Thuijl HF, et al. DNA Copy number analysis of fresh and formalin-fixed specimens by shallow whole-genome sequencing with identification and exclusion of problematic regions in the genome assembly. *Genome Res* (2014) 24(12):2022–32. doi: 10.1101/gr.175141.114

20. Zeng S, Ying Y, Xing N, Wang B, Qian Z, Zhou Z, et al. Noninvasive detection of urothelial carcinoma by cost-effective low-coverage whole-genome sequencing from urine-exfoliated cell DNA. *Clin Cancer Res Off J Am Assoc Cancer Res* (2020) 26(21):5646–54. doi: 10.1158/1078-0432.CCR-20-0401

21. Seshan VE, Olshen A. DNAcopy: DNA copy number data analysis. (2013). R package version 1.62.0. Available from: https://bioconductor.org/packages/release/bioc/html/DNAcopy.html.

22. Gharib H, Papini E, Garber JR, Duick DS, Harrell RM, Hegedüs L, et al. AMERICAN ASSOCIATION OF CLINICAL ENDOCRINOLOGISTS, AMERICAN COLLEGE OF ENDOCRINOLOGY, AND ASSOCIAZIONE MEDICI ENDOCRINOLOGI MEDICAL GUIDELINES FOR CLINICAL PRACTICE FOR THE DIAGNOSIS AND MANAGEMENT OF THYROID NODULES–2016 UPDATE. *Endocrine Pract Off J Am Coll Endocrinol Am Assoc Clin Endocrinol* (2016) 22(5):622–39. doi: 10.4158/EP161208.GL

23. Cibas ES, Ali SZ. The 2017 Bethesda system for reporting thyroid cytopathology. *Thyroid Off J Am Thyroid Assoc* (2017) 27(11):1341–6. doi: 10.1089/thy.2017.0500

24. Frasca F, Nucera C, Pellegriti G, Gangemi P, Attard M, Stella M, et al. BRAF (V600E) mutation and the biology of papillary thyroid cancer. *Endocrine-related Cancer* (2008) 15(1):191–205. doi: 10.1677/ERC-07-0212

25. Iwadate M, Mitsutake N, Matsuse M, Fukushima T, Suzuki S, Matsumoto Y, et al. The clinicopathological results of thyroid cancer with BRAFV600E mutation in the young population of fukushima. *J Clin Endocrinol Metab* (2020) 105(12): e4328–36. doi: 10.1210/clinem/dgaa573

26. Sugitani I, Ito Y, Takeuchi D, Nakayama H, Masaki C, Shindo H, et al. Indications and strategy for active surveillance of adult low-risk papillary thyroid microcarcinoma: Consensus statements from the Japan association of endocrine surgery task force on management for papillary thyroid microcarcinoma. *Thyroid Off J Am Thyroid Assoc* (2021) 31(2):183–92. doi: 10.1089/thy.2020.0330

27. Wu X, Li B, Zheng C, He X. Risk factors for central lymph node metastases in patients with papillary thyroid microcarcinoma. *Endocrine Pract Off J Am Coll Endocrinol Am Assoc Clin Endocrinol* (2018) 24(12):1057–62. doi: 10.4158/EP-2018-0305

28. Sheng L, Shi J, Han B, Lv B, Li L, Chen B, et al. Predicting factors for central or lateral lymph node metastasis in conventional papillary thyroid microcarcinoma. *Am J Surg* (2020) 220(2):334–40. doi: 10.1016/j.amjsurg.2019.11.032

29. Cheah WK, Arici C, Ituarte PH, Siperstein AE, Duh QY, Clark OH. Complications of neck dissection for thyroid cancer. *World J Surg* (2002) 26 (8):1013–6. doi: 10.1007/s00268-002-6670-4

30. Dismukes J, Fazendin J, Obiarinze R, Márquez GCH, Ramonell KM, Buczek E, et al. Prophylactic central neck dissection in papillary thyroid carcinoma: All risks, no reward. *J Surg Res* (2021) 264:230–5. doi: 10.1016/j.jss.2021.02.035

31. Giordano D, Frasoldati A, Gabrielli E, Pernice C, Zini M, Castellucci A, et al. Long-term outcomes of central neck dissection for cN0 papillary thyroid carcinoma. *Am J Otolaryngol* (2017) 38(5):576–81. doi: 10.1016/j.amjoto.2017.06.004

32. Liu Y, Lv H, Zhang S, Shi B, Sun Y. The impact of coexistent hashimoto's thyroiditis on central compartment lymph node metastasis in papillary thyroid carcinoma. *Front Endocrinol* (2021) 12:772071. doi: 10.3389/fendo.2021.772071

33. Zhang Q, Wang Z, Meng X, Duh QY, Chen G. Predictors for central lymph node metastases in CN0 papillary thyroid microcarcinoma (mPTC): A retrospective analysis of 1304 cases. *Asian J Surg* (2019) 42(4):571–6. doi: 10.1016/j.asjsur.2018.08.013

34. Stoler DL, Nowak NJ, Matsui S, Wiseman SM, Chen N, Dutt SS, et al. Comparative genomic instabilities of thyroid and colon cancers. *Arch Otolaryngol–head Neck Surg* (2007) 133(5):457–63. doi: 10.1001/archotol.133.5.457

35. Kitamura Y, Shimizu K, Tanaka S, Ito K, Emi M. Allelotyping of anaplastic thyroid carcinoma: frequent allelic losses on 1q, 9p, 11, 17, 19p, and 22q. *Genes Chromosomes Cancer* (2000) 27(3):244–51. doi: 10.1002/(SICI)1098-2264(200003)27:3<244::AID-GCC4>3.0.CO;2-7

36. Caria P, Vanni R. Cytogenetic and molecular events in adenoma and well-differentiated thyroid follicular-cell neoplasia. *Cancer Genet Cytogenet* (2010) 203 (1):21–9. doi: 10.1016/j.cancergencyto.2010.08.025

37. Kitamura Y, Shimizu K, Ito K, Tanaka S, Emi M. Allelotyping of follicular thyroid carcinoma: frequent allelic losses in chromosome arms 7q, 11p, and 22q. *J Clin Endocrinol Metab* (2001) 86(9):4268–72. doi: 10.1210/jcem.86.9.7853

frontiers | Frontiers in Endocrinology

TYPE Review
PUBLISHED 13 March 2024
DOI 10.3389/fendo.2024.1351776

OPEN ACCESS

EDITED BY
Christos K. Kontos,
National and Kapodistrian University of Athens, Greece

REVIEWED BY
Khawla S. Al-Kuraya,
King Faisal Specialist Hospital and Research Centre, Saudi Arabia
Katerina Katsaraki,
National and Kapodistrian University of Athens, Greece

*CORRESPONDENCE
Jinxing Quan
quanxt@sina.com

†These authors have contributed equally to this work and share first authorship

RECEIVED 07 December 2023
ACCEPTED 04 March 2024
PUBLISHED 13 March 2024

CITATION
Ma J, Xu J, Zhang X and Quan J (2024) The emerging role and clinical significance of circRNAs in papillary thyroid cancer. *Front. Endocrinol.* 15:1351776. doi: 10.3389/fendo.2024.1351776

The emerging role and clinical significance of circRNAs in papillary thyroid cancer

Jing Ma[1,2,3†], Jing Xu[4†], Xiaoqi Zhang[4] and Jinxing Quan[1,2,3*]

[1]The First Clinical Medical School, Lanzhou University, Lanzhou, Gansu, China, [2]Department of Endocrinology, Gansu Provincial Hospital, Lanzhou, Gansu, China, [3]Department of Endocrinology, Key Laboratory of Endocrine and Metabolic Diseases of Gansu Province, Lanzhou, Gansu, China, [4]The Second Clinical Medical School, Lanzhou University, Lanzhou, Gansu, China

Papillary thyroid cancer (PTC) is the most common type of thyroid malignancy, and its global incidence has been gradually increasing. For advanced PTC, the mortality rates are also increasing yearly. Despite advancements in diagnosis and treatment, some advanced PTC exhibit aggressive behaviors, leading to a poor prognosis. CircRNAs are a class of non-coding RNAs characterized by a covalently closed loop structure. Their stability and abundance have positioned them as promising diagnostic and prognostic biomarkers. Numerous studies have identified dysregulated circRNAs in PTC tissues and cell lines, suggesting their involvement in PTC initiation and progression. In this review, we provide an overview of circRNAs and systematically discuss their role in PTC. CircRNAs affect cancer progression by regulating the Wnt/β-catenin, PI3K/AKT, MAPK pathways, and others. Furthermore, circRNAs have been implicated in PTC metastasis and chemoresistance. We highlight their potential value as diagnostic markers, therapeutic targets, and prognostic indicators. In conclusion, circRNAs play a critical role in PTC, and dysregulated circRNAs influence multiple signaling pathways and cellular processes involved in tumorigenesis and metastasis. It represents a promising avenue for advancing the diagnosis, management, and treatment of PTC.

KEYWORDS

papillary thyroid cancer, circRNA, signaling pathway, biomarker, carcinogenesis

1 Introduction

Thyroid cancer (TC) is the most common endocrine malignancy and accounts for nearly one-third of all malignant tumors of the head and neck. For individuals with advanced TC, new systemic treatments and management are being investigated (1). The global prevalence of TC has been gradually increasing, particularly among young adults and teenagers. The age-standardized incidence of TC is approximately three times higher in women (10.1 per 100,000) than in men (3.1 per 100,000) (2). According to the latest cancer statistics reports in 2022, the number of TC survivors has jumped to the third highest rate

in women, and the high-risk age range is 30-45 years old (3). Based on the Adolescents and Young Adults (AYAs) 2020 statistics, the 15-29 age group has the highest incidence of TC (4). Furthermore, TC incidence rates also show significant differences across settings, such as more than a 15-fold difference in incidence rates among women in different regions of the world (2). There are three main histological types of TC, differentiated thyroid cancer (DTC), anaplastic thyroid cancer (ATC), and medullary thyroid cancer (MTC). DTC includes papillary thyroid cancer (PTC) and follicular thyroid cancer (FTC). PTC is the most common type of TC, accounting for nearly 85% of cases. Some aggressive PTC with local or distant metastasis, structural recurrence, and even progression to high-grade cancer can be life-threatening (5). The 5-year survival rate for patients with advanced PTC is only 59% (6). Recently, WHO has made significant adjustments to the classification of TC, highlighting differences in cellular origin, pathological features, molecular classification, and biological behavior into benign, low-risk, and malignant tumors, while also emphasizing the role of biomarkers in aiding diagnosis and determining prognosis (7).

Currently, sampling via ultrasound-guided fine-needle aspiration (FNA) is a commonly used diagnostic way for evaluating malignant thyroid nodules (8). Studies have shown that FNA reduces unnecessary thyroid surgery by 25%. Nonetheless, approximately 30% of thyroid nodules remain undiagnosed by pathology (6, 9), which even leads to misdiagnosis (9). In addition, the diagnostic value of FNA is relatively low for FTC (10). Unnecessary FNA can also add to the burden on the health care system and cause considerable anxiety for patients (11). Therefore, greater focus on accurate diagnosis, management, and treatment of TC is imperative. Understanding the underlying molecular mechanisms of TC can aid in the development of targeted and specialized treatments.

Circular RNAs (circRNAs) are a new class of non-coding RNA molecules and have been found to be widely expressed in various human cancers. Recently, they have emerged as a hot topic due to their potential role in carcinogenesis and tumor progression (12). Unlike linear RNA molecules, circRNAs are generated by head-to-tail splicing and form a closed-loop structure without 5' to 3' polarity and a polyadenylated tail. They are highly stable and resistant to degradation and play important regulatory roles in gene expression and other cellular processes (13–15). The study of circRNAs in PTC has been growing rapidly, and recent findings have shed light on their contribution to the development and progression of this disease (12–14). In this review, we give a brief description of circRNAs, then systematically discuss the role of circRNAs in PTC and their potential value in diagnosis, prognosis, and treatment.

2 Circular RNAs

CircRNAs were first discovered in the 1970s but were initially thought to be rare and non-functional byproducts of RNA splicing. It was not until the advent of high-throughput sequencing technologies in the early 2010s that circRNAs were found to be widespread and abundant in eukaryotic cells, including human cells. It has undergone rapid development in the past decade and has opened up new avenues for research into gene regulation, biological processes, and cellular signaling. They are mainly categorized according to their genomic origin and the way they are generated. Exonic circRNAs (ecircRNAs) are mainly derived from single or multiple exons, representing the majority of circRNAs (more than 80%). Intronic circRNAs (ciRNAs) contain only introns and are the most common transposons in the genome. Exon-intron circRNAs (EIciRNAs), which contain both exons and introns. In addition, a novel class of circRNAs, namely tRNA intronic circRNAs (tricRNAs), are formed by pre-tRNA splicing. Currently, most of the identified circRNAs belong to ecircRNA (16).

The massive number of circRNAs identified so far suggests that they may have complicated and diverse roles. To date, the functions of circRNAs that have been reported are diverse and include competing endogenous RNAs (ceRNAs) or miRNA sponges, interacting with RNA-binding proteins (RBPs), regulating the splicing or transcription of genes, translation into proteins or small peptides, epigenetic regulation, and modulating the stability of mRNAs (17). What's more, studies have reported that circRNAs can function in gene regulation by competing with linear splicing (18). Ho et al. (19) found that heterogeneous nuclear ribonucleoprotein M (HNRNPM) can control circRNA biogenesis and thus promote solid tumor development. The most thorough research has focused on circRNAs acting as miRNA sponges. CDR1as, also known as ciRS-7, harbors more than 70 conserved binding sites, is highly expressed in human and mouse brains and was reported to function as a sponge for miR-7 (20). In addition, circITCH, a recently discovered circRNA, similarly acts as a miRNA sponge via miR-7 to promote osteosarcoma migration and invasion (21). All these findings above indicate that circRNAs could function as miRNA sponges to contribute to the regulation of cancer. For the RBPs mechanism, it has been shown that EWS RNA-binding protein 1 (EWSR1) promotes circNEIL3 biogenesis in gliomas (22). Research found that NOVA2 can act as a neural-enriched RBP to promote circRNA biogenesis in the mouse brain (23).

There is also high tumor specificity in the peptide encoded by circRNAs. For example, Zhang et al. found that SHPRH-146aa generated from circSHPRH exhibited tumor specificity, and this encoded peptide was abundantly expressed in the normal human brain and downregulated in 81% of glioblastomas. SHPRH-146aa was able to protect full-length SHPRH from DTL-induced ubiquitination. As a key tumor suppressor, SHPRH contributes to the inhibition of tumorigenesis and progression (24). CircRHOT1 was highly expressed in advanced hepatocellular carcinoma (HCC) tissues and inhibited HCC progression by recruiting TIP60 to initiate NR2F6 transcription. It was strongly associated with the prognosis of HCC (25). Currently, there are two main known modes of translation initiation for circRNAs, the internal ribosome entry site (IRES) and the N6-methyladenosine (m6A).

m6A modification is one of the most common types of RNA modification in eukaryotes. It is widely involved in the regulation of biogenesis, splicing, translation, stability, and degradation of RNA. A recent study reviewed the functional crosstalk between m6A and circRNAs in cancer (26). Another mechanism has been proposed to activate the cap-independent pathway through the IRES, which is located in the 5′ UTR of mRNA. IRES initiates translation by directly recruiting ribosomes, an IRES-driven mechanism that has been explored in recent studies. Fan et al. (27) showed that certain short elements other than known IRES are sufficient to initiate circRNA translation. CircRNA-translated proteins also have certain biological roles. For example, during myogenesis, circZNF609 can undergo splice-dependent and cap non-dependent translation into proteins that specifically control myoblast proliferation (28).

In addition, the identification of differences in gene expression levels between cancer and control samples is a critical component of cancer biology research. Analyses involving multiple tumor cells and corresponding normal cells have found aberrant expression levels of circRNAs in different malignancies. A growing number of studies have shown that circRNAs are closely associated with the development of cancer and can be used as biomarkers (29–32). The main distinct advantage is their ability to be detected via RT-PCR of samples, as well as their great circulatory stability. Abnormal expression of circRNAs is correlated with tumor size, TNM stage, lymph node metastasis (LNM), and poor overall survival in TC (33). However, the relationship between PTC and circRNAs is still poorly understood. Those potential new roles of circRNAs need to be thoroughly investigated further.

3 CircRNAs in PTC

To date, a number of circRNAs have been found to be aberrantly expressed in PTC. They can regulate the progression of PTC through various aspects. However, the precise mechanisms by which circRNAs influence PTC development and progression remain unclear. Therefore, we summarize the dysregulated circRNAs in PTC reported in recent studies (Table 1). We can see most of the circRNAs are up-regulated in PTC. Moreover, they could act as miRNA sponges to carry out their functions. Some circRNAs have one or more miRNA binding sites that enable them to sequester miRNAs and further regulate the expression of their downstream target genes. illustrates the function of circRNAs in PTC. Further, we generalize the regulatory uniqueness of circRNAs in PTC in Figure 1.

3.1 CircRNAs act as ceRNAs involved in PTC biological processes

Current research has found that circRNAs could act as ceRNAs to absorb miRNAs and participate in the regulation of PTC. CeRNA was first proposed by Pandolfi's team in 2011 (83). They found that ceRNA molecules can compete to bind the same miRNAs through miRNA response elements (MREs) to regulate each other's expression levels. It is known that miRNAs can cause gene silencing by binding to the 3'-UTR matched by mRNAs through the seed region, while ceRNA can regulate gene expression by competitively binding miRNAs.

According to multiple previous studies, some circRNAs could participate in one or more miRNA sponge pathways. For example, CircFN1 (hsa_circ_0058124) acts as an oncogenic driver that promotes PTC cell proliferation, tumor invasion, and metastasis. It could bind miR-218-5p to modulate the expression of GATAD2A, which plays an important role in transcriptional regulation. Likewise, it can bind to miR-940, which regulates the expression of MAPK1, an essential MAP kinase that integrates various biochemical signals to regulate cellular processes such as proliferation, differentiation, and transcriptional regulation (34). Moreover, circFN1 interacts with miR-370-3p to modify the expression of LMO4, which has the potential to function as an oncogene or a transcriptional regulator (35). Additionally, circFN1 promotes the progression of PTC by sponging miR-873-5p while restraining the malignancy of PTC cells by binding to FSTL1 (84).

Chu et al. (36) found that circRUNX1_005 (hsa_circ_0002360) promoted DDHD2 expression by sponging miR-296-3p. This gene encodes the protein phospholipase DDHD2, which is involved in membrane transport between the endoplasmic reticulum and the Golgi apparatus, thereby enhancing the proliferation, migration, and invasion of PTC cells. Similarly, silencing of circPSD3 (hsa_circ_0004458) significantly downregulated RAC1 expression by sponging miR-885-5p. It produces small plasma membrane-associated GTPases that bind to a variety of effector proteins to regulate cellular responses, thereby promoting PTC cell cycle arrest and apoptosis (42).

CircPVT1 has been reported to promote the expression of VEGFA to induce endothelial cell proliferation, promoting cell migration, inhibiting apoptosis, and inducing vascular permeabilization by sponging miR-195 (38), or by evaluating Bax/Bcl-2/PCNA to regulate apoptosis or proliferation of cells by sponging miR-126 (39). Similarly, circMMP2 (hsa_circ_0039411) (40, 41) regulates SOX4 expression by sponging miR-423-5p and translating a transcription factor protein. CircMMP2 also sponges miR-1179 to regulate the expression of ABCA9, transporting and translocating various molecules through extracellular and intracellular membranes. Moreover, it can bind miR-1205 to regulate the expression of MTA1, which is involved in transcription, migration, invasion, and glycolysis of PTC cells.

According to recent research, circLDLR (hsa_circ_0003892) functions as a sponge for miR-195-5p to regulate the catalytic lipid-mediated enzyme, lipase H (LIPH) (43). Moreover, circLDLR interacts with miR-637 to impact the expression of LMO4 and also interacts with miR-326 to regulate the expression of LASP1. LASP1 encodes for an actin-dependent signaling protein that binds to the actin cytoskeleton at the cell membrane's extension to promote cell viability, migration, and invasion (44, 45). A novel oncogenic RNA, circBACH2, could be involved in the progression of PTC by acting as miR-139-5p sponge and then relieving suppression of the target LMO4 (64).

TABLE 1 Dysregulated circRNAs in PTC.

CircRNAs up-regulated (↑)	miRNA	Target gene/ Pathway	Biological Function	Reference
circFN1 _055 (hsa_circ_0058124)	↓ miR-218-5p ↓ miR-940	↑ NOTCH3/ GATAD2A	promotes cell proliferation, cell invasion, metastasis, and tumorigenicity	(34)
circFN1 _055 (hsa_circ_0058124)	↓ miR-370-3p	↑ LMO4	promotes cell viability, colony formation, migration, invasion and suppresses cell apoptosis	(35)
circRUNX1_005 (hsa_circ_0002360)	↓ miR-296-3p	↑ DDHD2	promotes cell proliferation, migration, and invasion	(36)
circARID1B_031 (hsa_circ_0001658)	↓ miR-671-5p	↑ PI3K/AKT/ITGA2	promotes cell proliferation and migration	(37)
circPVT1	↓ miR-195	↑ Wnt/β-catenin/VEGFA	promotes cell proliferation, migration, and invasion	(38)
circPVT1	↓ miR-126	↑ Bax/Bcl-2/PCNA	promotes cell viability, migration and invasion	(39)
circMMP2_005 (hsa_circ_0039411)	↓ miR-1179 ↓ miR-1205	↑ ABCA9 ↑MTA1	promotes cell growth, migration, invasion and suppresses cell apoptosis	(40)
circMMP2_005 (hsa_circ_0039411)	↓ miR-423-5p	↑ SOX4	promotes cell growth, migration, invasion, and glycolysis	(41)
circPSD3_017 (hsa_circ_0004458)	↓ miR-885-5p	↑ RAC1	promotes cell proliferation, suppresses cell cycle arrest and apoptosis	(42)
circLDLR_027 (hsa_circ_0003892)	↓ miR-195-5p	↑ LIPH	promotes cell proliferation, colony formation, migration, invasion and suppresses cell apoptosis	(43)
circLDLR _027 (hsa_circ_0003892)	↓ miR-637	↑ LMO4	promotes cell growth, migration, invasion and suppresses cell apoptosis	(44)
circLDLR_027 (hsa_circ_0003892)	↓ miR-326	↑ LASP1	promotes cell proliferation, migration, and invasion	(45)
circPRKCI _020 (hsa_circ_0067934)	↓ miR-1304	↑ CXCR1	promotes cell proliferation, migration, invasion and suppresses cell apoptosis	(46)
circPRKCI _020 (hsa_circ_0067934)	↓ miR-545-3p	↑ SLC7A11	promotes cell proliferation and suppresses cell apoptosis.	(47)
circPRKCI _020 (hsa_circ_0067934)	↓ miR-1301-3p	↑ HMGB1	promotes cell proliferation, migration, invasion and EMT	(48)
circNRIP1	↓ miR-195-5p	↑ P38 MAPK/ JAK/STAT	promotes cell proliferation, invasion, and suppresses apoptosis	(49)
circNRIP1	↓ miR-653-5p	↑ PBX3	promotes cell proliferation, migration, invasion and suppresses cell apoptosis	(50)
circNRIP1	↓ miR-541-5p ↓ miR-3064-5p	↑ PKM2	promotes cell proliferation and glycolysis	(51)
circKIAA1199_022 (hsa_circ_0000644)	↓ miR-1205	↑ E2F3	promotes cell growth, migration, invasion and suppresses cell apoptosis	(52)
circNDST1 _011 (hsa_circ_0006943)	–	↑ PI3K/AKT/EMT	promotes cell proliferation, migration, invasion, and EMT	(53)
circSSU72_007 (hsa_circ_0009294)	↓ miR-451a	↑ AKT/S1PR2	promotes cell proliferation, migration, and invasion	(54)
circRAPGEF5_001 (hsa_circ_0079558)	↓ miR-26b-5p	↑ MET/AKT	promotes cell proliferation, motility and suppresses cell apoptosis	(55)
circUBAP2_046 (hsa_circ_0003141)	↓ miR-370-3p	↑ PI3K/AKT/Wnt	promotes cell proliferation, invasion and suppresses cell apoptosis	(56)
circSMURF2 (hsa_circ_102171)	–	↑ Wnt/β-catenin/CTNNBIP1	promotes PTC progression by activating Wnt/β-catenin pathway in a CTNNBIP1-dependent way	(57)

(Continued)

TABLE 1 Continued

CircRNAs up-regulated (↑)	miRNA	Target gene/ Pathway	Biological Function	Reference
circUGGT2_065 (hsa_circ_0008274)	–	↑ mTOR/AMPK	promotes cell proliferation and invasion	(58)
hsa_circ_102002	↓ miR-488-3p	↑ HAS2	promotes cell proliferation, migration, and EMT	(59)
circPI4KA_028 (hsa_circ_0062389)	↓ miR-1179	↑ HMGB1	promotes cell proliferation, migration, and EMT	(60)
circPUM1	↓ miR-21-5p	↑ MAPK1	promotes cell proliferation, metastasis and glycolysis	(61)
circNOX4 _002 (hsa_circ_0023990)	↓ miR-485-5p	↑ FOXM1	promotes cell proliferation and glycolysis	(62)
hsa_circ_000121	↓ miR-4763 ↓ miR-6775	↑ SRC ↑ MMP-14	promotes the aggressiveness and lymph node metastasis	(63)
circBACH2_003 (hsa_circ_0001627)	↓ miR-139-5p	↑ LMO4	promotes cell proliferation, migration and invasion	(64)
circMET_004 (hsa_circ_0082003)	–	–	promotes cell proliferation, migration and invasion	(65)
circHMGA2_001 (hsa_circ_0027446)	↓ miR-129–5p	↑ CLDN1	promotes cell proliferation, migration, invasion and suppresses cell apoptosis	(66)
hsa_circ_0002111	–	–	promotes cell proliferation and invasion	(67)
hsa_circ_007148	–	–	associated with LNM	(68)
hsa_circ_007293	↓ miR-653-5p	↑ PAX6	promotes cell proliferation, invasion, migration, and EMT	(69)
circUGGT2_065 (hsa_circ_0008274)	↓ miR-154-3p	↑ SLC7A11	promotes cell migration and adhesion	(70)
circCCDC66	↓ miR-129-5p	↑ LARP1	promotes cell proliferation, invasion, and migration	(71)
circVANGL1	↓ miR-194	↑ ZEB1	promotes cell proliferation, invasion, migration, and EMT	(72)
circTMEM222_001 (hsa_circ_0011058)	↓ miR-335-5p	↑ YAP1	promotes cell proliferation, angiogenesis and radioresistance	(73)
circPSD3	↓ miR-7-5p	↑ METTL7B	promotes cell proliferation and invasion	(74)
circPRKCI_017 (hsa_circ_0122683)	↓ miR-335	↑ E2F3	promotes cell proliferation, invasion, and glycolysis	(75)
circRASSF2_009 (hsa_circ_0059354)	↓ miR-766-3p	↑ ARFGEF1	promotes cell proliferation, migration, invasion and angiogenesis	(76)
circSLAMF6_001 (hsa_circ_0000144)	↓ miR-1178-3p	↑ YWHAH	promotes cell proliferation, migration, invasion and angiogenesis	(77)
circFAM120B_004 (hsa_circ_0001666)	↓ miR-330-5p ↓ miR-193a-5p ↓ miR-326	↑ ETV4	promotes cell proliferation and arrest of cell cycle	(78)
circAGTPBP1_006 (hsa_circ_0087391)	↓ miR-34a-5p	↑ NOTCH1	promotes cell proliferation, migration, invasion, and metastasis	(79)
CircRNAs down-regulated (↓)	**miRNA**	**Target gene/ Pathway**	**Biological Function**	**Reference**
hsa_circ_047771	↑ miR-522-3p	–	associated with BRAFV600 mutation, LNM, and advanced TNM stage	(68)
circITCH	↑ miR-22-3p	↓ CBL/β-catenin	suppresses cell proliferation and invasion and promotes cell apoptosis	(80)
circFAM53B (hsa_circ_0000266)	↑ miR-183-5p	↓ CCDC6	suppresses cell proliferation, migration, and invasion	(81)
hsa_circ_100395	–	↓ PI3K/AKT/mTOR	suppresses cell migration, invasion, glycolysis and downregulated PI3K/ AKT/mTOR pathway	(82)

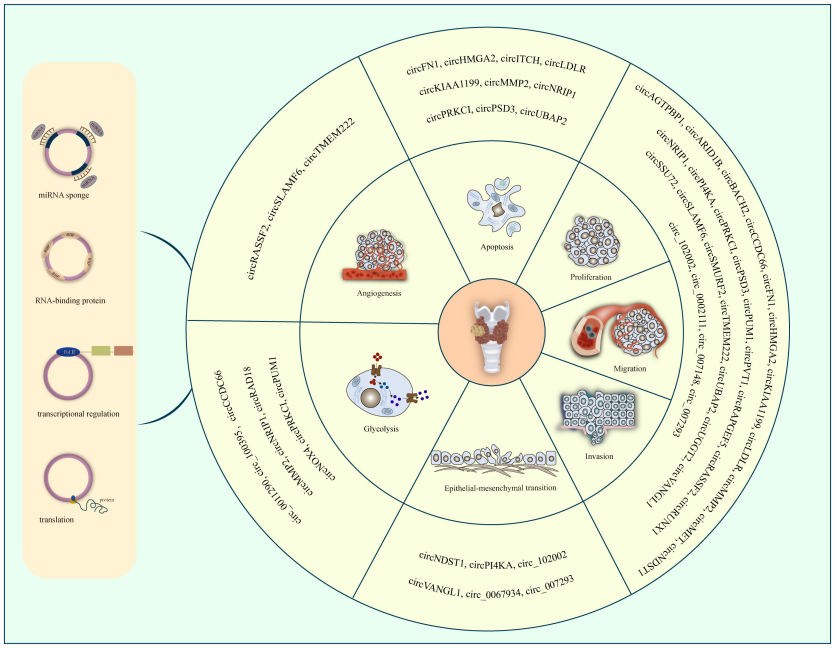

FIGURE 1
The regulatory uniqueness of circRNAs in PTC progression.

Furthermore, circPRKCI (hsa_circ_0067934) has been found to serve as a sponge for miR-1304 to modulate the expression of CXCR1, which encodes the receptor for IL8 (46). In addition, it interacts with miR-545-3p to modify the expression of SLC7A11 (47). This encoded protein has been recognized as the primary mediator of Kaposi's sarcoma-associated herpes and is allowed to follow fusion and entry into cells. Also, circPRKCI acts as a sponge for miR-1301-3p to modulate the expression of HMGB1, which encodes a non-histone nuclear DNA-binding protein that regulates transcription and DNA organization (48). This protein is involved in various cellular processes, such as inflammation, cell differentiation, and cell migration.

Recently, studies reported that circNRIP1 could bind miR-195-5p and miR-653-5p to regulate the expression of PBX3, a transcription regulator critical for animal organ and neuronal development, as well as regulation by RNA polymerase II (49, 50). Additionally, circNRIP1 can sponge miR-541-5p, playing a role in the regulation of PKM2, a crucial glycolytic enzyme (51).

Another hotly studied circRNA, circKIAA1199 (hsa_circ_0000644) can sponge miR-1205, which regulates the expression of E2F3 (52). Notably, E2F3 is involved in the regulation of genes essential for cell cycle progression and is a crucial oncogene in several tumors. Also, circKIAA1199 has been reported to function as a sponge for miR-671-5p, which leads to the regulation of ANXA2 expression (85). ANXA2 is a member of the membrane-linked protein family and acts as an autocrine factor, promoting osteoclast formation and bone resorption.

Overall, increasing efforts have been made to explore the mechanisms by which circRNAs regulate PTC progression. Such findings provide new insights into the physiological and pathological processes of PTC.

3.2 CircRNAs involved in associated signaling pathways in PTC

CircRNAs have been shown to function as tumor suppressors or oncogenes by regulating gene expression and modulating signaling pathways. Multiple signaling pathways are involved in the development and progression of PTC, including PI3K/AKT, Wnt/β-catenin, MAPK/ERK, AMPK/mTOR, and others. Figure 2 demonstrates the involvement of circRNAs in relevant signaling pathways in PTC. These pathways are frequently dysregulated in PTC and play critical roles in regulating cell proliferation, migration, invasion, metastasis, apoptosis, angiogenesis, glycolysis, and EMT.

3.2.1 PI3K/AKT signaling pathway

The PI3K/AKT pathway is frequently activated in various human cancers, making it an attractive therapeutic target (86). It is frequently activated by mutations in genes such as PIK3CA, PTEN, and AKT. In PTC, activation of the PI3K/AKT pathway increases cell survival and resistance to apoptosis, as well as angiogenesis and migration. PI3Ks are divided into three classes and contain many lipid kinase enzymes. Receptor tyrosine kinases (RTKs), G protein-coupled receptors (GPCRs), RAS, and Rho-GTPases all have the ability to activate Class IA PI3Ks. The downstream signaling events mediated by PIP3 result in cell growth, proliferation, autophagy, and apoptosis (87).

Several circRNAs have been found that regulate the PI3K/AKT pathway and induce PTC progression. For example, circNDST1 was reported to be significantly up-regulated in PTC. After knocking

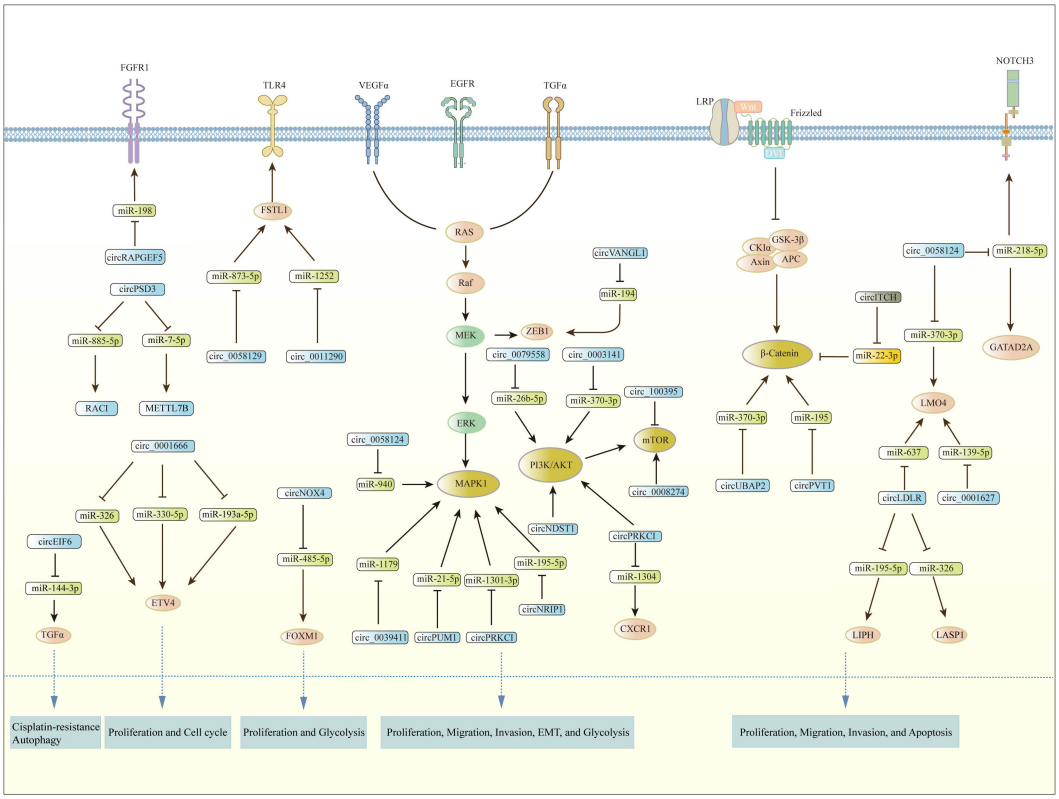

FIGURE 2
The involvement of circRNAs in relevant signaling pathways in PTC.

down circNDST1, the proliferation, migration, and invasion abilities of PTC cells were obviously suppressed. Meanwhile, it inhibited the activation of the PI3K/AKT pathway (53). The circSSU72/miR-451a/S1PR2 axis could also regulate PTC progression by the AKT pathway, which could serve as a novel therapeutic target in PTC (54). Moreover, circRAPGEF5 (hsa_circ_0079558) could activate the MET/AKT pathway via miR-26b-5p, which subsequently promoted the progression of PTC (55). CircUBAP2 (hsa_circ_0003141), an oncogenic molecule, is highly expressed in PTC tissues and cells. It may regulate PTC development through the PI3K/Akt pathway (56). Similarly, circ_0067934 was highly expressed in PTC. It was found to promote EMT and activate the PI3K/AKT pathway to facilitate the malignant behavior of PTC (88). In contrast, circ_100395 may play an anti-oncogenic role in PTC cells through the inhibition of the PI3K/AKT/mTOR pathway (82).

3.2.2 Wnt/β-catenin signaling pathway

The Wnt/β-catenin signaling pathway is a highly conserved signaling cascade that regulates cell proliferation, differentiation, and tissue homeostasis during embryonic development and in tissues. The pathway is activated by the binding of Wnt ligands to Frizzled (FZD) receptors and low-density lipoprotein receptor-related protein (LRP) co-receptors on the cell surface. It is transduced in cells via the β-catenin-dependent/canonical or β-catenin-independent/non-canonical pathways. It was reported that the abnormal activation of the Wnt/β-catenin signaling pathway is closely related to the progression of PTC. Moreover, dysregulation of the Wnt pathway is associated with the loss of tumor suppressor genes, such as APC and AXIN, and the activation of oncogenes, such as β-catenin and cyclin D1.

There are several circRNAs that have been reported to regulate the Wnt pathway in PTC (89). For instance, Chen et al. found that circNEK6 (hsa_circ_0088483) affects FDZ8 expression via the Wnt pathway. Its overexpression successfully enhanced the proliferation and invasion of PTC cells (90). Besides, it was reported that the Wnt/β-catenin signaling pathway was also significantly promoted by the overexpression of circPVT1 (38). Additionally, miR-370-3p was reported to regulate the Wnt pathway in a variety of cancers. Hsa_circ_0003141 was reported to regulate the Wnt pathway by miR-370-3p to play its role in PTC. Knockdown of hsa_circ_0003141 inhibited cell proliferation and invasion, while induced cell apoptosis of PTC (56). CTNNBIP1 is a β-catenin-interacting protein. CircRNA_102171 could exert a pro-carcinogenic role in PTC. It was found that circRNA_102171 could bind to CTNNBIP1, which in turn promoted the formation of the β-catenin/TCF complex and activated the Wnt/β-catenin pathway (57). Furthermore, FZD8 is reported as a Wnt receptor in the canonical Wnt signaling pathway that has been identified as a therapeutic target for cancer (91). MiR-345-5p, which was sponged by circPRS28 (hsa_circ_0049055), was a direct regulator of the functional gene FZD8 during PTC cell development (92). The relationship between circRPS28/miR-345-5p/FZD8 and the Wnt signaling pathway is left unexplored.

3.2.3 MAPK/ERK and AMPK signaling pathway

The MAPK pathway is a signal-transduction system. Its constitutive activation is crucial for the growth of PTC. Through critical proteins, such as receptor tyrosine kinases, MAPKs control crucial physiological processes involved in cell proliferation, differentiation, and development. Growth factor binding to a receptor tyrosine kinase receptor triggers the activation of downstream pathways. For example, Li C et al. (49) reported that up-regulation of circNRIP1 inverted the inhibitive function of miR-195-5p on the P38 MAPK pathway. The AMP-activated protein kinase (AMPK) is an energy-sensing protein that regulates cellular metabolism and maintains energy homeostasis. AMPK acts as a potential tumor suppressor since it is located at the entrance of a tumor suppression network that regulates cell growth and proliferation in stress responses. The AMPK pathway is activated by various stimuli that increase the cellular AMP/ATP ratio, such as nutrient deprivation, exercise, and hypoxia. It plays an important role in regulating tumor growth and metabolism, including in PTC. Activating AMPK may promote tumor survival and growth by maintaining AMPK activity and the ability to adapt to metabolic stress (93). CircUGGT2 (has_circ_0008274) deletion was found to impair the AMPK pathway by decreasing AMPK phosphorylation (p-AMPK) and promoting the mTOR pathway by increasing mTOR phosphorylation (p-mTOR) in TPC-1 cells. CircUGGT2 attenuation inhibited the AMPK/mTOR signaling pathway (58). Furthermore, studies have shown that AMPK activation can enhance the sensitivity of TC cells to chemotherapeutic agents, such as doxorubicin and cisplatin, suggesting that AMPK activation may be a promising therapeutic strategy for treatment.

3.2.4 Other signaling pathways

The NOTCH signaling pathway regulates cell differentiation and has been linked to several types of cancer, including PTC. It is frequently activated by mutations in genes, such as NOTCH1 and JAG1. The function of NOTCH1 in tumorigenesis has been extensively studied. *In vitro* studies have confirmed that overexpression of NOTCH1 was associated with resistance to cancer therapy. Research has identified that circAGTPBP1, as an oncogene, could regulate the NOTCH pathway through the miR-34a-5p/NOTCH1 axis and promote the progression of PTC (79). Besides, circFN1 was reported to promote PTC tumorigenesis and invasiveness through the NOTCH3 pathway. The knockdown of circFN1 significantly decreased cell viability, migration, and invasion. Furthermore, silencing circFN1 significantly suppressed cell migration (34). CircNRIP1 was found to modulate the JAK/STAT pathways and affect the cell functions and growth of xenografts (49).

In summary, the regulation of related signaling pathways plays a critical role in PTC progression. Those findings go far toward the progression of a novel therapy for PTC. However, the molecular mechanisms underlying the circRNAs' regulation of those pathways in PTC are largely unknown. The exploration of circRNAs may provide new insights into PTC pathogenesis, and targeting those pathways may be a promising therapeutic approach for treatment.

3.3 Role of circRNAs in EMT in PTC

Epithelial-mesenchymal transition (EMT) is a process in which epithelial cells acquire mesenchymal features. EMT confers metastatic properties to cancer cells by enhancing cell migration and invasion, which is considered a marker of carcinogenesis (94, 95). In recent years, a growing number of studies have focused on the role of circRNAs in EMT in PTC. A study reported that circNDST1 (hsa_circ_0006943) overexpression boosted PTC progression through the activation of EMT in a CSNK2A1-dependent manner (53). Circ_102002 was found to facilitate metastasis of PTC by regulating the miR-488-3p/HAS2 axis. Inhibition of circ_102002 downregulated HAS2 levels, suppressed the phosphorylation of FAK and AKT, regulated expressions of E-cadherin and N-cadherin, and inhibited PTC metastasis (59). CircPI4KA (hsa_circ_0062389) is also involved in EMT via sponging miR-1179 and thus regulates HMGB1 expression. They found that circPI4KA depletion significantly increased E-cadherin and decreased N-cadherin (60). Moreover, silencing of circ_007293 inhibited EMT, as indicated by suppressed N-cadherin and vimentin expressions and increased E-cadherin expression (69). Besides, circPRKCI (hsa_circ_0067934) had a similar effect on promoting PTC progression by regulating EMT (88). Overall, these important features in EMT confirm the potential role of circRNA in PTC therapy.

3.4 Role of circRNAs in glycolysis in PTC

A hallmark of cancer cells is a change in energy metabolism, characterized by the preferential use of glycolysis for energy production. Although not as efficient as oxidative phosphorylation in terms of net ATP production, cancer cells adapt by increasing glucose uptake and promoting the rate of glycolysis. Moreover, intermediates of glycolytic metabolism play a key role in macromolecular biosynthesis. Targeting glycolysis remains an attractive intervention, and recent preclinical studies support its efficacy. Several studies have explored potential therapeutic opportunities for the cancer-specific effects of glycolysis inhibitors (96).

There are several circRNAs that are involved in the glycolytic process in PTC. CircNRIP1 enhances glycolysis in PTC cells by upregulating PKM2 levels and sponging miR-541-3p and miR-3064-5p (51). Li Y et al. (61) showed that knockdown of circPUM1 impedes cell growth, metastasis, and glycolysis of PTC via enhancing MAPK1 expression by sponging miR-21-5p. Downregulation of circPUM1 resulted in decreased expression of hexokinase 2 (HK2) and blocked glycolysis in PTC. Hsa_circ_0023990 promotes tumor growth and glycolysis in dedifferentiated TC via positively regulating the miR-485-5p/FOXM1 axis (62). Data demonstrated that glucose uptake, lactate production, and glycolytic genes (GLUT1, HK2, and LDHA) were all inhibited by circ_100395 overexpression (82). Hsa_circ_0011290 regulates glycolysis by regulating the miR-1252/FSTL1 axis. Meanwhile, glucose metabolism was significantly switched with

10.3389/fendo.2024.1351776

decreased glucose uptake and lactate production (97). Also, it is found that circCCDC66 promotes the proliferation and migration of PTC cells by regulating miR-211-5p/PDK4, which in turn regulates glucose metabolism (98). CircRAD18 is involved in reprogramming glucose metabolism, and silencing of circRAD18 significantly inhibits cellular glucose uptake and lactate production in PTC cells by regulating miR-5166/PDK1 (99).

4 Clinical implications of circRNAs in PTC

Likewise, circRNAs have potential value as biomarkers in diagnosis, prognosis, and even treatment. Due to the lack of specific symptoms, PTC is often difficult to diagnose at an early stage. Early identification of the advanced PTC among many thyroid cancers is an urgent clinical issue to be addressed. A number of circRNAs have tissue-specific and developmental stage-specific expression patterns.

4.1 Role of circRNAs as diagnostic biomarkers

Most circRNAs have been found to be upregulated in PTC tissues or cells compared to normal. Bai C et al. (63) found that hsa_circ_000121 had good sensitivity and specificity for diagnosing PTC lymph node metastasis, with a cut-off value of 0.796. Cai X et al. (64) found that circBACH2 had a good diagnostic value for PTC with an AUC of 0.8631. In addition, hsa_circ_0082003 has potential as a biomarker for the diagnosis of PTC (65), as well as hsa_circ_0027446 (66). CircPSD3 (hsa_circ_0002111) was suggested as a potential diagnostic tumor marker for PTC, with an AUC of 0.833 (95% CI = 0.77-0.89, $p < 0.01$) (67). Similarly, circMAN1A2 has an AUC of 0.734 (100), hsa_circ_047771 has an AUC of 0.876 (95% CI = 0.78-0.94), and hsa_circ_007148 has an AUC of 0.846 (95% CI =0.75-0.96) (68). Studies have shown that exosomal circ_007293 regulated PTC cell invasion, migration, proliferation, and EMT, as well as induced PAX6 expression by sponging miR-653-5p (69). Further studies found that three differentially regulated circRNAs, including has_circ_007293, has_circ_031752, and has_circ_020135, were upregulated and confirmed in the serum of PTC patients (101). Additionally, these findings suggest that exosome circRNAs might be potential diagnostic molecular biomarkers for PTC.

4.2 Role of circRNAs as prognostic biomarkers

Recently, several studies have found that dysregulation of circRNAs is associated with a poor prognosis in PTC, including tumor size, LNM, TNM stage, and even postoperative recurrence. The correlation between circRNAs and clinical features of PTC is shown in Table 2.

TABLE 2 The correlation between circRNAs and clinical features of PTC.

Clinical features	Upregulated circRNAs	Downregulated circRNAs
Tumor size >3 cm	circLDLR (44), circPSD3 (74), circFOXM1 (102)	
Tumor size ≥2 cm	hsa_circ_0079558 (55), hsa_circ_0008274 (70)	
Tumor size ≥1cm	circPVT1 (38), circNRIP1 (50), hsa_circ_0000644 (52), hsa_circ_0079558 (55), hsa_circ_0003141 (56), circPUM1 (61), hsa_circ_0082003 (65), hsa_circ_0002111 (67), hsa_circ_0008274 (70), circCCDC66 (71), circVANGL1 (72), hsa_circ_0122683 (75), hsa_circ_0000144 (77), circAGTPBP1 (79), hsa_circ_0000266 (81)	
LNM	circLDLR (44), hsa_circ_0079558 (55), circBACH2 (64), hsa_circ_007293 (69), hsa_circ_0008274 (70), hsa_circ_0011058 (73), circPSD3 (74), hsa_circ_0001666 (78), circAGTPBP1 (79)	
TNM stage	circPVT1 (38), circLDLR (44), hsa_circ_0067934 (48), circNRIP1 (50), hsa_circ_0079558 (55), hsa_circ_0003141 (56), circPUM1 (61), circBACH2 (64), hsa_circ_0082003 (65), hsa_circ_0002111 (67), hsa_circ_007293 (69), hsa_circ_0008274 (70), circCCDC66 (71), circVANGL1 (72), hsa_circ_0011058 (73), circPSD3 (74), hsa_circ_0122683 (75), hsa_circ_0059354 (76), hsa_circ_0000144 (77), circAGTPBP1 (79)	hsa_circ_0000266 (81)

In addition, data obtained by COX regression analysis also supports the potential value of circRNAs in terms of prognosis. For example, it was found that patients with high expression of has_circ_0067934 showed a lower survival period. Cox model analysis indicated that hsa_circ_0067934 was an independent risk factor for prognosis (RR = 4.385, 95% CI = 1.087-17.544, p = 0.038) (88). Several high expression levels of circRNAs were associated with a poor prognosis of PTC, such as hsa_circ_102002 (59), circPUM1 (61), circBACH2 (64), hsa_circ_0027446 (66), hsa_circ_0008274 (70), circCCDC66 (71), and hsa_circ_0011058 (73). In contrast, low circ_100395 expression was linked to a poor prognosis in PTC (82). However, low hsa_circ_047771 expression was associated with the $BRAF^{V600}$ mutation, LNM, and TNM stage ($p < 0.05$). Furthermore, a high expression of hsa_circ_007148 was significantly correlated with LNM ($P < 0.05$) (68).

4.3 Role of circRNAs in treatment

CircRNAs have garnered growing interest in tumor research and hold promise for intervention or regulatory therapy. Drug

resistance is a key factor affecting cancer outcomes. Several studies have demonstrated the association of circRNAs with chemoresistance in cancer treatment. For instance, the circEIF6/miR-144-3p/TGF-α pathway was found to be associated with reduced sensitivity of ATC to cisplatin resistance. CircEIF6 could promote tumor growth by regulating miR-144-3p/TGF-α, while knockdown of circEIF6 enhanced cisplatin sensitivity *in vivo*. This finding suggests a potential therapeutic target for overcoming cisplatin resistance in TC (103). However, the downstream signaling molecules of TGF-α need to be further investigated. Additionally, due to the undifferentiated phenotype of TC and its aggressive nature, resistance to conventional treatments such as radiotherapy and chemotherapy is frequently observed in ATC, including cisplatin resistance (104). In breast cancer, circCDYL2 was able to maintain downstream AKT and ERK1/2 activity, thus promoting trastuzumab resistance in HER2-positive breast cancer patients (105). Furthermore, circCPM promoted resistance to 5-FU in gastric cancer and modulated autophagy by targeting PRKAA2 (106). In endometrial cancer, resistance to paclitaxel was found to be mediated by the key oncogenic circ0007534 (107). These studies suggest that circRNA-targeted therapy may have a role in reversing cancer chemoresistance.

In addition, circRNAs demonstrate promise as a drug carrier for the treatment of cancer. They exhibit robust stability and resistance to degradation by nucleases. These characteristics enable prolonged circulation in the body. CircRNAs can achieve targeted therapy by interacting with specific miRNAs. In PTC, certain miRNAs may be dysregulated, contributing to cancer progression. CircRNAs can be engineered to bind to these miRNAs, thereby restoring their normal levels and inhibiting cancer cell growth and dissemination. Also, aberrant expression of specific key genes closely correlates with cancer development in TC. CircRNAs serve as drug carriers, delivering specific siRNA or gene sequences to target genes. Pisignano G et al. (108) summarized ongoing research on evaluating the potential therapeutic effects of circRNA application in clinical practice for cancer patients. A study attempted to develop therapeutic mesenchymal stem cells (MSCs) containing a suicide-inducing gene, and they demonstrated the effectiveness of this approach in ATC therapy (109). The immunogenicity of extracellular vesicles derived from MSC is relatively low, making them potential alternatives to cell therapy. A recent review highlights the therapeutic options and biological applications of MSCs-derived extracellular vesicles. They are capable of transmitting signals or delivering biological materials to diseased sites in the body and then regulating therapy (110). However, the research on utilizing MSCs as carriers to load circRNAs for the treatment of TC remains in its early stages. More intensive studies in aggressive TC are highly needed to provide novel approaches for tumor therapy.

5 Discussion

PTC is a multifactorial disease, the prevalence of which is increasing year by year, and its diagnosis, treatment, and prognosis are still controversial in clinical practice (111). A recent study on the Chinese population found a rapid increase in the incidence of TC and a modest increase in mortality from 2005 to 2015 (112). In addition, based on decades of global epidemiological data, the overall incidence of TC was found to have increased by 3% per year between 1974 and 2013, with a concomitant 1.1% per year increase in mortality based on incidence. For advanced PTC, the incidence and mortality rates are also increasing annually in most countries (113). PTC accounts for approximately 85% of TC and includes follicular, diffuse sclerosing, hypercellular, and columnar cell subtypes. Of these, the diffuse sclerosing subtype has a 100% LNM rate, often occurs in children and young adults, and shows a poor prognosis. Tumor diagnosis and treatment have now moved into the era of precision medicine, and several molecular markers such as BRAF, RAS, RET/PTC, and PAX8/PPARγ have been used to improve the accuracy and timeliness of thyroid nodule diagnosis, as well as to reach the molecular level of the subtype classification of PTC. Recently, patients with RET/NTRK fusion were found to have worse clinical outcomes than patients with BRAF-mutated disease (114). Therefore, the early identification of highly aggressive, poorly differentiated, and poorly prognosed TC is of great importance. We provided a detailed review of recent findings in the field of circRNAs for PTC. Focusing on the biological functions of circRNAs and their related signaling pathways in PTC, as well as discussing the role of circRNAs in the EMT and glycolysis processes. Then, we discussed the clinical implications of circRNAs in PTC and found that circRNAs may be a new therapeutic approach for the treatment of TC.

CircRNAs have been found to be widely expressed in various cancers and are associated with tumorigenesis and progression. Because of the specific features of circRNAs, such as good stability, abundance, sensitivity, and specificity, they are gradually being proposed as biomarkers. The detection of circRNA in serum and FNA samples as a non-invasive diagnostic tool for PTC has several advantages over traditional diagnostic methods. Firstly, circRNA has the potential to improve the accuracy of PTC diagnosis as it is specific to cancer cells and could be used to differentiate between benign and malignant tumors. Secondly, it is less invasive than a tissue biopsy, and samples are more readily available. Further, this modality has the potential to improve the management of PTC by providing an early and accurate diagnosis, which could contribute to timely and appropriate treatment. Current studies have provided promising and informative evidence that confirms the viability of circRNAs as biomarkers.

With increasing evidence revealing the role that circRNAs play in multiple signaling pathway processes, this provides more focus points for PTC treatment. Among the processes associated with PTC, one of great importance is EMT. Several studies have reported that circRNAs have a distinct, easily measured, and observed corresponding expression during EMT, which is thought to be of potential value in inhibiting the malignant progression of TC. In spite of these exciting advances, the research on circRNAs still faces a few limitations. Firstly, due to the different sequencing methods, data analysis pipelines, and detection tools, the current databases of circRNAs are not uniform and very complete. This makes it difficult to compare the results of different studies. Furthermore, the limited sample sizes of studies make it difficult to generalize the

results to larger populations. Numerous circRNAs have been identified and found to have multiple functions through diverse mechanisms. This complexity makes it challenging to fully understand their role in PTC.

6 Future perspectives

In recent years, significant achievements have been made in the fields of circRNAs and PTC, yet the clinical application of circRNAs in PTC still faces numerous challenges. Firstly, existing studies are mainly focused on the PTC, while other subtypes of TC are insufficient, particularly MTC and ATC. Future research should allocate more attention to circRNAs in these subtypes. Secondly, due to the predominantly low expression levels of circRNAs, investigating efficient extraction and detection methods for circRNAs could enhance their utility as biomarkers. It is necessary to monitor relapse and progression using reliable biomarkers in long-term follow-up studies. Additionally, reliance on a single circRNA may not provide adequate support for cancer diagnosis or prognosis prediction. Hence, the utilization of a combination of cancer-related circRNA panels could prove valuable as biomarkers in the future. Moreover, despite the broad potential applications of circRNAs, current research predominantly focuses on their role as miRNA sponges, which is overly narrow. Other mechanisms of circRNAs warrant further investigation. Last but not least, an increasing number of studies are delving into the role of circRNAs in chemoresistance and cancer therapy. This represents a novel avenue for future investigation and merits thorough exploration. Nevertheless, additional research and validation are indispensable prior to the clinical implementation of circRNA-targeted treatments. Addressing concerns pertaining to safety, efficacy, drug release, and *in vivo* targeting is imperative.

In conclusion, circRNAs undoubtedly have enormous potential for cancer diagnosis and treatment. Through further research on circRNAs biogenesis and other mechanisms, alongside the development of detection technologies and comprehensive clinical trials, circRNAs will play a significant role in the diagnosis, monitoring, and treatment of PTC.

Author contributions

JM: Conceptualization, Data curation, Formal Analysis, Funding acquisition, Investigation, Validation, Writing – original draft. JX: Data curation, Formal Analysis, Investigation, Writing – original draft. XZ: Data curation, Formal Analysis, Software, Validation, Visualization, Writing – original draft. JQ: Supervision, Validation, Visualization, Writing – review & editing, Funding acquisition.

Funding

The author(s) declare that financial support was received for the research, authorship, and/or publication of this article. The study was supported by the Natural Science Foundation of Gansu Province (22JR5RA707), Gansu Provincial Health Commission (GSWSKY2017-03), Lanzhou Science and Technology Bureau (2022-ZD-50), and Gansu Provincial Hospital (19SYPYA-11, 21GSSYC-6).

Conflict of interest

The authors declare that the research was conducted in the absence of any commercial or financial relationships that could be construed as a potential conflict of interest.

Publisher's note

References

1. Chen DW, Lang BHH, McLeod DSA, Newbold K, Haymart MR. Thyroid cancer. *Lancet*. (2023) 401:1531–44. doi: 10.1016/S0140-6736(23)00020-X

2. Sung H, Ferlay J, Siegel RL, Laversanne M, Soerjomataram I, Jemal A, et al. Global cancer statistics 2020: globocan estimates of incidence and mortality worldwide for 36 cancers in 185 countries. *CA Cancer J Clin*. (2021) 71:209–49. doi: 10.3322/caac.21660

3. Miller KD, Nogueira L, Devasia T, Mariotto AB, Yabroff KR, Jemal A, et al. Cancer treatment and survivorship statistics, 2022. *CA Cancer J Clin*. (2022) 72:409–36. doi: 10.3322/caac.21731

4. Miller KD, Fidler-Benaoudia M, Keegan TH, Hipp HS, Jemal A, Siegel RL. Cancer statistics for adolescents and young adults, 2020. *CA Cancer J Clin*. (2020) 70:443–59. doi: 10.3322/caac.21637

5. Mould RC, van Vloten JP, AuYeung AWK, Karimi K, Bridle BW. Immune responses in the thyroid cancer microenvironment: making immunotherapy a possible mission. *Endocr Relat Cancer*. (2017) 24:T311–t29. doi: 10.1530/erc-17-0316

6. Kunavisarut T. Diagnostic biomarkers of differentiated thyroid cancer. *Endocrine*. (2013) 44:616–22. doi: 10.1007/s12020-013-9974-2

7. Christofer Juhlin C, Mete O, Baloch ZW. The 2022 who classification of thyroid tumors: novel concepts in nomenclature and grading. *Endocr Relat Cancer*. (2023) 30: e220293. doi: 10.1530/erc-22-0293

8. Ferraz C, Eszlinger M, Paschke R. Current state and future perspective of molecular diagnosis of fine-needle aspiration biopsy of thyroid nodules. *J Clin Endocrinol Metab*. (2011) 96:2016–26. doi: 10.1210/jc.2010-2567

9. Haugen BR. 2015 American thyroid association management guidelines for adult patients with thyroid nodules and differentiated thyroid cancer: what is new and what has changed? *Cancer*. (2017) 123:372–81. doi: 10.1002/cncr.30360

10. Yao Y, Xu P, Ying T, Wang Y, Wang X, Shu L, et al. Integrative analysis of DNA methylation and gene expression identified follicular thyroid cancer-specific diagnostic biomarkers. *Front Endocrinol (Lausanne)*. (2021) 12:736068. doi: 10.3389/fendo.2021.736068

11. Ha EJ, Na DG, Baek JH, Sung JY, Kim JH, Kang SY. Us fine-needle aspiration biopsy for thyroid Malignancy: diagnostic performance of seven society guidelines applied to 2000 thyroid nodules. *Radiology*. (2018) 287:893–900. doi: 10.1148/radiol.2018171074

12. He J, Xie Q, Xu H, Li J, Li Y. Circular Rnas and cancer. *Cancer Lett*. (2017) 396:138–44. doi: 10.1016/j.canlet.2017.03.027

13. Fagin JA, Wells SA Jr. Biologic and clinical perspectives on thyroid cancer. *N Engl J Med*. (2016) 375:1054–67. doi: 10.1056/NEJMra1501993

14. Zhang Y, Jia DD, Zhang YF, Cheng MD, Zhu WX, Li PF, et al. The emerging function and clinical significance of circRNAs in thyroid cancer and autoimmune thyroid diseases. *Int J Biol Sci*. (2021) 17:1731–41. doi: 10.7150/ijbs.55381

15. Liu CX, Chen LL. Circular Rnas: characterization, cellular roles, and applications. *Cell*. (2022) 185:2016–34. doi: 10.1016/j.cell.2022.04.021

16. Schmidt CA, Giusto JD, Bao A, Hopper AK, Matera AG. Molecular determinants of metazoan tricRNA biogenesis. *Nucleic Acids Res*. (2019) 47:6452–65. doi: 10.1093/nar/gkz311

17. Goodall GJ, Wickramasinghe VO. Rna in cancer. *Nat Rev Cancer*. (2021) 21:22–36. doi: 10.1038/s41568-020-00306-0

18. Ashwal-Fluss R, Meyer M, Pamudurti NR, Ivanov A, Bartok O, Hanan M, et al. Circrna biogenesis competes with pre-Mrna splicing. *Mol Cell*. (2014) 56:55–66. doi: 10.1016/j.molcel.2014.08.019

19. Ho JS, Di Tullio F, Schwarz M, Low D, Incarnato D, Gay F, et al. Hnrnpm controls circRNA biogenesis and splicing fidelity to sustain cancer cell fitness. *Elife*. (2021) 10:e59654. doi: 10.7554/eLife.59654

20. Hansen TB, Wiklund ED, Bramsen JB, Villadsen SB, Statham AL, Clark SJ, et al. Mirna-dependent gene silencing involving Ago2-mediated cleavage of a circular antisense Rna. *EMBO J*. (2011) 30:4414–22. doi: 10.1038/emboj.2011.359

21. Li H, Lan M, Liao X, Tang Z, Yang C. Circular Rna Cir-Itch promotes osteosarcoma migration and invasion through Cir-Itch/Mir-7/Egfr pathway. *Technol Cancer Res Treat*. (2020) 19:1533033819898728. doi: 10.1177/1533033819898728

22. Pan Z, Zhao R, Li B, Qi Y, Qiu W, Guo Q, et al. Ewsr1-induced Circneil3 promotes glioma progression and exosome-mediated macrophage immunosuppressive polarization via stabilizing Igf2bp3. *Mol Cancer*. (2022) 21:16. doi: 10.1186/s12943-021-01485-6

23. Knupp D, Cooper DA, Saito Y, Darnell RB, Miura P. Nova2 regulates neural circRNA biogenesis. *Nucleic Acids Res*. (2021) 49:6849–62. doi: 10.1093/nar/gkab523

24. Zhang M, Huang N, Yang X, Luo J, Yan S, Xiao F, et al. A novel protein encoded by the circular form of the Shprh gene suppresses glioma tumorigenesis. *Oncogene*. (2018) 37:1805–14. doi: 10.1038/s41388-017-0019-9

25. Wang L, Long H, Zheng Q, Bo X, Xiao X, Li B. Circular Rna Circrhot1 promotes hepatocellular carcinoma progression by initiation of Nr2f6 expression. *Mol Cancer*. (2019) 18:119. doi: 10.1186/s12943-019-1046-7

26. Huang X, Guo H, Wang L, Yang L, Shao Z, Zhang W. Recent advances in crosstalk between N6-methyladenosine (m6A) modification and circular RNAs in cancer. *Mol Ther Nucleic Acids*. (2022) 27:947–55. doi: 10.1016/j.omtn.2022.01.013

27. Fan X, Yang Y, Chen C, Wang Z. Pervasive translation of circular Rnas driven by short Ires-like elements. *Nat Commun*. (2022) 13:3751. doi: 10.1038/s41467-022-31327-y

28. Legnini I, Di Timoteo G, Rossi F, Morlando M, Briganti F, Sthandier O, et al. Circ-Znf609 is a circular Rna that can be translated and functions in myogenesis. *Mol Cell*. (2017) 66:22–37.e9. doi: 10.1016/j.molcel.2017.02.017

29. Li R, Jiang J, Shi H, Qian H, Zhang X, Xu W. Circrna: A rising star in gastric cancer. *Cell Mol Life Sci*. (2020) 77:1661–80. doi: 10.1007/s00018-019-03345-5

30. Wang YM, Zhao QW, Sun ZY, Lin HP, Xu X, Cao M, et al. Circular Rna Hsa_Circ_0003823 promotes the tumor progression, metastasis and apatinib resistance of esophageal squamous cell carcinoma by Mir-607/Crisp3 axis. *Int J Biol Sci*. (2022) 18:5787–808. doi: 10.7150/ijbs.76096

31. Yu L, Zhu H, Wang Z, Huang J, Zhu Y, Fan G, et al. Circular Rna circfirre drives osteosarcoma progression and metastasis through tumorigenic-angiogenic coupling. *Mol Cancer*. (2022) 21:167. doi: 10.1186/s12943-022-01624-7

32. Duan JL, Chen W, Xie JJ, Zhang ML, Nie RC, Liang H, et al. A novel peptide encoded by N6-methyladenosine modified circmap3k4 prevents apoptosis in hepatocellular carcinoma. *Mol Cancer*. (2022) 21:93. doi: 10.1186/s12943-022-01537-5

33. Franco AT, Ricarte-Filho JC, Isaza A, Jones Z, Jain N, Mostoufi-Moab S, et al. Fusion oncogenes are associated with increased metastatic capacity and persistent disease in pediatric thyroid cancers. *J Clin Oncol*. (2022) 40:1081–90. doi: 10.1200/jco.21.01861

34. Yao Y, Chen X, Yang H, Chen W, Qian Y, Yan Z, et al. Hsa_Circ_0058124 promotes papillary thyroid cancer tumorigenesis and invasiveness through the Notch3/Gatad2a axis. *J Exp Clin Cancer Res*. (2019) 38:318. doi: 10.1186/s13046-019-1321-x

35. Liu L, Yan C, Tao S, Wang H. Circ_0058124 aggravates the progression of papillary thyroid carcinoma by activating lmo4 expression via targeting Mir-370-3p. *Cancer Manag Res*. (2020) 12:9459–70. doi: 10.2147/cmar.S271778

36. Chu J, Tao L, Yao T, Chen Z, Lu X, Gao L, et al. Circular Rna circrunx1 promotes papillary thyroid cancer progression and metastasis by sponging Mir-296-3p and regulating Ddhd2 expression. *Cell Death Dis*. (2021) 12:112. doi: 10.1038/s41419-020-03350-8

37. Liu X, Wang C, Su Z, Cai S, Pan Q, Chen X. Circ_0001658 regulates Pi3k/Akt signaling via the Mir-671-5p/Itga2 axis and affects the progress of papillary thyroid carcinoma. *Ann Transl Med*. (2022) 10:1001. doi: 10.21037/atm-22-3650

38. Zeng L, Yuan S, Zhou P, Gong J, Kong X, Wu M. Circular Rna Pvt1 oncogene (Circpvt1) promotes the progression of papillary thyroid carcinoma by activating the Wnt/B-catenin signaling pathway and modulating the ratio of microrna-195 (Mir-195) to vascular endothelial growth factor a (Vegfa) expression. *Bioengineered*. (2021) 12:11795–810. doi: 10.1080/21655979.2021.2008639

39. Tao L, Yang L, Tian P, Guo X, Chen Y. Knockdown of circpvt1 inhibits progression of papillary thyroid carcinoma by sponging Mir-126. *RSC Adv*. (2019) 9:13316–24. doi: 10.1039/C9RA01820D

40. Yang Y, Ding L, Li Y, Xuan C. Hsa_Circ_0039411 promotes tumorigenesis and progression of papillary thyroid cancer by Mir-1179/Abca9 and Mir-1205/Mta1 signaling pathways. *J Cell Physiol*. (2020) 235:1321–29. doi: 10.1002/jcp.29048

41. Wen X, Du J, Wang X. Circ_0039411 promotes papillary thyroid carcinoma development through mediating the Mir-423-5p/Sox4 signaling. *Int J Biol Markers*. (2021) 36:10–20. doi: 10.1177/17246008211043128

42. Jin X, Wang Z, Pang W, Zhou J, Liang Y, Yang J, et al. Upregulated Hsa_Circ_0004458 contributes to progression of papillary thyroid carcinoma by inhibition of Mir-885-5p and activation of Rac1. *Med Sci Monit*. (2018) 24:5488–500. doi: 10.12659/msm.911095

43. Gui X, Li Y, Zhang X, Su K, Cao W. Circ_Ldlr promoted the development of papillary thyroid carcinoma via regulating Mir-195-5p/Liph axis. *Cancer Cell Int*. (2020) 20:241. doi: 10.1186/s12935-020-01327-3

44. Jiang YM, Liu W, Jiang L, Chang H. Circldlr promotes papillary thyroid carcinoma tumorigenicity by regulating Mir-637/Lmo4 axis. *Dis Markers*. (2021) 2021:3977189. doi: 10.1155/2021/3977189

45. Han P, Liu J, Zhao Q, Li H, Zhang T, Li B, et al. Circular Rna Hsa_Circ_0003892 promotes the development of papillary thyroid carcinoma by regulating the Mir-326/Lasp1 axis. *Histol Histopathol*. (2023) 38:585–95. doi: 10.14670/hh-18-546

46. Zhang H, Ma XP, Li X, Deng FS. Circular Rna Circ_0067934 exhaustion expedites cell apoptosis and represses cell proliferation, migration and invasion in thyroid cancer via sponging Mir-1304 and regulating cxcr1 expression. *Eur Rev Med Pharmacol Sci*. (2019) 23:10851–66. doi: 10.26355/eurrev_201912_19789

47. Wang HH, Ma JN, Zhan XR. Circular Rna Circ_0067934 attenuates ferroptosis of thyroid cancer cells by Mir-545-3p/Slc7a11 signaling. *Front Endocrinol (Lausanne)*. (2021) 12:670031. doi: 10.3389/fendo.2021.670031

48. Dong LP, Chen LY, Bai B, Qi XF, Liu JN, Qin S. Circ_0067934 promotes the progression of papillary thyroid carcinoma cells through Mir-1301-3p/Hmgb1 axis. *Neoplasma*. (2022) 69:1–15. doi: 10.4149/neo_2021_210608N771

49. Li C, Zhu L, Fu L, Han M, Li Y, Meng Z, et al. Circrna Nrip1 promotes papillary thyroid carcinoma progression by sponging Mir-195-5p and modulating the P38 Mapk and Jak/stat pathways. *Diagn Pathol*. (2021) 16:93. doi: 10.1186/s13000-021-01153-9

50. Fu L, Huo J, Fitrat H, Kong Y, Zhang L, Shang C, et al. Circnrip1 exerts oncogenic functions in papillary thyroid carcinoma by sponging Mir-653-5p and regulating Pbx3 expression. *J Oncol*. (2022) 2022:2081501. doi: 10.1155/2022/2081501

51. Ji X, Lv C, Huang J, Dong W, Sun W, Zhang H. Alkbh5-induced circular Rna Nrip1 promotes glycolysis in thyroid cancer cells by targeting Pkm2. *Cancer Sci*. (2023) 114:2318–34. doi: 10.1111/cas.15772

52. Nie C, Han J, Bi W, Qiu Z, Chen L, Yu J, et al. Circular Rna Circ_0000644 promotes papillary thyroid cancer progression via sponging mir-1205 and regulating E2f3 expression. *Cell Cycle*. (2022) 21:126–39. doi: 10.1080/15384101.2021.2012334

53. Shu C, Wang S, Hu J, Xu M, Deng H, Maimaiti Y, et al. Circndst1 promotes papillary thyroid cancer progression via its interaction with Csnk2a1 to activate the Pi3k-Akt pathway and epithelial-mesenchymal transition. *J Endocrinol Invest*. (2023) 46:545–57. doi: 10.1007/s40618-022-01928-x

54. Zhang Z, Xia F, Yao L, Jiang B, Li X. Circssu72 promotes cell proliferation, migration and invasion of papillary thyroid carcinoma cells by targeting Mir-451a/S1pr2 axis. *Front Cell Dev Biol*. (2022) 10:817028. doi: 10.3389/fcell.2022.817028

55. Zheng H, Fu Q, Ma K, Shi S, Fu Y. Circ_0079558 promotes papillary thyroid cancer progression by binding to Mir-26b-5p to activate Met/Akt signaling. *Endocr J*. (2021) 68:1247–66. doi: 10.1507/endocrj.EJ20-0498

56. Xiong H, Yu J, Jia G, Su Y, Zhang J, Xu Q, et al. Emerging roles of circubap2 targeting Mir-370-3p in proliferation, apoptosis, and invasion of papillary thyroid cancer cells. *Hum Cell*. (2021) 34:1866–77. doi: 10.1007/s13577-021-00585-1

57. Bi W, Huang J, Nie C, Liu B, He G, Han J, et al. Circrna Circrna_102171 promotes papillary thyroid cancer progression through modulating ctnnbip1-dependent activation of B-catenin pathway. *J Exp Clin Cancer Res*. (2018) 37:275. doi: 10.1186/s13046-018-0936-7

58. Zhou GK, Zhang GY, Yuan ZN, Pei R, Liu DM. Has_Circ_0008274 promotes cell proliferation and invasion involving Ampk/Mtor signaling pathway in papillary thyroid carcinoma. *Eur Rev Med Pharmacol Sci*. (2018) 22:8772–80. doi: 10.26355/eurrev_201812_16644

59. Zhang W, Liu T, Li T, Zhao X. Hsa_Circrna_102002 facilitates metastasis of papillary thyroid cancer through regulating Mir-488-3p/Has2 axis. *Cancer Gene Ther*. (2021) 28:279–93. doi: 10.1038/s41417-020-00218-z

60. Wang Y, Zong H, Zhou H. Circular Rna Circ_0062389 modulates papillary thyroid carcinoma progression via the Mir-1179/high mobility group box 1 axis. *Bioengineered*. (2021) 12:1484–94. doi: 10.1080/21655979.2021.1914470

61. Li Y, Qin J, He Z, Cui G, Zhang K, Wu B. Knockdown of circpum1 impedes cell growth, metastasis and glycolysis of papillary thyroid cancer via enhancing mapk1

expression by serving as the sponge of Mir-21-5p. *Genes Genomics*. (2021) 43:141–50. doi: 10.1007/s13258-020-01023-6

62. Zhang Q, Wu L, Liu SZ, Chen QJ, Zeng LP, Chen XZ, et al. Hsa_Circ_0023990 promotes tumor growth and glycolysis in dedifferentiated Tc via targeting mir-485-5p/Foxm1 axis. *Endocrinology*. (2021) 162:bqab172. doi: 10.1210/endocr/bqab172

63. Bai C, Yang W, Ouyang R, Li Z, Zhang L. Study of Hsa_circrna_000121 and Hsa_circrna_004183 in papillary thyroid microcarcinoma. *Open Life Sci*. (2022) 17:726–34. doi: 10.1515/biol-2022-0080

64. Cai X, Zhao Z, Dong J, Lv Q, Yun B, Liu J, et al. Circular RNA circBACH2 Plays a Role in Papillary Thyroid Carcinoma by Sponging miR-139-5p and Regulating LMO4 Expression. *Cell Death Dis*. (2019) 10:184. doi: 10.1038/s41419-019-1439-y

65. Ye J, Feng JW, Wu WX, Qi GF, Wang F, Hu J, et al. Microarray profiling identifies Hsa_Circ_0082003 as a novel tumor promoter for papillary thyroid carcinoma. *J Endocrinol Invest*. (2023) 46:509–22. doi: 10.1007/s40618-022-01922-3

66. Zhang H, Zhou Q, Jiang J. Circ_0027446 induces cldn1 expression to promote papillary thyroid cancer cell Malignancy by binding to Mir-129-5p. *Pathol Res Pract*. (2022) 238:154095. doi: 10.1016/j.prp.2022.154095

67. Du G, Ma R, Li H, He J, Feng K, Niu D, et al. Increased expression of Hsa_Circ_0002111 and its clinical significance in papillary thyroid cancer. *Front Oncol*. (2021) 11:644011. doi: 10.3389/fonc.2021.644011

68. Ren H, Liu Z, Liu S, Zhou X, Wang H, Xu J, et al. Profile and clinical implication of circular Rnas in human papillary thyroid carcinoma. *PeerJ*. (2018) 6:e5363. doi: 10.7717/peerj.5363

69. Lin Q, Qi Q, Hou S, Chen Z, Jiang N, Zhang L, et al. Exosomal circular Rna Hsa_Circ_007293 promotes proliferation, migration, invasion, and epithelial-mesenchymal transition of papillary thyroid carcinoma cells through regulation of the microrna-653-5p/paired box 6 axis. *Bioengineered*. (2021) 12:10136–49. doi: 10.1080/21655979.2021.2000745

70. Ma J, Kan Z. Circular Rna Circ_0008274 enhances the Malignant progression of papillary thyroid carcinoma via modulating solute carrier family 7 member 11 by sponging Mir-154-3p. *Endocr J*. (2021) 68:543–52. doi: 10.1507/endocrj.EJ20-0453

71. Li P, Chen J, Zou J, Zhu W, Zang Y, Li H. Circular Rna coiled-coil domain containing 66 regulates Malignant development of papillary thyroid carcinoma by upregulating la ribonucleoprotein 1 via the sponge effect on Mir-129-5p. *Bioengineered*. (2022) 13:7181–96. doi: 10.1080/21655979.2022.2036304

72. Xiang Y, Wang W, Gu J, Shang J. Circular Rna vangl1 facilitates migration and invasion of papillary thyroid cancer by modulating the Mir-194/Zeb1/Emt axis. *J Oncol*. (2022) 2022:4818651. doi: 10.1155/2022/4818651

73. Zhang Z, Wang W, Su Z, Zhang J, Cao H. Circ_0011058 facilitates proliferation, angiogenesis and radioresistance in papillary thyroid cancer cells by positively regulating yap1 via acting as mir-335-5p sponge. *Cell Signal*. (2021) 88:110155. doi: 10.1016/j.cellsig.2021.110155

74. Zhu J, Wang Y, Yang C, Feng Z, Huang Y, Liu P, et al. Circ-Psd3 promoted proliferation and invasion of papillary thyroid cancer cells via regulating the Mir-7-5p/Mettl7b axis. *J Recept Signal Transduct Res*. (2022) 42:251–60. doi: 10.1080/10799893.2021.1910706

75. Liu Y, Chen G, Wang B, Wu H, Zhang Y, Ye H. Silencing circrna protein kinase C iota (Circ-prkci) suppresses cell progression and glycolysis of human papillary thyroid cancer through Circ-Prkci/Mir-335/E2f3 Cerna axis. *Endocr J*. (2021) 68:713–27. doi: 10.1507/endocrj.EJ20-0726

76. Li Z, Xu J, Guan H, Lai J, Yang X, Ma J. Circ_0059354 aggravates the progression of papillary thyroid carcinoma by elevating arfgef1 through sponging mir-766-3p. *J Endocrinol Invest*. (2022) 45:825–36. doi: 10.1007/s40618-021-01713-2

77. Ma Y, Yang D, Guo P. Circ_0000144 acts as a mir-1178-3p decoy to promote cell Malignancy and angiogenesis by increasing Ywhah expression in papillary thyroid cancer. *J Otolaryngol Head Neck Surg*. (2022) 51:28. doi: 10.1186/s40463-022-00574-w

78. Qi Y, He J, Zhang Y, Wang L, Yu Y, Yao B, et al. Circular Rna Hsa_Circ_0001666 sponges Mir−330−5p, Mir−193a−5p and Mir−326, and promotes papillary thyroid carcinoma progression via upregulation of Etv4. *Oncol Rep*. (2021) 45:50. doi: 10.3892/or.2021.8001

79. Dai L, Zhang W, Wang Y, Yu K, Le Q, Wu X. CircAGTPBP1 Promotes the Progression of Papillary Thyroid Cancer Through the Notch Pathway via the miR-34a-5p/notch1 Axis. *iScience*. (2023) 26:107564. doi: 10.1016/j.isci.2023.107564

80. Wang M, Chen B, Ru Z, Cong L. Circrna Circ-itch suppresses papillary thyroid cancer progression through Mir-22-3p/Cbl/B-catenin pathway. *Biochem Biophys Res Commun*. (2018) 504:283–88. doi: 10.1016/j.bbrc.2018.08.175

81. Zhang C, Gu H, Liu D, Tong F, Wei H, Zhou D, et al. The Circ_Fam53b-Mir-183-5p-Ccdc6 axis modulates the Malignant behaviors of papillary thyroid carcinoma cells. *Mol Cell Biochem*. (2022) 477:2627–41. doi: 10.1007/s11010-022-04465-6

82. Chen L, Zhuo D, Yuan H. Circ_100395 impedes Malignancy and glycolysis in papillary thyroid cancer: involvement of Pi3k/Akt/Mtor signaling pathway. *Immunol Lett*. (2022) 246:10–7. doi: 10.1016/j.imlet.2022.04.004

83. Salmena L, Poliseno L, Tay Y, Kats L, Pandolfi PP. A cerna hypothesis: the rosetta stone of a hidden Rna language? *Cell*. (2011) 146:353–8. doi: 10.1016/j.cell.2011.07.014

84. Tan X, Zhao J, Lou J, Zheng W, Wang P. Hsa_Circ_0058129 regulates papillary thyroid cancer development via mir-873-5p/follistatin-like 1 axis. *J Clin Lab Anal*. (2022) 36:e24401. doi: 10.1002/jcla.24401

85. Li HG, Zhao LH, Liu JZ, Liu KP, Liu JB, Su ZJ, et al. Silencing Circ_0000644 inhibits papillary thyroid cancer cell Malignancy by combining with mir-671-5p to release the inhibition on Anxa2. *J Endocrinol Invest*. (2023) 46:749–61. doi: 10.1007/s40618-022-01930-3

86. Aoki M, Fujishita T. Oncogenic roles of the Pi3k/Akt/Mtor axis. *Curr Top Microbiol Immunol*. (2017) 407:153–89. doi: 10.1007/82_2017_6

87. Hawkins PT, Stephens LR. Pi3k signalling in inflammation. *Biochim Biophys Acta*. (2015) 1851:882–97. doi: 10.1016/j.bbalip.2014.12.006

88. Wang H, Yan X, Zhang H, Zhan X. Circrna Circ_0067934 overexpression correlates with poor prognosis and promotes thyroid carcinoma progression. *Med Sci Monit*. (2019) 25:1342–49. doi: 10.12659/msm.913463

89. Stamos JL, Weis WI. The B-catenin destruction complex. *Cold Spring Harb Perspect Biol*. (2013) 5:a007898. doi: 10.1101/cshperspect.a007898

90. Chen F, Feng Z, Zhu J, Liu P, Yang C, Huang R, et al. Emerging roles of circrna_Nek6 targeting mir-370-3p in the proliferation and invasion of thyroid cancer via Wnt signaling pathway. *Cancer Biol Ther*. (2018) 19:1139–52. doi: 10.1080/15384047.2018.1480888

91. Le PN, McDermott JD, Jimeno A. Targeting the Wnt pathway in human cancers: therapeutic targeting with a focus on Omp-54f28. *Pharmacol Ther*. (2015) 146:1–11. doi: 10.1016/j.pharmthera.2014.08.005

92. Mao Y, Huo Y, Li J, Zhao Y, Wang Y, Sun L, et al. Circrps28 (Hsa_Circ_0049055) is a novel contributor for papillary thyroid carcinoma by regulating cell growth and motility via functioning as cerna for Mir-345-5p to regulate frizzled family receptor 8 (Fzd8). *Endocr J*. (2021) 68:1267–81. doi: 10.1507/endocrj.EJ21-0072

93. Faubert B, Vincent EE, Poffenberger MC, Jones RG. The Amp-activated protein kinase (Ampk) and cancer: many faces of a metabolic regulator. *Cancer Lett*. (2015) 356:165–70. doi: 10.1016/j.canlet.2014.01.018

94. Mittal V. Epithelial mesenchymal transition in tumor metastasis. *Annu Rev Pathol*. (2018) 13:395–412. doi: 10.1146/annurev-pathol-020117-043854

95. Pastushenko I, Blanpain C. Emt transition states during tumor progression and metastasis. *Trends Cell Biol*. (2019) 29:212–26. doi: 10.1016/j.tcb.2018.12.001

96. Ganapathy-Kanniappan S, Geschwind JF. Tumor glycolysis as a target for cancer therapy: progress and prospects. *Mol Cancer*. (2013) 12:152. doi: 10.1186/1476-4598-12-152

97. Hu Z, Zhao P, Zhang K, Zang L, Liao H, Ma W. Hsa_Circ_0011290 regulates proliferation, apoptosis and glycolytic phenotype in papillary thyroid cancer via Mir-1252/ Fstl1 signal pathway. *Arch Biochem Biophys*. (2020) 685:108353. doi: 10.1016/j.abb.2020.108353

98. Ren H, Song Z, Chao C, Mao W. Circccdc66 promotes thyroid cancer cell proliferation, migratory and invasive abilities and glycolysis through the Mir-211-5p/Pdk4 axis. *Oncol Lett*. (2021) 21:416. doi: 10.3892/ol.2021.12677

99. Chen W, Zhang T, Bai Y, Deng H, Yang F, Zhu R, et al. Upregulated Circrad18 promotes tumor progression by reprogramming glucose metabolism in papillary thyroid cancer. *Gland Surg*. (2021) 10:2500–10. doi: 10.21037/gs-21-481

100. Fan CM, Wang JP, Tang YY, Zhao J, He SY, Xiong F, et al. Circman1a2 could serve as a novel serum biomarker for Malignant tumors. *Cancer Sci*. (2019) 110:2180–88. doi: 10.1111/cas.14034

101. Yang C, Wei Y, Yu L, Xiao Y. Identification of altered circular Rna expression in serum exosomes from patients with papillary thyroid carcinoma by high-throughput sequencing. *Med Sci Monit*. (2019) 25:2785–91. doi: 10.12659/msm.915658

102. Ye M, Hou H, Shen M, Dong S, Zhang T. Circular Rna circfoxm1 plays a role in papillary thyroid carcinoma by sponging Mir-1179 and regulating Hmgb1 expression. *Mol Ther Nucleic Acids*. (2020) 19:741–50. doi: 10.1016/j.omtn.2019.12.014

103. Liu F, Zhang J, Qin L, Yang Z, Xiong J, Zhang Y, et al. Circular Rna Eif6 (Hsa_Circ_0060060) sponges Mir-144-3p to promote the cisplatin-resistance of human thyroid carcinoma cells by autophagy regulation. *Aging (Albany NY)*. (2018) 10:3806–20. doi: 10.18632/aging.101674

104. Lee SI, Kim DK, Seo EJ, Choi EJ, Kwon YW, Jang IH, et al. Role of Krüppel-like factor 4 in the maintenance of chemoresistance of anaplastic thyroid cancer. *Thyroid*. (2017) 27:1424–32. doi: 10.1089/thy.2016.0414

105. Ling Y, Liang G, Lin Q, Fang X, Luo Q, Cen Y, et al. Circcdyl2 promotes trastuzumab resistance via sustaining Her2 downstream signaling in breast cancer. *Mol Cancer*. (2022) 21:8. doi: 10.1186/s12943-021-01476-7

106. Fang L, Lv J, Xuan Z, Li B, Li Z, He Z, et al. Circular Cpm promotes chemoresistance of gastric cancer via activating Prkaa2-mediated autophagy. *Clin Transl Med*. (2022) 12:e708. doi: 10.1002/ctm2.708

107. Yi H, Han Y, Li S. Oncogenic Circular RNA circ_0007534 Contributes to Paclitaxel Resistance in Endometrial Cancer by Sponging miR-625 and Promoting ZEB2 Expression. *Front Oncol*. (2022) 12:985470. doi: 10.3389/fonc.2022.985470

108. Pisignano G, Michael DC, Visal TH, Pirlog R, Ladomery M, Calin GA. Going circular: history, present, and future of circRNAs in cancer. *Oncogene*. (2023) 42:2783–00. doi: 10.1038/s41388-023-02780-w

109. Kalimuthu S, Oh JM, Gangadaran P, Zhu L, Lee HW, Jeon YH, et al. Genetically engineered suicide gene in mesenchymal stem cells using a tet-on system for anaplastic thyroid cancer. *PLoS One*. (2017) 12:e0181318. doi: 10.1371/journal.pone.0181318

110. McLaughlin C, Datta P, Singh YP, Lo A, Horchler S, Elcheva IA, et al. Mesenchymal stem cell-derived extracellular vesicles for therapeutic use and in bioengineering applications. *Cells*. (2022) 11:3366. doi: 10.3390/cells11213366

111. McLeod DSA, Zhang L, Durante C, Cooper DS. Contemporary debates in adult papillary thyroid cancer management. *Endocr Rev*. (2019) 40:1481–99. doi: 10.1210/er.2019-00085

112. Wang J, Yu F, Shang Y, Ping Z, Liu L. Thyroid cancer: incidence and mortality trends in China, 2005-2015. *Endocrine*. (2020) 68:163–73. doi: 10.1007/s12020-020-02207-6

113. Lim H, Devesa SS, Sosa JA, Check D, Kitahara CM. Trends in thyroid cancer incidence and mortality in the United States, 1974-2013. *JAMA*. (2017) 317:1338–48. doi: 10.1001/jama.2017.2719

114. Najafian A, Noureldine S, Azar F, Atallah C, Trinh G, Schneider EB, et al. Ras mutations, and Ret/Ptc and Pax8/Ppar-gamma chromosomal rearrangements are also prevalent in benign thyroid lesions: implications thereof and a systematic review. *Thyroid*. (2017) 27:39–48. doi: 10.1089/thy.2016.0348

frontiers | Frontiers in Endocrinology

TYPE Original Research
PUBLISHED 22 July 2024
DOI 10.3389/fendo.2024.1397794

OPEN ACCESS

EDITED BY
Francesca Coperchini,
University of Pavia, Italy

REVIEWED BY
Andrea Gutierrez Maria,
National Cancer Institute (NIH), United States
Nawaz Zahid,
Genome Institute of Singapore (A*STAR), Singapore

*CORRESPONDENCE
Dengqiang Wu
wdq19940727@163.com

RECEIVED 08 March 2024
ACCEPTED 10 July 2024
PUBLISHED 22 July 2024

CITATION
Li Y and Wu D (2024) Identification of signature genes and immune infiltration analysis in thyroid cancer based on PANoptosis related genes.
Front. Endocrinol. 15:1397794.
doi: 10.3389/fendo.2024.1397794

Identification of signature genes and immune infiltration analysis in thyroid cancer based on PANoptosis related genes

Yujie Li[1] and Dengqiang Wu[2*]

[1]Department of Clinical Laboratory, The Affiliated LiHuiLi Hospital of Ningbo University, Ningbo, China, [2]Department of Clinical Laboratory, Ningbo No. 6 Hospital, Ningbo, China

Background: Thyroid cancer is the most common malignancy of the endocrine system. PANoptosis is a specific form of inflammatory cell death. It mainly includes pyroptosis, apoptosis and necrotic apoptosis. There is increasing evidence that PANoptosis plays a crucial role in tumour development. However, no pathogenic mechanism associated with PANoptosis in thyroid cancer has been identified.

Methods: Based on the currently identified PANoptosis genes, a dataset of thyroid cancer patients from the GEO database was analysed. To screen the common differentially expressed genes of thyroid cancer and PANoptosis. To analyse the functional characteristics of PANoptosis-related genes (PRGs) and screen key expression pathways. The prognostic model was established by LASSO regression and key genes were identified. The association between hub genes and immune cells was evaluated based on the CIBERSORT algorithm. Predictive models were validated by validation datasets, immunohistochemistry as well as drug-gene interactions were explored.

Results: The results showed that eight key genes (NUAK2, TNFRSF10B, TNFRSF10C, TNFRSF12A, UNC5B, and PMAIP1) exhibited good diagnostic performance in differentiating between thyroid cancer patients and controls. These key genes were associated with macrophages, CD4+ T cells and neutrophils. In addition, PRGs were mainly enriched in the immunomodulatory pathway and TNF signalling pathway. The predictive performance of the model was confirmed in the validation dataset. The DGIdb database reveals 36 potential therapeutic target drugs for thyroid cancer.

Conclusion: Our study suggests that PANoptosis may be involved in immune dysregulation in thyroid cancer by regulating macrophages, CD4+ T cells and activated T and B cells and TNF signalling pathways. This study suggests potential targets and mechanisms for thyroid cancer development.

KEYWORDS

thyroid cancer, PANoptosis, immune infiltration, predictive models, candidate genes

Introduction

Thyroid cancer (THCA) is one of the most common malignant tumours in the world, and in recent years, the incidence of thyroid cancer has been increasing every year. Compared with the total data in 2000, the incidence of thyroid cancer has increased 20 times (1, 2). The incidence of thyroid cancer in women is 3-4 times higher than in men. According to clinical and pathological typing thyroid cancer can be divided into papillary thyroid carcinoma (PTC), follicular thyroid carcinoma (FTC), medullary thyroid carcinoma (MTC), and undifferentiated thyroid carcinoma (ATC) (3, 4). PTC and FTC collectively referred to as differentiated thyroid carcinoma (DTC) is the most common pathological type of thyroid cancer, accounting for more than 90% of all thyroid cancers. The treatment of choice for most patients with thyroid cancer is surgical resection, and thyroid-stimulating hormone suppression and radioactive iodine (RAI) therapy are required for patients with high-risk features, with some patients with thyroid cancer progressing to RAI-refractory thyroid cancer and death (5). There is a lack of effective treatment strategies for patients with advanced thyroid cancer. The development, invasion, and metastasis of thyroid cancer are closely related to changes at the gene level and dysfunctional regulation of related signal transduction pathway. These molecular changes are the hallmarks of thyroid cancer diagnosis and prognosis, as well as potential targets for biological therapy.

PANoptosis is an inflammation-driven programmed cell death that combines key features of pyroptosis, apoptosis and necrotic apoptosis, yet cannot be characterised by any of these modes of death alone (6, 7). PANoptosis was first named in 2019 by the American scholar Malireddi, who proposed that the innate immune sensors ZBP1 and TAK1 kinase play important roles in the regulation of the PANoptosis vesicle complex (7). Three types of PANoptosis vesicles have been identified, ZBP1 PANoptosis vesicles, RIPK1 PANoptosis vesicles and AIM2 PANoptosis vesicles. Viruses, bacteria and other non-infectious factors such as cytokines in tumours can trigger host cells to undergo PANoptosis (8, 9). Pancytopenia is closely related to homeostasis maintenance, embryonic development, and immune regulation.

BRAF V600E and RAS gene variants are the most common mutations in thyroid cancer. These mutations constitutively activate the MAPK signalling pathway, and patients with advanced thyroid cancer develop other genetic variants in addition to these common mutations and become more aggressive and less differentiated (10, 11). The genetic variants and mechanisms that drive the development of thyroid cancer are becoming better understood, but researchers still do not fully understand the determinants and functional basis of certain genetic variants (12). The study of genomic profiles of thyroid cancer patients can help predict the prognosis of thyroid cancer patients and for subsequent immunotherapy. PANoptosis plays a crucial role in many diseases such as infections, tumours, and inflammatory diseases (13–16). There are no data from studies evaluating the impact of PANoptosis-related genes in THCA disease progression. Therefore, the present study proposes that PANoptosis-related genes may also be involved in thyroid cancer disease progression. We first analysed the expression levels of PANoptosis-related genes in THCA. The pathogenic mechanisms of PANoptosis-related genes were explored based on functional enrichment analysis. A PANoptosis risk score model was established by LASSO regression, and the diagnostic efficiency of key genes was verified in the validation dataset. Finally, we analysed the immune infiltration characteristics of THCA to reveal the association between key genes and the immune microenvironment. We aimed to explore the potential link between PANoptosis-related genes affecting the genetic variants of THCA, and to provide a theoretical basis for guiding the prognosis and immunotherapy of thyroid cancer patients.

Materials and methods

Data acquisition

The thyroid cancer datasets GSE33630 and GSE3467 were downloaded from the Gene Expression Omnibus (GEO) database (https://www.ncbi.nlm.nih.gov/gds). The training dataset GSE33630 consisted of 60 THCA patient samples and 45 control samples. Transcriptome information for 512 thyroid cancer samples was obtained from The Cancer Genome Atlas (TCGA) database (https://portal.gdc.cancer.gov/). The validation dataset GSE3467 included 9 THCA patient samples and 9 controls. The obtained dataset was analysed based on R software (version 4.3.1). PANoptosis-related genes were downloaded from the GeneCards database (https://www.genecards.org/).

Analysis of PANoptosis related differentially expressed genes

We used the "combat" function in "sva" to remove the batch-to-batch difference to obtain the differentially expressed genes between the THCA group and the control group (17). The screening criteria were $|\log FC| > 1.5$, p-value < 0.05. The obtained differentially expressed genes and PANoptosis related genes were imported into the jvenn online platform (https://jvenn.toulouse.inrae.fr/app/example.html) to obtain PANoptosis related differentially expressed genes (PRGs).

Functional enrichment analysis

Differentially expressed genes were imported into the DAVID (https://david.ncifcrf.gov/) online platform for Gene Ontology (GO) and Kyoto Encyclopedia of Genes and Genomes (KEGG) analyses. GO mainly includes molecular function (MF), biological

pathway (BP) and cellular component (CC). Visualization was performed using the "ggplot2" package in R software (18). The interaction network between PRGs was constructed using the STRING database. In addition, the metscape database (https://metascape.org/) was used to explore the functional mechanisms among PRGs.

Screening for prognostic markers

Least Absolute Shrinkage and Selection Operator (LASSO) regression is a regularization method for linear regression problems, which can be used to reduce the complexity of the model, prevent overfitting, and select important feature variables (19). We used the LASSO regression model to screen for diagnostic markers. Patients with THCA in the training dataset were divided into high-risk and low-risk groups. Predictive model accuracy was assessed by area under the receiver operating characteristic curve (ROC). GSE3467 was used as a validation dataset to validate the expression of the key genes mentioned above and the area under ROC (AUC) value to measure the predictive power of the algorithm($P<0.05$). We validated the predictive power of the algorithm in the Human Protein Atlas (HPA) database (https://www.proteinatlas.org/) to verify the expression levels of key genes in thyroid cancer tissues. The relationship between the core genes and the prognosis of thyroid cancer patients was explored by the clinical information in the TCGA database.

Immune cell correlation analysis

The CIBERSORT algorithm was used to calculate the immune cell infiltration between the thyroid cancer group and the control group in the training dataset (20). Stacked plots were used to show the distribution of immune cells in each sample. Box plots show the relative proportions of the immune cell types between the two groups. The "ggcorrplot" package was used to explore the correlation between biomarkers and immune cell infiltration.

Drug screening and predicting transcription factor regulatory networks

The Drug Gene Interaction Database (DGIbd) is a database for exploring drug-gene interactions. Transcription factors are key regulators of gene expression, and the activity of these proteins determines cellular function and response to environmental perturbations. We predicted TF regulatory networks and TF-miRNA regulatory networks of key genes by NetworkAnalyst 3.0 online tool (https://www.networkanalyst.ca/) (21). Analyses and presentations were performed using Cytoscape 3.7.2.

Results

Identification of differentially expressed genes of THCA

We obtained a total of 2219 differentially expressed genes by analysing the training dataset GSE33630. The screening criteria were $|logFC|>1.5$, $P>0.05$. The volcano plots and heatmaps in Supplementary Figures 1A, B demonstrate the differential expression patterns of DEGs in the dataset GSE3360. These DEGs were mainly enriched in the positive regulation of inflammatory response, cell migration, extracellular matrix structure, and protein fusion (Figure 1A). KEGG pathway analysis focused on Phagosome、Cytokine-cytokine receptor interaction、Rheumatoid arthritis and ECM-receptor interaction (Figure 1B).

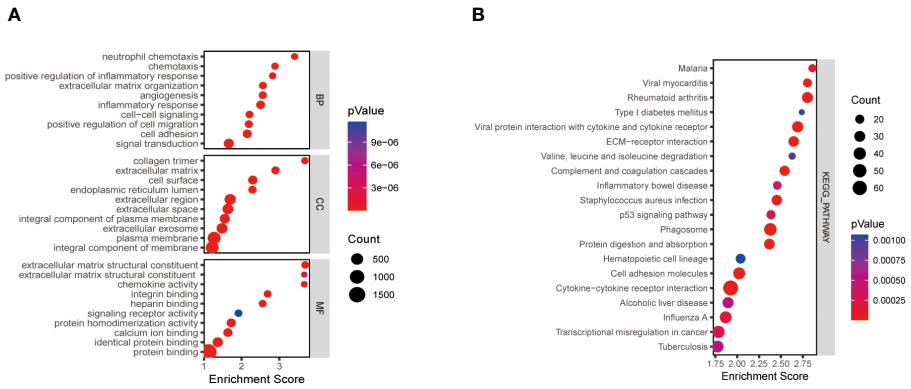

FIGURE 1
Functional enrichment analysis of thyroid cancer-related differentially expressed genes. The size of the ball represents the number of genes. The colours of the balls correspond to different P values. **(A)** The top 10 significantly enriched GO annotations, including biological process, cellular component, and molecular function, were selected separately. **(B)** The top 20 significantly enriched KEGG pathway analyses. GO, the Gene Ontology; KEGG, the Kyoto Encyclopedia of Genes and Genomes analyses.

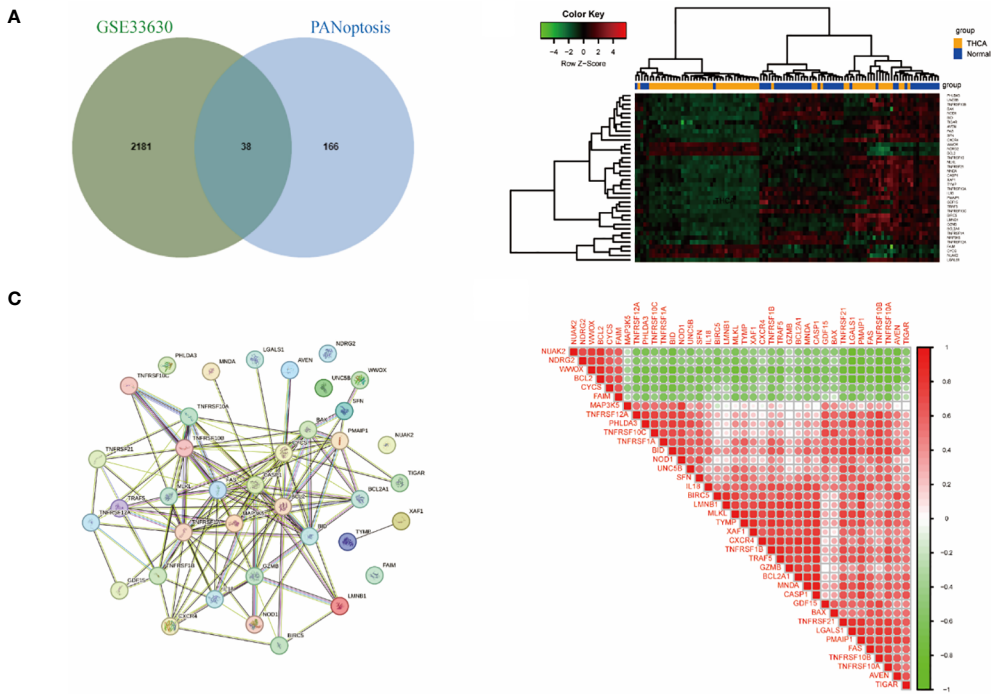

FIGURE 2
Identification of PANoptosis -related differentially expressed genes in the thyroid cancer training dataset. **(A)** Venn plots of 204 PANoptosis genes and 2216 DEGs. **(B)** Heatmap of the expression of 38 PRGs in the training dataset. Red: low expression level; green: high expression level **(C)** Interaction network graph of PRGs in the STRING database. **(D)** Correlation heatmap of PRGs in the training dataset. THCA, thyroid cancer; DEGs, differentially expressed genes.

Identification of differentially expressed genes associated with PANoptosis

A total of 2219 DEGs were obtained in GSE33630 and 204 PANoptosis genes were obtained from GeneCards, and the intersection of the two datasets was taken to obtain 38 PRGs as shown in Figure 2A. The heatmap in Figure 2B demonstrates the differential expression of the 38 PRGs in GSE33630. We constructed a protein interaction network in which 31 genes had interaction relationships (Figure 2C). To explore the links between these genes, we calculated their correlations using the "corrplot" package (Figure 2D) and found significant synergistic effects, with most of the genes being significantly positively correlated with each other.

Constructing functionally enriched networks

To investigate the relationship between PANoptosis genes and the pathogenesis of thyroid cancer, we further explored the functional pathways of PRGs through the metscape database. Functional enrichment analysis showed that the 38 genes were mainly enriched in the positive regulation of apoptosis, pyroptosis, cytokine signalling in the immune system, and regulation of lymphocyte proliferation, etc. (Figure 3A). KEGG analysis showed that the genes were mainly related to the TNF signalling pathway. The network graph between the enriched pathways is shown in Figure 3B. Nodes with the same pathways tend to cluster together.

Construction of a PANoptosis risk score model for thyroid cancer

To further screen PRGs for key genes that play a regulatory role in thyroid cancer disease progression, we constructed a PANoptosis risk score model based on the TCGA database using LASSO regression against 38 PRGs. The LASSO analysis identified eight genes associated with THCA prognosis: NUAK2, TNFRSF10B, TNFRSF10C, TNFRSF12A, UNC5B, PMAIP1, IL18 and GZMB. We established a PANoptosis risk score and survival analysis for THCA as well as the differential expression of these 8 genes in this model (Figure 4). We chose the following formula as the risk score formula: lambda.min=0.0062 Riskscore=(0.4977)*NUAK2+(0.0437)*TNFRSF10B+(-0.385)*TNFRSF10C+(-0.2139)*TNFRSF12A+(0.0165)*UNC5B+(0.5133)*PMAIP1+(-0.253)*IL18+(-0.006)*GZMB. We also analysed the ROC curves of this risk model at different times with AUC. the AUC values for 3-year, 5-year and 10-year OS were 0.854, 0.736 and 0.868, respectively (Figure 4C). Where the higher AUC value indicates the better predictive ability of the model. In addition, we also calculated the AUC values of these eight

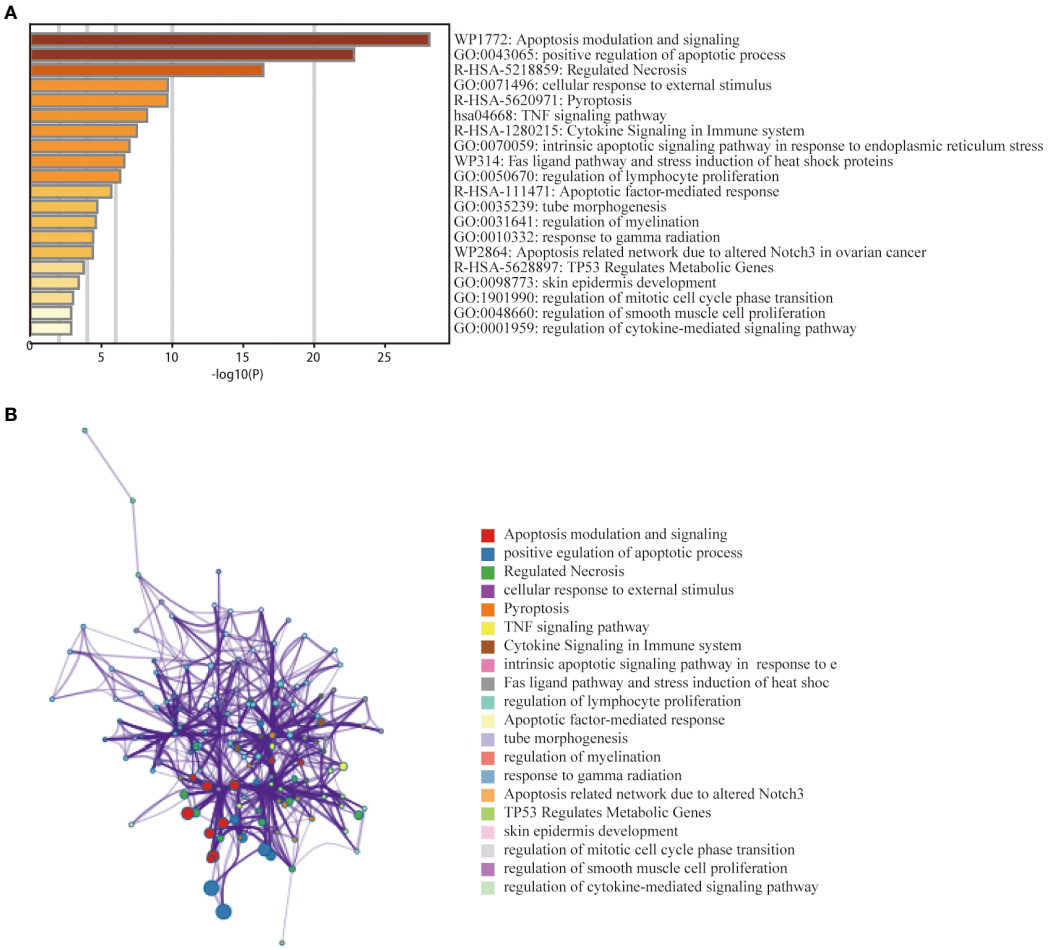

FIGURE 3
Functional enrichment analysis of PANoptosis -related differentially expressed genes in the thyroid cancer training dataset. **(A)** Bar graph of 20 enriched biological pathways, coloured by p–values. **(B)** Network of enriched terms for specified genes analysed by Metascape, coloured by cluster ID.

candidate genes in the GSE33630 dataset, and all of them, except GZMB, had an AUC greater than 0.7 (Figures 5A–H).

Immune cell infiltrability analysis of the training dataset

The immune system of THCA patients plays an important role in disease progression. To investigate the differences in immune cell infiltration between THCA patients and controls, we used the CIBERSORT algorithm. The proportions of immune cells between the two groups are shown in Figure 6A. The THCA group showed significantly higher proportions of activated T cells, activated DC cells, naïve B cells, NK cells, and helper T cells compared with the control group (Figure 6C). Neutrophils were positively correlated with seven genes except NUAK2. TNFRSF10B, TNFRSF10C, and TNFRSF12A were positively correlated with macrophages, DC cells, and mast cells (Figure 6B).

Construction of hub gene-TF-miRNA transcriptional network

To further explore the potential biological processes of candidate genes in thyroid cancer, we analysed the interactions among candidate genes, transcription factors and miRNAs through the Networkanalyst platform. The TF-gene interaction network was constructed in the ENCODE (https://www.encodeproject.org/) database (Supplementary Figure S2A). The TF-miRNA interaction network was obtained in the Regnetwork (http://www.regnetworkweb.org) database (Supplementary Figure S2B). The regulatory network was then imported into Cytoscape 3.7.2 for visualization. Combining the regulatory networks revealed that IKZF1 potentially transcriptionally activates PMAIP1, TNFRSF10B and GZMB. The TF-genes network contained 179 TFs, 8 hub genes, and 248 edges. In the TF-miRNA regulatory network, a total of 90 edges and 81 miRNAs interacted with 7 hub genes.

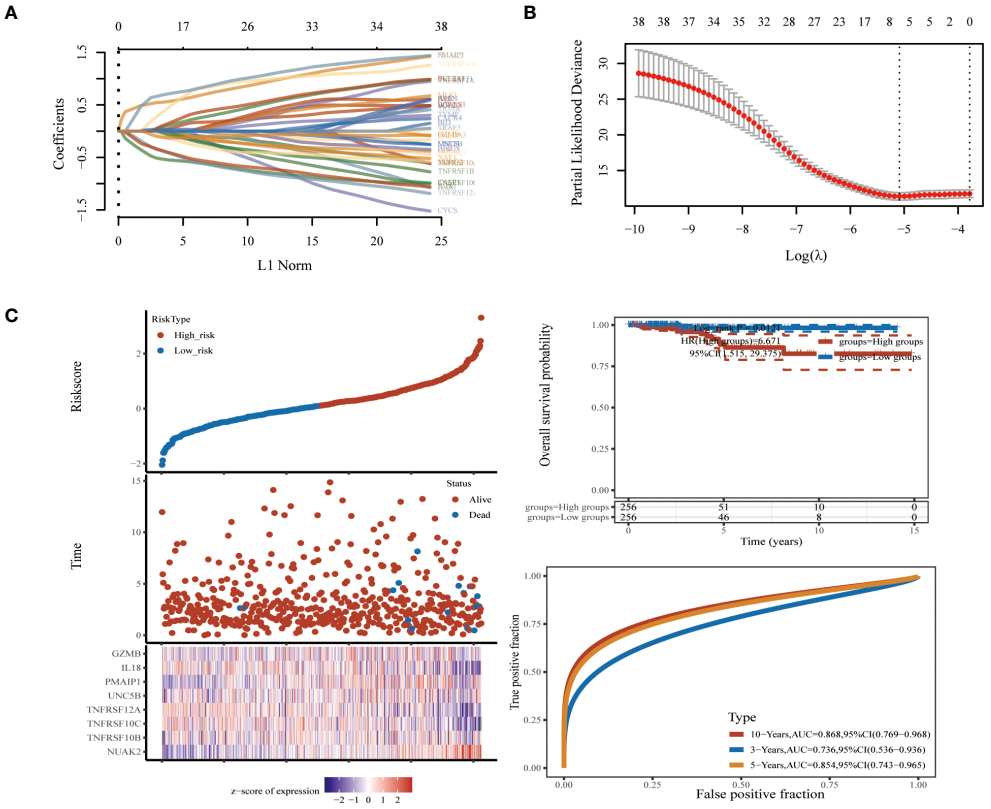

FIGURE 4
Biomarker identification using LASSO regression based on thyroid cancer dataset in TCGA database. **(A)** Least absolute shrinkage and selection operator (LASSO) regression analysis. **(B)** Cross validation for adjusting parameter selection in LASSO regression. **(C)** Modelling of pan-apoptotic risk score and survival analysis.

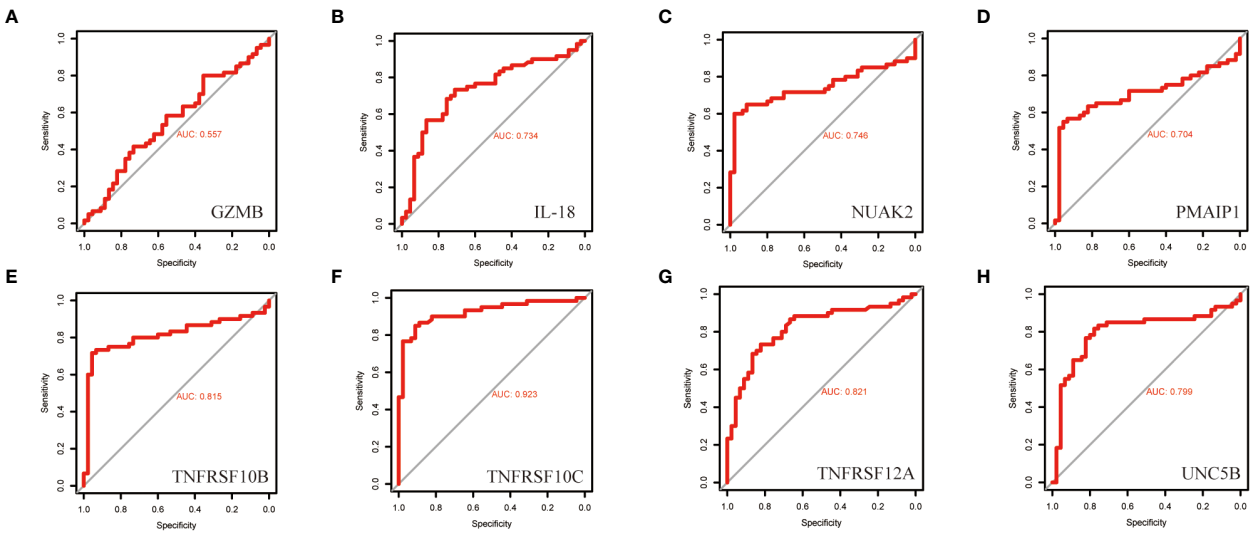

FIGURE 5
ROC curves of the diagnostic value of the eight biomarkers in the thyroid cancer training dataset. **(A–H)** Subject operating characteristic curves (ROC) of candidate diagnostic markers NUAK2, TNFRSF10B, TNFRSF10C, TNFRSF12A, UNC5B, PMAIP1, IL18 and GZMB in the training dataset.

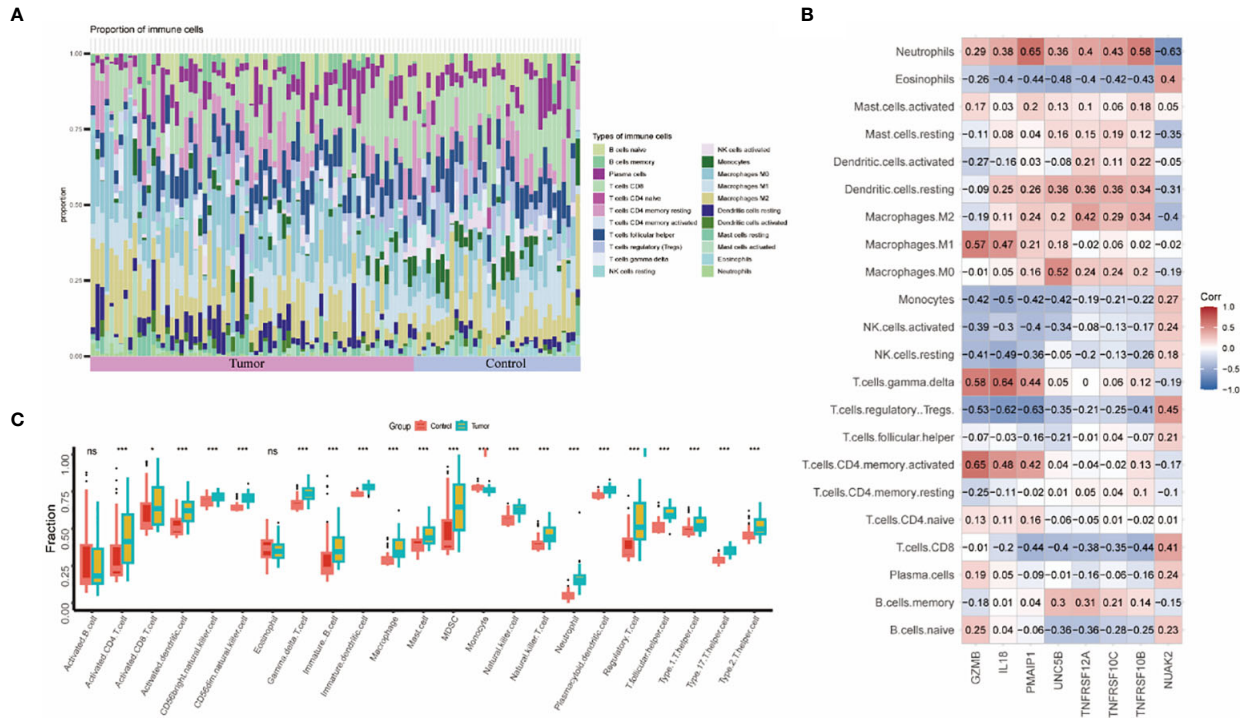

FIGURE 6
Assessment and visualization of immune cell infiltration in the thyroid cancer training dataset. **(A)** Proportion of immune cell infiltration in the thyroid cancer group and control group. **(B)** Heatmap of 8 biomarkers correlating with immune cells. **(C)** Box line plot of immune cells differentially expressed between thyroid cancer group and control group. (* represented P < 0.05, ** represented P < 0.01 and *** represented P < 0.001).

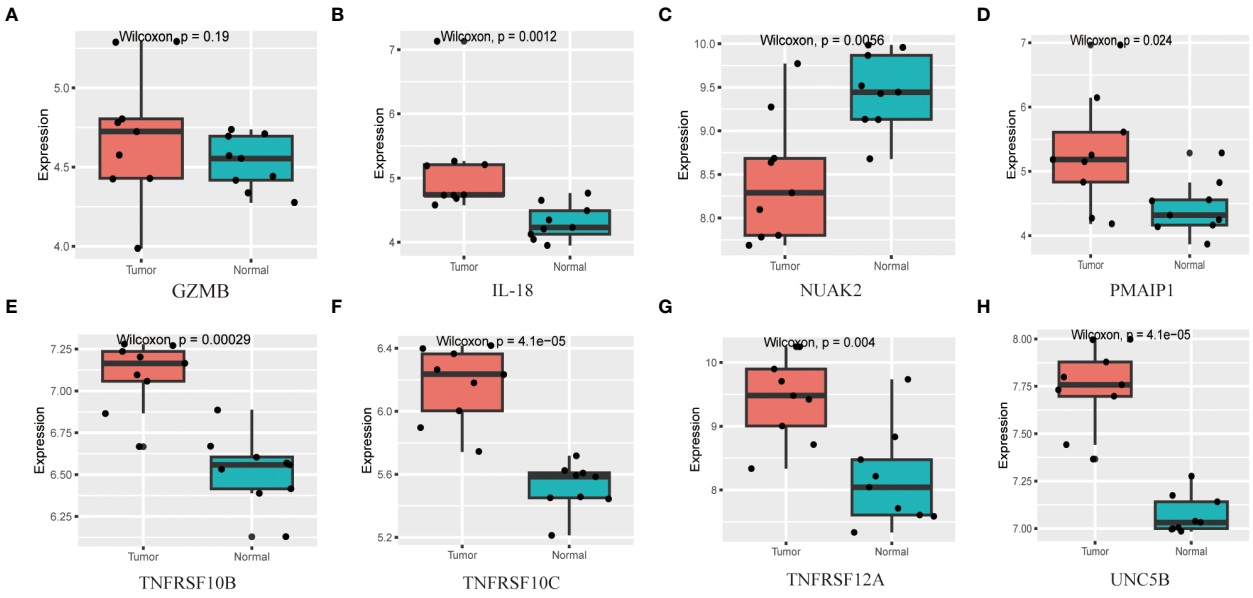

FIGURE 7
Expression analysis of biomarkers in 8 in the thyroid cancer validation dataset. **(A–H)** Expression levels of candidate diagnostic markers NUAK2, TNFRSF10B, TNFRSF10C, TNFRSF12A, UNC5B, PMAIP1, IL18 and GZMB in the validation dataset.

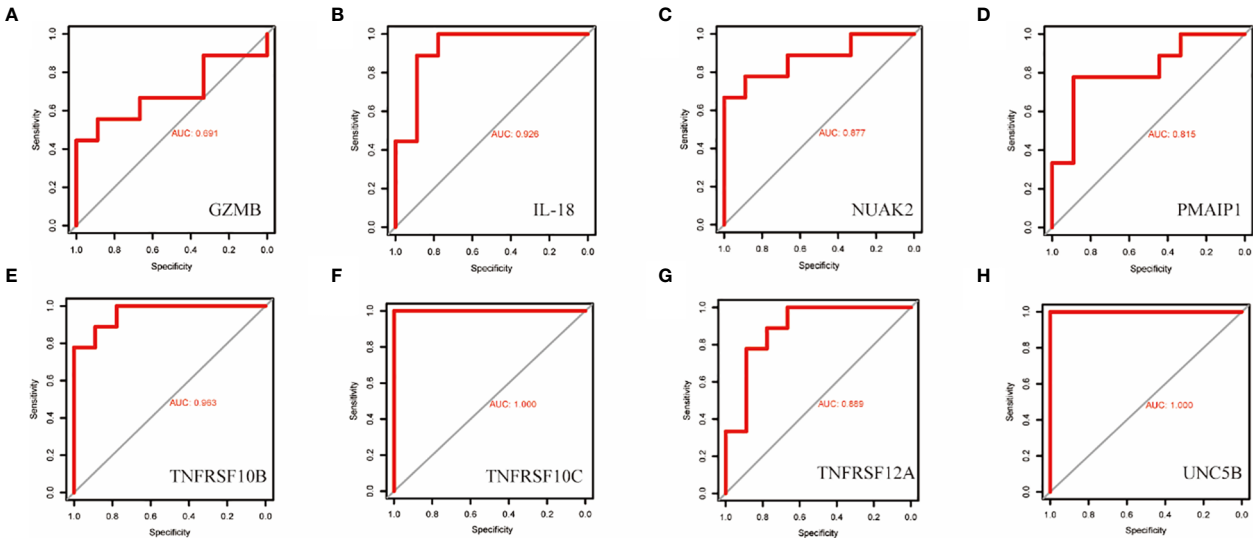

FIGURE 8
ROC curves for the diagnostic value of the eight biomarkers in the thyroid cancer validation dataset. **(A–H)** Subject operating characteristic curves (ROC) of candidate diagnostic markers NUAK2, TNFRSF10B, TNFRSF10C, TNFRSF12A, UNC5B, PMAIP1, IL18 and GZMB in the validation dataset.

Validation of candidate diagnostic markers

To validate the accuracy of the prediction model, we examined the expression of the candidate genes in the validation dataset GSE3467 and ROC analysis. The results showed good diagnostic performance of the predictive model. It is possible that the sample size of the analysis was limited and the difference in the expression of GZMB in the validation dataset was not statistically significant (Figure 7A). NUAK2, TNFRSF10B, TNFRSF10C, TNFRSF12A, UNC5B, PMAIP1, and IL18 were expressed in the validation dataset in agreement with the analysis of the assay dataset (Figures 7B–H). TNFRSF10B, TNFRSF10C, TNFRSF12A, UNC5B, PMAIP1, and IL18 had increased expression in thyroid cancer tissues, while NUAK2 was decreased. The ROC curves showed that the AUC values of the seven candidate genes were greater than 0.8 except for GZMB (Figures 8A–H). Then we verified the protein expression of the candidate genes in the tissues at the protein level. The results showed that except for TNFRSF10B, the expression of other genes was generally consistent with the above analysis. It proved that the PANoptosis prediction model based on 8 key genes was feasible (Figures 9A–H).

Drug-gene interaction prediction

We imported 8 key targets from the above screening into the DGIbd database for screening small molecule compounds for the treatment of thyroid cancer. In total, 36 drugs interacted with TNFRSF10C, TNFRSF12A, PMAIP1, IL18, GZMB and TNFRSF10B. Visualization was performed using Cytoscape (Figure 10). 1 drug targets TNFRSF12A. 1 drug targets PMAIP1. 9 drugs target TNFRSF10B. 19 drugs target IL18. 1 drug targets TNFRSF10C. 5 drugs target GZMB. No potential drugs were identified for UNC5B and NUAK2. Details of these drugs are in Supplementary Table S1.

Discussion

Thyroid cancer has become the most common endocrine system malignancy. The incidence of thyroid cancer is increasing at the highest rate among all malignant tumours. Treatment options for patients with advanced thyroid cancer are very limited. In recent years, with the rapid development of multi-omics research, the understanding of the pathogenesis of different thyroid cancer subtypes has been greatly enhance (22). In particular, the discovery of new thyroid cancer biomarkers has brought hope for the treatment of advanced thyroid cancer. PANoptosis is a novel mode of programmed cell death. PANoptosis has been extensively studied in colorectal, prostate and gastric cancers and some inflammatory diseases (23–27). No study has yet found a link between PANoptosis and thyroid cancer disease progression. The aim of this study was to explore the role of PANoptosis in thyroid cancer disease progression, with the hope of providing new therapeutic targets for the treatment of thyroid cancer.

In this study, a total of 2219 DEGs were identified by analysing the training dataset. In obtained 38 genes that were differentially expressed in thyroid cancer tissues by taking the intersection set. The functional enrichment of the 38 PRGs was mainly related to the regulation of the immune system, with the most significant

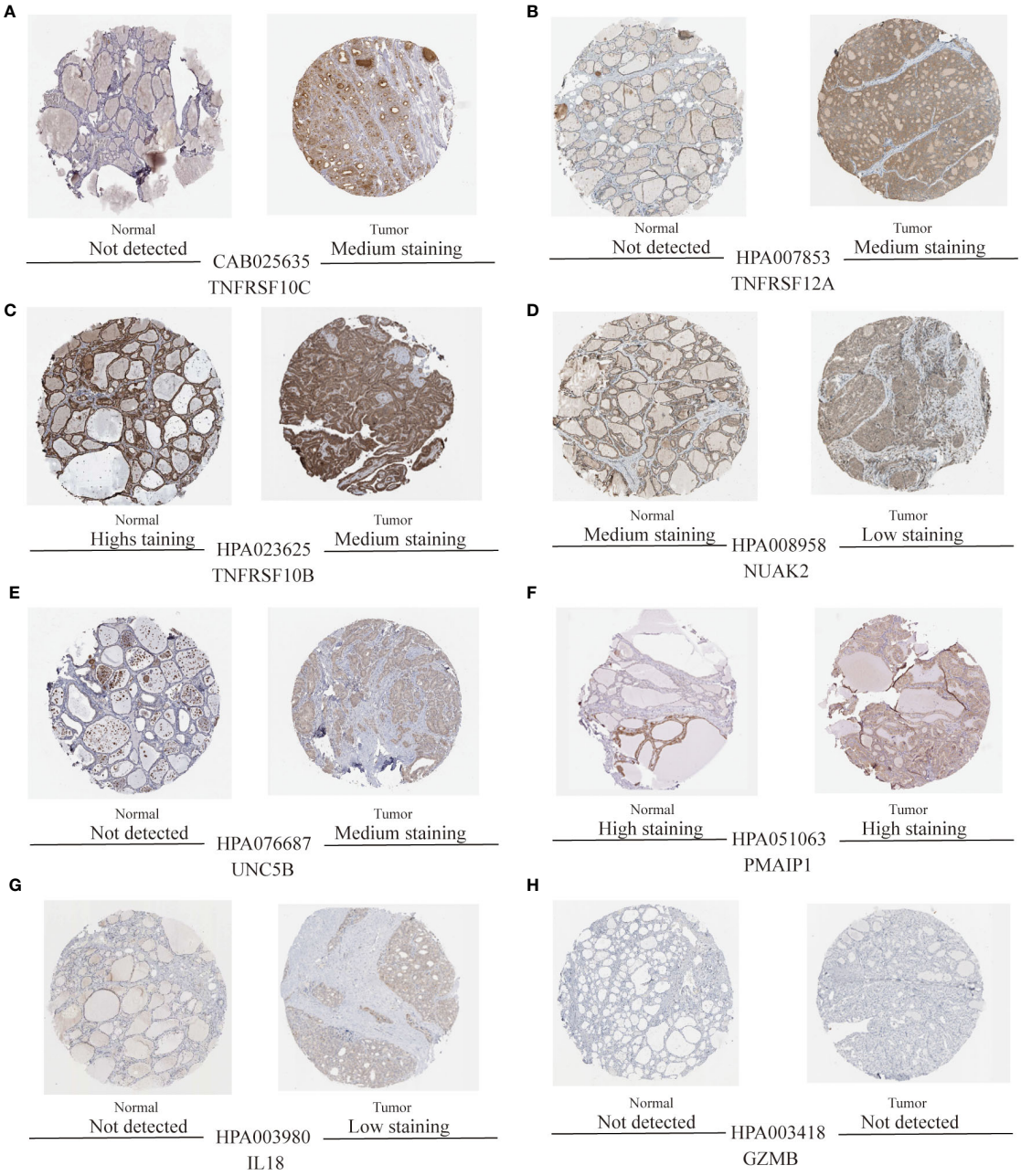

FIGURE 9
Protein expression levels of eight thyroid cancer biomarkers were analysed based on the HPA database. **(A–H)** Protein expression of candidate diagnostic markers TNFRSF10C, TNFRSF12A, TNFRSF10B, NUAK2, UNC5B, PMAIP1, IL18, and GZMB in thyroid normal and tumour tissues.

enrichment in the TNF pathway. We further identified 8 meaningful signature genes using LASSO regression. Then the diagnostic efficacy of these eight genes for thyroid cancer was verified by ROC curves. Among them, the AUC values of TNFRSF10B, TNFRSF10C and TNFRSF12A in the training dataset were all greater than 0.8. TNFRSF10B, TNFRSF10C and TNFRSF12A belong to the tumour necrosis factor receptor superfamily (TNFRSF) which can bind to the tumour necrosis factor superfamily (TNFSF) through the cysteine-rich domains (CRDs). The TNFRSF system contains 19 ligands and 29 receptors, some of which can bind to multiple receptors and regulate complex cellular networks. TNFRSF can assist in the regulation of a variety of cellular functions, including immune responses, inflammatory responses, and cell proliferation, differentiation, and apoptosis (28–31).

In addition, we also analysed the immune cell infiltration in the thyroid cancer group versus the control group in the training dataset. The results showed that activated T cells, NK cells, bone marrow-derived suppressor cells (MDSC), and helper T cells were significantly higher in the tumour group. PANoptosis may be involved in thyroid

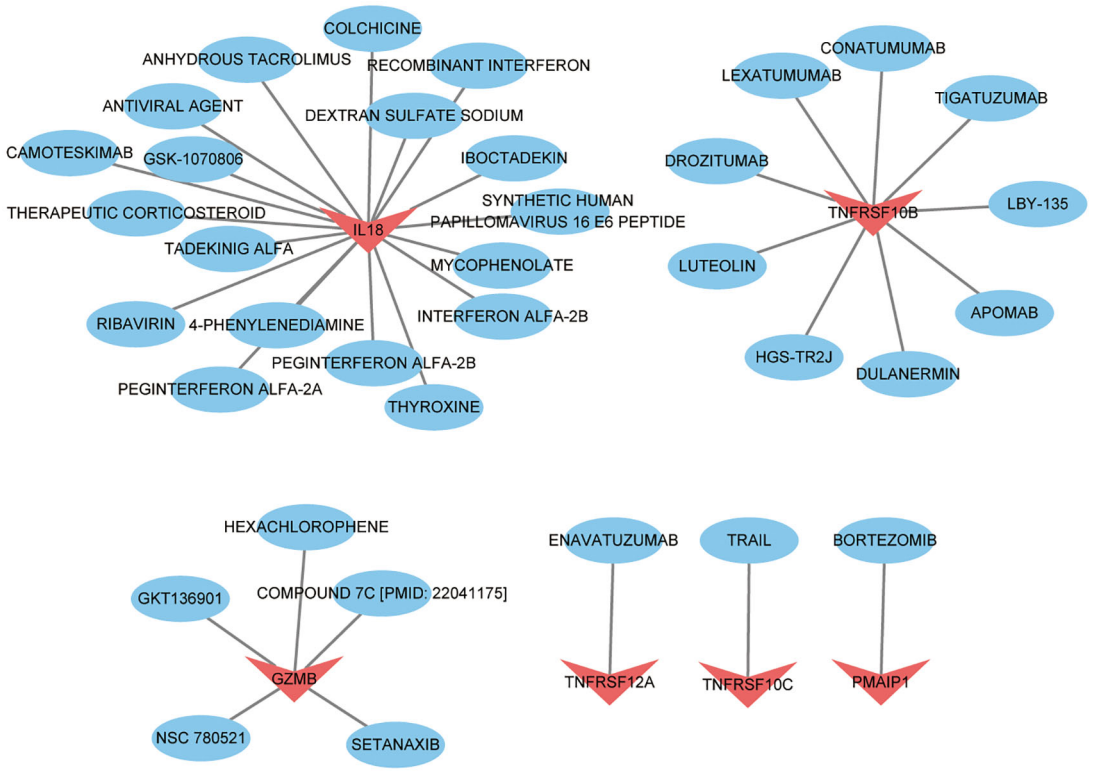

FIGURE 10
Drug prediction based on key targets in thyroid cancer. Red represents key targets and blue represents predicted drugs.

cancer progression through the immune system. These genes we studied were strongly correlated with mast cell and macrophage infiltration. During the progression of ATC, macrophages shift from the M1 state to the M2 state. The role of macrophages in thyroid cancer progression is worthy of further investigation (2). TNFRSF family-mediated signalling has been a hot topic of research in the field of tumour immunotherapy, with notable findings in CAR-T cell therapy (30, 32, 33). Given that TNFRSF10B, TNFRSF10C and TNFRSF12A are up-regulated in thyroid cancer tissues and correlate with macrophages. They may be able to play an important role in CAR-macrophage therapy in the future. In order to make our study more convincing, the above results were verified again by the validation dataset GSE3467.The expression differences of NUAK2, TNFRSF10B, TNFRSF10C, TNFRSF12A, UNC5B, PMAIP1, and IL18 in the validation dataset were statistically significant. And the AUC values of these genes were all greater than 0.8. The PANoptosis diagnostic model based on 8 key genes performed well in the HPA database, except for TNFRSF10B. Although there are individual differences in the expression of TNFRSF10B, this still proves that our predictive model is feasible.

Conclusion

our study has some limitations. The results of our analyses were mainly obtained from public databases and lacked sufficient clinical samples for validation. And our study also requires later molecular biology experiments to further explore the hypothesis of the results of this study. However, we finally identified eight PRDEGs as potential targets for thyroid cancer diagnosis and treatment and predicted potential therapeutic agents through this study. The immune microenvironment of thyroid cancer and the link with PRGs were explored by immune infiltration analysis. It gives us a clearer understanding of thyroid cancer and PANoptosis and provides some new ideas for the clinical treatment of thyroid cancer disease.

Data availability statement

The datasets presented in this study can be found in online repositories. The original contributions presented in the study are included in the article/Supplementary Material. Further inquiries can be directed to the corresponding author.

Author contributions

DW: Writing – review & editing. YL: Writing – original draft.

Funding

The author(s) declare that no financial support was received for the research, authorship, and/or publication of this article.

Conflict of interest

The authors declare that the research was conducted in the absence of any commercial or financial relationships that could be construed as a potential conflict of interest.

Publisher's note

All claims expressed in this article are solely those of the authors and do not necessarily represent those of their affiliated organizations, or those of the publisher, the editors and the reviewers. Any product that may be evaluated in this article, or claim that may be made by its manufacturer, is not guaranteed or endorsed by the publisher.

Supplementary material

The Supplementary Material for this article can be found online at: https://www.frontiersin.org/articles/10.3389/fendo.2024.1397794/full#supplementary-material

References

1. Chen DW, Lang BHH, McLeod DSA, Newbold K, Haymart MR. Thyroid cancer. *Lancet*. (2023) 401:1531–44. doi: 10.1016/S0140-6736(23)00020-X

2. Lu L, Wang JR, Henderson YC, Bai S, Yang J, Hu M, et al. Anaplastic transformation in thyroid cancer revealed by single-cell transcriptomics. *J Clin Invest*. (2023) 133:e169653. doi: 10.1172/JCI169653

3. Laha D, Nilubol N, Boufraqech M. New therapies for advanced thyroid cancer. *Front Endocrinol (Lausanne)*. (2020) 11:82. doi: 10.3389/fendo.2020.00082

4. Grimm D. Recent advances in thyroid cancer research. *Int J Mol Sci*. (2022) 23:4631. doi: 10.3390/ijms23094631

5. Cabanillas ME, McFadden DG, Durante C. Thyroid cancer. *Lancet*. (2016) 388:2783–95. doi: 10.1016/S0140-6736(16)30172-6

6. Sun X, Yang Y, Meng X, Li J, Liu X, Liu H. PANoptosis: Mechanisms, biology, and role in disease. *Immunol Rev*. (2024) 321:246–62. doi: 10.1111/imr.13279

7. Malireddi RKS, Kesavardhana S, Kanneganti TD. ZBP1 and TAK1: master regulators of NLRP3 inflammasome/pyroptosis, apoptosis, and necroptosis (PAN-optosis). *Front Cell Infect Microbiol*. (2019) 9:406. doi: 10.3389/fcimb.2019.00406

8. Karki R, Sundaram B, Sharma BR, Lee S, Malireddi RKS, Nguyen LN, et al. ADAR1 restricts ZBP1-mediated immune response and PANoptosis to promote tumorigenesis. *Cell Rep*. (2021) 37:109858. doi: 10.1016/j.celrep.2021.109858

9. Zhu P, Ke ZR, Chen JX, Li SJ, Ma TL, Fan XL. Advances in mechanism and regulation of PANoptosis: Prospects in disease treatment. *Front Immunol*. (2023) 14:1120034. doi: 10.3389/fimmu.2023.1120034

10. Traversi F, Stooss A, Dettmer MS, Charles RP. BRAF(V600E) overrides NOTCH signaling in thyroid cancer. *Thyroid*. (2021) 31:787–99. doi: 10.1089/thy.2019.0595

11. Jimenez-Mora E, Gallego B, Diaz-Gago S, Lasa M, Baquero P, Chiloeches A. (V600E)BRAF inhibition induces cytoprotective autophagy through AMPK in thyroid cancer cells. *Int J Mol Sci*. (2021) 22:6033. doi: 10.3390/ijms22116033

12. Zhang P, Guan H, Yuan S, Cheng H, Zheng J, Zhang Z, et al. Targeting myeloid derived suppressor cells reverts immune suppression and sensitizes BRAF-mutant papillary thyroid cancer to MAPK inhibitors. *Nat Commun*. (2022) 13:1588. doi: 10.1038/s41467-022-29000-5

13. Messaoud-Nacer Y, Culerier E, Rose S, Maillet I, Rouxel N, Briault S, et al. STING agonist diABZI induces PANoptosis and DNA mediated acute respiratory distress syndrome (ARDS). *Cell Death Dis*. (2022) 13:269. doi: 10.1038/s41419-022-04664-5

14. Sundaram B, Pandian N, Mall R, Wang Y, Sarkar R, Kim HJ, et al. NLRP12-PANoptosome activates PANoptosis and pathology in response to heme and PAMPs. *Cell*. (2023) 186:2783–2801 e2720. doi: 10.1016/j.cell.2023.05.005

15. Karki R, Lee S, Mall R. ZBP1-dependent inflammatory cell death, PANoptosis, and cytokine storm disrupt IFN therapeutic efficacy during coronavirus infection. *Sci Immunol*. (2022) 7:eabo6294. doi: 10.1126/sciimmunol.abo6294

16. Bi Y, Xu H, Wang X, Zhu H, Ge J, Ren J, et al. FUNDC1 protects against doxorubicin-induced cardiomyocyte PANoptosis through stabilizing mtDNA via interaction with TUFM. *Cell Death Dis*. (2022) 13:1020. doi: 10.1038/s41419-022-05460-x

17. Chen S, Yang D, Lei C, Li Y, Sun X, Chen M, et al. Identification of crucial genes in abdominal aortic aneurysm by WGCNA. *PeerJ*. (2019) 7:e7873. doi: 10.7717/peerj.7873

18. Gustavsson EK, Zhang D, Reynolds RH. ggtranscript: an R package for the visualization and interpretation of transcript isoforms using ggplot2. *Bioinformatics*. (2022) 8:3844–6. doi: 10.5281/zenodo.6374061

19. Alhamzawi R, Ali HTM. The Bayesian adaptive lasso regression. *Math Biosci*. (2018) 303:75–82. doi: 10.1016/j.mbs.2018.06.004

20. Chen B, Khodadoust MS, Liu CL, Newman AM, Alizadeh AA. Profiling tumor infiltrating immune cells with CIBERSORT. *Methods Mol Biol*. (2018) 1711:243–59. doi: 10.1007/978-1-4939-7493-1_12

21. Xia J, Gill EE, Hancock RE. NetworkAnalyst for statistical, visual and network-based meta-analysis of gene expression data. *Nat Protoc*. (2015) 10:823–44. doi: 10.1038/nprot.2015.052

22. Hong K, Cen K, Chen Q, Dai Y, Mai Y, Guo Y. Identification and validation of a novel senescence-related biomarker for thyroid cancer to predict the prognosis and immunotherapy. *Front Immunol*. (2023) 14:1128390. doi: 10.3389/fimmu.2023.1128390

23. Zhang Z, Zhang F, Pang P, Li Y, Chen X, Sun S, et al. Identification of PANoptosis-relevant subgroups to evaluate the prognosis and immune landscape of patients with liver hepatocellular carcinoma. *Front Cell Dev Biol*. (2023) 11:1210456. doi: 10.3389/fcell.2023.1210456

24. Sun W, Li P, Wang M, Xu Y, Shen D, Zhang X, et al. Molecular characterization of PANoptosis-related genes with features of immune dysregulation in systemic lupus erythematosus. *Clin Immunol*. (2023) 253:109660. doi: 10.1016/j.clim.2023.109660

25. Pan H, Pan J, Li P, Gao J. Characterization of PANoptosis patterns predicts survival and immunotherapy response in gastric cancer. *Clin Immunol*. (2022) 238:109019. doi: 10.1016/j.clim.2022.109019

26. Tong J, Lan XT, Zhang Z, Liu Y, Sun DY, Wang XJ, et al. Ferroptosis inhibitor liproxstatin-1 alleviates metabolic dysfunction-associated fatty liver disease in mice: potential involvement of PANoptosis. *Acta Pharmacol Sin*. (2023) 44:1014–28. doi: 10.1038/s41401-022-01010-5

27. Lin JF, Hu PS, Wang YY, Tan YT, Yu K, Liao K, et al. Phosphorylated NFS1 weakens oxaliplatin-based chemosensitivity of colorectal cancer by preventing PANoptosis. *Signal Transduct Target Ther*. (2022) 7:54. doi: 10.1038/s41392-022-00889-0

28. Obermajer N, Zwolak A, Wajant H. Editorial: TNFRSF agonists: mode of action and therapeutic opportunities. *Front Immunol*. (2023) 14:1328100. doi: 10.3389/fimmu.2023.1328100

29. Liu L, Wu Y, Ye K, Cai M, Zhuang G, Wang J. Antibody-targeted TNFRSF activation for cancer immunotherapy: the role of fcgammaRIIB cross-linking. *Front Pharmacol*. (2022) 13:924197. doi: 10.3389/fphar.2022.924197

30. He Y, Vlaming M, van Meerten T, Bremer E. The implementation of TNFRSF co-stimulatory domains in CAR-T cells for optimal functional activity. *Cancers (Basel)*. (2022) 14:299. doi: 10.3390/cancers14020299

31. Hashimoto K. CD137 as an attractive T cell co-stimulatory target in the TNFRSF for immuno-oncology drug development. *Cancers (Basel)*. (2021) 13:2288. doi: 10.3390/cancers13102288

32. Si W, Fan YY, Qiu SZ, Li X, Wu EY, Ju JQ, et al. Design of diversified chimeric antigen receptors through rational module recombination. *iScience*. (2023) 26:106529. doi: 10.1016/j.isci.2023.106529

33. Zaitseva O, Hoffmann A, Otto C, Wajant H. Targeting fibroblast growth factor (FGF)-inducible 14 (Fn14) for tumor therapy. *Front Pharmacol*. (2022) 13:935086. doi: 10.3389/fphar.2022.935086

frontiers | Frontiers in Endocrinology

TYPE Original Research
PUBLISHED 16 September 2024
DOI 10.3389/fendo.2024.1339473

OPEN ACCESS

EDITED BY
Anna Perri,
Magna Græcia University of Catanzaro, Italy

REVIEWED BY
Virginia Brancato,
University Milano Bicocca, Italy
Katia Aviña-Padilla,
Unidad Irapuato (CINVESTAV), Mexico

*CORRESPONDENCE
Yanyan Sun
601589@hrbmu.edu.cn
Denan Zhang
zhangdenan@ems.hrbmu.edu.cn
Xiujie Chen
chenxiujie@ems.hrbmu.edu.cn

†These authors have contributed equally to this work

RECEIVED 05 December 2023
ACCEPTED 05 July 2024
PUBLISHED 16 September 2024

CITATION
Ma H, Li G, Huo D, Su Y, Jin Q, Lu Y, Sun Y, Zhang D and Chen X (2024) Impact of Hashimoto's thyroiditis on the tumor microenvironment in papillary thyroid cancer: insights from single-cell analysis. *Front. Endocrinol.* 15:1339473. doi: 10.3389/fendo.2024.1339473

Impact of Hashimoto's thyroiditis on the tumor microenvironment in papillary thyroid cancer: insights from single-cell analysis

Hongzhe Ma[1†], Guoqi Li[1†], Diwei Huo[2†], Yangguang Su[1], Qing Jin[1], Yangxu Lu[1], Yanyan Sun[3*], Denan Zhang[1*] and Xiujie Chen[1*]

[1]Department of Pharmacogenomics, College of Bioinformatics and Science Technology, Harbin Medical University, Harbin, China, [2]Department of Urology Surgery, The Fourth Affiliated Hospital of Harbin Medical University, Harbin, China, [3]Department of General Surgery, The Fourth Affiliated Hospital of Harbin Medical University, Harbin, China

This study investigates the impact of Hashimoto's thyroiditis (HT), an autoimmune disorder, on the papillary thyroid cancer (PTC) microenvironment using a dataset of 140,456 cells from 11 patients. By comparing PTC cases with and without HT, we identify HT-specific cell populations (HASCs) and their role in creating a TSH-suppressive environment via mTE3, nTE0, and nTE2 thyroid cells. These cells facilitate intricate immune–stromal communication through the MIF–(CD74+CXCR4) axis, emphasizing immune regulation in the TSH context. In the realm of personalized medicine, our HASC-focused analysis within the TCGA-THCA dataset validates the utility of HASC profiling for guiding tailored therapies. Moreover, we introduce a novel, objective method to determine K-means clustering coefficients in copy number variation inference from bulk RNA-seq data, mitigating the arbitrariness in conventional coefficient selection. Collectively, our research presents a detailed single-cell atlas illustrating HT–PTC interactions, deepening our understanding of HT's modulatory effects on PTC microenvironments. It contributes to our understanding of autoimmunity–carcinogenesis dynamics and charts a course for discovering new therapeutic targets in PTC, advancing cancer genomics and immunotherapy research.

KEYWORDS

single-cell analysis, thyroid-stimulating hormone, immune cell communication, cancer genomics, TCGA-THCA

1 Introduction

As the most common endocrine malignancy in the world, the incidence of thyroid cancer has been increasing over the last three decades (1). The global incidence rate in women is three times higher than in men, and the global cancer burden in women is 5.1% (2). Among them, papillary thyroid cancer (PTC) is the most common subtype of thyroid

cancer (accounting for 70%~85.9%) (3). Although PTC progresses slowly, a significant proportion of patients have metastases by the time of diagnosis. In the case of metastasis, the combination of surgery, radioactive iodine (RAI) ablation, and thyroid-stimulating hormone (TSH) suppression can still get a favorable prognosis for most cases. However, there are still some metastatic cases that do not benefit from the above treatment strategies (4, 5). Based on traditional genome and transcriptome sequencing techniques, several diagnostic and progressive genes of PTC, such as BRAF and RAS, have been discovered (6). However, this approach ignores the high heterogeneity of PTC. Different tumor microenvironments around PTC will affect the occurrence, development, and drug resistance of tumors. Several studies have reported the effect of tumor-infiltrating immune cells on prognosis in patients with thyroid cancer (7, 8). Myeloid cells increase in proportion in cancer patients and reduce survival time through immunosuppressive function (9). Tumor-associated macrophages vary in frequency in different subtypes of thyroid cancer (10). Natural killer (NK) cells also play a central role in the immune surveillance of thyroid cancer (11). Lymphocyte density was associated with the overall survival and recurrence rate of PTC (12). These immune cells play their respective roles from different aspects. Therefore, systematic evaluation of the tumor immune microenvironment of PTC is helpful to understand the pathogenesis of cancer and guide clinical rational treatment. Hashimoto's thyroiditis (HT), also known as chronic lymphocytic thyroiditis (CLT), is a common autoimmune endocrine disease, causing hypothyroidism or hyperthyroidism, and the incidence is also increasing year by year. Approximately 18.9% to 23.2% of PTC patients have been reported to have HT, and PTC patients with HT have a better prognosis than PTC patients without HT. However, at the same time, HT is considered to be a chronic inflammatory response, and various inflammatory cells infiltrating around the thyroid of patients with HT can damage the DNA of interstitial cells, leading to erroneous DNA repair, thereby promoting the occurrence of PTC. When HT and PTC occur at the same time, experts at home and abroad have different opinions on whether the former has a protective or promoting effect on the latter (13–17). This indicates that the role of HT in the formation of the tumor immune microenvironment of PTC is still unclear. Therefore, this research will focus on HT development to promote or inhibit PTC.

In the past, the inferCNV algorithm was usually used to distinguish malignant epithelial cells from non-malignant epithelial cells, which is an effective method and widely used. However, the existing problem is how to screen the results obtained by the inferCNV algorithm. The usual selection of the clustering coefficient K with copy number variation is subjective, which will lead to inaccurate results. To solve this problem, we proposed a method to determine the best clustering coefficient K based on TCGA data, which can effectively solve the problem of subjectivity in coefficient selection and provide a new strategy for the clustering coefficient selection of the inference results of single-cell copy number variation in the future.

With the development of single-cell RNA sequencing (scRNA-seq), solving tumor heterogeneity from the perspective of cells has become a hot spot at the forefront. Several studies have reported the use of scRNA-seq in thyroid cancer, such as a recent study on gender differences in the tumor microenvironment in PTC patients (18), the progression of follicular thyroid cancer and medullary thyroid cancer (19, 20), and the dedifferentiation of anaplastic thyroid cancer and PTC (21). To explore whether HT promotes or inhibits the generation and development of PTC, we conducted a comprehensive analysis of the paratumors, primary tumors, lymph nodes, and distant metastasis sites of 11 PTC patients and systematically compared the differences in tumor microenvironments of PTC patients with and without HT. The developmental trajectories of malignant thyroid epithelial cells (mTEs) and non-malignant thyroid epithelial cells (nTEs) and their interaction with HASCs were indicated. This discovery can help us better understand how HT inhibits the development of PTC by affecting its tumor microenvironment. To expand the role of HASCs, we found the relationship between HASCs and prognosis at the single-cell level, and clinical features in TCGA-THCA were further investigated to find the value of HASCs in clinical application. Based on the HASC subtypes, studies have identified unique genomic and drug sensitivity profiles of different molecular subtypes, and this provides a new idea for the personalized treatment of PTC.

2 Methods

2.1 scRNA-seq data processing

We obtained the number GSE184362 from the Gene Expression Omnibus (GEO) database (22) (https://www.ncbi.nlm.nih.gov/geo/), and a total of 23 samples (6 paratumors, 7 primary tumors, and 10 metastatic tumors), which consisted of 8 samples with HT and 15 samples without HT, were used for analysis via the Seurat R package (23). For each sample, genes were retained with detected expression in more than three cells. Cells with less than 200 detected genes were excluded. Finally, 171,524 cells were preserved. Before correcting batch effects, we used the NormalizeData() function in Seurat to normalize the raw gene expression value by the global-scaling normalization method "Log-Normalize":

$$Exp_{Normalized} = log^{\frac{Exp_{Raw}}{Exp_{Total}} * 10000 + 1}$$

where Exp(Normalized), Exp(Raw), and Exp(Total) stand for raw gene expression value, normalized gene expression, and the total expression of all genes in one cell, respectively. Then, the "vst" method of the FindVariableFeatures function was used to find the highly variable genes (top 5,000) in each sample. In the process of batch effect correction, we went through three steps. First of all, the SelectIntegrationFeatures function was used to select the integrated dataset required features, and then, the FindIntegrationAnchors function was used to find each anchor point between two datasets. In the end, the IntegrateData function completes the merge of the dataset according to the anchor points identified in the previous step. After batch effect correction, there were 14,0456 cells left over here, and we selected the top 5,000 highly variable genes through the FindVariableFeatures() function, and the top 20 principal components (PCs) were selected based on the JackStraw() function. According to the top 20 PCs, the FindNeighbors() and FindClusters() functions were applied to cluster the cells. The

cluster identified 14 cell clusters at a resolution of 0.1, which were annotated into six cell types by marker genes of myeloid cells (LYZ, FCER1G, LYZ, TYROBP), T/NK cells (CD3D, CD3E, IL7R, IL32, TRAC), B cells (CD79A, CD79B, MS4A1, IGKC, CD74), thyroid epithelial cells (TG, CLU, FN1, MGST1, S100A13), fibroblasts (RGS5, IGFBP7, TAGLN, COL1A2, ACTA2), and endothelial cells (TIMP3, RAMP2, CLDN5, TFPI, MGP) (24).

2.2 CNV analysis of epithelial cells

To distinguish malignant thyroid epithelial cells (mTEs) from non-malignant thyroid epithelial cells (nTEs), we used the inferCNV R package to predict the copy-number alterations (CNAs) of cells and compared them to the reference "normal" cells (this refers to paratumor cells) from scRNA-seq data (25). By setting the cutoff parameter of the inferCNV package's run function to 0.1, the HMM_type parameter to i6, and the HMM_report_by parameter to cell, we get the CNA score for each cell. According to the CNA scores of cells on 22 chromosomes, all cells (including paratumors, primary tumors, and metastatic tumors) were clustered using K-means clustering, and the number of clustering K values ranged from 6 to 15.

2.3 Developmental trajectory inference of mTEs and nTEs

The Monocle2 R package was used to perform the trajectory analysis for mTEs and nTEs (26). Function newCellDataSet() converted the Seurat object to CellDataSet object, and function estimateSizeFactors() and function estimateDispersions() were used to standardize and normalize the gene expression data of cells, respectively. The genes with average log2 fold change greater than 0.5 and adjusted *P*-values less than 0.05 between HT and non-HT of T/NK cells were used as ordering genes in the trajectory analysis. The DDRTree method of the reduceDimension function was used for dimension reduction. Furthermore, the differentially expressed genes (DEGs) (average log2 fold change >1, adjusted *P*-value<0.05, and *q*-value<0.01) that changed along with the pseudotime were identified by the differentialGeneTest() function. The BEAM function was used to find genes that are regulated in a branching way.

2.4 Cell–cell interaction analysis of HASCs

Here, we defined the subset of cells that had a significantly higher percentage of content in PTC samples with HT than in PTC samples without HT as HT-associated specific cells (HASCs). At the same time, the significant difference of this cell subset should be $P<0.05$, while HASCs are more capable of exhibiting differences in the tumor microenvironment between PTC samples with and without HT. Cell–cell communications among HASCs were mapped using the CellChat R package, a common repository of ligands, receptors, cofactors, and their interactions (27). For cell interaction analysis, expression levels were calculated relative to the total read map of the same set of coding genes in all transcriptomes. Expression values were averaged across each single-cell cluster/cell sample.

2.5 Identification of molecular subtypes based on HASCs in TCGA-THCA

Transcriptome data from The Cancer Genome Atlas (TCGA) of THCA were downloaded from UCSC XENA (28) (https://xena.ucsc.edu/). Consensus clustering is a method that provides quantitative evidence for determining the number and membership of possible clusters in a dataset. This approach has been widely used in cancer genomics, where new disease molecular subtypes have been discovered. To discover various molecular patterns based on HASCs, the ConsensusClusterPlus R package was employed (29).

2.6 The characteristics of molecular subtypes

The ESTIMATE algorithm, which comes true with the IOBR R package, was applied to evaluate the immune score and stroma score of the samples for validation of the molecular subtype signatures found (30, 31). Between the molecular subtypes, the variation in the distribution of genes was depicted by the maftools R package (32). At the same time, the drug sensitivity (IC50 value) of 138 GDSC database drugs was predicted by the pRRophetic R package (33).

2.7 Statistical analysis

All statistical analyses were performed using the R tool (v.4.1.1). The Wilcoxon test was applied to compare the differences between two groups, and the Kruskal–Wallis test was used to compare differences between multiple groups of samples. Here, ns indicates $P>0.05$, * indicates $P<0.05$, ** indicates $P<0.01$, *** indicates $P<0.001$, and **** indicates $P<0.0001$. Among them, $P<0.05$ indicates a significant difference. The Kaplan–Meier survival analysis was carried out using the R packages survival and survminer.

2.8 Workflow of the experimental design and analysis

The workflow of this study was divided into four steps as follows (Figure 1): the first step is the processing of single-cell data, the second part is the copy-number variation analysis based on the inferCNV algorithm to distinguish malignant and non-malignant epithelial cells, the third step is the acquisition of HASCs, and the fourth step is the molecular typing of TCGA-THCA samples based on HASCs.

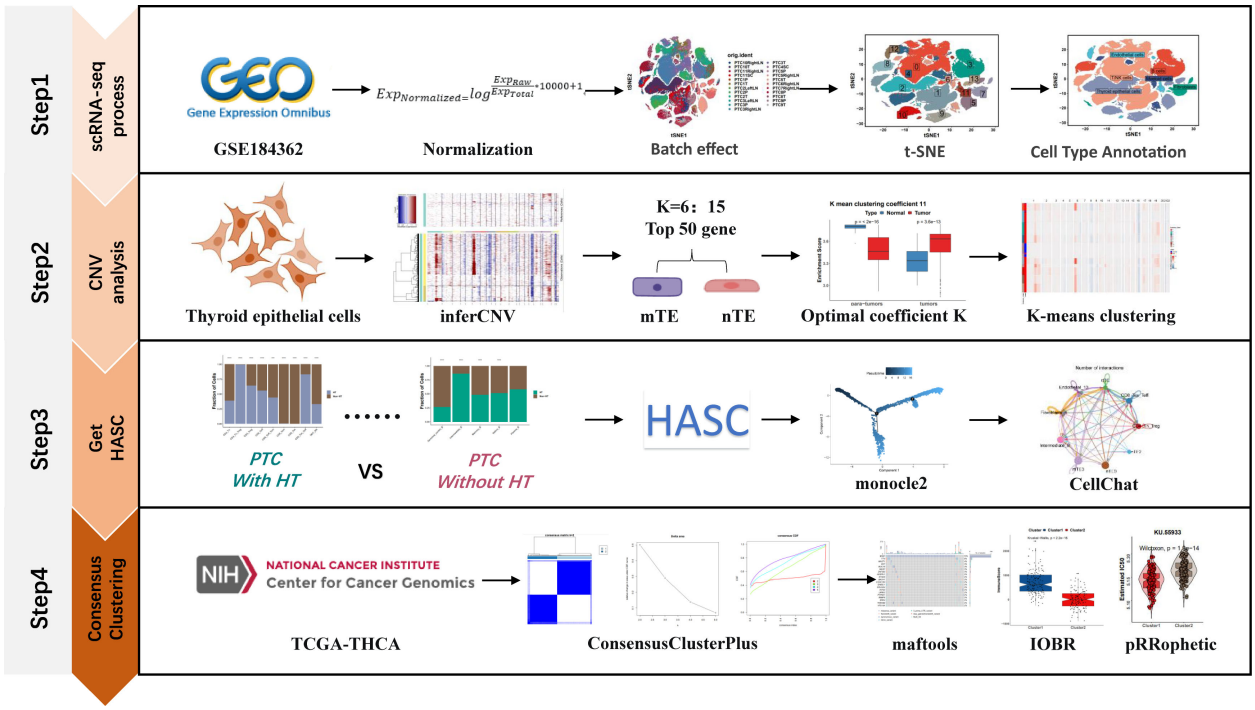

FIGURE 1
Workflow of the effect of HT on the PTC tumor microenvironment at the single-cell level.

3 Results

3.1 Landscape of PTC by scRNA-seq

After rigorous quality screening, a total of 140,456 cells were retained for further analysis (Figure 2A). Six cell types, namely, endothelial cells (TIMP3, RAMP2, CLDN5, TFPI, MGP), fibroblasts (RGS5, IGFBP7, TAGLN, COL1A2, ACTA2), thyroid epithelial cells (TG, CLU, FN1, MGST1, S100A13), B cells (CD79A, CD79B, MS4A1, IGKC, CD74), T/NK cells (CD3D, CD3E, IL7R, IL32, TRAC), and myeloid cells (LYZ, FCER1G, LYZ, TYROBP), were obtained by using t-SNE dimension reduction clustering at low resolution (Figure 2B). All these cell subtypes were shared among tissue sources (Figure 2C), whether with or without HT (Figure 2D), and among samples (Figure 2E). It has a mixed biological origin and was not affected by data preprocessing. Overall, compared with non-HT patients, the immune system was significantly activated in HT patients, with more T/NK cells, B cells, and myeloid cells at the cancer site and fewer fibroblast cells. HT, as an autoimmune disease, leads to excessive activation of the immune system, which may inhibit the development of PTC by alleviating the immunosuppressive effect of tumors (Figure 2F). The chi-square test revealed significant differences in the content of the six types of cells between HT and non-HT (Figure 2G). Among them, the content of immune cells was higher in patients with HT although T/NK cells were excluded, which may be due to the low content of T/NK cells in the HT samples of paratumor tissues. Either way, it is clear that the immune systems of the HT samples were better activated.

3.2 Distinguishing between malignant and non-malignant thyroid epithelial cells

Based on the fact that PTC has abundant copy number variation, we infer chromosome copy number variation (CNV) of cells based on RNA expression profile to distinguish mTEs and nTEs. First, according to the results of cell-type annotation, all thyroid epithelial cells were extracted and the CNV of each cell was inferred by using the cells in the paratumors as the reference standard (Figure 3B). Then, *K*-mean clustering was used to cluster CNV profiles. To determine the optimal clustering coefficient *K*, single sample gene set enrichment analysis (ssGSEA) was conducted in the TCGA-THCA dataset with the gene set composed of the top 50 genes that were differentially expressed between mTEs and nTEs in the clustering results of each *K* value (Figure 3A). This was the method that was created to determine the best *K*-means clustering coefficient. When $K = 11$, the difference in the enrichment fraction between tumor and paracancer samples showed the smallest *P*-value. Therefore, we used $K = 11$ to cluster CNV profiles. *K*-means clustering subgroups 5 and 6 were nTEs, and the rest of the subgroups were mTEs (Figure 3C). Overall, in the original mTEs, there were 8 distant metastases, 251 lymph nodes, and 701 primary tumor mTE cells classified as paratumor nTEs, and in the original nTEs, there were 346 paratumor nTE cells classified as primary tumor mTEs.

To further investigate the function of mTEs and nTEs, these two cell subsets were reclustered. mTEs were reclustered into 14 clusters (Supplementary Figure S1A), and the mTE3 clusters in

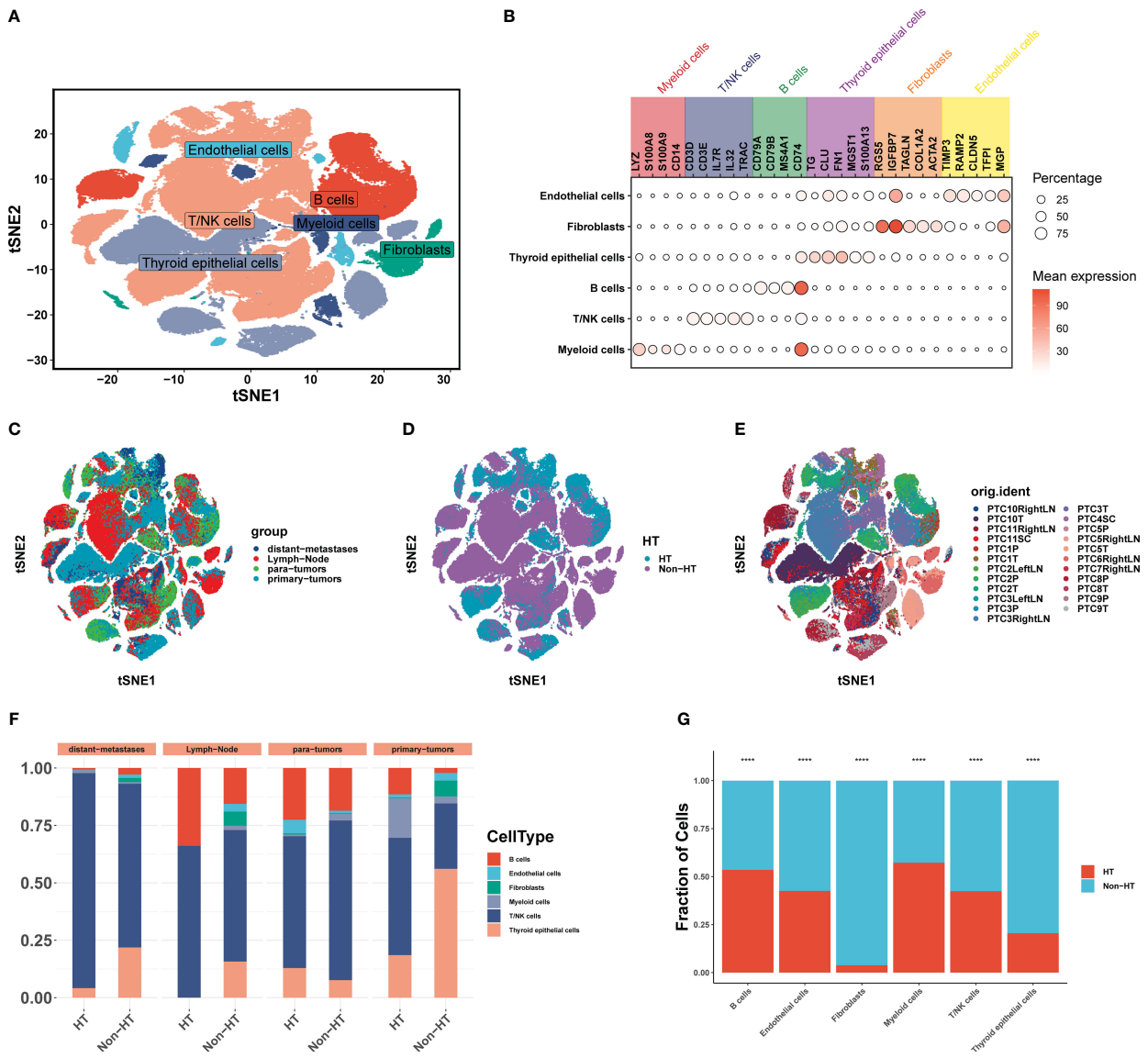

FIGURE 2
Overview of scRNA-seq analysis across 11 PTC patients. **(A)** t-SNE plot visualizing 14 distinct clusters encompassing 140,456 cells from all samples (n = 23), colored by cell type (n = 6). **(B)** Bubble plots showing the expression levels of marker genes for each cell type. **(C)** t-SNE plot visualizing cell clusters colored by tissue of origin. **(D)** t-SNE plot visualizing cell clusters colored by HT and non-HT. **(E)** t-SNE plot visualizing cell clusters colored by samples. **(F)** Horizontal bar charts showing the relative abundance of various cell types between HT and non-HT in each tissue of origin. **(G)** *Post-hoc* analysis of each cell between HT and non-HT; *P< 0.05, **P< 0.01, ***P< 0.001, ****P< 0.0001.

HT patients were significantly higher than those in non-HT patients (Supplementary Figure S1B). Although all mTE clusters were significantly different between HT and non-HT patients, mTE3 clusters had a significant preponderance in HT patients (Supplementary Figure S1C). To understand the function of each mTE cluster, GO enrichment analysis was performed. The results showed that the mTE3 cluster was mainly enriched in the thyroid hormone metabolic process and thyroid hormone generation pathways (Supplementary Table S1). Activation of these pathways would produce more thyroid hormones, which would inhibit the secretion of TSH and thus form a TSH-inhibited environment. One of the effective treatment methods for thyroid cancer is TSH inhibition, indicating that HT patients form a TSH-inhibited environment through the high proportion of mTE3 clusters. Moreover, the occurrence and development of thyroid cancer is delayed. After that, nTEs were reclustered into 11 clusters (Supplementary Figure S2A). Similar to mTEs, the proportion of nTE0 and nTE2 clusters in HT patients is significantly higher than that in non-HT patients (Supplementary Figures S2B, C), and these two clusters are also enriched in the thyroid hormone metabolic process and thyroid hormone generation pathways (Supplementary Figure S2D; Supplementary Table S2). The above results indicate that the TSH-inhibiting environment formed by a high proportion of mTE3, nTE0, and nTE2 clusters in HT patients has an inhibitory effect on PTC.

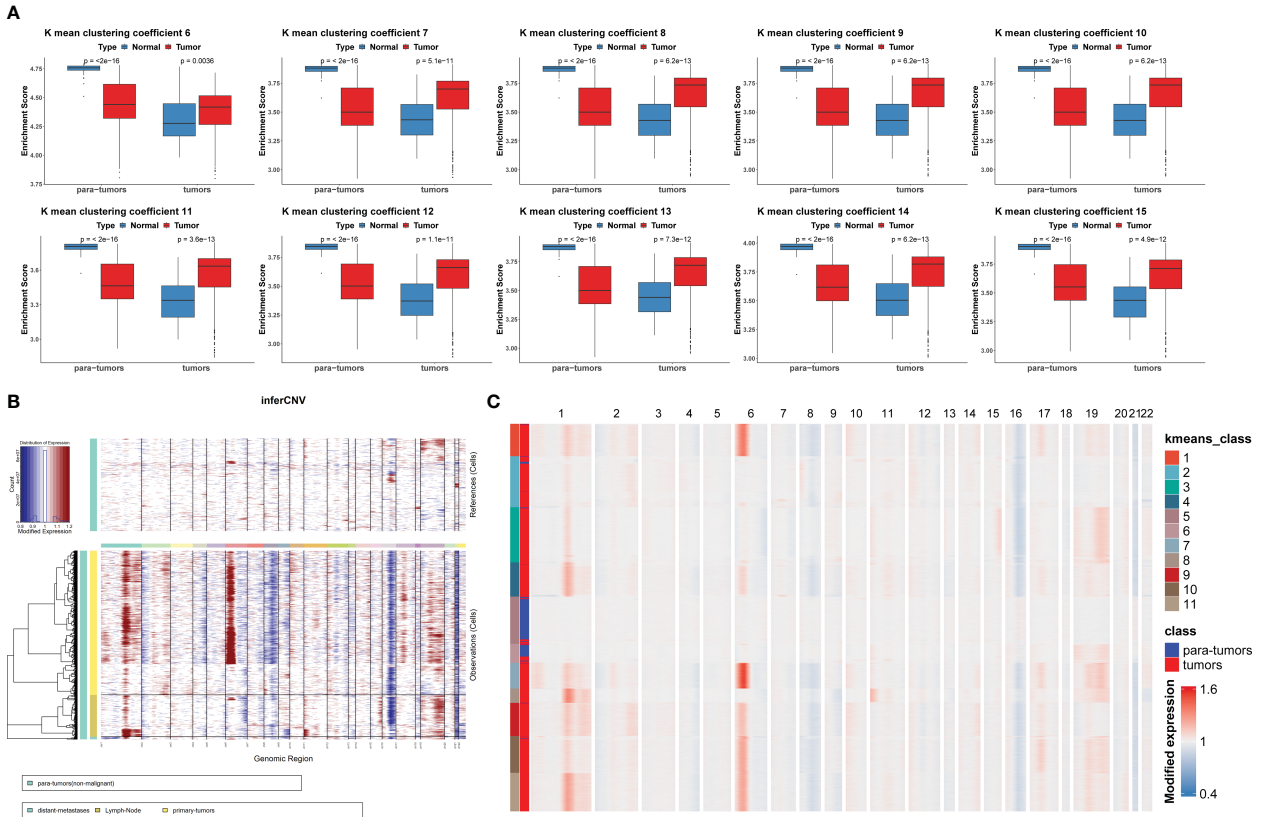

FIGURE 3
The copy number variation (CNV) profile analysis distinguishing malignant thyroid epithelial cells (mTEs) and non-malignant thyroid epithelial cells (nTEs). **(A)** The differentially expressed genes of mTEs and nTEs obtained at different *K* values were used as the ssGSEA results of the gene set in TCGA-THCA tumor and paratumor samples. **(B)** Chromosomal CNV plots of thyroid epithelial cells. The above box was the control group. The lower box shows the tumor groups. **(C)** Clustering heatmap of CNV on 22 chromosomes at $K = 11$.

3.3 Pseudotime analysis of thyroid cells

We next explored the mTE3, nTE0, and nTE2 cluster differentiation trajectories in HT patients by inferring the state trajectories using Monocle2. This analysis showed that nTE0 and nTE2 were at the beginning of the trajectory path, whereas mTE3 was at a terminal state (Figures 4A, B). Furthermore, mTE3 is mainly derived from mTE10, and nTE0 and nTE2 are mainly differentiated into nTE6, nTE8, and nTE10 (Figure 4B). At time transition point 1, the characteristic genes of mTE3 clusters were more likely to change from low expression to high expression, while the characteristic genes of nTE0 and nTE2 clusters were more likely to change from high expression to low expression, which was also found at time transition point 2, which further emphasized the results that nTE0 and nTE2 clusters were in the early stage of differentiation and mTE3 clusters were in the late stage of differentiation (Figures 4C–H). These results indicate that in HT patients, nTE0 and nTE2 clusters may differentiate into mTE3 clusters, but some cells transform into other nTE clusters, which does not affect the environment of TSH inhibition, because mTE10 clusters will differentiate into mTE3 clusters, making up for the increase of TSH caused by the decrease of nTE0 and nTE2. This dynamic transformation creates a TSH-inhibiting microenvironment that effectively inhibits PTC in HT patients.

3.4 Different tumor immune microenvironments between HT and non-HT patients

Innate immunity and adaptive immunity play important roles in the development of PTC (34). By clustering T/NK cells, B cells, and myeloid cells and counting the differences in the proportion of immune cells, differences in the tumor immune microenvironment (TIM) between HT and non-HT patients were discovered. First, T/NK cells were divided into nine cell types: 1) CD4+ T-cell subsets ($n = 3$), including naive T (Tn), regulatory T (Treg), and Tn_Treg; 2) CD8+ T-cell subsets ($n = 5$), including effector T (Teff), exhausted T (Tex), effector memory T (Tem), Tex_Teff, and Teff_Tem cells; and 3) NK cell subsets ($n = 1$), including NKT_NK cells (Figures 5A, B). The high proportion of CD4_Tn_Treg and CD8_Tex_Teff in HT patients indicates the activation of the immune system (Figures 5C, D). More CD8_Teff and less CD8_Tex can effectively mobilize the immune system to kill PTC, while the high percentage of CD4_Tn_Treg can prevent the excessive activation of the immune system and thus maintain immune homeostasis (35). Second, B cells were divided into five cell types, namely, Plasma_B (MZB1, CD38), Native_B (MS4A1, IGHD), Memory_B (MS4A1, CD27), Intermediate_B (IGHD, CD27) and Germinal_center_B (MS4A1, NEIL1) (Figures 5E,

10.3389/fendo.2024.1339473

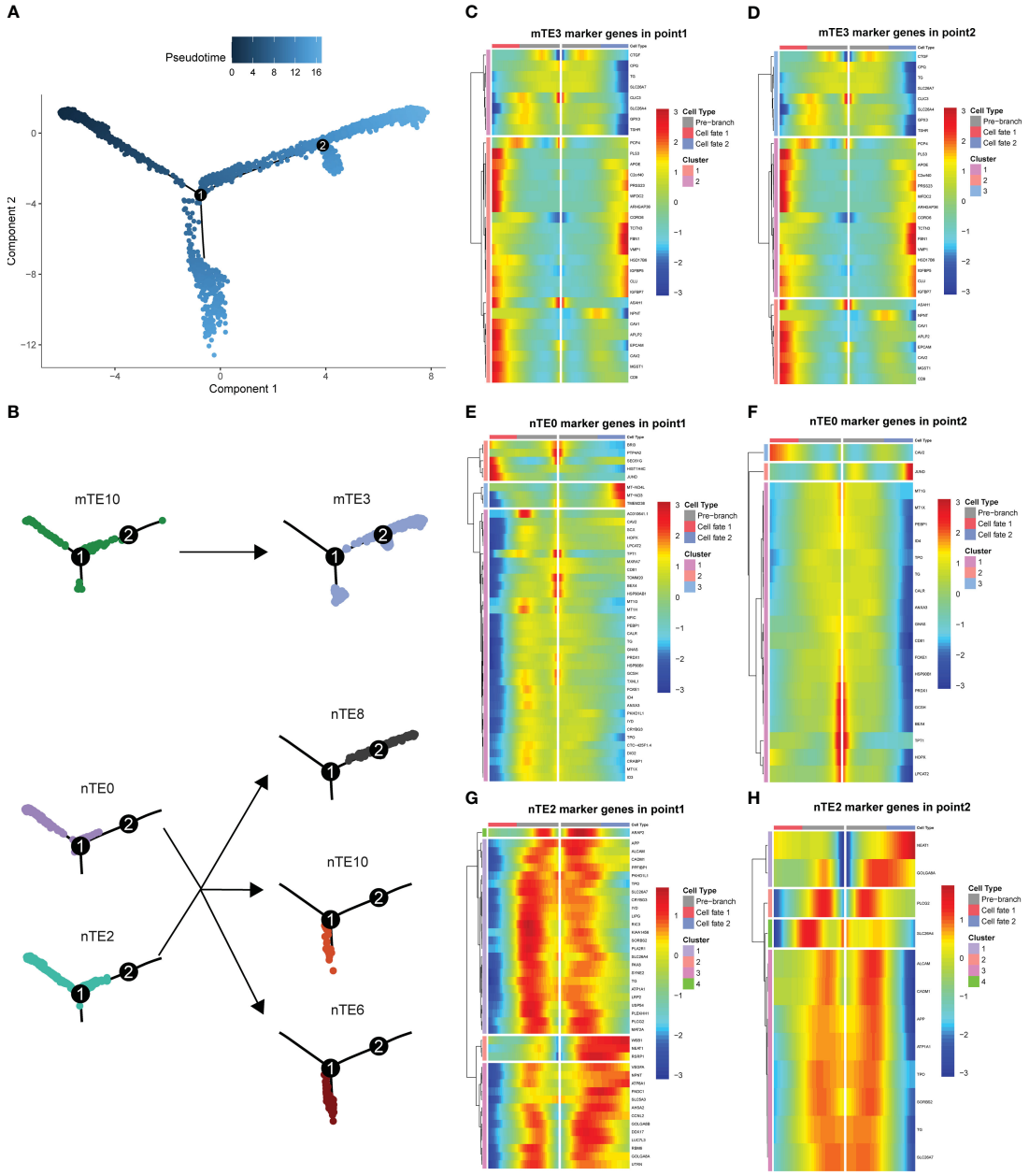

FIGURE 4
Trajectory analysis of mTE3, nTE0, and nTE2. **(A, B)** The trajectory analysis of mTE3, nTE0, and nTE2. mTE3 was from mTE10 and nTE0 and nTE2 were divided into nTE8, nTE10, and nTE6. **(C)** Heatmap showing two-gene clusters of mTE3 marker genes with different expression signatures at pseudotime point 1. **(D)** Heatmap showing three-gene clusters of mTE3 marker genes with different expression signatures at pseudotime point 2. **(E)** Heatmap showing three-gene clusters of nTE0 marker genes with different expression signatures at pseudotime point 1. **(F)** Heatmap showing three-gene clusters of nTE0 marker genes with different expression signatures at pseudotime point 2. **(G)** Heatmap showing four-gene clusters of nTE2 marker genes with different expression signatures at pseudotime point 1. **(H)** Heatmap showing four-gene clusters of nTE2 marker genes with different expression signatures at pseudotime point 2.

F). Intermediate_B was the only cell with a significantly high proportion in HT patients (Figures 5G, H). Myeloid cells were divided into three cell types, and macrophage cells are the primary type (Figures 5I, J). However, high infiltration of conventional dendritic cells (cDCs) in HT patients predicted stronger activation of T cells. Although plasmacytoid dendritic cells (pDCs) could also activate T cells, their activation capacity was smaller (Figures 5K, L). The above proportion of immune cells indicates that HT patients can better activate their own immune system, and the presence of PTC prevents excessive activation of the immune system to reach homeostasis, which forms a dynamic balance between autoimmune diseases and cancer. This finding enables us to clearly see that HT inhibits the development of PTC by mobilizing CD4_Tn_Treg, CD8_Tex_Teff, Intermediate_B, and cDC.

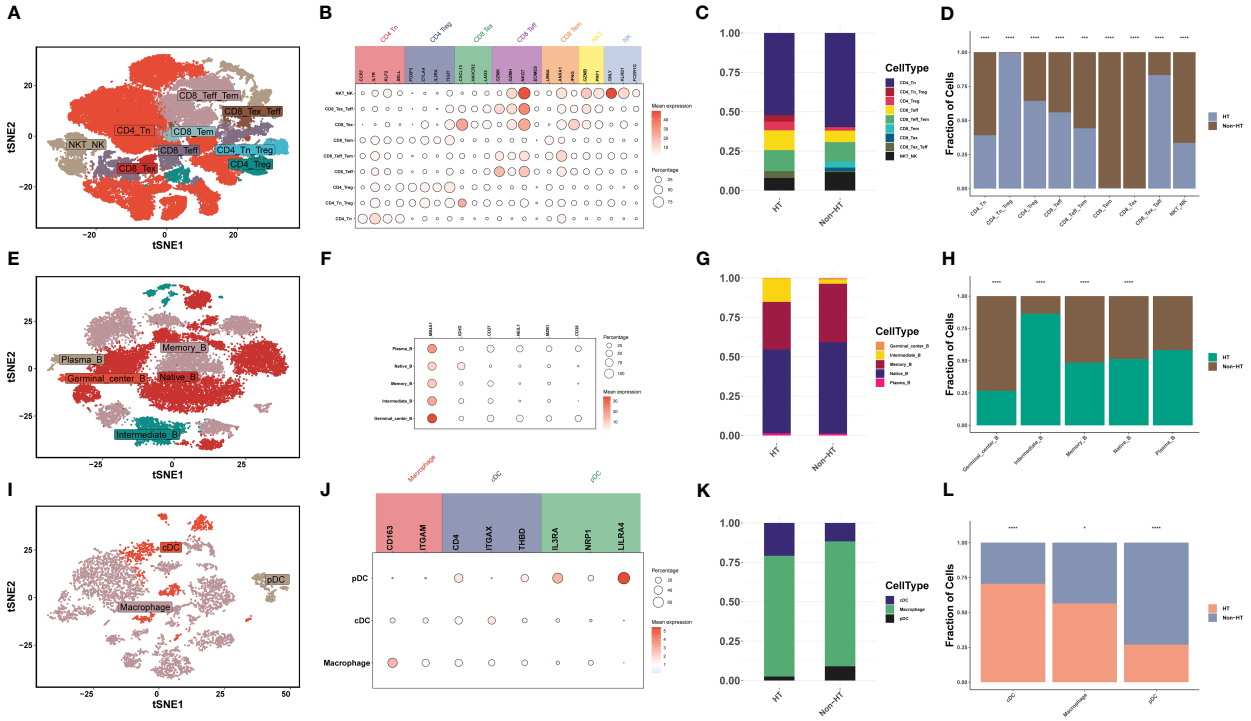

FIGURE 5
The scRNA-seq landscape of immune cells. **(A)** t-SNE plot visualizing 28 distinct clusters of T/NK cells, colored by cell type (*n* = 9). **(B)** Bubble plots showing the expression levels of marker genes for each cell type. **(C)** Horizontal bar charts showing the relative abundance of various cell types between HT and non-HT. **(D)** *Post-hoc* analysis of each cell type between HT and non-HT. **(E)** t-SNE plot visualizing 20 distinct clusters of B cells, colored by cell type (*n* = 5). **(F)** Bubble plots showing the expression levels of marker genes for each cell type. **(G)** Horizontal bar charts showing the relative abundance of various cell types between HT and non-HT. **(H)** *Post-hoc* analysis of each cell type between HT and non-HT. **(I)** t-SNE plot visualizing 20 distinct clusters of myeloid cells, colored by cell type (*n* = 3). **(J)** Bubble plots showing the expression levels of marker genes for each cell type. **(K)** Horizontal bar charts showing the relative abundance of various cell types between HT and non-HT. **(L)** *Post-hoc* analysis of each cell type between HT and non-HT. *P< 0.05, **P< 0.01, ***P< 0.001, ****P< 0.0001.

3.5 Identification of diverse subtypes of stromal cells

Stromal cells are mainly composed of fibroblasts and endothelial cells. The fibroblasts were divided into 11 cell clusters (Figure 6A), which were cell-type-annotated according to the characteristic genes of the four cancer-associated fibroblasts (CAFs) (36). The characteristic genes of myCAFs were highly expressed in most cell subsets, but iCAFs and irCAFs were highly expressed in cell clusters 4, 7, and 8 (Figure 6B). In particular, cell cluster 4 is an important component of CAF in HT patients, and the expression level of PDGFRA, a marker gene of iCAFs, is the highest (Figures 6B–D). The inflammatory and immune environments formed by iCAFs and irCAFs indicate that CAF in HT patients is more benign, which is superior to myCAF's role in tissue repair during cancer development. Furthermore, endothelial cells were divided into 15 cell clusters (Figure 6E), and endothelial cell cluster 13 almost only existed in HT patients (Figures 6F, G). In order to understand its biological function, GO enrichment analysis was conducted on all endothelial cell clusters, and consistent with nTE0, nTE2, and mTE3 clusters, the marker gene of endothelial cell cluster 13 was mainly enriched in the thyroid hormone metabolic process and thyroid hormone generation pathways (Figure 6H; Supplementary Table S3). In conclusion, a high proportion of fibroblast cluster 4 and endothelial cell cluster 13 in stromal cells is a major feature of HT patients, which will better inhibit the development of PTC.

3.6 Multiple cell crosstalk reveals the regulatory mechanism of tumor microenvironment

Through the above systematic analysis, we found that nTE0, nTE2, and mTE3 contents were abundant in HT patients, and the environment that causes TSH inhibition can effectively control the development of PTC. At the same time, it was noticed that the tumor microenvironment of HT patients has a significantly high proportion of CD4_Tn_Treg, CD8_Tex_Teff, Intermediate_B, cDC, fibroblast cluster 4, and endothelial cell cluster 13, indicating that there may be a cross-talk among these cells. We refer to these cells as HASCs. To further understand the underlying regulatory mechanisms, we used CellChat to infer intercellular communication between nTE0, nTE2, and mTE3 and other cell types based on the ligand–receptor (L–R). mTE3 and nTE0 interact more closely with other cells, both in terms of the number and intensity of interactions, and more as senders of cell communication. On the other hand, immune and stromal cells

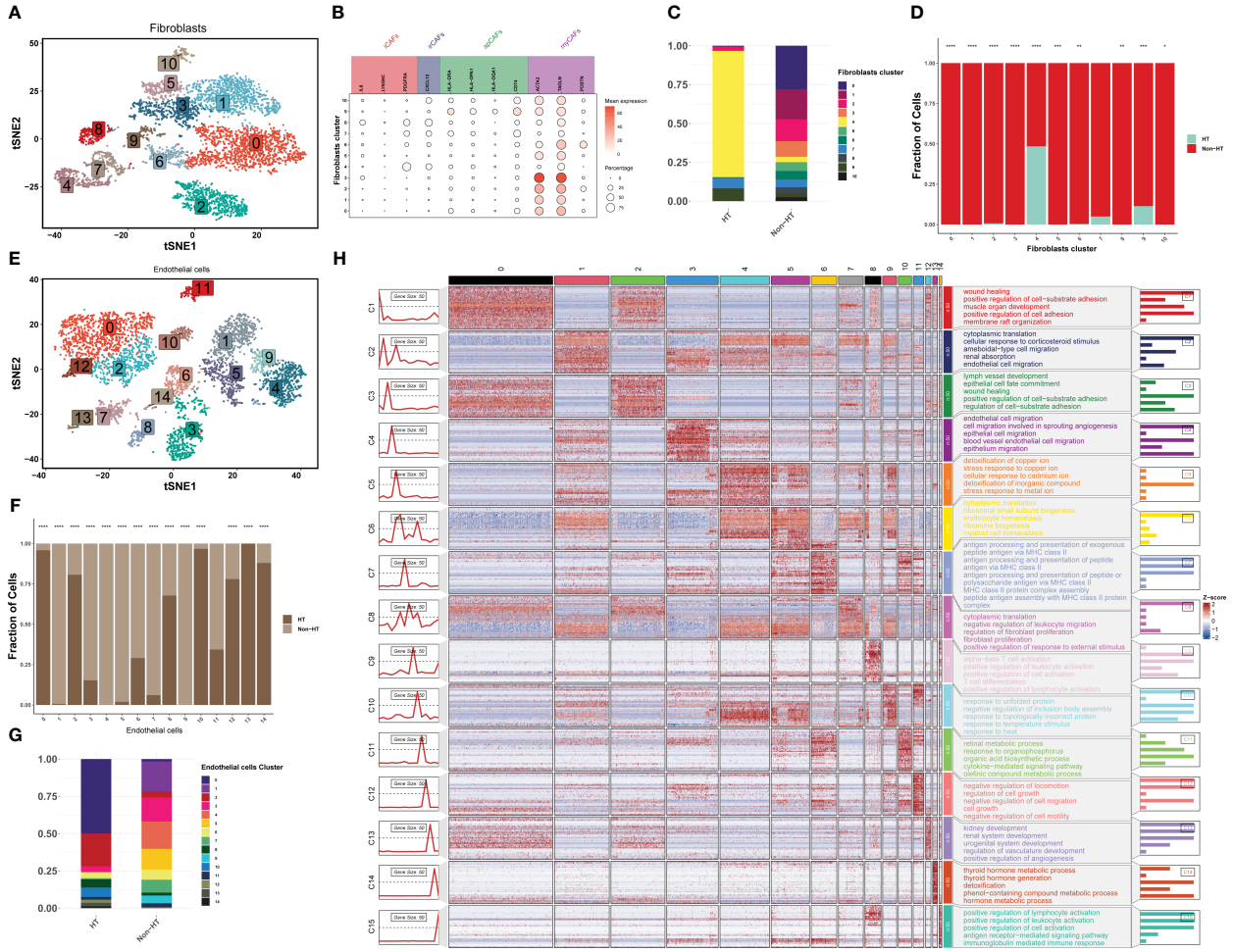

FIGURE 6
The scRNA-seq landscape of stromal cells. **(A)** t-SNE plot visualizing 11 distinct clusters of fibroblasts, colored by cell type (n = 4). **(B)** Bubble plots showing the expression levels of marker genes for each cell type. **(C)** Horizontal bar charts showing the relative abundance of various cell types between HT and non-HT. **(D)** *Post-hoc* analysis of each cell type between HT and non-HT. **(E)** t-SNE plot showing endothelial cells colored by clusters (n = 15). **(F)** Horizontal bar charts showing the relative abundance of various clusters between HT and non-HT. **(G)** *Post-hoc* analysis of each cluster between HT and non-HT. **(H)** GO enrichment analysis of the top 50 marker genes in 15 clusters. *P< 0.05, **P< 0.01, ***P< 0.001, ****P< 0.0001.

interact with other cells more as receivers of cell communication (Figure 7A). nTE0, nTE2, and mTE3 interact primarily with MIF signaling pathways mediated by CD74 and CXCR4 receptors on immune and stromal cells via MIF ligands (Figure 7B). In the MIF signaling pathway network, nTE0, nTE2, and mTE3 showed a similar interaction relationship with all other cells, that is, nTE0 and mTE3 had interactions with all other cells (Figure 7C), and MIF–(CD74+CXCR4) was dominant in these interactions (Figure 7D). Further studies showed that in the MIF–(CD74 +CXCR4) signaling pathway, CD4_Tn_Treg, CD8_Tex_Teff, cDC, and Intermediate_B interact with many other cells in the signaling network (Figure 7E), which can also be seen by the expression value of the L–R pairs (Figure 7F). To further determine the role of these cells in the MIF signaling pathway, a cellular communication network system analysis was performed. The results were consistent with the previous results: nTE0 and mTE3 were mainly signal transmitters, while all the other cells except E were receivers, and CD4_Tn_Treg and CD8_Tex_Teff were very active, playing the four roles of signal sending, receiving, mediating, and influencing (Figure 7G). To more intuitively define the role of all cells in the MIF signaling pathway, we visualized the dominant sender (source) and receiver (target) in 2D space (Figure 7H). There was no doubt that nTE0 and mTE3 were the senders of the signal; Intermediate_B, cDC, and fibroblast cluster 4 were the receivers of the signal; CD4_Tn_Treg, endothelial cell cluster 13, and CD8_Tex_Teff were both the sender and the receiver; and nTE2 was almost neither the sender nor the receiver.

3.7 Relationship between HASC infiltration and clinical features in bulk RNA-seq

First, we investigated the association of HASC infiltration with PTC prognosis. Patients in groups CD4_Tn_Treg, CD8_Tex_Teff, and mTE3 with high infiltration had a better prognosis although

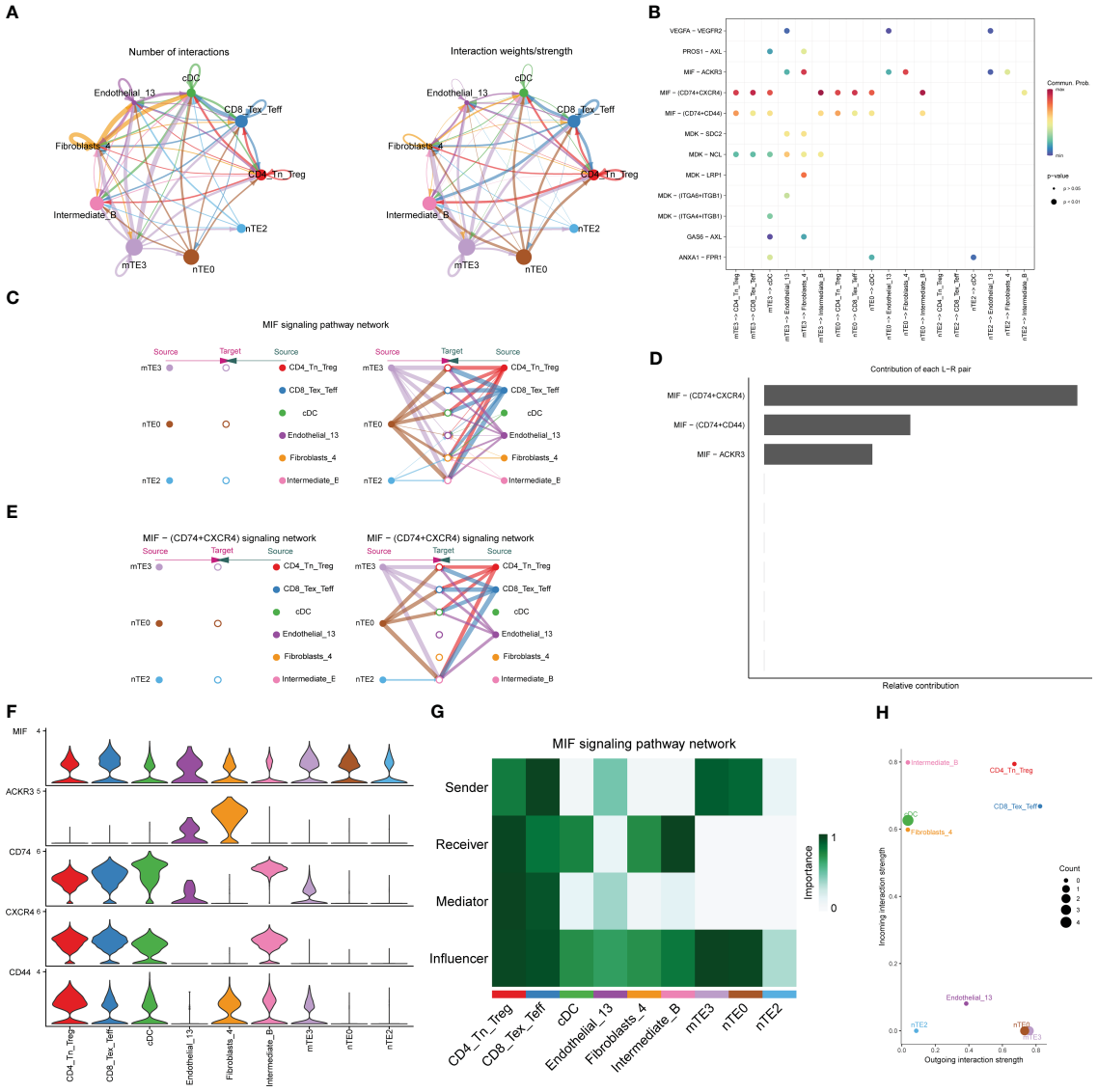

FIGURE 7
Cell–cell communication analysis of HASCs. **(A)** Net count map of HASC interactions. HASC interaction weight map. The thicker the line, the greater the number of interactions and the greater the weight/intensity of interactions between the two cell types. **(B)** The significantly related ligand–receptor interactions from the main thyroid epithelial cells to other immune and stromal cells. **(C)** Hierarchy plot of interactions between selected target cells and other cells in the MIF signaling pathway network. **(D)** Relative contribution of each ligand–receptor pair to the overall communication network of signaling pathways, which is the ratio of the total communication probability of the inferred network of each ligand–receptor pair to that of the signaling pathways. **(E)** Hierarchy plot of interactions between selected target cells and other cells in the MIF–(CD74+CXCR4) signaling network. **(F)** Violin plot showing the expression patterns of signaling genes involved in the inferred signaling network. **(G)** The network centrality index of each cell population was calculated to identify the role of each type of cell in the MIF signaling pathway. **(H)** Scatter plot visualizing the dominant sender (source) and receiver (target) in the MIF signaling pathway in 2D space.

survival differences were not significant ($P > 0.05$) (Figures 8A, B, G), which was consistent with previous intercellular communication results that CD4_Tn_Treg and CD8_Tex_Teff play multiple roles in critical cell communication. Since the environment of TSH suppression was mainly created by the high infiltration of mTE3, nTE0, and nTE2, it was logical that patients in the high infiltration group of mTE3 would have a better prognosis, but we observed a paradoxical phenomenon that patients with high infiltration of nTE0 and nTE2 would have a worse prognosis (Figures 8H, I). Through the previous trajectory analysis, we found that nTE0 and nTE2 were in the early stage of differentiation, while mTE3 was in the late stage of differentiation. The high infiltration of nTE0 and nTE2 implies that cell differentiation had not begun or was just beginning when the characteristic genes of nTE0 and nTE2 were not immediately functional and the TSH-suppressive environment had not yet formed. In contrast, the high infiltration of mTE3 cells indicated that cell differentiation was nearing completion, the signature genes of mTE3 had completed their role in thyroid hormone production, and the TSH-suppressed environment effectively prolonged patient survival. The high infiltration of cDC, fibroblast cluster 4, and Intermediate_B as receivers of cell communication meant that cell

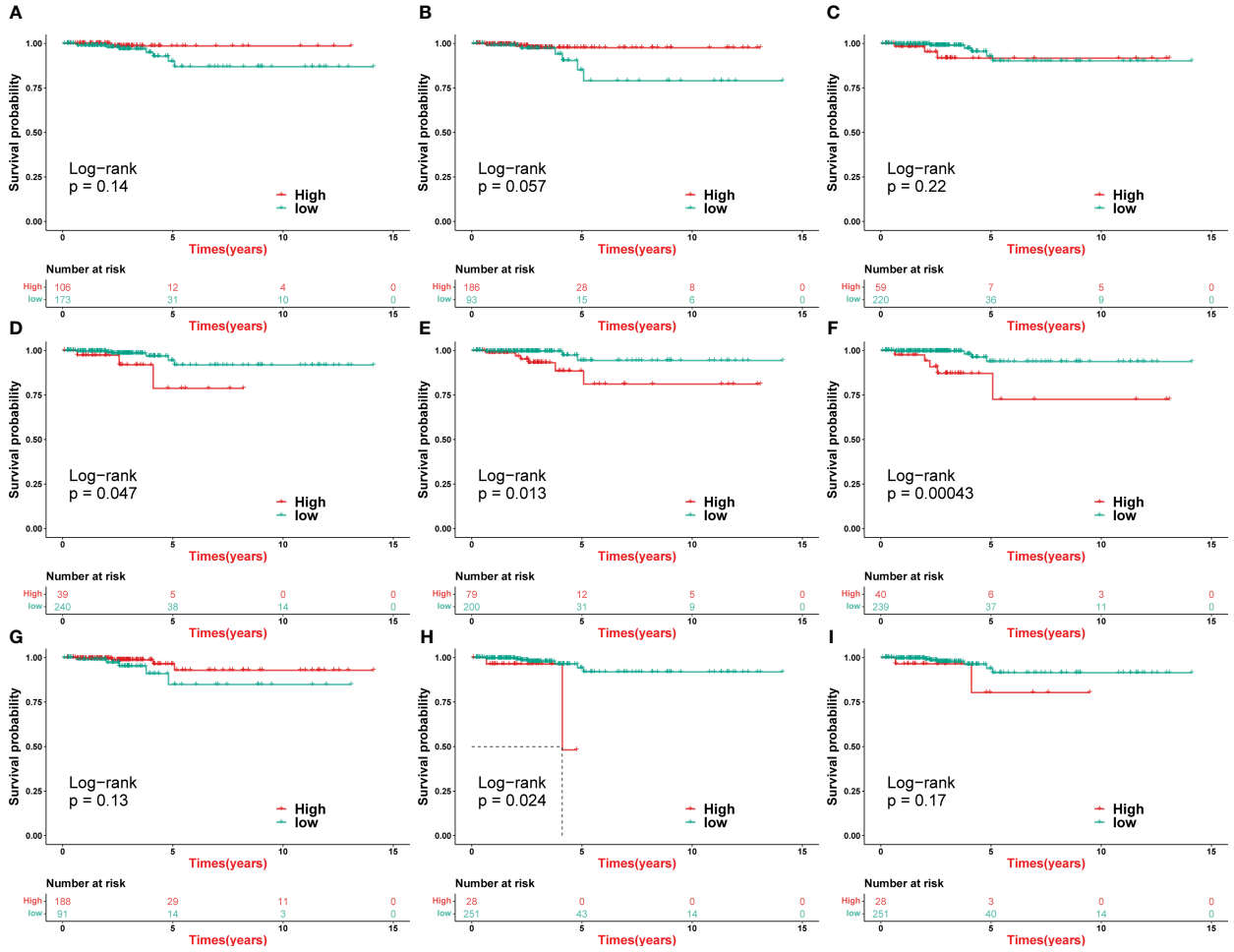

FIGURE 8
Survival analysis of HASCs in TCGA-THCA. **(A–I)** Kaplan–Meier curve of OS according to CD4_Tn_Treg (log-rank test: $P = 0.14$) **(A)**, CD8_Tex_Teff (log-rank test: $P = 0.057$) **(B)**, cDC (log-rank test: $P = 0.22$) **(C)**, endothelial cell cluster 13 (log-rank test: $P = 0.047$) **(D)**, fibroblast cluster 4 (log-rank test: $P = 0.013$) **(E)**, Intermediate_B (log-rank test: $P = 0.00043$) **(F)**, mTE3 (log-rank test: $P = 0.13$) **(G)**, nTE0 (log-rank test: $P = 0.024$) **(H)**, and nTE2 (log-rank test: $P = 0.17$) **(I)**.

differentiation had fully started, the TSH-suppressive environment had been established, and the patient's prognosis was naturally better (Figures 8C, E, F). As a group of tissues that can phagocytose foreign bodies, bacteria, necrosis, and aging and participate in the immune activities of the body, patients with high infiltration of endothelial cell cluster 13 would have a better survival time (Figure 8D). Then, we examined the association of HASCs with clinical features. mTE3 was significantly enriched in patients younger than 60, validating the results of the survival analysis (Supplementary Figure S3A). Significant differences in terms of gender were found in CD4_Tn_Treg and Intermediate_B, where CD4_Tn_Treg was significantly enriched in female patients, while Intermediate_B was significantly enriched in male patients (Supplementary Figure S3B). In terms of tumor metastasis, CD8_Tex_Teff and cDC were enriched in patients without metastasis, revealing their role in preventing tumor metastasis (Supplementary Figure S3C). Most of the HASCs were significantly differentially enriched in the presence or absence of regional lymph node metastasis, indicating that regional lymph node metastasis is an important feature of PTC (Supplementary Figure S3D). The results of tumor T stage and AJCC stage showed the same enrichment trend of HASCs. The changes of mTE3, nTE0, and nTE2 were not obvious, but the immune cells CD4_Tn_Treg, CD8_Tex_Teff, and cDC showed a fluctuating change trend, that was from high to low (Supplementary Figures S3E, F), which reflected the dynamic changes of immune cells in the development of cancer. However, advanced patients usually have fewer immune cells, which is consistent with some existing studies (37).

3.8 Consensus clustering of TCGA-THCA based on HASCs

The HASCs were further utilized for consensus clustering analysis. When the clustering coefficient $K = 2$, the clustering effect was the best, and the internal consistency and stability of the subgroups were good (Figures 9A–C). Cluster 1 was more abundant in immune cells, in contrast to cluster 2, which was more abundant in stromal cells (Figure 9D). This finding was validated by the results of sample immune scoring and stromal scoring evaluated

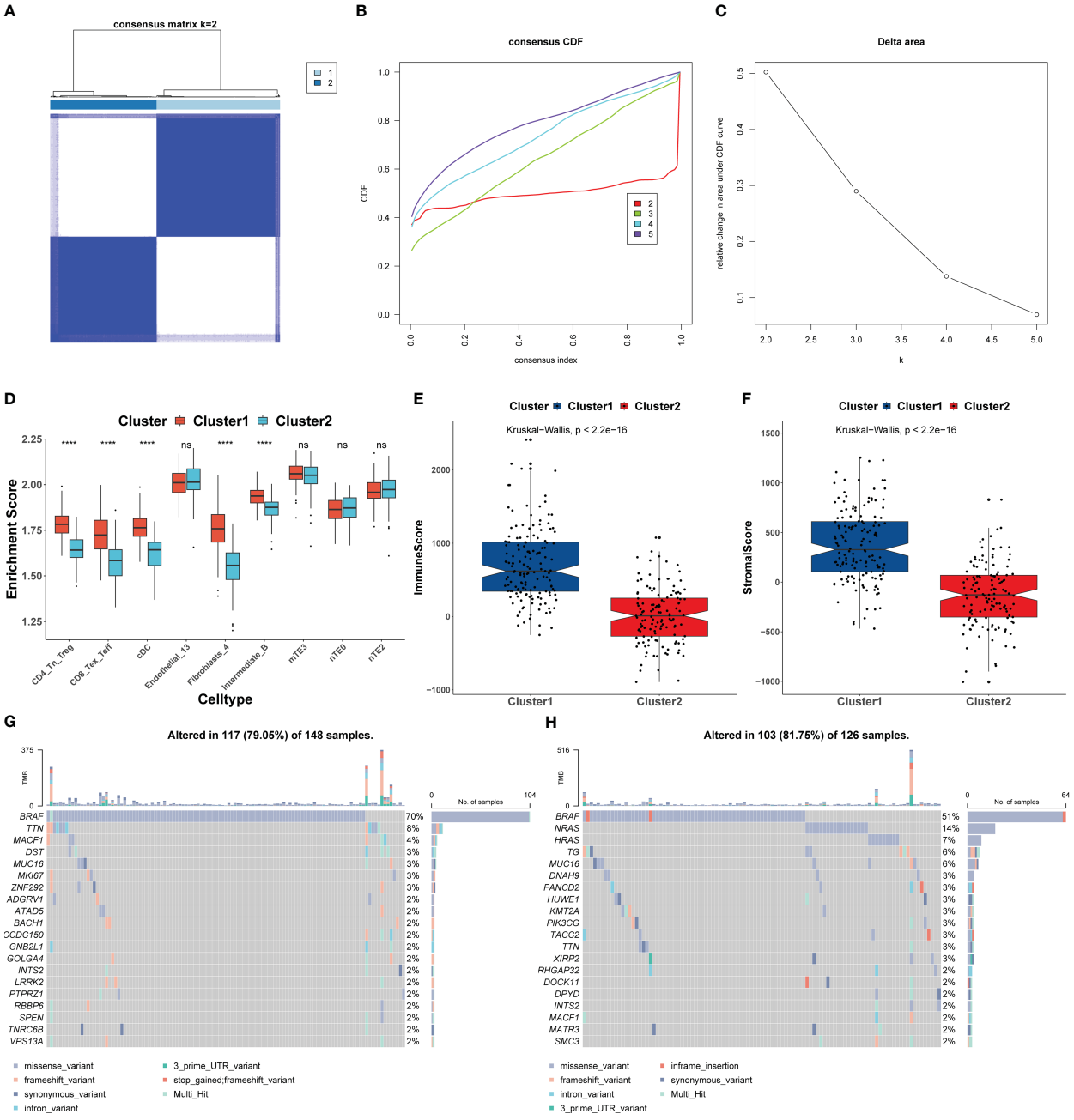

FIGURE 9
Identification of different molecular subtypes based on HASCs. **(A)** Consensus clustering matrix when *K* = 2. **(B)** Consensus clustering CDF with *K* values of 2 to 9. **(C)** Relative change in area under the CDF curve for *K* = 2. **(D)** Box plot of the HASC content between cluster 1 and cluster 2. **(E, F)** Box plot of the difference between immune scores **(E)** and stromal scores **(F)** in subtypes based on the ESTIMATE algorithm. **(G, H)** SNV waterfall of the top 20 (mutation frequency) genes in cluster 1 (*n* = 148) **(G)** and cluster 2 (*n* = 126) **(H)**. *P< 0.05, **P< 0.01, ***P< 0.001, ****P< 0.0001.

by the ESTIMATE algorithm (Figures 9E, F). Previous studies have confirmed that high infiltration of immune cells such as CD8+ T cells and CD4+ T cells predicts better prognosis. Next, we compared the mutation status of cluster 1 and cluster 2 and found that the overall tumor mutation burden (TMB) of cluster 1 was higher, indicating that cluster 1 could benefit better from immunotherapy (38). At the same time, we found that the BRAF gene mutation frequency was the highest in both subgroups, which was consistent with previous studies (6). However, we also found that cluster 1 and cluster 2 showed different mutation patterns. Mutations in cluster 1 mainly occurred in TTN and MACF1 genes, while mutations in cluster 2 mainly occurred in NRAS and HRAS genes of the RAS gene family (Figures 9G, H). The IC50 value of 138 drugs in the Genomics of Drug Sensitivity in Cancer (GDSC) database was predicted based on the expression profile of TCGA-THCA. The top 9 drugs with significant differences in drug sensitivity between

subgroups were shown here, which were BMS.536924 (Figure 10A), parthenolide (Figure 10B), sunitinib (Figure 10C), AICAR (Figure 10D), VX.680 (Figure 10E), paclitaxel (Figure 10F), KU.55933 (Figure 10G), vinblastine (Figure 10H), and BMS.509744 (Figure 10I). Among them, sunitinib, VX.680, paclitaxel, and vinblastine are anticancer drugs, and cluster 1 showed a stronger drug sensitivity to these drugs, indicating that this cluster had a better response to drug treatment, which was consistent with the previous results of higher TMB. The classification of molecular subtypes in TCGA-THCA samples allows us to more precisely target drug therapy, and this new finding will help in the treatment of PTC patients.

4 Discussion

The present investigation addresses a critical gap in our understanding of PTC by leveraging scRNA-seq, transcending the limitations of conventional bulk RNA-seq methodologies that inadequately delineate cellular heterogeneity (39, 40). By

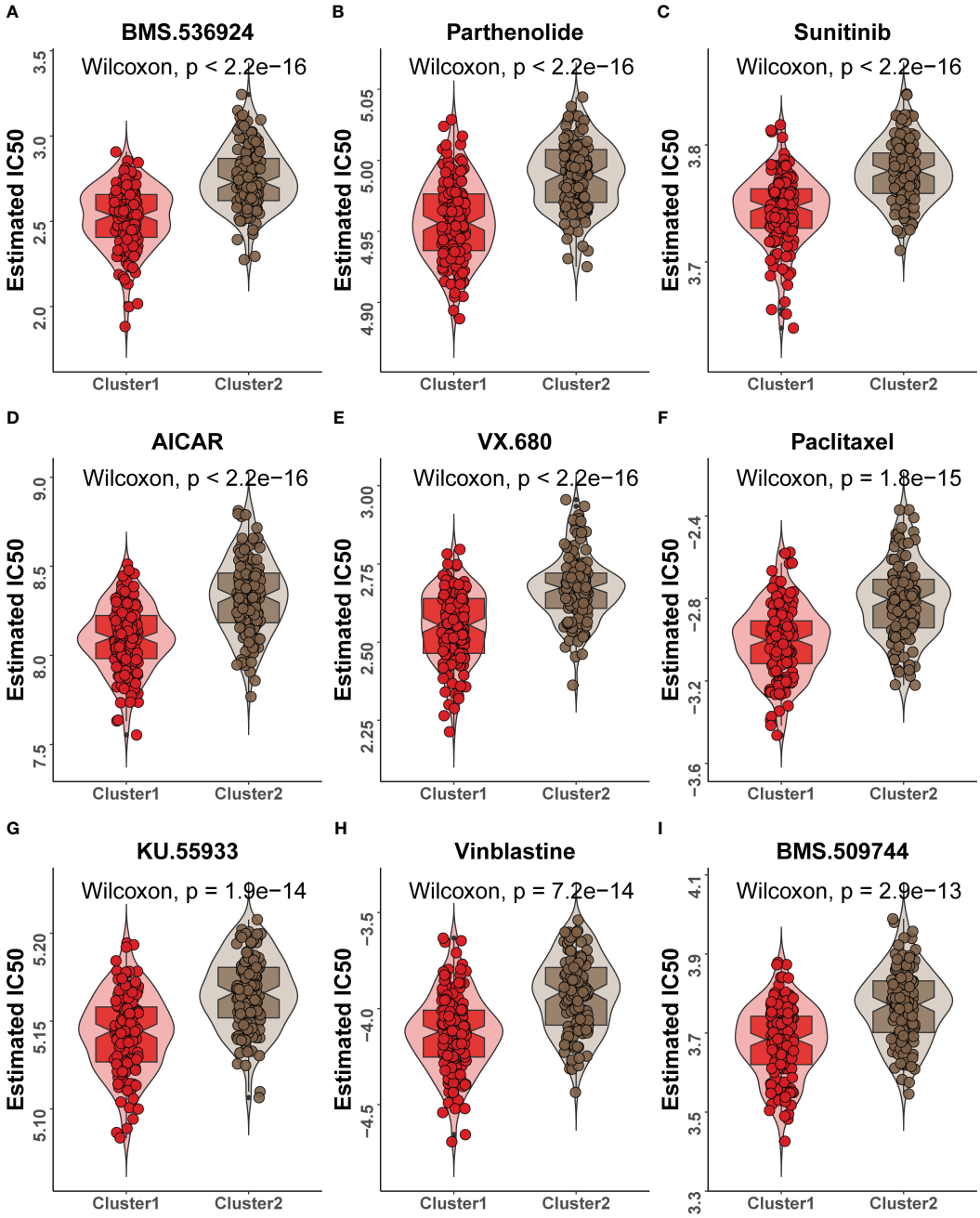

FIGURE 10
Variations in drug sensitivity between cluster 1 and cluster 2. **(A–I)** IC50 box diagram of the nine drugs with significant difference in drug sensitivity in cluster 1 and cluster 2, respectively, in which red indicated cluster 1 and brown indicated cluster 2.

harnessing the high-resolution capabilities of scRNA-seq, we align with prior research highlighting its significance in PTC exploration (41), offering a refined perspective on the disease. Given the autoimmune nature of HT and its potential to modulate immune cell activity—a pivotal factor in PTC management (42)—our study underscores the necessity to elucidate HT's impact on PTC.

Our work innovates in the approach to distinguish malignant from non-malignant cells, a challenge traditionally addressed through inferential CNV analyses in cancer research (25, 43–48). To overcome the impediment of low CNV variability in PTC, we employed *K*-means clustering informed by the statistical significance of differential enrichment scores derived from TCGA data. This novel methodology optimizes CNV-based classification, contributing a robust tool for future scRNA-seq studies.

A pivotal discovery lies in the identification of HT-associated specific cell populations (HASCs). Our findings resonate with the therapeutic efficacy of TSH suppression in PTC management (49), revealing that HASC subsets—marked by mTE3, nTE0, and nTE2 cells enriched in thyroid hormone pathways—are conducive to a TSH-suppressive milieu, thereby affirming HT's positive influence on PTC progression through these cell clusters (50).

Additionally, our study elucidates the intricate interplay between immune and stromal cells with thyroid cells, pinpointing specific cell clusters such as CD4+ Tn Tregs, CD8+ Teff, and others, where the MIF–(CD74+CXCR4) axis emerges as a crucial mediator. This pathway, previously implicated in PTC immunotherapy (51), highlights immune cells' centrality in TSH milieu regulation, underscoring their potential as therapeutic targets. Notably, CD4_Tn_Treg and CD8_Tex_Teff cell subsets were found to play multiple roles in the cellular communication of HASCs, which was consistent with previous studies on the role of T cells in PTC (24).

A preceding meta-analysis has affirmed the differential impacts of immune and stromal cells in the tumor microenvironment (50). Consequently, we ventured to elucidate the prognostic implications of HASCs at the tissue level. Our findings revealed heterogeneous effects of individual cell types on disease prognosis, with CD4+ Tn Tregs, CD8+ Tex Teffs, and mTE3 exhibiting elevated enrichment in M0, T1, and stage I, concurrently associated with younger patient age. No discernible variation was noted concerning gender or N-stage classification. This cellular heterogeneity underscores the complexity of tumor ecosystems, a characteristic well-documented in TCGA-THCA cohorts (51). To further dissect this heterogeneity, molecular stratification emerges as the premier strategy, endorsed extensively in the literature. Thus, consensus clustering was employed to segregate TCGA-THCA cases into two distinct clusters (cluster 1 and cluster 2), where cluster 1 displayed heightened HASC enrichment, indicative of a correlation with HT, an observation corroborated by the ESTIMATE algorithm. Additionally, our investigation of drug responsiveness revealed cluster 1 to be more susceptible to chemotherapeutic agents like sunitinib, VX-680, paclitaxel, and vinblastine, reinforcing the hypothesis that cluster 1 represents HT-positive PTC, with its enriched immune landscape enhancing sensitivity to anticancer therapies, a pivotal insight for therapeutic strategies.

In aggregate, our research constitutes a comprehensive exploration of cellular subset disparities between HT-positive and HT-negative PTC patients at the single-cell resolution. By isolating HASCs from differential cell populations, we facilitated an in-depth examination of intercellular communication dynamics, unearthing regulatory mechanisms. Expanding upon prior studies, we quantified HASC abundance in bulk transcriptomic datasets and conducted cluster analysis on TCGA samples. This work underscores the significance of HT in modulating PTC progression and identifies the MIF–(CD74+CXCR4) axis as a potential therapeutic target. While acknowledging limitations, our study undeniably illuminates the favorable influence of HT on PTC outcomes, thereby furnishing a fresh perspective and theoretical foundation for subsequent inquiries.

Data availability statement

The original contributions presented in the study are included in the article/Supplementary Material. Further inquiries can be directed to the corresponding authors.

Author contributions

HM: Conceptualization, Data curation, Writing – review & editing. GL: Investigation, Methodology, Resources, Validation, Visualization, Writing – original draft, Writing – review & editing. DH: Conceptualization, Writing – original draft. YGS: Resources, Writing – original draft. QJ: Conceptualization, Writing – original draft. YL: Conceptualization, Writing – original draft. YS: Conceptualization, Writing – original draft. DZ: Conceptualization, Writing – original draft. XC: Conceptualization, Writing – original draft.

Funding

The author(s) declare financial support was received for the research, authorship, and/or publication of this article. This research was funded by the National Natural Science Foundation of China (grant numbers 61971166 and 62072144) and the Post-Doctoral Foundation of Heilongjiang Province (grant numbers LBH-Z22207 and LBH-Q20159).

Acknowledgments

At the same time, we thank Dr. Pan Byron Fei from the United States for his help in revising the English language of the article.

Conflict of interest

The authors declare that the research was conducted in the absence of any commercial or financial relationships that could be construed as a potential conflict of interest.

Publisher's note

All claims expressed in this article are solely those of the authors and do not necessarily represent those of their affiliated organizations, or those of the publisher, the editors and the reviewers. Any product that may be evaluated in this article, or claim that may be made by its manufacturer, is not guaranteed or endorsed by the publisher.

Supplementary material

The Supplementary Material for this article can be found online at: https://www.frontiersin.org/articles/10.3389/fendo.2024.1339473/full#supplementary-material

References

1. Pellegriti G, Frasca F, Regalbuto C, Squatrito S, Vigneri R. Worldwide increasing incidence of thyroid cancer: update on epidemiology and risk factors. *J Cancer Epidemiol.* (2013) 2013:965212. doi: 10.1155/2013/965212

2. Bray F, Ferlay J, Soerjomataram I, Siegel RL, Torre LA, Jemal A. Global cancer statistics 2018: GLOBOCAN estimates of incidence and mortality worldwide for 36 cancers in 185 countries. *CA Cancer J Clin.* (2018) 68:394–424. doi: 10.3322/caac.21492

3. Kwak JY, Kim EK, Kim JK, Han JH, Hong SW, Park TS, et al. Dual priming oligonucleotide-based multiplex PCR analysis for detection of BRAFV600E mutation in FNAB samples of thyroid nodules in BRAFV600E mutation-prevalent area. *Head Neck.* (2010) 32:490–8. doi: 10.1002/hed.21210

4. Tiedje V, Fagin JA. Therapeutic breakthroughs for metastatic thyroid cancer. *Nat Rev Endocrinol.* (2020) 16:77–8. doi: 10.1038/s41574-019-0307-2

5. Mehnert JM, Varga A, Brose MS, Aggarwal RR, Lin CC, Prawira A, et al. Safety and antitumor activity of the anti-PD-1 antibody pembrolizumab in patients with advanced, PD-L1-positive papillary or follicular thyroid cancer. *BMC Cancer.* (2019) 19:196. doi: 10.1186/s12885-019-5380-3

6. Kebebew E, Weng J, Bauer J, Ranvier G, Clark OH, Duh QY, et al. The prevalence and prognostic value of BRAF mutation in thyroid cancer. *Ann Surg.* (2007) 246:466–70. doi: 10.1097/SLA.0b013e318148563d

7. Gooden MJ, Bock GH, Leffers N, Daemen T, Nijman HW. The prognostic influence of tumour-infiltrating lymphocytes in cancer: a systematic review with meta-analysis. *Br J Cancer.* (2011) 105:93–103. doi: 10.1038/bjc.2011.189

8. Gentles AJ, Newman AM, Liu CL, Bratman SV, Feng W, Kim D, et al. The prognostic landscape of genes and infiltrating immune cells across human cancers. *Nat Med.* (2015) 21:938–45. doi: 10.1038/nm.3909

9. Gabrilovich DI, Nagaraj S. Myeloid-derived suppressor cells as regulators of the immune system. *Nat Rev Immunol.* (2009) 9:162–74. doi: 10.1038/nri2506

10. Jung KY, Cho SW, Kim YA, Kim D, Oh BC, Park DJ, et al. Cancers with higher density of tumor-associated macrophages were associated with poor survival rates. *J Pathol Transl Med.* (2015) 49:318–24. doi: 10.4132/jptm.2015.06.01

11. Lee EK, Sunwoo JB. Natural killer cells and thyroid diseases. *Endocrinol Metab (Seoul).* (2019) 34:132–7. doi: 10.3803/EnM.2019.34.2.132

12. Gupta S, Patel A, Folstad A, Fenton C, Dinauer CA, Tuttle RM, et al. Infiltration of differentiated thyroid carcinoma by proliferating lymphocytes is associated with improved disease-free survival for children and young adults. *J Clin Endocrinol Metab.* (2001) 86:1346–54. doi: 10.1210/jc.86.3.1346

13. Ahn D, Heo SJ, Park JH, Kim JH, Sohn JH, Park JY, et al. Clinical relationship between Hashimoto's thyroiditis and papillary thyroid cancer. *Acta Oncol.* (2011) 50:1228–34. doi: 10.3109/0284186X.2011.602109

14. Konturek A, Barczyński M, Wierzchowski W, Stopa M, Nowak W. Coexistence of papillary thyroid cancer with Hashimoto thyroiditis. *Langenbecks Arch Surg.* (2013) 398:389–94. doi: 10.1007/s00423-012-1021-x

15. Lee JH, Kim Y, Choi JW, Kim YS. The association between papillary thyroid carcinoma and histologically proven Hashimoto's thyroiditis: a meta-analysis. *Eur J Endocrinol.* (2013) 168:343–9. doi: 10.1530/EJE-12-0903

16. Zhang Y, Dai J, Wu T, Yang N, Yin Z. The study of the coexistence of Hashimoto's thyroiditis with papillary thyroid carcinoma. *J Cancer Res Clin Oncol.* (2014) 140:1021–6. doi: 10.1007/s00432-014-1629-z

17. Resende de Paiva C, Grønhøj C, Feldt-Rasmussen U, von Buchwald C. Association between Hashimoto's thyroiditis and thyroid cancer in 64,628 patients. *Front Oncol.* (2017) 7:53. doi: 10.3389/fonc.2017.00053

18. Peng M, Wei G, Zhang Y, Li H, Lai Y, Guo Y, et al. Single-cell transcriptomic landscape reveals the differences in cell differentiation and immune microenvironment of papillary thyroid carcinoma between genders. *Cell Biosci.* (2021) 11:39. doi: 10.1186/s13578-021-00549-w

19. Ceolin L, Siqueira DR, Romitti M, Ferreira CV, Maia AL. Molecular basis of medullary thyroid carcinoma: the role of RET polymorphisms. *Int J Mol Sci.* (2012) 13:221–39. doi: 10.3390/ijms13010221

20. Mohammadi M, Hedayati M. A brief review on the molecular basis of medullary thyroid carcinoma. *Cell J.* (2017) 18:485–92. doi: 10.22074/cellj.2016.4715

21. Luo H, Xia X, Kim GD, Liu Y, Xue Z, Zhang L, et al. Characterizing dedifferentiation of thyroid cancer by integrated analysis. *Sci Adv.* (2021) 7. doi: 10.1126/sciadv.abf3657

22. Barrett T, Wilhite SE, Ledoux P, Evangelista C, Kim IF, Tomashevsky M, et al. NCBI GEO: archive for functional genomics data sets–update. *Nucleic Acids Res.* (2013) 41:D991–5. doi: 10.1093/nar/gks1193

23. Stuart T, Butler A, Hoffman P, Hafemeister C, Papalexi E, Mauck WM, et al. Comprehensive integration of single-cell data. *Cell.* (2019) 177:1888–902. doi: 10.1016/j.cell.2019.05.031

24. Pu W, Shi X, Yu P, Zhang M, Liu Z, Tan L, et al. Single-cell transcriptomic analysis of the tumor ecosystems underlying initiation and progression of papillary thyroid carcinoma. *Nat Commun.* (2021) 12:6058. doi: 10.1038/s41467-021-26343-3

25. Patel AP, Tirosh I, Trombetta JJ, Shalek AK, Gillespie SM, Wakimoto H, et al. Single-cell RNA-seq highlights intratumoral heterogeneity in primary glioblastoma. *Science.* (2014) 344:1396–401. doi: 10.1126/science.1254257

26. Qiu X, Hill A, Packer J, Lin D, Ma YA, Trapnell C. Single-cell mRNA quantification and differential analysis with Census. *Nat Methods.* (2017) 14:309–15. doi: 10.1038/nmeth.4150

27. Jin S, Guerrero-Juarez CF, Zhang L, Chang I, Ramos R, Kuan CH, et al. Inference and analysis of cell-cell communication using CellChat. *Nat Commun.* (2021) 12:1088. doi: 10.1038/s41467-021-21246-9

28. Goldman MJ, Craft B, Hastie M, Repecka K, McDade F, Kamath A, et al. Visualizing and interpreting cancer genomics data via the Xena platform. *Nat Biotechnol.* (2020) 38:675–8. doi: 10.1038/s41587-020-0546-8

29. Wilkerson MD, Hayes DN. ConsensusClusterPlus: a class discovery tool with confidence assessments and item tracking. *Bioinformatics.* (2010) 26:1572–3. doi: 10.1093/bioinformatics/btq170

30. Aran D, Sirota M, Butte AJ. Systematic pan-cancer analysis of tumour purity. *Nat Commun.* (2015) 6:8971. doi: 10.1038/ncomms9971

31. Zeng D, Ye Z, Shen R, Yu G, Wu J, Xiong Y, et al. IOBR: multi-omics immuno-oncology biological research to decode tumor microenvironment and signatures. *Front Immunol.* (2021) 12:687975. doi: 10.3389/fimmu.2021.687975

32. Mayakonda A, Lin DC, Assenov Y, Plass C, Koeffler HP. Maftools: efficient and comprehensive analysis of somatic variants in cancer. *Genome Res.* (2018) 28:1747–56. doi: 10.1101/gr.239244.118

33. Geeleher P, Cox N, Huang RS. pRRophetic: an R package for prediction of clinical chemotherapeutic response from tumor gene expression levels. *PloS One.* (2014) 9:e107468. doi: 10.1371/journal.pone.0107468

34. Ferrari SM, Fallahi P, Elia G, Ragusa F, Ruffilli I, Paparo SR, et al. Thyroid autoimmune disorders and cancer. *Semin Cancer Biol.* (2020) 64:135–46. doi: 10.1016/j.semcancer.2019.05.019

35. de Candia P, Procaccini C, Russo C, Lepore MT, Matarese G. Regulatory T cells as metabolic sensors. *Immunity.* (2022) 55:1981–92. doi: 10.1016/j.immuni.2022.10.006

36. Lavie D, Ben-Shmuel A, Erez N, Scherz-Shouval R. Cancer-associated fibroblasts in the single-cell era. *Nat Cancer.* (2022) 3:793–807. doi: 10.1038/s43018-022-00411-z

37. Sajid A, Rahman H, Ambudkar SV. Advances in the structure, mechanism and targeting of chemoresistance-linked ABC transporters. *Nat Rev Cancer.* (2023) 23:762–779. doi: 10.1038/s41568-023-00612-3

38. Anagnostou V, Bardelli A, Chan TA, Turajlic S. The status of tumor mutational burden and immunotherapy. *Nat Cancer*. (2022) 3:652–6. doi: 10.1038/s43018-022-00382-1

39. He J, Zhou M, Yin J, Wan J, Chu J, Jia J, et al. METTL3 restrains papillary thyroid cancer progression via m(6)A/c-Rel/IL-8-mediated neutrophil infiltration. *Mol Ther*. (2021) 29:1821–37. doi: 10.1016/j.ymthe.2021.01.019

40. Buj R, Mallona I, Díez-Villanueva A, Zafon C, Mate JL, Roca M, et al. Kallikreins stepwise scoring reveals three subtypes of papillary thyroid cancer with prognostic implications. *Thyroid*. (2018) 28:601–12. doi: 10.1089/thy.2017.0501

41. Wang T, Shi J, Li L, Zhou X, Zhang H, Zhang X, et al. Single-cell transcriptome analysis reveals inter-tumor heterogeneity in bilateral papillary thyroid carcinoma. *Front Immunol*. (2022) 13:840811. doi: 10.3389/fimmu.2022.840811

42. Ehlers M, Schott M. Hashimoto's thyroiditis and papillary thyroid cancer: are they immunologically linked? *Trends Endocrinol Metab*. (2014) 25:656–64. doi: 10.1016/j.tem.2014.09.001

43. Chen K, Wang Y, Hou Y, Wang Q, Long D, Liu X, et al. Single cell RNA-seq reveals the CCL5/SDC1 receptor-ligand interaction between T cells and tumor cells in pancreatic cancer. *Cancer Lett*. (2022) 545:215834. doi: 10.1016/j.canlet.2022.215834

44. Liu Y, He S, Wang XL, Peng W, Chen QY, Chi DM, et al. Tumour heterogeneity and intercellular networks of nasopharyngeal carcinoma at single cell resolution. *Nat Commun*. (2021) 12:741. doi: 10.1038/s41467-021-21043-4

45. Puram SV, Tirosh I, Parikh AS, Patel AP, Yizhak K, Gillespie S, et al. Single-cell transcriptomic analysis of primary and metastatic tumor ecosystems in head and neck cancer. *Cell*. (2017) 171:1611–1624 e24. doi: 10.1016/j.cell.2017.10.044

46. Müller S, Liu SJ, Di Lullo E, Malatesta M, Pollen AA, Nowakowski TJ, et al. Single-cell sequencing maps gene expression to mutational phylogenies in PDGF- and EGF-driven gliomas. *Mol Syst Biol*. (2016) 12:889. doi: 10.15252/msb.20166969

47. Tirosh I, Venteicher AS, Hebert C, Escalante LE, Patel AP, Yizhak K, et al. Single-cell RNA-seq supports a developmental hierarchy in human oligodendroglioma. *Nature*. (2016) 539:309–13. doi: 10.1038/nature20123

48. Chen YP, Yin JH, Li WF, Li HJ, Chen DP, Zhang CJ, et al. Single-cell transcriptomics reveals regulators underlying immune cell diversity and immune subtypes associated with prognosis in nasopharyngeal carcinoma. *Cell Res*. (2020) 30:1024–42. doi: 10.1038/s41422-020-0374-x

49. Gild ML, Bullock M, Robinson BG, Clifton-Bligh R. Multikinase inhibitors: a new option for the treatment of thyroid cancer. *Nat Rev Endocrinol*. (2011) 7:617–24. doi: 10.1038/nrendo.2011.141

50. Xu J, Ding K, Mu L, Huang J, Ye F, Peng Y, et al. Hashimoto's thyroiditis: A "Double-edged sword" in thyroid carcinoma. *Front Endocrinol (Lausanne)*. (2022) 13:801925. doi: 10.3389/fendo.2022.801925

51. Minna E, Romeo P, Dugo M, De Cecco L, Todoerti K, Pilotti S, et al. Correction: miR-451a is underexpressed and targets AKT/mTOR pathway in papillary thyroid carcinoma. *Oncotarget*. (2018) 9:12534. doi: 10.18632/oncotarget.v9i15

frontiers | Frontiers in Endocrinology

TYPE Original Research
PUBLISHED 24 January 2025
DOI 10.3389/fendo.2025.1508404

OPEN ACCESS

EDITED BY
Marialuisa Appetecchia,
Hospital Physiotherapy Institutes (IRCCS), Italy

REVIEWED BY
Poupak Fallahi,
University of Pisa, Italy
Marina Muzzaltalian,
Auxological Institute (IRCCS), Italy

*CORRESPONDENCE
Yu Wu
headandneck2018@126.com

RECEIVED 09 October 2024
ACCEPTED 02 January 2025
PUBLISHED 24 January 2025

CITATION
Liu J, Gao W, Zheng X, Wu S, Shi Y, Wang F and Wu Y (2025) Molecular testing stratifies the risk of structural recurrence in high risk differentiated thyroid cancer: a retrospective cohort study.
Front. Endocrinol. 16:1508404.
doi: 10.3389/fendo.2025.1508404

Molecular testing stratifies the risk of structural recurrence in high risk differentiated thyroid cancer: a retrospective cohort study

Jie Liu[1], Wensi Gao[2], Xiong Zheng[1], Shuping Wu[1], Yi Shi[3], Feng Wang[1] and Yu Wu[1]*

[1]Department of Head and Neck Surgery, Clinical Oncology School of Fujian Medical University, Fujian Cancer Hospital, Fuzhou, China, [2]Department of Breast Surgery, Clinical Oncology School of Fujian Medical University, Fujian Cancer Hospital, Fuzhou, China, [3]Department of Molecular Pathology, Clinical Oncology School of Fujian Medical University, Fujian Cancer Hospital, Fuzhou, China

Background: High-risk differentiated thyroid cancer in 2015 American Thyroid Association risk stratification system (ATA-RSS) exhibits a significantly increased probability of recurrence and poor outcomes. This study aimed to investigate the molecular profiles of high-risk differentiated thyroid cancer and to assess the role of molecular testing in enhancing prognostic risk stratification.

Methods: In a single-center study conducted at Fujian Cancer Hospital, Fujian Province, China, a consecutive cohort of differentiated thyroid cancer patients identified as high-risk under 2015 ATA-RSS criteria were retrospectively assessed, spanning from November 1, 2019, to March 31, 2022. Molecular characterize groups were conducted using an 18-gene next-generation sequencing assay. Patients harboring mutations in the *TERT* promoter, *TP53*, or *PIK3CA* genes were categorized as the high molecular risk group, while all others were assigned to the non-high molecular risk group.

Results: Among the 108 cases, 32 (29.6%) fell into the high molecular risk group, characterized by a significantly older mean age (57.8 vs. 42.6 years, $p < 0.001$), larger tumor size (3.1 cm vs. 2.0 cm, $p = 0.003$), a higher incidence of aggressive pathological subtypes (43.8% vs. 7.9%, $p < 0.001$), and an increased occurrence of distant metastasis (34.4% vs. 7.9%, $p = 0.001$). Over a median follow-up period of 32.5 months, this high-risk group demonstrated an elevated risk of local recurrence (32.1% vs. 9.5%, HR: 3.18, 95% CI: 1.15-8.78) and metachronous distant metastasis (38.1% vs. 2.9%, HR: 12.54, 95% CI: 2.60-60.41). Multivariate COX regression analysis confirmed that molecular characterize groups (HR: 5.77, 95% CI: 2.18-15.23, $p < 0.001$) and tumor size (HR: 1.32, 95% CI: 1.00-1.74, $p = 0.047$) independently predicted recurrence-free survival.

Conclusion: ATA-RSS high-risk differentiated thyroid cancer often presents with late-hit genetic alterations, which are strongly associated with increased likelihood of structural recurrence. Molecular testing offers a precise approach to recurrence risk stratification in high-risk cases, enabling personalized follow-up and treatment strategies tailored to the specific prognostic profile.

KEYWORDS

thyroid cancer, risk stratification, molecular testing, recurrence, molecular profile

1 Introduction

Thyroid cancer has demonstrated the most rapid rise in incidence among endocrine malignancies globally in recent decades. By 2020, the global incidence surpassed 500,000 new cases annually, with over 200,000 in China alone (1, 2). Despite differentiated thyroid cancer (DTC) comprising the majority of cases, often associated with favorable outcomes and low mortality, a subset of patients will experience relapse or metastasis, developing resistance to radioactive iodine (RAI), thus creating a substantial therapeutic obstacle (3). Postoperative management of DTC now primarily relies on risk-based assessments, prioritizing individualized approaches and ongoing adjustments. Prognostic evaluation is currently guided by the 8th edition of the American Joint Committee on Cancer Tumor-Node-Metastasis (AJCC TNM) staging system and the 2015 American Thyroid Association risk stratification system (ATA RSS), both of which are widely adopted methodologies (4). The 8th edition of the AJCC TNM staging system provides a more precise reflection of mortality risk. However, for evaluating postoperative recurrence risk in DTC patients with favorable prognoses, greater reliance on supplementary risk assessment tools is warranted (5). The 2015 ATA RSS serves as a key prognostic framework following DTC surgery. In a study with a median follow-up of 4 years, 31% of patients in the ATA high-risk group achieved no evidence of disease (NED), compared to 52% in the intermediate-risk group and 78% in the low-risk group (6). A separate short-term study reported recurrence rates of 22.8%, 6.7%, and 2.9% for the high-, intermediate-, and low-risk groups, respectively (7). These findings indicate that the ATA RSS stratifies recurrence risk with greater precision. In various regions, including China, the ATA RSS remains a foundational tool for postoperative risk assessment. However, the ATA RSS framework omits several critical individual variables, such as pathological subtypes, multifocality, extranodal invasion, and molecular profiles, resulting in substantial prognostic variability even among cases classified within the same risk group (4). Continued research and accumulating evidence are required to refine and enhance the accuracy of this stratification system. In the three risk classes, persistent and recurrent lesions frequently occur in high-risk DTC cases, posing significant obstacles to effective treatment (8, 9). Further investigation into prognostic factors for patients within this risk category remains essential.

Research into the molecular mechanisms of thyroid cancer has evolved over several decades, with early studies identifying key mutations in *BRAF* and *RAS*, along with fusion events in the *RET* and *NTRK* genes (10, 11). These genetic alterations critically affect the clinical and pathological characteristics of thyroid cancer by activating the mitogen activated protein kinase (MAPK) and/or PI3K/AKT/mTOR signaling pathways. Such oncogene mutations are present throughout all stages of thyroid cancer and are now recognized as early drivers of tumorigenesis (12). Molecular diagnostic tools that detect common early driver genes, such as *BRAF* V600E, *RAS*, *RET*, and *PAX8*/*PPARG*, when combined with fine needle aspiration biopsy (FNAB), have been shown to substantially enhance diagnostic accuracy, a finding supported by numerous studies and widely accepted in the field (13–16). Some of these driver alterations, such as *BRAF* V600E, *RET*, *NTRK* fusion, and *ALK* fusion, also serve as therapeutic targets for selective kinase inhibitors. Compared to multi-targeted kinase inhibitors, these agents are often preferred due to their superior efficacy and safety profiles, underscoring the heightened clinical value of molecular testing in managing aggressive and RAI-refractory thyroid cancers (17). Mutations in the PI3K/AKT/mTOR pathway, including *PIK3CA*, *AKT1* and *PTEN* are infrequent in thyroid cancer, though they can act as early driver mutations in certain RAS-like subtypes. More commonly, however, they co-occur with other driver mutations in advanced, poorly differentiated cases (12, 18). Additionally, mutations in the *TERT* promoter (*TERT*p) and tumor suppressor genes like *TP53* and *CNKN2A* frequently co-mutate with driver genes. These mutations are closely linked to adverse prognostic indicators, such as recurrence, metastasis, and iodine resistance. Importantly, they are regarded as late-stage mutations that drive thyroid cancer dedifferentiation and progression to high-grade or undifferentiated forms (12, 18). These previous findings have enabled prognostic stratification of certain thyroid cancers through the integration of specific genetic markers in molecular testing. In recent years, several studies have sought to elucidate the association between the molecular profiles of thyroid cancer and clinical risk and prognosis. Yip et al. conducted a case-control study

analyzing the genetic variation in DTC patients with distant metastases, proposing molecular risk stratification based on these variations, with distinct groups showing differing predicted rates of distant metastasis (19). Liu et al. and Schumm et al. further validated the relationship between this molecular risk stratification and tumor recurrence through retrospective cohort studies (7, 20). Collectively, these studies have highlighted the feasibility of molecular testing in enhancing current risk assessment models and introduced novel perspectives for its application in thyroid cancer management.

The molecular profiles of ATA high-risk DTC patients and its association with prognosis remain unexplored. This retrospective cohort study analyzed the clinical characteristics and follow-up data of ATA high-risk individuals who underwent 18-gene next-generation sequencing (NGS) test, aiming to evaluate the potential of incorporating molecular profiles to refine postoperative recurrence risk stratification in this high-risk population.

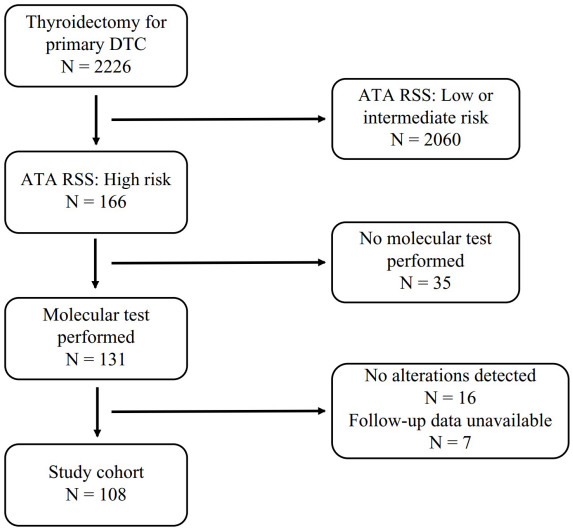

FIGURE 1
Flowchart of patient inclusion and exclusion. DTC, Differentiated Thyoid Cancer; ATA RSS, 2015 ATA Risk Stratification System.

2 Materials and methods

2.1 Patients and clinicopathologic data

This retrospective cohort study analyzed medical records from consecutive patients who underwent primary thyroidectomy with a pathological diagnosis of DTC at Fujian Cancer Hospital, Fujian Province, China, between November 1, 2019, and March 31, 2022, utilizing the hospital's electronic medical record system. This study was approved by the Ethics Committee of Fujian Cancer Hospital, Fuzhou, China (Ethics Number: K2024-400-01). Preoperative assessment, surgical extent, and postoperative management adhered to the 2015 ATA guidelines and the Chinese National Health Commission's thyroid cancer diagnosis and treatment protocols. The ATA high-risk category was assigned based on the criteria outlined in the 2015 ATA guidelines (4). This retrospective cohort study analyzed medical records from consecutive patients who underwent primary thyroidectomy with a pathological diagnosis of DTC at Fujian Cancer Hospital, Fujian Province, China, between November 1, 2019, and March 31, 2022, utilizing the hospital's electronic medical record system. Preoperative assessment, surgical extent, and postoperative management adhered to the 2015 ATA guidelines and the Chinese National Health Commission's thyroid cancer diagnosis and treatment protocols. The ATA high-risk category was assigned based on the criteria outlined in the 2015 ATA guidelines (Figure 1). Preoperative variables included patient age, sex, and tumor size. Imaging results from Doppler ultrasound, computed tomography (CT), and magnetic resonance imaging were assessed to verify the characteristics of the primary tumor, lymph node involvement, and distant metastasis. Surgical records were examined to determine macroscopic extrathyroidal extension (ETE) and extranodal extension (ENE) based on descriptions of primary tumors and regional lymph nodes. Postoperative pathology reports, reviewed by experienced pathologists, provided confirmation of pathological subtypes, lymph node metastasis, ETE, ENE, multifocality, and other relevant data. Notably, since molecular testing was conducted postoperatively, pathologists were unaware of these molecular findings at the time of initial pathological diagnosis of surgical specimens.

2.2 Molecular testing and molecular characterize groups

Molecular testing for thyroid tumors has not been routinely integrated into the diagnostic and therapeutic protocols in China. At our institution, such testing was recommended post-surgery for cases identified as high risk according to ATA RSS, where its potential clinical benefit was considered substantial. Patients were fully briefed on the associated costs and clinical implications, followed by informed consent if they opted for the testing. Sequencing libraries were constructed using the thyroid cancer 18-genes panel (RigenBio) in adherence to the manufacturer's protocol. This panel, a multiplex PCR-based NGS assay, was designed to detect point mutations, insertions/deletions, and gene fusions across 18 genes implicated in thyroid cancer, including *AKT1*, *BRAF*, *CTNNB1*, *EZH1*, *GNAS*, *HRAS*, *KRAS*, *NRAS*, *NTRK*, *PAX8/PPARG*, *RET*, *PIK3CA*, *PTEN*, *SPOP*, *TERT*p, *TP53*, *TSHR*, and *ZNF148*. Genomic DNA and total RNA were extracted from formalin-fixed, paraffin-embedded (FFPE) thyroid nodule specimens utilizing the FFPE DNA/RNA Extraction Kit (RigenBio). Total RNA was reverse-transcribed into cDNA, and both DNA and cDNA were amplified via multiplex PCR targeting specific genomic regions. Each amplified library underwent indexing and adapter ligation through an additional round of PCR. Purified indexed libraries were quantified using a Qubit fluorometer (Thermo Fisher), and sequencing was performed on the NovaSeq 6000 platform (Illumina) with 150 bp paired-end reads. Adapter sequences at the 3' and 5' ends of the reads were

trimmed using Trimmomatic (v0.38) prior to alignment. SNV and InDel calling was performed using VarScan (v2.3.9), and variants were annotated with VEP. Gene fusions were identified by analyzing fusion transcript sequences with a customized script. Following previously reported molecular risk stratification methods (7, 20–22) and integrating the molecular variation data from this study, molecular characterize groups (MCGs) were categorized based on missense mutations, insertions/deletions, and gene fusions identified in molecular testing. Cases with "negative" molecular testing results were excluded from the study cohort. Patients harboring any of the four gene mutations—*TERT*p, *TP53*, *PIK3CA*, and *AKT1*—were classified into the high molecular risk (HMR) group, while those without these mutations were assigned to the non-HMR group.

2.3 Postoperative management and follow-up

Postoperative assessments were conducted to classify pTNM stage followed the AJCC 8th edition. During follow-up, abnormal neck findings on ultrasound or CT were further evaluated using ultrasound-guided FNAB to confirm structural recurrence (SR). Local recurrence encompassed lymph node metastasis in the neck and upper mediastinum, as well as other thyroid-originating lesions in these regions. Metachronous distant metastasis was primarily identified through biochemical markers, including serum thyroglobulin and thyroglobulin antibodies, alongside imaging modalities such as CT and RAI whole-body scans. Final diagnoses were made by a multidisciplinary team consisting of specialists in thyroid surgery, endocrinology, radiotherapy, radiology, and pathology. The diagnosis of RAI-refractory disease adhered to the criteria specified in the 2015 ATA guidelines (4). The study assessed all-cause mortality using data from medical records and telephone follow-ups, with the endpoint defined as the date of the patient's last follow-up or death. The follow-up records were concluded as of March 31, 2024.

2.4 Statistical analysis

Normally distributed continuous variables were presented as mean ± standard deviation, and inter-group differences were assessed via Student's t-test. For non-normally distributed variables, data were expressed as median ± interquartile range (IQR), with the Mann-Whitney U test used for between-group comparisons. Categorical variables were evaluated using the χ^2 test, with Fisher's exact test applied when necessary. Univariate logistic regression was employed to assess the association between MCGs and both local recurrence and metachronous distant metastasis. The Kaplan-Meier method was applied to assess the relationship between MCGs and recurrence-free survival (RFS). For the COX regression model, univariate regression analysis initially identified potential variables associated with RFS, focusing on established prognostic factors such as age (<55 or ≥55 years), gender, tumor size (cm), pathological subtype, multifocality, ETE, ENE, N stage, and RAI ablation (23, 24). To avoid omitting potential prognostic variables that could be correlated with the outcome in the multivariable analysis, we have relaxed the significance threshold for this step to $p < 0.10$, variables with $p \geq 0.10$ were excluded. Multivariate analysis then incorporated the remaining variables from the univariate screening alongside MCGs. A proportional hazard regression model was constructed using the likelihood ratio test (Forward: LR) with maximum partial likelihood estimation to identify independent factors related to RFS. Statistical analysis and visualization were performed using IBM SPSS Statistics version 22.0 (IBM Corp., NY, USA). All statistical tests were two-sided, with $p < 0.05$ deemed statistically significant.

3 Results

3.1 Clinical features

In a cohort of 108 ATA high-risk DTC patients, 59 (54.6%) were female, with a mean age of 47.1 years (SD: 14.6) and a median tumor size of 2.1 cm (IQR: 1.3–4.0). The majority of patients (97.2%) underwent total thyroidectomy with concurrent cervical lymph node dissection, while 3 patients received lobectomy with central lymph node dissection. Postoperative pathology confirmed papillary thyroid carcinoma (PTC) in 105 cases (97.2%), of which 17 (15.7%) exhibited invasive features, including 16 tall cell and 1 columnar cell variant. The remaining 3 cases were identified as widely invasive follicular thyroid carcinoma (FTC). In this cohort, high-risk ATA criteria encompassed macroscopic ETE (93.5%), distant metastasis (14.8%), metastatic lymph nodes with a maximum diameter ≥3 cm (13.9%), incomplete tumor resection (5.6%), FTC exhibiting more than 4 vascular invasions (2.8%), and postoperative serum thyroglobulin (Tg) levels suggestive of distant metastasis (1.9%). Most cases presented with central (89.8%) or lateral neck (54.6%) lymph node metastasis. Among the 17 cases with initial distant metastasis, lung involvement predominated (82.4%), followed by bone metastasis (23.5%). Other metastatic sites included the abdomen and brain, with one case each (5.9%). Among the clinical characteristics, 48 cases (44.4%) presented with ENE, and 70 cases (64.8%) exhibited multifocal lesions. Three patients who initially underwent thyroid lobectomy did not proceed with the recommended total thyroidectomy. Postoperative assessment, which included imaging and RAI whole-body scans for cases with elevated Tg levels, identified 90 patients (83.3%) as NED. Of these, 71.1% underwent RAI ablation or adjuvant therapy as prescribed, while the remainder received only thyroid-stimulating hormone suppression therapy and routine follow-up. The 18 patients with unresectable locally persistent disease or distant metastasis were treated with therapeutic RAI.

3.2 Molecular profiles and molecular characterize groups

A total of 134 genetic variants across eight genes were identified in the study cohort, including 93 missense mutations, 26 upstream

promoter mutations, and 15 fusion mutations, with the *BRAF* V600E mutation being the most prevalent (75%), followed by *TERT*p mutations (24.1%), *RET* fusions (12.0%), and *PIK3CA* mutations (5.6%) (Figure 2). Early driver mutations, such as *BRAF* V600E, *RET* fusion, *NTRK* fusion, and *KRAS*/*NRAS* mutations, were present in 92.6% of cases. Of the 8 cases with unidentified driver genes, 7 exhibited the single *TERT*p C228T mutation, while 1 presented with the single *TP53* E271K mutation. Based on the MCGs outlined earlier, 32 cases (29.6%) were assigned to the HMR group, and the remaining 76 cases were categorized as non-HMR. The HMR group demonstrated an older mean age (57.8 vs. 42.6, $p < 0.001$), more aggressive pathological subtypes (43.8% vs. 7.9%, $p < 0.001$), larger primary tumors (3.1 cm vs. 2.0 cm, $p = 0.003$), and a greater incidence of distant metastasis (34.4% vs. 7.9%, $p = 0.001$) (Table 1). Postoperatively, fewer patients in the HMR group achieved NED status (65.6% vs. 90.8%, $p = 0.001$). In cases achieving NED after initial treatment, 81.0% of the HMR group and 68.1% of the non-HMR group completed RAI ablation or adjuvant therapy, with no statistically significant difference observed between the groups ($p = 0.256$). A significant difference was found in ETE ($p = 0.025$), where 97.4% of the non-HMR group exhibited macroscopic ETE, compared to 84.4% in the HMR group. The female proportion was 40.6% in the HMR group and 60.5% in the non-HMR group, but this difference lacked statistical significance ($p = 0.058$). Regarding initial surgery, incomplete local tumor resection occurred in 12.5% of the HMR group and 2.6% of the non-HMR group, though this difference was also not statistically significant ($p = 0.062$).

3.3 Outcomes

As of March 31, 2024, the median follow-up for the 108 cases was 32.5 months (IQR: 28–38), with no statistically significant difference in follow-up duration across groups ($p = 0.159$) (Table 2). In the HMR group, 17 cases (53.1%) and in the non-HMR group, 8 cases (10.5%) underwent therapeutic RAI for distant metastases or inoperable local lesions. Among these, 13 cases (76.5%) in the HMR group and 3 cases (37.5%) in the non-HMR group met RAI refractory criteria, although this difference did not reach statistical significance ($p = 0.075$). The HMR group exhibiting an elevated risk of local recurrence (HR: 3.18, 95% CI: 1.15-8.78) and metachronous distant metastasis (HR: 12.54, 95% CI: 2.60-60.41). Survival analysis indicated a strong association between MCGs and RFS ($p < 0.001$) (Figure 3). As described above, we first performed univariate analysis to preliminarily screen the initially identified variables, the results suggested that age, tumor size, N stage, and invasive pathological subtype may influence RFS ($p < 0.10$). Upon constructing the multivariate regression model, only MCGs (HR: 5.77, 95% CI: 2.18-15.23) and tumor size (HR: 1.32, 95% CI: 1.00-1.74) emerged as independent factors associated with RFS. During the follow-up period, 3 patients (9.4%) in the HMR group died, with survival times of 7, 15, and 22 months, respectively, all deaths attributable to the tumor. No deaths occurred in the non-HMR group, and the difference in mortality between the groups was statistically significant ($p = 0.039$).

4 Discussion

ATA high-risk cases in DTC pose significant treatment challenges and are associated with poorer outcomes. Research on these high-risk cases remains limited, with considerable variation in reported characteristics across studies. A Dutch single-center study by Van Velsen et al., involving 236 ATA high-risk DTC patients, identified FTC in 32% of cases, ETE in 32%, cervical lymph node dissection in 45%, and distant metastasis in 33% (19). In contrast, a retrospective single-center study by Shah et al. in the United States, analyzing 320 ATA high-risk DTC cases, reported FTC in 4.1%, ETE in 94%, cervical lymph node metastasis (N1a+N1b) in 62.5%, and distant metastasis in 13.4%. The cohort characteristics observed in this study align with those reported by Shah et al., with a minimal

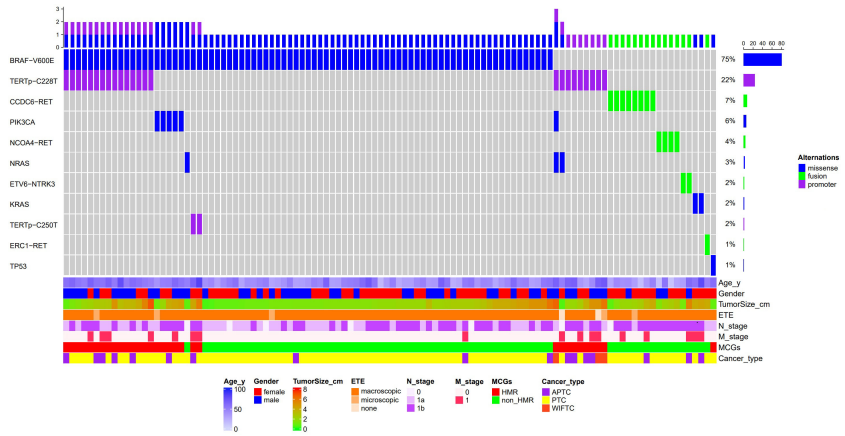

FIGURE 2
Waterfall plot of molecular profiles and clinical features of 108 patients with ATA high risk differentiated thyroid cancer. ETE, Extrathyroidal extension; MCGs, Molecular characterize groups; HMR, High Molecular Risk; APTC, aggressive papillary thyroid cancer; PTC, papillary thyroid cancer; WIFTC, widely invasive follicular thyroid cancer.

10.3389/fendo.2025.1508404

TABLE 1 Demographic characteristics and clinical features of patients with ATA high risk differentiated thyroid cancer at initial surgery by Molecular Characterize Groups.

Variable		Molecular characterize groups, No. (%)		*p*
		Non-HMR	HMR	
No. of patients		76(70.4)	32(29.6)	
Age(Mean ± SD, years)		42.6 ± 13.4	57.8 ± 11.6	<0.001
SEX	Female	46(60.5)	13(40.6)	0.058
Cancer type	Non-Aggressive PTC,	70(92.1)	18(56.3)	<0.001
	Aggressive PTC	6(7.9)	11(34.4)	
	Widely invasive FTC	0	3(9.4)	
Initial surgery	Lobectomy and CND	2(2.6)	1(3.1)	0.959
	Total thyroidectomy and CND	33(43.4)	13(40.6)	
	Total thyroidectomy and LND	41(53.9)	18(56.3)	
	R2 resection	2(2.6)	4(12.5)	0.062
T stage	1	1(1.3)	2(6.3)	0.452
	2	1(1.3)	1(3.1)	
	3	30(39.5)	13(40.6)	
	4	44(57.9)	16(50.0)	
N stage	0	6(7.9)	1(3.1)	0.655
	1a	29(38.2)	13(40.6)	
	1b	41(53.9)	18(56.3)	
M stage	1	6(7.9)	11(34.4)	0.001
Extrathyroidal extension	Macroscopic	74(97.4)	27(84.4)	0.025
	Microscopic	2(2.6)	3(9.4)	
Extra-nodal invasion		31(40.8)	18(56.3)	0.204
Tumor size, median(IQR)		2.0(1.3-2.9)	3.1(2.0-4.5)	0.003
Multifocal		49(64.5)	21(65.6)	0.637
NED after initial surgery		69(90.8)	21(65.6)	0.001

ATA, American Thyroid Association; HMR, High Molecular Risk; PTC, papillary thyroid cancer; FTC, follicular thyroid cancer; CND, central neck dissection; LND, lateral neck dissection; NED, no evidence of disease.

incidence of FTC, most complicated by ETE, and 14.8% presenting with distant metastasis. These variations likely stem from differences in the pathological composition. In contrast, the higher proportion of FTC in van Velsen et al.'s study may explain the lower rates of ETE and lymph node metastasis, alongside a higher incidence of distant metastasis. Notably, the rate of cervical lymph node metastasis in this study exceeded that of the two aforementioned studies. Potential explanations include: (1) China's diagnostic and treatment protocols still recommend routine prophylactic central cervical lymph node dissection, leading to the detection of subclinical metastases in cases, including those initially staged as cN0; (2) this study employed a more positive pre-treatment evaluation strategy for lateral cervical lymph nodes. For suspicious lesions detected on ultrasound or CT, ultrasound-guided FNAB combined with Tg measurement in puncture eluent enhanced the detection rate of lateral cervical lymph node metastasis (25). Additionally, 64.8% of the cases in this study involved multifocal lesions, with more than half (54.6%) exhibiting lateral cervical lymph node metastasis, and 44.4% showing ENE. These features align with previous reports on the characteristics of advanced DTC (3).

The NGS molecular assay used in this study incorporated an 18-gene panel, shown in prior research to improve diagnostic precision for FNAB (15). In contrast to widely adopted large NGS panel like ThyroSeq V3 and Afirma GSC, this assay targets the 18 most prevalent genes in Chinese thyroid cancer cases, optimizing cost-effectiveness. Previous studies employing large NGS panel reported variant detection rates ranging from 86.5% to 95.2% (20, 26, 27). In this study, clinically significant variants were identified in 87.8% of ATA high-risk DTC cases, with driver variants detected in 92.6%, reflecting comparable detection efficiency. Additionally, this molecular test covers several key prognosis-related genes, including

10.3389/fendo.2025.1508404

TABLE 2 Outcome of patients with ATA high risk differentiated thyroid cancer by Molecular Characterize Groups.

Outcome		Molecular characterize groups, No. (%)		*p*
		Non-HMR	HMR	
Duration of follow-up, month, median(IQR)		32.5(27.0-36.0)	32.5(30.3-44.0)	0.159
Structural recurrence	Locally recurrence[1]	7(9.5)	9(32.1)	0.012
	Metachronous distant metastasis[2]	2(2.9)	8(38.1)	<0.001
Death		0	3(9.4)	0.039
RAI	Ablation or adjuvant therapy	47(68.1)	17(81.0)	0.256
	Therapeutic RAI	8(10.5)	17(53.1)	<0.001
	RAI-refractory disease	3(37.5)	13(76.5)	0.075

[1]2 patients in Non-HMR group and 4 patients in HMR group who had locally persistent disease were not included.
[2]6 patients in Non-HMR group and 11 patients in HMR group who had distant metastasis at presentation were not included.
ATA, American Thyroid Association; HMR, High Molecular Risk; RAI, radioactive iodine.

*TERT*p, *TP53*, *PIK3CA*, *AKT1*, and *PTEN*, enhancing the ability to identify high-risk molecular profiles. Nevertheless, given the limited scope of molecular testing in this study, we believe that the molecular backgrounds of the "no alteration detected" cases remains unknown and may vary on an individual basis, which is why they were excluded from the study. Among the ATA high-risk cohort, the most prevalent driver variants were *BRAF* V600E, *NRAS*, *KRAS* mutations, and *RET* and *NTRK* fusions, aligning with findings from a recent Chinese study focused primarily on DTC (26). This distribution is also consistent with another report from China involving PTC cases with high recurrence risk (28). In this cohort, *TERT*p and *PIK3CA* mutations were identified in 24.1% and 5.6% of cases, respectively, notably exceeding the frequencies reported in other cohorts with varying recurrence risks. For instance, Du et al. reported *TERT*p and *PIK3CA* mutations in 6.3% and 1.5% of cases, respectively (26). Similarly, in a meta-analysis focusing solely on PTC, the average incidence of *TERT*p mutations was 10.1% (21). The elevated frequency of high-risk molecular alterations in the ATA high-risk DTC cohort suggests that prognostic gene detection in this group may hold enhanced clinical relevance. This study found that high-risk molecular alterations were consistently associated with *BRAF* V600E or *NRAS* mutations, while no such mutations were detected in the 15 cases exhibiting *RET* or *NTRK* fusions, aligning with findings from other large-scale studies. For instance, TCGA reports indicate that *TERT*p mutations are linked to driver mutations or arm-level somatic copy number alterations, rather than *BRAF* mutations or gene fusions (29). In the study by Du et al., only one case of *RET* fusion and one of *NTRK1* fusion were accompanied by *TERT*p mutations (26). However, other studies have noted the co-existence of *RET* fusions and *TERT*p mutations, which may impact prognosis and the response to *RET* and *MEK* targeted therapies (30). Further investigation into the association between gene fusion variants and late-stage alterations, such as *TERT*p mutations, is warranted as additional data becomes available.

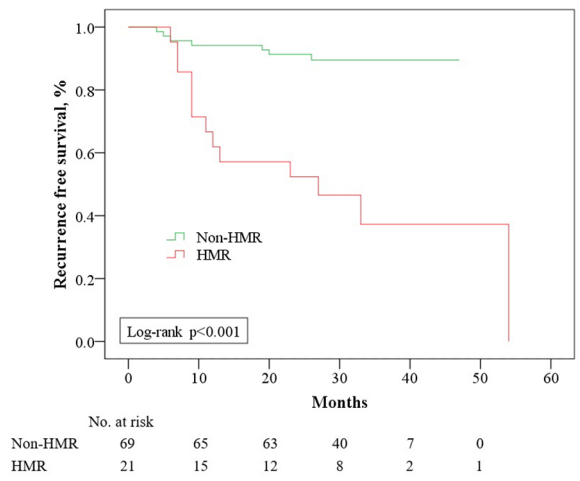

FIGURE 3
Recurrence free survival among 90 patients with ATA high risk differentiated thyroid cancer who had no evidence of disease after initial treatment, stratified by Molecular Characterize Groups. HMR, High Molecular Risk.

A 2021 study by Yip et al. first proposed a novel molecular risk classification divided into three categories based on ThyroSeq, version 3 molecular testing and ThyroSeq Cancer Risk Classifier (19). This classification has since been adopted in several subsequent studies, with its clinical relevance consistently validated (7, 20, 22). The present study adapted this classification, modifying the risk grouping to align with the specific molecular tests used and the unique characteristics of the study cohort. Due to the limitations of molecular testing in this study in detecting certain early driver genes (e.g., *ALK*, *DICER1*, *EIF1AX*, etc.) and specific variant forms (e.g., gene expression alterations, copy number alterations, etc.), "concurrent early variants" were not considered a requirement for inclusion in the HMR group. Additionally, possibly influenced by the cohort characteristics, only two cases exhibited "RAS-like" molecular profiles, which were defined as "low molecular risk". Consequently, the sample size for analyzing "low-risk" cases was insufficient, the non-HMR cases were not further stratified into "low-risk" or "intermediate-risk". In the study by Liu et al., increasing molecular risk was associated with higher mean patient age, a lower proportion of female patients, larger median tumor size, and more frequent occurrences of aggressive PTC subtypes, ETE, cervical lymph node metastasis, and synchronous distant metastasis (22). Schumm et al. also identified a correlation

between higher molecular risk groups and more aggressive clinical features, including larger primary tumors, ETE, and positive surgical margins (20). Similarly, in the HMR group of this study, clinical parameters such as age, tumor size, aggressive pathological subtypes, and distant metastasis demonstrated comparable patterns. Although *TERT*p mutations are well-documented as being significantly associated with RAI resistance (21, 31), the relationship between molecular risk stratification and RAI refractory status has not been explored. In this cohort, 25 patients underwent therapeutic RAI for unresectable lesions. While the HMR group exhibited a higher prevalence of RAIR cases, the difference was not statistically significant, likely due to the limited sample size. Further investigation is required to determine whether MCGs can reliably predict RAI treatment efficacy, with larger sample sizes necessary.

Previous studies have demonstrated a significant correlation between high-risk molecular variants and both RFS and SR following DTC surgery, with a strong link to distant metastasis. For example, Liu et al. observed a substantially lower 36-month RFS in the high molecular risk group compared to the intermediate and low-risk groups, with a recurrence risk exceeding threefold that of the latter two groups (22). Similarly, Schumm et al. found that patients in the high molecular risk group exhibited an elevated risk of SR (HR: 9.31) and distant metastasis (HR: 42.7) compared to those in the intermediate-risk group (20). In our study, a median follow-up of 32.5 months revealed significant differences in key prognostic indicators, including local recurrence, metachronous distant metastasis, and RFS across various MCGs following initial surgery. Notably, 80% of metachronous distant metastasis cases occurred in the HMR group. In contrast, the non-HMR group exhibited markedly lower rates of SR (10.1%) and metachronous distant metastasis (2.9%) compared to the overall study cohort, and significantly below historical data for ATA high-risk DTC (8, 9). All three recorded deaths occurred within the HMR group. Although between-group differences in mortality were significant, the limited follow-up duration and small number of death cases precluded survival analysis. These results indicate that for ATA high-risk DTC, the presence of high-risk variants serves as a strong predictor of adverse prognostic events during the initial treatment phase.

Some prognostic factors, such as age, tumor size, and pathological subtype, exhibit variability across different MCGs as previously noted, are currently employed to evaluate prognostic risk during the initial treatment phase of DTC (23). We hypothesized that high-risk genetic alterations contribute to the correlation between risk-related clinical features and poor prognosis, a relationship supported by emerging evidence. For instance, age is widely recognized as a key prognostic factor in DTC, as demonstrated in numerous studies (5, 32), and is a critical factor in the 8th AJCC TNM staging system. Nevertheless, research by Heo et al. found that *TERT*p mutations mediated the effect of age at diagnosis on the mortality rate by 36% in DTC (33). In this study, while age, tumor size, pathological subtype, and N stage appeared to be associated with RFS during initial univariate analysis, only MCGs (HR: 5.77) and tumor size (HR: 1.32) remained independently linked to RFS after incorporating the MCGs variable into a multivariable model. This finding aligns with reports by Liu et al. and Schumm et al., whose multivariate models similarly indicated that recurrence risk was solely related to tumor size and molecular risk (7, 20). Despite differences in cohort composition, the consistent results across these three DTC studies suggest that molecular profiles may be independently and more directly predictive of prognosis.

Several studies on "molecular risk stratification" have highlighted the importance of integrating routine molecular testing via preoperative FNAB, as it offers valuable insights into the molecular risk stratification prior to surgery, thereby shaping the initial treatment approach (7, 20, 22). However, despite its efficacy in informing clinical decisions, the broad adoption of NGS with large panels is hindered by substantial costs and limited access, restricting its routine application in many regions for thyroid cancer management. This study indicated that when NGS testing was employed for prognostic risk stratification in thyroid cancer, the use of small panels targeting key prognostic loci (such as *TERT*p, *PIK3CA*, *TP53*, *AKT1*, etc.) offered comparable efficiency in risk grouping. In regions where routine preoperative molecular testing is not feasible, a more targeted and cost-effective approach would be better to perform supplementary postoperative molecular testing specifically for ATA high-risk cases, allowing for accurate risk stratification. Given the elevated risk of recurrence and distant metastasis in patients with both high-risk ATA RSS and adverse molecular profiles, closer follow-up is warranted. Further research is needed to determine whether more positive RAI adjuvant therapies or alternative treatments may offer enhanced benefits for this subgroup.

Despite strengths, several limitations affect this study. First, as a retrospective cohort study, only cases with completed molecular testing were included, introducing potential selection bias due to the two-stage process of physician explanation and patient consent required for testing. Second, compliance issues led to incomplete RAI treatment in some cases, potentially skewing overall prognostic outcomes compared to patients who received the full standard treatment. Additionally, this non-compliance complicates a standardized analysis of postoperative serum Tg levels and biochemical incomplete responses within the study cohort. Given the lack of significant differences in case distribution across various MCG groups, this factor is unlikely to decisively affect the prognostic variation between the groups. Additionally, the small sample size limits the feasibility of performing propensity score matching based on different characteristics, which could have enhanced the precision of the statistical analysis. Furthermore, the short follow-up period constrains the study to short-term prognostic outcomes, and the long-term prognostic implications of different MCGs will require extended follow-up for more comprehensive assessment.

In conclusion, our study indicated a higher incidence of structural recurrence and poorer RFS in ATA RSS high risk DTC presented with high molecular risk. Molecular testing and MCGs offer significant potential for refining prognosis in high-risk DTC cases and merit broader application. The potential need for specialized postoperative management strategies for ATA high-risk cases with high molecular risk warrants further investigation.

Data availability statement

The datasets presented in this study can be found in online repositories. The names of the repository/repositories and accession number(s) can be found in the article/Supplementary Material.

Ethics statement

The studies involving humans were approved by The Ethics Committee of Fujian Cancer Hospital, Fuzhou, China (Ethics Number: K2024-400-01). The studies were conducted in accordance with the local legislation and institutional requirements. Written informed consent for participation was not required from the participants or the participants' legal guardians/next of kin in accordance with the national legislation and institutional requirements.

Author contributions

JL: Conceptualization, Formal analysis, Writing – original draft, Writing – review & editing. YW: Conceptualization, Writing – review & editing. WG: Data curation, Investigation, Writing – review & editing. XZ: Methodology, Writing – review & editing. SW: Investigation, Writing – review & editing. YS: Validation, Writing – review & editing. FW: Data curation, Writing – review & editing.

Funding

The author(s) declare financial support was received for the research, authorship, and/or publication of this article. This work was funded by Natural Science Foundation of Fujian province (Grant/Award Number: 2024J011069).

Conflict of interest

The remaining authors declare that the research was conducted in the absence of any commercial or financial relationships that could be construed as a potential conflict of interest.

Generative AI statement

The author(s) declare that no Generative AI was used in the creation of this manuscript.

Publisher's note

Supplementary material

The Supplementary Material for this article can be found online at: https://www.frontiersin.org/articles/10.3389/fendo.2025.1508404/full#supplementary-material

References

1. Pizzato M, Li M, Vignat J, Laversanne M, Singh D, La Vecchia C, et al. The epidemiological landscape of thyroid cancer worldwide: GLOBOCAN estimates for incidence and mortality rates in 2020. *Lancet Diabetes Endocrinol.* (2022) 10:264–72. doi: 10.1016/S2213-8587(22)00035-3

2. Zheng R, Zhang S, Zeng H, Wang S, Sun K, Chen R, et al. Cancer incidence and mortality in China, 2016. *J Natl Cancer Cent.* (2022) 2:1–9. doi: 10.1016/j.jncc.2022.02.002

3. Boucai L, Zafereo M, Cabanillas ME. Thyroid cancer: A review. *JAMA.* (2024) 331:425–35. doi: 10.1001/jama.2023.26348

4. Haugen BR, Alexander EK, Bible KC, Doherty GM, Mandel SJ, Nikiforov YE, et al. 2015 American thyroid association management guidelines for adult patients with thyroid nodules and differentiated thyroid cancer: the american thyroid association guidelines task force on thyroid nodules and differentiated thyroid cancer. *Thyroid.* (2016) 26:1–133. doi: 10.1089/thy.2015.0020

5. Gan T, Huang B, Chen Q, Sinner HF, Lee CY, Sloan DA, et al. Risk of recurrence in differentiated thyroid cancer: A population-based comparison of the 7th and 8th editions of the american joint committee on cancer staging systems. *Ann Surg Oncol.* (2019) 26:2703–10. doi: 10.1245/s10434-019-07275-1

6. Pitoia F, Bueno F, Urciuoli C, Abelleira E, Cross G, Tuttle RM. Outcomes of patients with differentiated thyroid cancer risk-stratified according to the American thyroid association and Latin American thyroid society risk of recurrence classification systems. *Thyroid.* (2013) 23:1401–7. doi: 10.1089/thy.2013.0011

7. Liu JB, Baugh KA, Ramonell KM, McCoy KL, Karslioglu-French E, Morariu EM, et al. Molecular testing predicts incomplete response to initial therapy in differentiated thyroid carcinoma without lateral neck or distant metastasis at presentation: retrospective cohort study. *Thyroid.* (2023) 33:705–14. doi: 10.1089/thy.2023.0060

8. van Velsen EFS, Stegenga MT, van Kemenade FJ, Kam BLR, van Ginhoven TM, Visser WE, et al. Evaluating the 2015 american thyroid association risk stratification system in high-risk papillary and follicular thyroid cancer patients. *Thyroid.* (2019) 29:1073–9. doi: 10.1089/thy.2019.0053

9. Shah S, Boucai L. Effect of age on response to therapy and mortality in patients with thyroid cancer at high risk of recurrence. *J Clin Endocrinol Metab.* (2018) 103:689–97. doi: 10.1210/jc.2017-02255

10. Kimura ET, Nikiforova MN, Zhu Z, Knauf JA, Nikiforov YE, Fagin JA. High prevalence of BRAF mutations in thyroid cancer: genetic evidence for constitutive activation of the RET/PTC-RAS-BRAF signaling pathway in papillary thyroid carcinoma. *Cancer Res.* (2003) 63:1454–7.

11. Greco A, Pierotti MA, Bongarzone I, Pagliardini S, Lanzi C, Della Porta G. TRK-T1 is a novel oncogene formed by the fusion of TPR and TRK genes in human papillary thyroid carcinomas. *Oncogene.* (1992) 7:237–42.

12. Landa I, Cabanillas ME. Genomic alterations in thyroid cancer: biological and clinical insights. *Nat Rev Endocrinol.* (2024) 20:93–110. doi: 10.1038/s41574-023-00920-6

13. DiGennaro C, Vahdatzad V, Jalali MS, Toumi A, Watson T, Gazelle GS, et al. Assessing bias and limitations of clinical validation studies of molecular diagnostic tests for indeterminate thyroid nodules: systematic review and meta-analysis. *Thyroid.* (2022) 32:1144–57. doi: 10.1089/thy.2022.0269

14. Chudova D, Wilde JI, Wang ET, Wang H, Rabbee N, Egidio CM, et al. Molecular classification of thyroid nodules using high-dimensionality genomic data. *J Clin Endocrinol Metab.* (2010) 95:5296–304. doi: 10.1210/jc.2010-1087

15. Ren M, Yao Q, Bao L, Wang Z, Wei R, Bai Q, et al. Diagnostic performance of next-generation sequencing and genetic profiling in thyroid nodules from a single center in China. *Eur Thyroid J.* (2022) 11:e210124. doi: 10.1530/ETJ-21-0124

16. Ferrari SM, Fallahi P, Ruffilli I, Elia G, Ragusa F, Paparo SR, et al. Molecular testing in the diagnosis of differentiated thyroid carcinomas. *Gland Surg.* (2018) 7:S19–29. doi: 10.21037/gs.2017.11.07

17. Elia G, Patrizio A, Ragusa F, Paparo SR, Mazzi V, Balestri E, et al. Molecular features of aggressive thyroid cancer. *Front Oncol.* (2022) 12:1099280. doi: 10.3389/fonc.2022.1099280

18. Yoo SK, Song YS, Lee EK, Hwang J, Kim HH, Jung G, et al. Integrative analysis of genomic and transcriptomic characteristics associated with progression of aggressive thyroid cancer. *Nat Commun.* (2019) 10:2764. doi: 10.1038/s41467-019-10680-5

19. Yip L, Gooding WE, Nikitski A, Wald AI, Carty SE, Karslioglu-French E, et al. Risk assessment for distant metastasis in differentiated thyroid cancer using molecular profiling: A matched case-control study. *Cancer.* (2021) 127:1779–87. doi: 10.1002/cncr.33421

20. Schumm MA, Shu ML, Hughes EG, Nikiforov YE, Nikiforova MN, Wald AI, et al. Prognostic value of preoperative molecular testing and implications for initial surgical management in thyroid nodules harboring suspected (Bethesda V) or known (Bethesda VI) papillary thyroid cancer. *JAMA Otolaryngol Head Neck Surg*. (2023) 149:735–42. doi: 10.1001/jamaoto.2023.1494

21. Liu C, Liu Z, Chen T, Zeng W, Guo Y, Huang T. TERT promoter mutation and its association with clinicopathological features and prognosis of papillary thyroid cancer: A meta-analysis. *Sci Rep*. (2016) 6:36990. doi: 10.1038/srep36990

22. Liu JB, Ramonell KM, Carty SE, McCoy KL, Schaitkin BM, Karslioglu-French E, et al. Association of comprehensive thyroid cancer molecular profiling with tumor phenotype and cancer-specific outcomes. *Surgery*. (2023) 173:252–9. doi: 10.1016/j.surg.2022.05.048

23. Chen DW, Carr G, Worden FP, Veenstra CM, Haymart MR, Banerjee M. Survival prognostication in patients with differentiated thyroid cancer and distant metastases: A SEER population-based study. *Thyroid*. (2024) 34:837–45. doi: 10.1089/thy.2023.0709

24. Ginzberg SP, Sharpe J, Passman JE, Amjad W, Wirtalla CJ, Soegaard Ballester JM, et al. Revisiting the relationship between tumor size and risk in well-differentiated thyroid cancer. *Thyroid*. (2024) 34:980–9. doi: 10.1089/thy.2023.0327

25. Grani G, Fumarola A. Thyroglobulin in lymph node fine-needle aspiration washout: a systematic review and meta-analysis of diagnostic accuracy. *J Clin Endocrinol Metab*. (2014) 99:1970–82. doi: 10.1210/jc.2014-1098

26. Du Y, Zhang S, Zhang G, Hu J, Zhao L, Xiong Y, et al. Mutational profiling of Chinese patients with thyroid cancer. *Front Endocrinol (Lausanne)*. (2023) 14:1156999. doi: 10.3389/fendo.2023.1156999

27. Hu MI, Waguespack SG, Dosiou C, Ladenson PW, Livhits MJ, Wirth LJ, et al. Afirma genomic sequencing classifier and xpression atlas molecular findings in consecutive bethesda III-VI thyroid nodules. *J Clin Endocrinol Metab*. (2021) 106:2198–207. doi: 10.1210/clinem/dgab304

28. Li M, Jia H, Qian Q, Wen P, Chen C, Hua Y, et al. Genomic characterization of high-recurrence risk papillary thyroid carcinoma in a southern Chinese population. *Diagn Pathol*. (2020) 15:49. doi: 10.1186/s13000-020-00962-8

29. Cancer Genome Atlas Research N. Integrated genomic characterization of papillary thyroid carcinoma. *Cell*. (2014) 159:676–90. doi: 10.1016/j.cell.2014.09.050

30. Zhang W, Lin S, Wang Z, Zhang W, Xing M. Coexisting RET/PTC and TERT promoter mutation predict poor prognosis but effective RET and MEK targets in thyroid cancer. *J Clin Endocrinol Metab*. (2024) 109:3166–75. doi: 10.1210/clinem/dgae327

31. Cao J, Zhu X, Sun Y, Li X, Yun C, Zhang W. The genetic duet of BRAF V600E and TERT promoter mutations predicts the poor curative effect of radioiodine therapy in papillary thyroid cancer. *Eur J Nucl Med Mol Imaging*. (2022) 49:3470–81. doi: 10.1007/s00259-022-05820-x

32. Shah S, Boucai L. Effect of age on response to therapy and mortality in patients with thyroid cancer at high risk of recurrence. *J Clin Endocrinol Metab*. (2018) 103:689–97. doi: 10.1210/jc.2017-02255

33. Heo J, Lee S, Park J, Yang H, Park H, Ki CS, et al. Age-associated mortality is partially mediated by TERT promoter mutation status in differentiated thyroid carcinoma. *PloS One*. (2023) 18:e0294145. doi: 10.1371/journal.pone.0294145

frontiers | Frontiers in Oncology

TYPE Original Research
PUBLISHED 29 January 2025
DOI 10.3389/fonc.2025.1502391

OPEN ACCESS

EDITED BY
Juan Pablo Nicola,
National University of Cordoba, Argentina

REVIEWED BY
Laura Fozzatti,
CONICET Centre for Research in Clinical Biochemistry and Immunology (CIBICI), Argentina
Cesar Seigi Fuziwara,
University of São Paulo, Brazil

*CORRESPONDENCE
Zengren Zhao
zhaozengren@hebmu.edu.cn
Bo Liu
Lb123@hebmu.edu.cn
Xia Jiang
jiangxia0925@hebmu.edu.cn

†These authors have contributed equally to this work and share first authorship

RECEIVED 26 September 2024
ACCEPTED 08 January 2025
PUBLISHED 29 January 2025

CITATION
Wang H, Shang F, Wang Y, Pang B, Kang L, Zhou C, Li D, Li Z, Jiang X, Liu B and Zhao Z (2025) PMAIP1 regulates the progression of follicular thyroid carcinoma through the Wnt3/FOSL1 pathway. *Front. Oncol.* 15:1502391. doi: 10.3389/fonc.2025.1502391

PMAIP1 regulates the progression of follicular thyroid carcinoma through the Wnt3/FOSL1 pathway

Haobo Wang[1†], Fangjian Shang[1†], Yifang Wang[1], Bo Pang[1,2], Longfei Kang[1,2], Chuanmin Zhou[1,2], Dongyun Li[1,2], Zhongxin Li[1,2], Xia Jiang[1,2*], Bo Liu[1*] and Zengren Zhao[1*]

[1]Department of General Surgery, The First Hospital of Hebei Medical University, Shijiazhuang, China, [2]Gastrointestinal Disease Diagnosis and Treatment Center, Hebei Key Laboratory of Colorectal Cancer Precision Diagnosis and Treatment, The First Hospital of Hebei Medical University, Shijiazhuang, China

Introduction: In thyroid carcinoma (TC), follicular thyroid carcinoma (FTC) represents the second most prevalent pathological type following papillary thyroid carcinoma. Notably, FTC exhibits a more aggressive clinical course and a higher propensity for distant metastasis. However, the underlying mechanisms governing the progression of FTC remain poorly understood. PMAIP1 is a gene implicated in various cancers and biological processes. Investigating the role and mechanism of PMAIP1 in FTC is crucial for enhancing our understanding of FTC and informing clinical treatment strategies.

Methods: This study examined the expression level of PMAIP1 in FTC through comprehensive analysis of databases, tumor tissues, and cell lines. Following the establishment of a stably transfected plasmid in cell lines, a series of functional assays and subcutaneous xenograft experiment were conducted to investigate the role of PMAIP1 in FTC. Additionally, transcriptome sequencing was employed to identify potential signaling pathways associated with PMAIP1. Mechanistic studies involved a series of rescue experiments to elucidate the regulatory mechanisms of PMAIP1 in FTC.

Results: PMAIP1 was found to be highly expressed in FTC, and its knockdown significantly inhibited the proliferation and metastasis of FTC cells both *in vivo* and *in vitro*. The results of transcriptome sequencing analysis indicated that PMAIP1 may influence the progression of FTC via the Wnt signaling pathway. Subsequent investigations revealed a direct correlation between PMAIP1 expression levels and those of Wnt3 and FOSL1 in FTC. A series of rescue experiments further substantiated the regulatory role of PMAIP1 on Wnt3/FOSL1 in FTC.

Discussion: In conclusion, our research demonstrated that PMAIP1 emerges as a novel pro-cancer factor in FTC, and its knockdown significantly inhibited the proliferation and metastasis of FTC both *in vivo* and *in vitro*. Mechanistically, PMAIP1 regulated FOSL1 by modulating the Wnt signaling pathway, thereby promoting FTC progression. Targeting PMAIP1 may present a promising therapeutic strategy for FTC.

KEYWORDS

follicular thyroid carcinoma, PMAIP1, Wnt3, FOSL1, progression

1 Introduction

Thyroid cancer (TC) is the most prevalent endocrine malignancy, accounting for 586,000 cases globally and ranking ninth in incidence in 2020 (1, 2). The increased utilization of diagnostic imaging and surveillance has revealed a clear trend of rejuvenation in TC, making it a significant type of cancer that warrants attention (3). Among differentiated thyroid cancers, follicular thyroid carcinoma (FTC) has an incidence rate of approximately 10% to 15%, second only to papillary thyroid carcinoma (PTC), but it is notably more invasive (4). FTC is considered a high-risk cancer due to its propensity for hematogenous metastasis to distant sites, particularly the lungs and bones (5). Despite significant advancements in the diagnosis and treatment of FTC, the underlying mechanisms of FTC remain largely obscure. Consequently, investigating potential biomarkers and elucidating their molecular mechanisms in FTC is of paramount importance to address this research gap. Concurrently, such investigations may facilitate the development of novel therapeutic targets for FTC, thereby expanding the repertoire of clinical treatment options.

PMAIP1 (Phorbol-12-myristate-13-acetate-induced protein 1), also known as NOXA or APR, located on chromosome 18q21.32, is a member of the BCL-2 protein family (6). Research indicated that insulin activates the AKT signaling pathway, which subsequently inhibits the RNA translation of NOXA/PMAIP1, thereby promoting the survival of human pluripotent stem cells (7). NOXA/PMAIP1 has the potential as a predictive marker for response and survival in patients undergoing CAR T-cell transfusion. Targeting NOXA/PMAIP1 may enhance the therapeutic efficacy of CAR T cells. However, the functional significance of PMAIP1 in FTC remains unexplored (8). Furthermore, azacitidine was observed to upregulate the expression of PMAIP1, thereby enhancing the sensitivity of preclinical models of acute myeloid leukemia to venetoclax. This finding provided evidence for novel therapeutic strategies aimed at overcoming resistance to current acute myeloid leukemia treatments (9). These studies indicated that PMAIP1 plays a significant role in the biological progression of various diseases and may serve as a potential therapeutic target. Additionally, PMAIP1 was implicated in the pathogenesis and progression of multiple cancers. Research indicated that NOXA/PMAIP1 serves as a marker for an aggressive subtype of pancreatic ductal adenocarcinoma, with NOXA/PMAIP1 expression inducing synthetic lethality upon RUNX1 inhibition in pancreatic cancer (10). The co-expression of PUMA and NOXA/PMAIP1 proteins in benign epithelial cells has been predictive of recurrence following radical prostatectomy (11). Additionally, a study involving 160 patients with colorectal cancer and adjacent tissues demonstrated that NOXA/PMAIP1 was overexpressed in colorectal cancer tumors, even at early stages (12). However, the functional significance of PMAIP1 in FTC remains unexplored.

In this study, we conducted a comprehensive analysis utilizing the databases, supplemented by validation with clinical tumor samples and cell lines, and identified elevated expression levels of PMAIP1 in FTC. Consequently, we postulated that PMAIP1 contributes to the progression of FTC. To substantiate this hypothesis, we examined the impact of PMAIP1 on FTC proliferation and metastasis through both *in vivo* and *in vitro* experiments. Additionally, we employed transcriptome sequencing to elucidate the potential pathway through which PMAIP1 may exert its effects in FTC, and subsequently verified the association between PMAIP1 and the pathway by rescue experiments. In this study, we examined the expression levels, functional roles, molecular mechanisms, and clinical significance of PMAIP1 in FTC.

2 Materials and methods

2.1 Clinical samples

Pairs of FTC and adjacent non-tumorous tissue specimens (n=8) were procured from the Department of General Surgery at The First Hospital of Hebei Medical University. The study received ethical approval from the Ethics Committee of The First Hospital of Hebei Medical University (NO: 20230203), and informed consent was obtained from all patients for the collection of tissue samples.

2.2 Bioinformatics analysis

RNA-sequencing expression profiles and corresponding clinical data of FTC were obtained from The Cancer Genome Atlas (TCGA) dataset (https://portal.gdc.cancer.gov/). Normal control datasets were sourced from the Genotype-Tissue Expression (GTEx) data portal (https://www.gtexportal.org/home/datasets). Statistical analyses were conducted using R software (Version 3.5.0). The two-gene correlation map was generated using the ggstatsplot package in R, employing Spearman's correlation analysis to assess the relationship between quantitative variables that do not follow a normal distribution. $P<0.05$ was considered statistically significant.

2.3 Cell lines

The FTC cell lines (FTC133 and FTC238) and the non-tumoral thyroid cell line (NTHY-ORI3-1) were used in this study. The human FTC orthotopic cell lines FTC133 (1×10^6) and the non-tumoral thyroid cell line NTHY-ORI3-1 (1×10^6) were procured from Procell Life Science&Technology Co, Ltd (Cat NO.: CL-0644; CL-0817). The human FTC lung metastasis cell line FTC238 was procured from YUCHI Biology Co, Ltd (Cat NO.: SC-1458). FTC133 and NTHY-ORI3-1 were maintained in RPMI-1640 medium (Thermo, Gibco, UK) and FTC238 was maintained in DMEM F-12 medium (Thermo, Gibco, UK), all supplemented with 10% fetal bovine serum (Thermo, Gibco, UK) and 1% penicillin-streptomycin (Thermo, Gibco, UK). All cell lines were incubated at 37°C with 5% CO_2.

2.4 RNA extraction and quantitative real –time polymerase chain reaction

Total RNA was extracted utilizing the RNA EASY reagent (R701-01, Vazyme, China), followed by reverse transcription with the Prime Script RT Reagent Kit (RR047A, TaKaRa, Japan). The Quantitative real-time polymerase chain reaction (qRT- PCR) system (LightCycler 480II, USA) was prepared using the ChamQ Universal SYBR qPCR Master Mix (Q711, Vazyme, China), cDNA, and specific primers. PCR amplification reactions were conducted in triplicate for each cDNA sample, with β-actin serving as the internal reference gene. All gene-specific primers were designed using NCBI (https://www.ncbi.nlm.nih.gov/) resources and synthesized by Sangon Biotech Co., Ltd (Shanghai, China) (Table 1). Relative gene expression levels were calculated using the $2^{-\Delta\Delta Ct}$ method.

2.5 Establishment of knockdown and overexpression cell lines

Knockdown plasmid of PMAIP1 (sh-PMAIP1: 5'-GTGCTAC TCAACTCAGGAGAT -3'), sh-negative control (sh-NC), over-expression plasmid of PMAIP1 (NM_001382618.1), Vector, knockdown plasmid of Wnt3 (sh-Wnt3: 5'-GCGCTTCTGCCG CAATTACAT-3'), siRNA of FOSL1 (siFOSL1:5'-CCUCAGCUC AUCGCAAGAGUA-3') and siNC were ordered form Guangzhou Fulengen Co, Ltd. 5μg plasmids (or 5μmol siRNA) were transfected into FTC133 and FTC238 by using Lipofectamine 3000 (Invitrogen, USA) according to the manufacturer's instructions. The cells were then selected using 1 μg/mL puromycin (Solarbio, China).

2.6 Western blot analysis

Protein was extracted from the cells using RIPA lysis buffer (PMSF: RIPA = 1:100), and the protein concentration was semi-quantified using a BCA protein assay kit. Equal amounts of protein were separated by 12% SDS-PAGE (BIO-RAD kit) and subsequently transferred to a PVDF membrane. The PVDF membrane was blocked with 5% BSA in TBST at room temperature for 2 hours. Following three washes with TBST, the membrane was incubated with primary antibody at 4°C overnight. Afterward, it was washed three times with TBST and then incubated with a secondary antibody at room temperature for one hour. Finally, the protein bands were visualized and analyzed. This experiment was repeated three times.

TABLE 1 Primer sequences used in this study.

Gene name	Primer sequences	Length (bp)
PMAIP1	F: AGGAACAAGTGCAAGTAGCTG	153
	R: GGAGTCCCCTCATGCAAGTT	
Wnt3	F: TGACTCGCATCATAAGGGGC	181
	R: GTGGTCCAGGATAGTCGTGC	
FOSL1	F: GTGCCAAGCATCAACACCAT	126
	R: CCAGTTTGTCAGTCTCCTGTTC	
β-actin	F: ACTTAGTTGCGTTACACCCTT	155
	R: GTCACCTTCACCGTTCCA	

2.7 Cell counting kit–8 assay

Cells were digested and quantified during the logarithmic growth phase, subsequently seeded in 96-well plates at a density of $1x10^3$ cells per well, and incubated at 37°C with 5% CO_2. Each experimental group included four replicates. Upon cell adherence, 10μL of cell counting kit-8 (CCK-8) reagent (Abbkine, China) was added to each well at 0h, 24h, 48h, and 72h, followed by incubation at 37°C. After a 2h incubation period, the absorbance of the 96-well plates was measured at 450 nm using a microplate reader.

2.8 Colony formation assay

Cells were digested and counted during the logarithmic growth phase, and 2mL of the medium was added to a 6-well plate, with the cell suspension seeded at a density of 1,000 cells per well. Cells were cultured in a 5% CO_2 incubator at 37°C for a duration of 10-14 days, with the medium being replaced every 3 to 4 days. The experiment was terminated upon the observation of significant clonal cell groups. Following the removal of the medium, the cells were washed twice with PBS. Subsequently, 1 mL of 4% paraformaldehyde (Biosharp, China) was added to each well for fixation over a period of 15 minutes. This was followed by the addition of 1 mL of crystal violet ammonium oxalate solution (Solarbio, China) for 30 minutes at room temperature. The wells were then gently rinsed with double-distilled water. After allowing the cells to air dry, the cell clusters were photographed and counted. This experiment was conducted in triplicate.

2.9 Wound healing assay

Following trypsinization and cell counting, the cells were seeded into 6-well plates at a density of 50×10^4 cells per well. Once the cells had reached confluence, scratches were made perpendicular to the initial horizontal line. Cell debris was subsequently removed using PBS, after administering mitomycin treatment to the cells for a duration of one hour, proceed to wash them with PBS, and fresh medium was added. The cells were then cultured at 37°C in a 5% CO_2 atmosphere. The widths of the scratches were measured and recorded at 0h and 24h using an inverted biological microscope, with three fields of view captured at each time point.

2.10 Migration and invasion assay

Add 700 μL of medium (20% FBS, no P/S) to each well of a 24-well plate and subsequently place the chamber into the well containing the medium. Introduce 100 μL of the diluted cell suspension into the

chamber, ensuring a total cell count of 10×10^4. Incubate the cells under standard culture conditions for 24h (37°C, 5% CO_2). After the incubation period, remove the chamber from the 24-well plate and gently eliminate any non-migrated cells and residual medium from the polycarbonate membrane using a cotton swab. Fix the cells with 4% paraformaldehyde for 30 minutes, followed by staining with 0.1% crystal violet for 15 minutes. Take a picture under the microscope and count the number of cells. The experiment was repeated 3 times.

2.11 Subcutaneous xenograft

NTG mice (4-6 weeks old) were purchased from Beijing Sibeifu Biotechnology Co., Ltd, and housed under special pathogen-free conditions. Animal experiments were conducted with the approval of the Animal Ethics Committee (NO: MDL2024-04-05-01), ensuring that all mice were provided with adequate water and food. Stable transfection of FTC133 and FTC238 cells with sh-PMAIP1 or sh-NC was conducted, followed by selection using puromycin. Subsequently, FTC133 and FTC238 cells with stable PMAIP1 knockdown were digested and resuspended in PBS at a concentration of 5×10^6 cells per 100μL. These cells were then injected into the left axillary region of randomly assigned mice (5 mice per group) within one hour. The condition of the mice was monitored, and tumor volume measurements commenced on day 3. Tumor volume was assessed every 3 days using calipers and calculated using the formula: volume (mm^3) = 0.5 × length × width^2. After the mice were euthanized, the tumors were subsequently isolated, photographed, and weighed. The excised tissues were either fixed in 10% neutral-buffered formalin or processed further. Tumor sections from paraffin-embedded blocks were utilized for histological examination.

2.12 Immunohistochemical staining

Following dewaxing and rehydration, the tissue sections were immersed in 0.01M citrate buffer and subjected to microwave heating to restore antigenicity. After incubation at room temperature for 10 minutes, the sections were treated with PBS and 1% periodate. Subsequently, the sections were incubated with the primary antibody overnight at 4°C, followed by a 30-minute incubation with the secondary antibody on the subsequent day. The sections were then subjected to a staining protocol that included diaminobenzidine staining, PBS washes, hematoxylin counterstaining, distilled water washes, and PBS rebluing. Dehydration was performed using a graded series of alcohols, with each stage lasting 5 minutes, and concluded with a 10-minute treatment in xylene. Finally, the sections were sealed with neutral gum for microscopic examination. Subsequently, three images of each tissue slice were randomly captured using a microscope, and the staining intensity of these images was analyzed utilizing Aipathwell software (Wuhan servicebio technology Co, Ltd). The staining intensity of the sections was evaluated based on the rate of positive cells and the positive area rate.

2.13 Transcriptome sequencing and analysis

Each experimental group comprised three samples, with each sample containing a volume of 1×10^7 cells. Following RNA extraction, the integrity of the RNA was rigorously assessed using the Agilent 2100 Bioanalyzer. Upon completion of library construction, preliminary quantification was conducted using the Qubit 2.0 Fluorometer, and the libraries were subsequently diluted to a concentration of 1.5 ng/μL. Following the completion of quality checks, various libraries were pooled in accordance with the manufacturer's guidelines, taking into account the necessary effective concentration and desired sequencing output. These pooled libraries were then subjected to Illumina sequencing. The resulting raw data underwent quality control and were aligned to the reference genome HG38 for annotation purposes. Comparative analysis of gene expression profiles was performed between sh-PMAIP1 cells and the control group. Subsequently, differentially expressed genes were identified, and enrichment analyses for Kyoto Encyclopedia of Genes and Genomes (KEGG) pathways were conducted utilizing the R (Version 3.5.0).

2.14 Statistical analysis

In vitro experiments were performed in triplicates. All statistical tests were performed using Graphpad Prism 8.0 (Graphpad Software Inc., San Diego, CA) or the SPSS program (Version 22.0; SPSS, Chicago, IL). The mean ± standard deviation was used for statistical description and the t-test for statistical analysis. Statistical significance was determined at $P < 0.05$. $^*P < 0.05$, $^{**}P < 0.01$, $^{***}P < 0.001$.

3 Results

3.1 PMAIP1 was upregulated in FTC

We acquired data on 106 FTC samples and 653 normal tissue samples from TCGA and GTEx databases. Comparative analysis of PMAIP1 expression between FTC and normal tissues revealed a significant overexpression of PMAIP1 in FTC tissues (Figure 1A). Additionally, we examined PMAIP1 expression across stages I-IV of FTC relative to normal tissues, finding elevated mRNA levels of PMAIP1 in FTC samples (Figure 1B). To further validate these findings, we collected 8 pairs of FTC and adjacent non-cancerous tissues and assessed PMAIP1 expression differences. The results demonstrated a significant upregulation of PMAIP1 expression in FTC tissues compared to adjacent non-cancerous tissues (Figure 1C). Subsequently, we assessed the expression levels of PMAIP1 across three cell lines. Among these, PMAIP1 was markedly overexpressed in the FTC cell lines FTC133 and FTC238 relative to NTHY-ORI3-1 (Figure 1D). These findings indicated that PMAIP1 was upregulated in FTC.

10.3389/fonc.2025.1502391

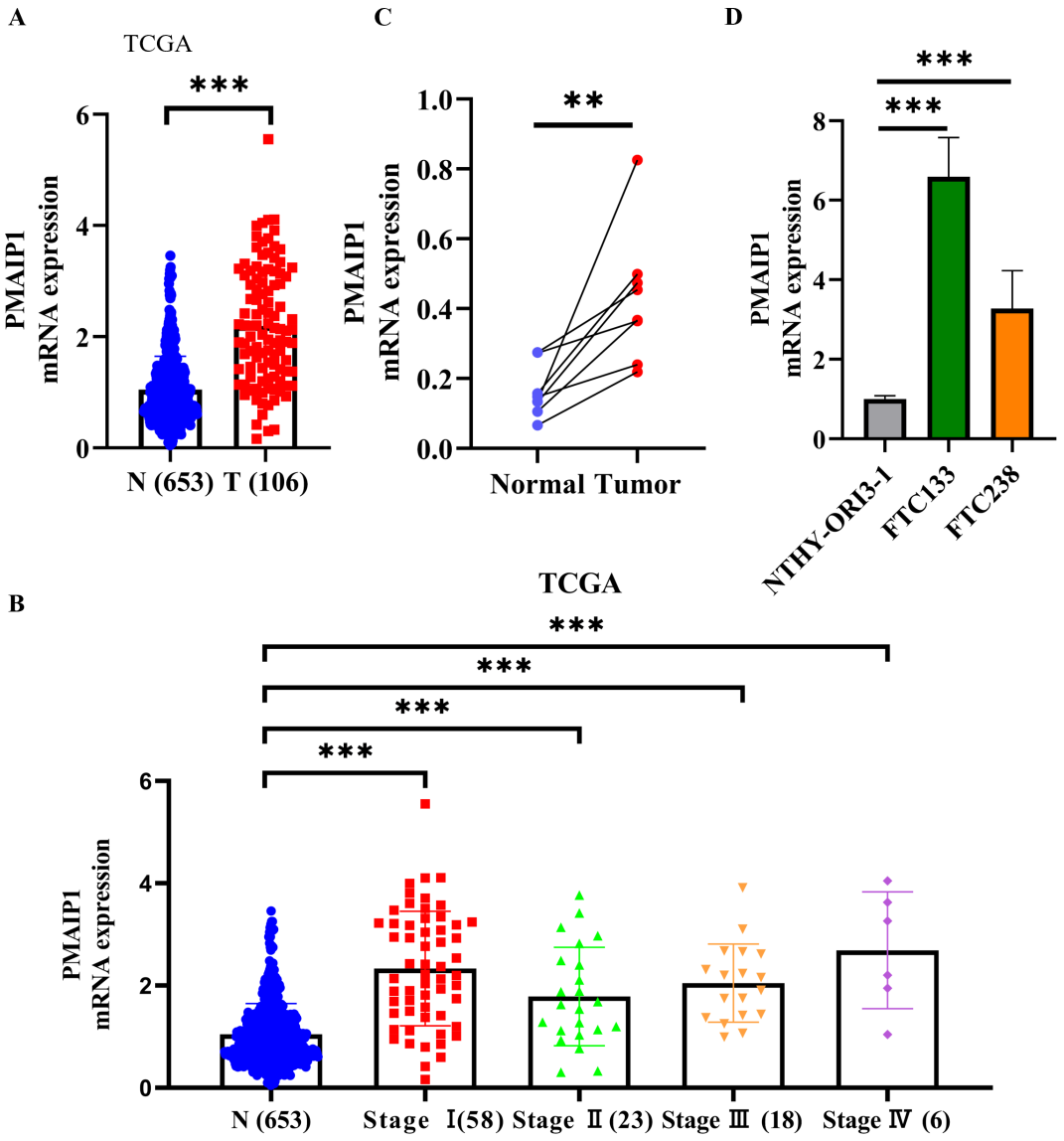

FIGURE 1
PMAIP1 was upregulated in FTC. **(A)** RNA-sequencing expression profiles and corresponding clinical data for FTC (n=106) were obtained from TCGA dataset. Normal control datasets (n=653) were sourced from the GTEx data portal. PMAIP1 mRNA expression was higher in FTC tissues relative to normal tissues at all stages, ***$P < 0.001$. **(B)** In stages I (n=58), II (n=23), III (n=18), and IV (n=6), the expression level of PMAIP1 was all significantly elevated in FTC tissues compared to normal tissues (n=653), ***$P < 0.001$. **(C)** 8 FTC tissues and 8 paired adjacent normal tissues were detected by qRT-PCR, showing that PMAIP1 expression was upregulated in FTC tissues compared with paired adjacent normal tissues, **$P < 0.01$. **(D)** Cell lines were used to explore the PMAIP1 level. Compared with NTHY-ORI3-1, PMAIP1 expression was upregulated in both FTC133 and FTC238, ***$P < 0.001$.

3.2 Knockdown of PMAIP1 significantly inhibited the proliferation and metastasis of FTC *in vitro*

To construct cell lines with PMAIP1 knockdown, FTC133 and FTC238 cells were transfected with plasmids and subsequently screened using puromycin to construct cell lines with stable knockdown of PMAIP1 and detected by WB. The results indicated that PMAIP1 exhibits a high and stable knockdown efficiency in FTC133 and FTC238 cell lines (Figure 2A). CCK-8 assays demonstrated that the knockdown of PMAIP1 in these cell lines resulted in decreased cell proliferation (Figure 2B). Additionally, the knockdown of PMAIP1 significantly inhibited the colony formation ability of both FTC133 and FTC238 (Figure 2C). To further elucidate the impact of PMAIP1 on the migratory and invasive capabilities of FTC133 and FTC238 cells, wound healing and transwell assays were conducted. Quantitative analysis revealed that the wound healing rate was significantly reduced in the shPMAIP1 group compared to the shNC group (Figure 2D). Migration and invasion assays demonstrated that, in comparison to the shNC group, the knockdown of PMAIP1 significantly decreased the numbers of invasion and migration cells of FTC133 and FTC238 (Figures 2E, F).

10.3389/fonc.2025.1502391

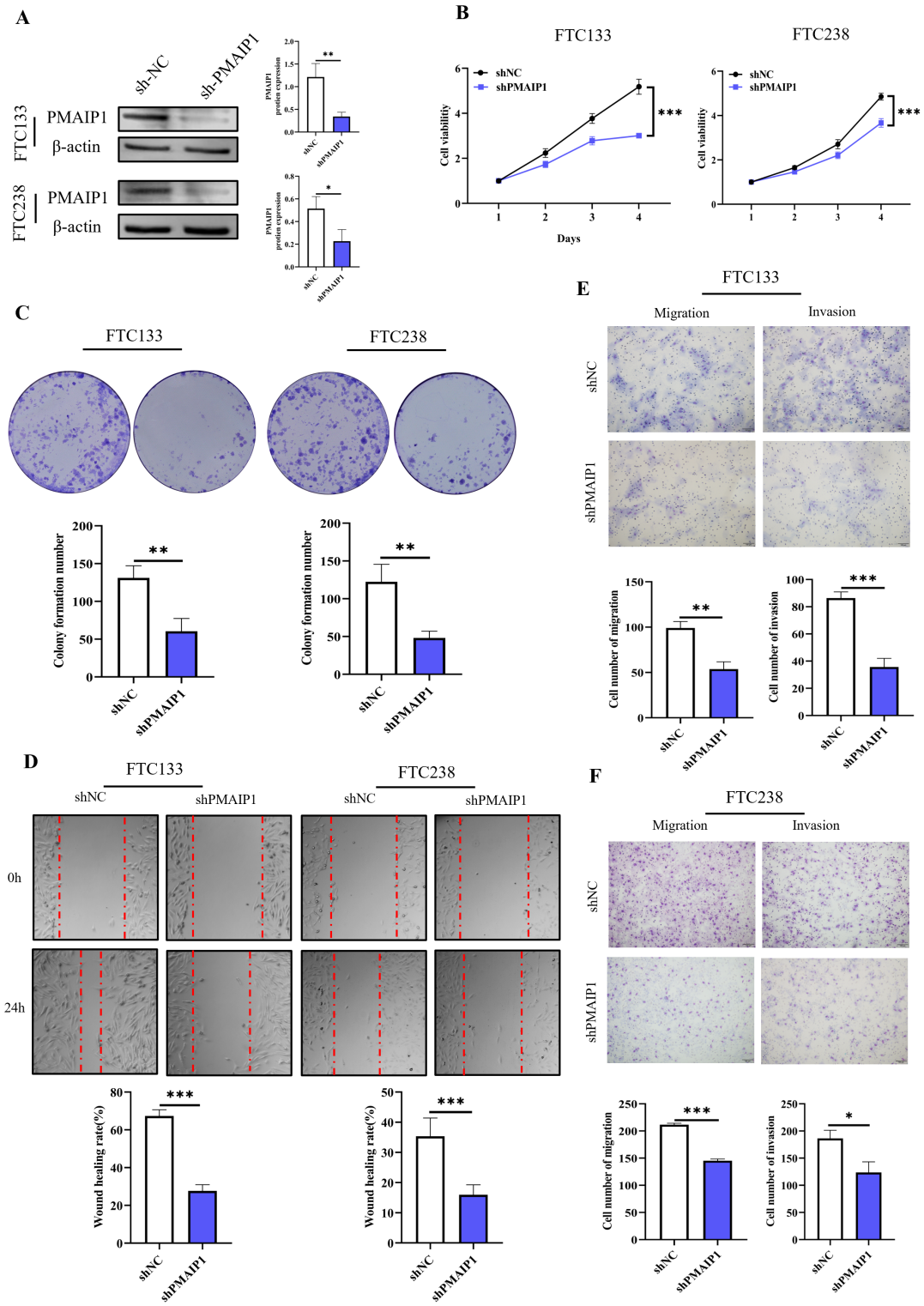

FIGURE 2
Knockdown of PMAIP1 significantly inhibited the proliferation and metastasis of FTC *in vitro*. **(A)** Stable knockdown of PMAIP1 by shRNA in FTC133 and FTC238 was confirmed by WB, $^{*}P < 0.05$, $^{**}P < 0.01$. **(B)** CCK-8 assay showed that the knockdown of PMAIP1 in FTC133 and FTC238 cells resulted in a significant decrease in cell proliferation compared with the NC group, $^{***}P < 0.001$. **(C)** Colony formation assay showed the knockdown of PMAIP1 markedly decreased the colony formation number of FTC133 and FTC238 cells compared with the NC group, $^{**}P < 0.01$. **(D)** The wound healing assay suggested the knockdown of PMAIP1 substantially impaired the wound-healing ability of FTC133 and FTC238 cells, $^{***}P < 0.001$. **(E)** Migration and invasion assay showed the knockdown of PMAIP1 significantly reduced the number of invasive and migrating FTC133 cells, $^{**}P < 0.01$, $^{***}P < 0.001$. **(F)** Migration and invasion assay showed the knockdown of PMAIP1 significantly decreased the number of invasive and migrating FTC238 cells, $^{***}P < 0.001$, $^{*}P < 0.05$.

3.3 Knockdown of PMAIP1 significantly inhibited the proliferation and metastasis of FTC *in vivo*

Initially, NTG mice underwent one week of adaptive feeding. Subsequently, FTC133 and FTC238 cells, with stable PMAIP1 knockdown and negative control, were subcutaneously injected into the left forelimb armpit of NTG mice, and tumor tissues were dissected post-experiment for further analysis (Figure 3A). The findings indicated that PMAIP1 knockdown significantly reduced tumor weight and tumor volume. In parallel, the mice in the shPMAIP1 group exhibited a significant increase in body weight compared to those in the shNC group (Figures 3B, C). To assess the impact of PMAIP1 knockdown on tumor proliferation and metastasis, we utilized the proliferation marker Ki67 and the metastasis markers MMP2 and MMP9 for further analysis. The expression levels of Ki67, MMP2, and MMP9 in tumor tissues were determined via immunohistochemical (IHC). The findings revealed that the expression levels of Ki67, MMP2, and MMP9 were reduced in the shPMAIP1 group compared with the shNC group (Figures 3D, E).

3.4 PMAIP1 activated the Wnt signaling pathway

We extracted RNA from cells of the shNC and shPMAIP1 groups in both FTC133 and FTC238 cell lines, followed by transcriptome sequencing. Differentially expressed genes were annotated to identify disease-associated genes. Intersection analysis of down-regulated genes from both cell lines revealed 82 genes (Figure 4A). Subsequent enrichment analysis of these 82 genes identified their association with several KEGG pathways, including the Apelin signaling pathway, Melanogenesis, Gastric cancer and the Wnt signaling pathway, et al. (Figure 4B). The schematic diagram of the Wnt signaling pathway shows that when PMAIP1 is knocked down, the expression levels of Wnt3, FOSL1, and PLC in the Wnt signaling pathway are correspondingly reduced. Interestingly, FOSL1 is a downstream gene of Wnt3. Therefore, we decided to explore the mechanism of the PMAIP1/Wnt3/FOSL1 pathway in FTC (Figure 4C). Additionally, we extracted data from 106 FTC patients from the TCGA database and conducted a correlation analysis, which revealed a direct proportional relationship between the expression levels of PMAIP1 and those of Wnt3 and FOSL1 (Figure 4D). These findings were consistent with the results obtained from the transcriptome sequencing analysis conducted in this study. Furthermore, we assessed the expression levels of Wnt3 and FOSL1 in both the shNC and shPMAIP1 groups and the results indicated that the knockdown of PMAIP1 led to a reduction in the expression levels of Wnt3 and FOSL1 (Figure 4E).

3.5 PMAIP1 modulated the proliferation and metastasis of FTC by regulating the Wnt signaling pathway

To elucidated the role of PMAIP1 in FTC cancer progression via the Wnt pathway, we conducted a rescue experiment employing shWnt3. Initially, we engineered FTC133 and FTC238 cell lines to overexpress PMAIP1 (Figure 5A). The results indicated that the overexpression of PMAIP1 led to elevated levels of Wnt3 and FOSL1. Conversely, the expression levels of Wnt3 and FOSL1 were significantly diminished in the Vector+shWnt3 group compared to the Vector+shNC group; in the meantime, a comparative analysis revealed that the expression levels of Wnt3 and FOSL1 were significantly reduced in the PMAIP1+shWnt3 group relative to the PMAIP1+shNC group (Figure 5A). This indicated that the knockdown of Wnt3 was successful. The CCK-8 assays demonstrated that cell proliferation in the PMAIP1+shNC group was increased compared with the Vector+shNC group. Furthermore, compared with the Vector+shNC group, proliferation of cells of the Vector+shWnt3 group was significantly decreased. Compared with the PMAIP1+shNC group, proliferation of cells of the PMAIP1 +shWnt3 group was significantly decreased (Figure 5B). Cell colony formation numbers of the PMAIP1+shNC group was increased compared with the Vector+shNC group. Compared with the Vector+shNC group, cell colony formation numbers of the Vector+shWnt3 group was significantly decreased. Compared to the PMAIP1+shNC group, cell colony formation numbers of the PMAIP1+shWnt3 group was significantly decreased (Figure 5C). The wound healing assays demonstrated that the wound healing rate of the PMAIP1+shNC group was increased compared with the Vector +shNC group. Furthermore, compared with the Vector+shNC group, the wound healing rate of the Vector+shWnt3 group was significantly decreased. Compared to the PMAIP1+shNC group, the wound healing rate of the PMAIP1+shWnt3 group was significantly decreased (Figure 5D). Migration and invasion assays revealed that the cell invasion and migration numbers of the PMAIP1+shNC group was increased compared with the Vector+shNC group. Compared with the Vector+shNC group, cell numbers of the Vector+shWnt3 group was significantly decreased. Compared to the PMAIP1+shNC group, cell numbers of the PMAIP1+shWnt3 group was significantly decreased (Figures 5E, F).

3.6 PMAIP1 regulated the proliferation and metastasis of FTC by FOSL1

These experimental results suggested that PMAIP1 influences the cancer progression of FTC through the Wnt pathway. However, the potential involvement of FOSL1 in this process remains to be elucidated. To investigate this, we transfected FTC133 and FTC238 cells with siRNA targeting FOSL1. The results indicated that, in

10.3389/fonc.2025.1502391

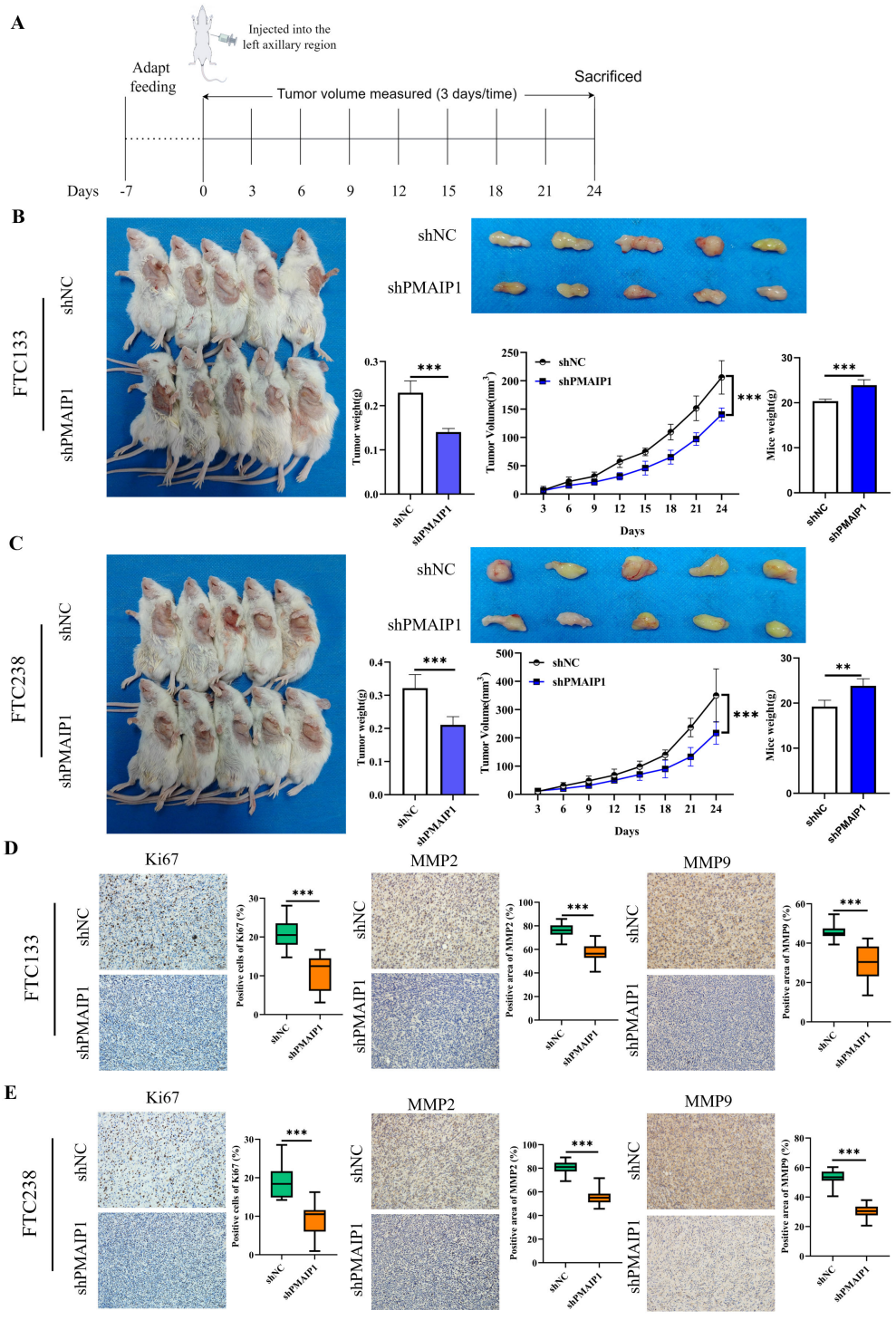

FIGURE 3
Knockdown of PMAIP1 significantly inhibited the proliferation and metastasis of FTC *in vivo*. **(A)** Experimental flowchart of subcutaneous tumor transplantation in NTG mice. **(B)** Compared with the NC group, the weight and volume of tumors of FTC133 were significantly reduced (***$P < 0.001$) and the body weight of mice was increased (***$P < 0.001$) by knockdown of PMAIP1. **(C)** Compared with the NC group, the weight and volume of tumors of FTC238 were significantly reduced (***$P < 0.001$) and the body weight of mice was increased (**$P < 0.01$) by knockdown of PMAIP1. **(D)** Knockdown of PMAIP1 decreased the Ki67 positive cells percentage, MMP2 and MMP9 positive area percentage in FTC133 subcutaneous xenografts determined by IHC staining, ***$P < 0.001$. **(E)** Knockdown of PMAIP1 decreased the Ki67 positive cells percentage, MMP2 and MMP9 positive area percentage in FTC238 subcutaneous xenografts determined by IHC staining, ***$P < 0.001$.

10.3389/fonc.2025.1502391

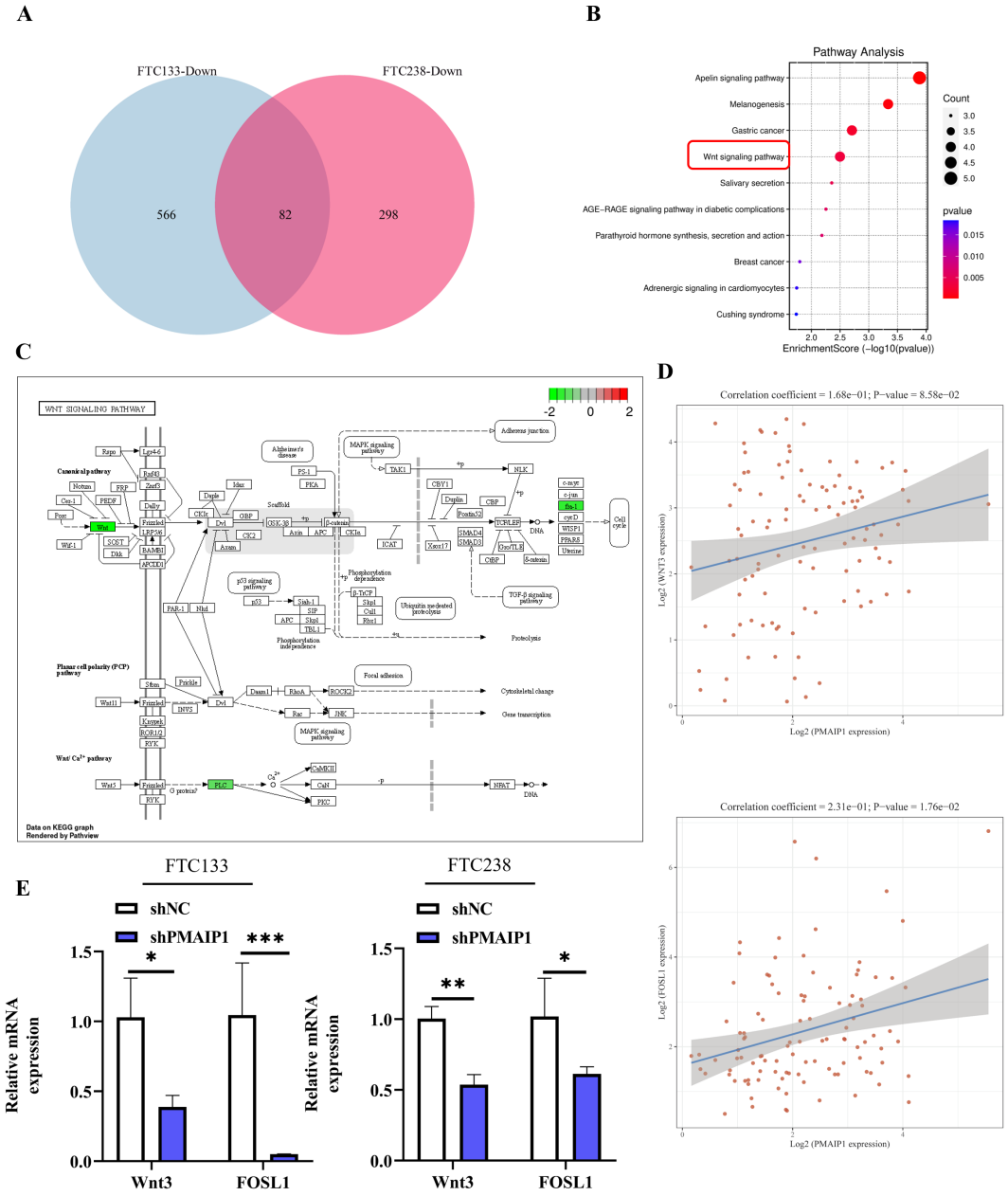

FIGURE 4
PMAIP1 activated the Wnt signaling pathway. **(A)** Venn diagram of downregulated genes in FTC133 and FTC238 cells and 82 common genes were detected. **(B)** The top 10 enrichment KEGG pathways of 82 intersection genes were shown. **(C)** As the Wnt signaling pathway showed, expression of Wnt, fra-1, and PLC were decreased after the knockdown of PMAIP1. **(D)** Spearman's correlation analysis of TCGA dataset suggested that the expression level of PMAIP1 was directly proportional to Wnt3 in FTC and the expression levels of PMAIP1 are directly proportional to FOSL1 in FTC. **(E)** In FTC133 and FTC238 cell lines, the expression levels of Wnt3 and FOSL1 were both decreased after PMAIP1 was knocked down, $*P < 0.05$, $**P < 0.01$, $***P < 0.001$.

comparison to the Vector+siNC group, the expression level of FOSL1 was significantly reduced in the Vector+siFOSL1 group: in comparison to the PMAIP1+siNC group, the expression level of FOSL1 in the PMAIP1+ siFOSL1 group was significantly reduced, indicating successful siRNA transfection (Figure 6A). The CCK-8 assays demonstrated that, compared with the Vector+siNC group, proliferation of cells of the Vector+siFOSL1 group was significantly decreased. Compared with the PMAIP1+siNC group, proliferation of cells of the PMAIP1+ siFOSL1 group was significantly decreased (Figure 6B). Compared with the Vector+siNC group, cell colony formation numbers of the Vector+siFOSL1 group was significantly decreased. Compared to the PMAIP1+siNC group, cell colony formation numbers of the PMAIP1+siFOSL1 group was significantly decreased (Figure 6C). The wound healing assays demonstrated that, compared with the Vector+siNC group, the wound healing rate of the Vector+siFOSL1 group was significantly decreased. Compared to the PMAIP1+siNC group, the wound healing rate of the PMAIP1+siFOSL1 group was significantly

10.3389/fonc.2025.1502391

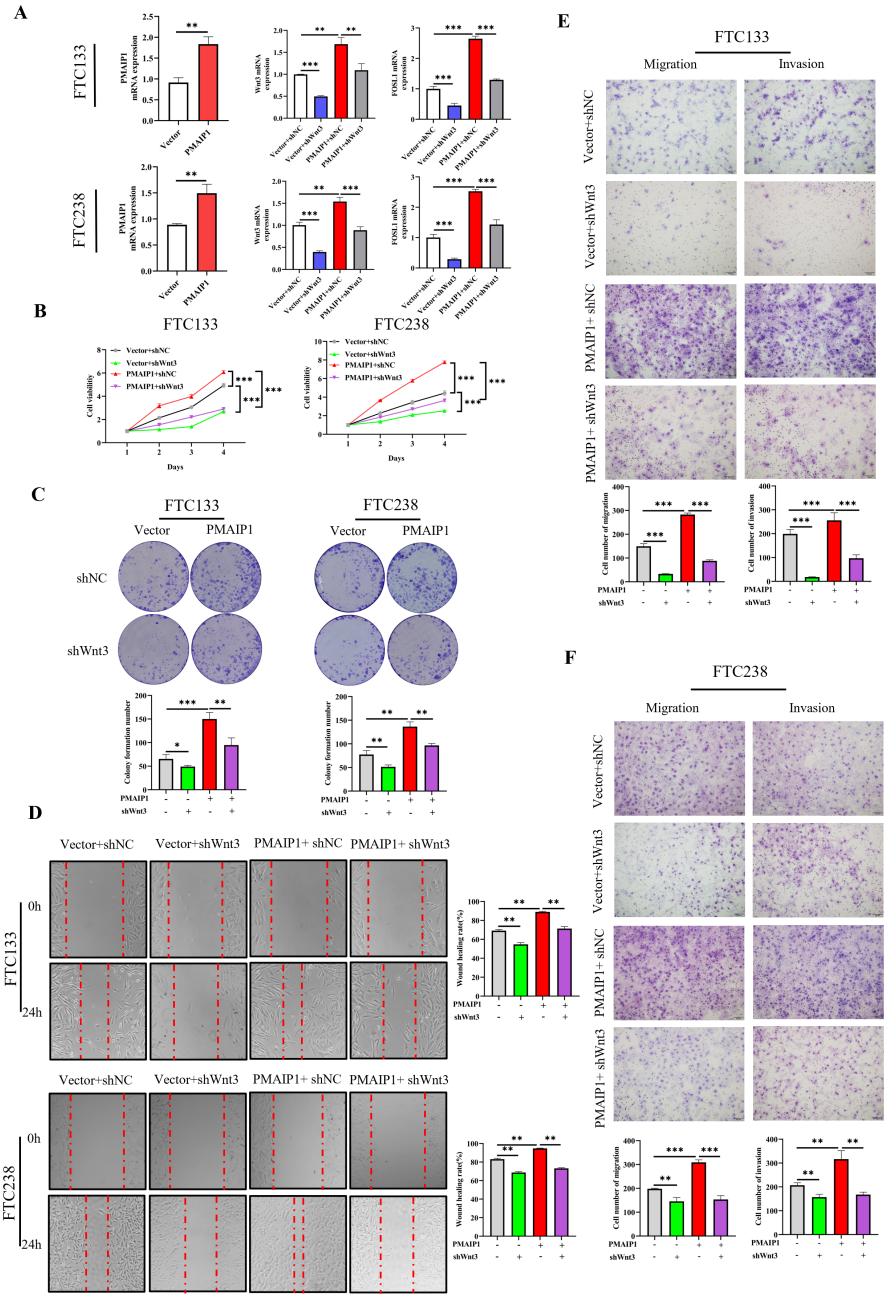

FIGURE 5
PMAIP1 modulated the proliferation and metastasis of FTC by regulating the Wnt signaling pathway. **(A)** Overexpression of PMAIP1 in FTC133 and FTC238 was confirmed by qRT-PCR. The overexpression of PMAIP1 led to elevated levels of Wnt3 and FOSL1. Conversely, the expression levels of Wnt3 and FOSL1 were significantly diminished in the Vector+shWnt3 group compared to the Vector+shNC group; in the meantime, a comparative analysis revealed that the expression levels of Wnt3 and FOSL1 were significantly reduced in the PMAIP1+shWnt3 group relative to the PMAIP1+shNC group, $^{**}P < 0.01$, $^{***}P < 0.001$. **(B)** CCK-8 assay was used to determine the proliferation ability of cells. The proliferation ability of FTC133 and FTC238 in the PMAIP1+shNC group were promoted compared with the Vector+shNC group, $^{***}P < 0.001$. Compared with the Vector+shNC group, the knockdown of Wnt3 significantly decreased the proliferation ability of FTC133 and FTC238 in the Vector+shWnt3 group, $^{***}P < 0.001$. Compared with the PMAIP1+shNC group, the knockdown of Wnt3 significantly decreased the proliferation ability of FTC133 and FTC238 in the PMAIP1+shWnt3 group, $^{***}P < 0.001$. **(C)** The colony formation numbers of FTC133 and FTC238 in the PMAIP1+shNC group were promoted compared with the Vector+shNC group, $^{**}P < 0.01$, $^{***}P < 0.001$. Compared with the Vector +shNC group, knockdown of Wnt3 significantly decreased the colony formation numbers of FTC133 and FTC238 in the Vector+shWnt3 group, $^{*}P < 0.05$, $^{**}P < 0.01$. Compared with the PMAIP1+shNC group, knockdown of Wnt3 significantly decreased the colony formation numbers of FTC133 and FTC238 in the PMAIP1+shWnt3 group, $^{**}P < 0.01$. **(D)** The wound-healing rates of FTC133 and FTC238 in the PMAIP1+shNC group were promoted compared with the Vector+shNC group, $^{**}P < 0.01$. Compared with the Vector+shNC group, the knockdown of Wnt3 significantly decreased the wound-healing rate of FTC133 and FTC238 in the Vector+shWnt3 group, $^{**}P < 0.01$. Compared with the PMAIP1+shNC group, the knockdown of Wnt3 significantly decreased the wound-healing rate of FTC133 and FTC238 in the PMAIP1+shWnt3 group, $^{**}P < 0.01$. **(E, F)** Migration and invasion cell numbers of FTC133 and FTC238 in the PMAIP1 +shNC group were increased compared with the Vector+shNC group, $^{**}P < 0.01$, $^{***}P < 0.001$. Compared with the Vector+shNC group, migration and invasion cells of FTC133 and FTC238 significantly decreased in the Vector+shWnt3 group, $^{**}P < 0.01$, $^{***}P < 0.001$. Compared with the PMAIP1+shNC group, migration and invasion cells of FTC133 and FTC238 significantly decreased in the PMAIP1+shWnt3 group, $^{**}P < 0.01$, $^{***}P < 0.001$.

10.3389/fonc.2025.1502391

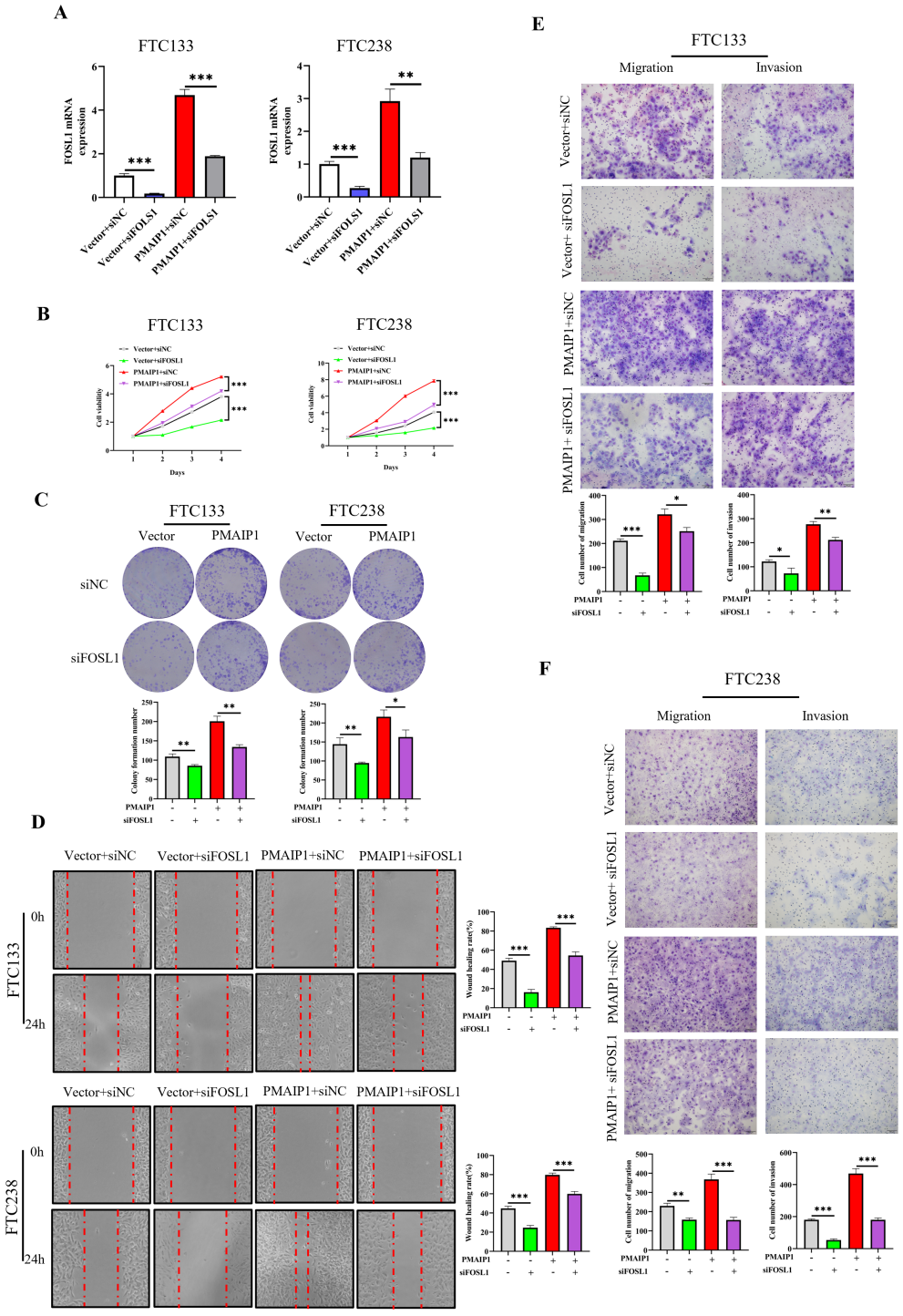

FIGURE 6
PMAIP1 regulated the proliferation and metastasis of FTC by FOSL1. **(A)** Knockdown of FOSL1 in FTC133 and FTC238 was confirmed by qRT-PCR. The expression level of FOSL1 were significantly diminished in the Vector+siFOSL1 group compared to the Vector+siNC group; the expression level of FOSL1 were significantly reduced in the PMAIP1+ siFOSL1 group relative to the PMAIP1+siNC group, $^{**}P < 0.01$, $^{***}P < 0.001$. **(B)** Compared with the Vector+siNC group, the knockdown of FOSL1 significantly decreased the proliferation ability of FTC133 and FTC238 in the Vector+siFOSL1 group, $^{***}P < 0.001$. Compared with the PMAIP1+siNC group, the knockdown of FOSL1 significantly decreased the proliferation ability of FTC133 and FTC238 in the PMAIP1+siFOSL1 group, $^{***}P < 0.001$. **(C)** Compared with the Vector+siNC group, the knockdown of FOSL1 significantly decreased the colony formation numbers of FTC133 and FTC238 in the Vector+siFOSL1 group, $^{*}P < 0.05$, $^{**}P < 0.01$. Compared with the PMAIP1 +siNC group, knockdown of FOSL1 significantly decreased the colony formation numbers of FTC133 and FTC238 in the PMAIP1+siFOSL1 group, $^{**}P < 0.01$. **(D)** Compared with the Vector+siNC group, knockdown of FOSL1 significantly decreased the wound-healing rate of FTC133 and FTC238 in the Vector+siFOSL1 group, $^{***}P < 0.001$. Compared with the PMAIP1+siNC group, knockdown of FOSL1 significantly decreased the wound-healing rate of FTC133 and FTC238 in the PMAIP1+siFOSL1 group, $^{***}P < 0.001$. **(E, F)** Compared with the Vector+ siNC group, migration and invasion cells of FTC133 and FTC238 significantly decreased in the Vector+siFOSL1 group, $^{*}P < 0.05$, $^{**}P < 0.01$, $^{***}P < 0.001$. Compared with the PMAIP1+siNC group, migration and invasion cells of FTC133 and FTC238 significantly decreased in the PMAIP1+ siFOSL1 group, $^{*}P < 0.05$, $^{**}P < 0.01$, $^{***}P < 0.001$.

decreased (Figure 6D). Migration and invasion assays revealed that, compared with the Vector+siNC group, cell numbers of the Vector +siFOSL1 group was significantly decreased. Compared to the PMAIP1+siNC group, cell numbers of the PMAIP1+siFOSL1 group was significantly decreased (Figures 6E, F).

4 Discussion

Our study innovatively confirmed that PMAIP1 could impact the progression of FTC by regulating the Wnt3/FOSL1 pathway, thereby offered new therapeutic possibilities for FTC. FTC is the second most common histotype of differentiated thyroid cancer, often overshadowed by the more prevalent PTC (13). However, the propensity of FTC for distant metastasis and poor prognosis renders it a critical subtype of thyroid cancer that warrants significant attention (5). Despite the growing body of research on FTC over the years, its pathogenesis remains largely elusive. Identifying potential biomarkers is crucial for advancing our understanding of FTC pathogenesis and for identifying potential therapeutic targets. In this study, we analyzed data from FTC and normal tissues available in the TCGA and GETx databases. Our findings revealed that the expression level of PMAIP1 was significantly elevated in FTC tissues compared to normal tissues. Notably, PMAIP1 was also overexpressed in FTC stages I-IV, suggested that its overexpression may influence the progression of FTC. Furthermore, validation using collected FTC tissues and FTC cell lines yielded results consistent with our initial analysis. Consequently, we hypothesized that PMAIP1 is overexpressed in FTC and may exert a pro-cancer effect.

To validate our hypothesis, we achieved stable knockdown of PMAIP1 in two cell lines, FTC133 and FTC238, resulting in a marked inhibition of cell proliferation and metastatic capability. Additionally, we established a subcutaneous xenograft model using immunodeficient mice. The findings demonstrated that PMAIP1 knockdown significantly suppressed the growth of FTC tumors *in vivo*, as evidenced by reductions in both tumor weight and volume. This study demonstrated that the knockdown of PMAIP1 inhibited the progression of FTC both *in vivo* and *in vitro*. Ki67 was utilized as a significant marker for cell proliferation, while MMP2 and MMP9 served as critical markers for distant metastasis (14–16). IHC results revealed that the knockdown of PMAIP1 was associated with reduced expression levels of Ki67, MMP2, and MMP9. These findings suggested that targeting PMAIP1 could effectively inhibit FTC growth and metastasis, thereby expanding clinical treatment options for FTC.

Additionally, PMAIP1 has been implicated in various biological processes. For instance, long non-coding RNA LOC101928963 regulated the proliferation and apoptosis of spinal glioma by interacting with PMAIP1, providing a foundation for targeted therapy of spinal glioma (17). Plant Homeo Domain Finger Protein 8 regulated mesodermal and cardiac differentiation of embryonic stem cells by mediating the histone demethylation of PMAIP1 (18). Another study elucidated a novel non-epigenetic mechanism of action for the hypomethylating agent 5-azacitidine and its synergistic activity with the BCL-2 selective inhibitor venetoclax. This combination, through the ISR-mediated induction of PMAIP1, could reduce drug resistance in acute myeloid leukemia (19). These findings suggested that PMAIP1 was a critical regulator in disease development and treatment. However, there are limited studies on the role of PMAIP1 in TC. Bortezomib sensitized TC cells to Vemurafenib through mitochondrial dysregulation and the induction of apoptosis, which was accompanied by an increased expression of NOXA/PMAIP1 (20). In this study, the knockdown of PMAIP1 significantly inhibited the proliferation and metastasis of FTC. To elucidate the pro-cancer role of PMAIP1 in FTC, we conducted further investigations. Transcriptome sequencing was utilized to identify differentially expressed genes associated with PMAIP1. Enrichment analysis of the down-regulated gene set revealed an inhibition of the Wnt signaling pathway, accompanied by the down-regulation of Wnt3 and FOSL1. Bioinformatics analysis revealed a direct proportionality between PMAIP1 and the expression levels of Wnt3 and FOSL1, corroborating the findings from transcriptome sequencing. Additionally, we verified that the expression patterns of Wnt3 and FOSL1 were consistent with those of PMAIP1. Overexpression of PMAIP1 resulted in increased expression levels of Wnt3 and FOSL1 as well. Simultaneously, we conducted rescue experiments and verified that the concurrent knockdown of Wnt3, in the context of PMAIP1 overexpression, significantly inhibited the proliferation and metastasis of FTC. These findings suggesteded that PMAIP1 may influence the proliferation and metastasis of FTC through modulation of the Wnt signaling pathway. It is well established that the Wnt signaling pathway was among the most frequently dysregulated pathways in human malignancies, playing pivotal roles in tumorigenesis and targeted therapy (21, 22). Currently, the functional mechanisms of the Wnt signaling pathway have been reported in breast cancer (23), PTC (24), prostate cancer (25) and gastric cancer (26). Notably, the relationship between PMAIP1 and the Wnt signaling pathway has not been previously documented in the literature. Our study may be the first to elucidated the regulation of FTC by PMAIP1 via the Wnt signaling pathway. Consequently, the findings of this research offered a more practical and feasible approach to the clinical management of FTC.

Current research on the apelin pathway primarily centered on its implications for cardiovascular and metabolic disorders. Apelin, a peptide ubiquitously expressed throughout the body, engaged the apelin receptor to facilitate endothelium-dependent vasodilation and inotropy, lower blood pressure, and promote angiogenesis. The apelin system was posited to confer protection against arrhythmias, inhibit thrombosis, and exert significant anti-fibrotic effects (27). Additionally, empirical studies have demonstrated that apelin influences glucose and lipid metabolism and modulates insulin secretion (28). Moreover, evidence suggested that the apelin system was involved in inflammatory responses (29). On the other hand, components of the Wnt signaling pathway have been established as reliable biomarkers and potential targets for cancer therapy. Ongoing or completed clinical trials involving Wnt signaling pathway components indicated that Wnt-targeted therapies hold promising applications in clinical settings (30). Furthermore, updates on inhibitors, antagonists, and activators of

the Wnt signaling pathway presented innovative strategies for personalized cancer treatment (21). This emphasized our focus on the Wnt signaling pathway. Our discovery found that PMAIP1 played a cancer-promoting role in FTC, representing a significant finding and identifying a potential target for FTC treatment. This rationale was compelling. However, we aimed for our research to inform clinical practices in the treatment of FTC and to facilitate the rapid translation of these findings into patient benefits. Therefore, investigating the regulatory relationship between the novel FTC oncogene PMAIP1 and the Wnt pathway during FTC progression opened new avenues for dual-targeted therapy of this malignancy, which holds substantial clinical significance. While we prioritized our investigation into the Wnt pathway, we did not overlook Apelin's potential role in FTC. Moving forward, we will continue to monitor and explore various signaling pathways in FTC—including the Apelin signaling pathway.

Although we have demonstrated that PMAIP1 exerts its effects on FTC through the Wnt signaling pathway. Furthermore, modulation of PMAIP1 expression, either through knockdown or overexpression, correspondingly resulted in the down-regulation or up-regulation of FOSL1 expression levels. FOSL1 (also known as FRA-1) functions downstream of the Wnt signaling pathway and was implicated in promoting metastasis in head and neck squamous cell carcinoma, suggested its role as an oncogene (31). This raised the question of whether PMAIP1 exerts a pro-cancer effect on FTC by regulating FOSL1 downstream of Wnt. To address this, a series of rescue experiments were conducted in this study. The results demonstrated that the proliferation and metastasis of FTC cells were significantly inhibited following the knockdown of FOSL1. The same results were observed when FOSL1 was knocked down in the FTC cell line stably overexpressing PMAIP1. Consequently, we posited that our study substantiates, at least in part, the role of PMAIP1 in regulating the cancer progression of FTC via modulation of the Wnt3/FOSL1 pathway. FOSL1, a transcription factor, has been shown in previous studies to be highly upregulated in bile duct cancer in both humans and mice, correlating with poorer survival outcomes (32). Additionally, FOSL1 has been demonstrated to promote the proliferation, invasion, migration, and epithelial-mesenchymal transition of colorectal cancer cells, and was significantly associated with poor prognosis (33). These findings align with our research outcomes. Our results indicated that FOSL1 contributes to the oncogenesis of FTC by enhancing its proliferation and metastasis, a process regulated by PMAIP1 through the Wnt signaling pathway. This mechanism, which we have identified, could be critical for the progression of FTC and holds potential clinical significance.

Our study has several limitations. Firstly, the sample size of FTC tissues was limited, attributable to the difficulties associated with the clinical diagnosis of FTC. Secondly, the precise interaction between PMAIP1 and the Wnt signaling pathway remains unclear. In future studies, we will continue to collect FTC samples to further substantiate our findings. Concurrently, we will delve deeper into the mechanisms of action of PMAIP1.

In conclusion, our research demonstrated that PMAIP1 was overexpressed in FTC and correlated with the clinical stage of the disease. PMAIP1 emerged as a novel pro-cancer factor in FTC, and its knockdown significantly inhibited the proliferation and metastasis of FTC both *in vivo* and *in vitro*. Mechanistically, PMAIP1 regulated FOSL1 by modulating the Wnt signaling pathway, thereby promoting FTC progression. Targeting PMAIP1 may present a promising therapeutic strategy for FTC.

Data availability statement

The RNA data presented in this article has been deposited to the NCBI Repository, under accession numbers PRJNA1212579.

Ethics statement

The studies involving humans were approved by The Ethics Committee of The First Hospital of Hebei Medical University. The participants provided their written informed consent to participate in this study. The animal study was approved by the experimental animal Ethics Committee of Hebei Kangtai Medical Laboratory Service Co., LTD. The studies were conducted in accordance with the local legislation and institutional requirements.

Author contributions

HW: Writing – original draft, Writing – review & editing, Investigation, Supervision. FS: Writing – original draft, Writing – review & editing, Investigation, Supervision. YW: Investigation, Supervision, Writing – review & editing. BP: Investigation, Supervision, Writing – review & editing. LK: Investigation, Supervision, Writing – review & editing. CZ: Data curation, Formal analysis, Writing – review & editing. DL: Data curation, Formal analysis, Writing – review & editing. ZL: Data curation, Formal analysis, Writing – review & editing. XJ: Writing – original draft, Writing – review & editing, Investigation, Supervision. BL: Writing – original draft, Writing – review & editing, Investigation, Supervision. ZZ: Writing – original draft, Writing – review & editing, Investigation, Supervision.

Funding

The author(s) declare financial support was received for the research, authorship, and/or publication of this article. This study was supported by Natural science foundation of Hebei Province (No.H2022206418 and H2024206117), Hebei Province Key Science and Technology Research Program (No.20240188), Hebei Provincial Department of Science and Technology Health Innovation Project (No. 20231063, 22372409D and 242W7702Z), Hebei Medical University Innovation Team Project (B-12), Hebei Medical University Graduate Innovation Funding Project (XCXZZB202310). Hebei introduction of foreign expert intelligence projects (YZ202201), Hebei clinical medicine excellent talents project of Province (ZF2025038).

Acknowledgments

Our gratitude goes to the teachers of the Department of General Surgery and Gastrointestinal Disease Diagnosis and Treatment Center of the First Hospital of Hebei Medical University for their help.

Conflict of interest

The authors declare that the research was conducted in the absence of any commercial or financial relationships that could be construed as a potential conflict of interest.

Generative AI statement

The author(s) declare that no Generative AI was used in the creation of this manuscript.

Publisher's note

References

1. Kitahara CM, Sosa JA. Understanding the ever-changing incidence of thyroid cancer. *Nat Rev Endocrinol*. (2020) 16:617–8. doi: 10.1038/s41574-020-00414-9

2. Sung H, Ferlay J, Siegel RL, Laversanne M, Soerjomataram I, Jemal A, et al. Global cancer statistics 2020: globocan estimates of incidence and mortality worldwide for 36 cancers in 185 countries. *CA: A Cancer J Clin*. (2021) 71:209–49. doi: 10.3322/caac.21660

3. Miller KD, Fidler-Benaoudia M, Keegan TH, Hipp HS, Jemal A, Siegel RL. Cancer statistics for adolescents and young adults, 2020. *CA: A Cancer J Clin*. (2020) 70:443–59. doi: 10.3322/caac.21637

4. Daniels GH. Follicular thyroid carcinoma: A perspective. *Thyroid*. (2018) 28:1229–42. doi: 10.1089/thy.2018.0306

5. Cabanillas ME, McFadden DG, Durante C. Thyroid cancer. *Lancet*. (2016) 388:2783–95. doi: 10.1016/s0140-6736(16)30172-6

6. Janus P, Toma-Jonik A, Vydra N, Mrowiec K, Korfanty J, Chadalski M, et al. Pro-death signaling of cytoprotective heat shock factor 1: upregulation of noxa leading to apoptosis in heat-sensitive cells. *Cell Death Differ*. (2020) 27:2280–92. doi: 10.1038/s41418-020-0501-8

7. Zhou X, Ren Z, Xu J, Deng C, Zhang Z, Godoy-Parejo C, et al. Insulin directs dichotomous translational regulation to control human pluripotent stem cell survival, proliferation and pluripotency. *Int J Biol Sci*. (2022) 18:3562–75. doi: 10.7150/ijbs.71199

8. Yan X, Chen D, Wang Y, Guo Y, Tong C, Wei J, et al. Identification of noxa as a pivotal regulator of resistance to car T-cell therapy in B-cell Malignancies. *Signal Transduction Targeted Ther*. (2022) 7:98. doi: 10.1038/s41392-022-00915-1

9. Cojocari D, Smith BN, Purkal JJ, Arrate MP, Huska JD, Xiao Y, et al. Pevonedistat and azacitidine upregulate noxa (Pmaip1) to increase sensitivity to venetoclax in preclinical models of acute myeloid leukemia. *Haematologica*. (2021) 107:825–35. doi: 10.3324/haematol.2020.272609

10. Doffo J, Bamopoulos SA, Köse H, Orben F, Zang C, Pons M, et al. Noxa expression drives synthetic lethality to runx1 inhibition in pancreatic cancer. *Proc Natl Acad Sci*. (2022) 119:e2105691119. doi: 10.1073/pnas.2105691119

11. Clairefond S, Péant B, Ouellet V, Barrès V, Tian Z, Trudel D, et al. Puma and noxa expression in tumor-associated benign prostatic epithelial cells are predictive of prostate cancer biochemical recurrence. *Cancers*. (2020) 12:3187. doi: 10.3390/cancers12113187

12. Kosmidou V, Vlassi M, Anagiotos K, Raftopoulou S, Kalogerakou E, Skarmalioraki S, et al. Noxa upregulation and 5-gene apoptotic biomarker panel in colorectal cancer. *Eur J Clin Invest*. (2020) 51:e13353. doi: 10.1111/eci.13353

13. Grani G, Lamartina L, Durante C, Filetti S, Cooper DS. Follicular thyroid cancer and hürthle cell carcinoma: challenges in diagnosis, treatment, and clinical management. *Lancet Diabetes Endocrinol*. (2018) 6:500–14. doi: 10.1016/s2213-8587(17)30325-x

14. La Rosa S. Diagnostic, prognostic, and predictive role of ki67 proliferative index in neuroendocrine and endocrine neoplasms: past, present, and future. *Endocrine Pathol*. (2023) 34:79–97. doi: 10.1007/s12022-023-09755-3

15. Murugan AK, Al-Amr A, Al-Ansari MM, Manogaran PS, Al-Hindi H, Alzahrani AS. Single nucleotide polymorphisms in matrix metalloproteinase 2 (Mmp2) enhance brafv600e mutation-mediated oncogenicity and invasiveness of papillary thyroid cancer cells. *Endocrine-Related Cancer*. (2021) 28:273–89. doi: 10.1530/erc-20-0242

16. Shang W, Wang Y, Liang X, Li T, Shao W, Liu F, et al. Setdb1 promotes gastric carcinogenesis and metastasis via upregulation of ccnd1 and mmp9 expression. *J Pathol*. (2020) 253:148–59. doi: 10.1002/path.5568

17. Zheng Y-J, Liang T-S, Wang J, Zhao J-Y, Yang D-K, Liu Z-S. Silencing lncrna loc101928963 inhibits proliferation and promotes apoptosis in spinal cord glioma cells by binding to pmaip1. *Mol Ther - Nucleic Acids*. (2019) 18:485–95. doi: 10.1016/j.omtn.2019.07.026

18. Tang Y, Hong Y-Z, Bai H-J, Wu Q, Chen CD, Lang J-Y, et al. Plant homeo domain finger protein 8 regulates mesodermal and cardiac differentiation of embryonic stem cells through mediating the histone demethylation of pmaip1. *Stem Cells*. (2016) 34:1527–40. doi: 10.1002/stem.2333

19. Jin S, Cojocari D, Purkal JJ, Popovic R, Talaty NN, Xiao Y, et al. 5-azacitidine induces NOXA to prime AML cells for venetoclax-mediated apoptosis. *Clin Cancer Res*. (2020) 26:3371–83. doi: 10.1158/1078-0432

20. Tsumagari K, Abd Elmageed ZY, Sholl AB, Green EA, Sobti S, Khan AR, et al. Bortezomib sensitizes thyroid cancer to braf inhibitor *in vitro* and *in vivo*. *Endocrine-Related Cancer*. (2018) 25:99–109. doi: 10.1530/erc-17-0182

21. Zhang Y, Wang X. Targeting the wnt/B-catenin signaling pathway in cancer. *J Hematol Oncol*. (2020) 13:165. doi: 10.1186/s13045-020-00990-3

22. Song P, Gao Z, Bao Y, Chen L, Huang Y, Liu Y, et al. Wnt/B-catenin signaling pathway in carcinogenesis and cancer therapy. *J Hematol Oncol*. (2024) 17:46. doi: 10.1186/s13045-024-01563-4

23. Li X, Chen W, Huang L, Zhu M, Zhang H, Si Y, et al. Sinomenine hydrochloride suppresses the stemness of breast cancer stem cells by inhibiting Wnt signaling pathway through down-regulation of WNT10B. *Pharmacol Res*. (2022) 179:106222. doi: 10.1016/j.phrs.2022.106222

24. Lv P, Xue Y. Ets like-1 protein elk1-induced lncrna linc01638 accelerates the progression of papillary thyroid cancer by regulating axin2 through wnt/B-catenin signaling pathway. *Bioengineered*. (2021) 12:3873–85. doi: 10.1080/21655979.2021.1935404

25. Zhang X, Li H, Wang Y, Zhao H, Wang Z, Chan FL. Nuclear receptor NURR1 functions to promote stemness and epithelial-mesenchymal transition in prostate cancer via its targeting of Wnt/β-catenin signaling pathway. *Cell Death Dis*. (2024) 15:234. doi: 10.1038/s41419-024-06621-w

26. Zhang J, Wang H, Wu J, Yuan C, Chen S, Liu S, et al. GALNT1 enhances Malignant phenotype of gastric cancer via modulating CD44 glycosylation to activate the wnt/β-catenin signaling pathway. *Int J Biol Sci*. (2021) 18:6068–83. doi: 10.7150/ijbs.73431

27. Chapman FA, Maguire JJ, Newby DE, Davenport AP, Dhaun N. Targeting the apelin system for the treatment of cardiovascular diseases. *Cardiovasc Res*. (2023) 119:2683–96. doi: 10.1093/cvr/cvad171

28. Bertrand C, Valet P, Castan-Laurell I. Apelin and energy metabolism. *Front Physiol*. (2015) 6:115. doi: 10.3389/fphys.2015.00115

29. Wang X, Zhang L, Li P, Zheng Y, Yang Y, Ji S. Apelin/APJ system in inflammation. *Int Immunopharmacol*. (2022) 109:108822. doi: 10.1016/j.intimp.2022.108822

30. Neiheisel A, Kaur M, Ma N, Havard P, Shenoy AK. Wnt pathway modulators in cancer therapeutics: An update on completed and ongoing clinical trials. *Int J Cancer*. (2022) 150:727–40. doi: 10.1002/ijc.33811

31. Zhang M, Hoyle RG, Ma Z, Sun B, Cai W, Cai H, et al. Fosl1 promotes metastasis of head and neck squamous cell carcinoma through super-enhancer-driven transcription program. *Mol Ther*. (2021) 29:2583–600. doi: 10.1016/j.ymthe.2021.03.024

32. Vallejo A, Erice O, Entrialgo-Cadierno R, Feliu I, Guruceaga E, Perugorria MJ, et al. Fosl1 promotes cholangiocarcinoma via transcriptional effectors that could be therapeutically targeted. *J Hepatol*. (2021) 75:363–76. doi: 10.1016/j.jhep.2021.03.028

33. Liu Y, Yue M, Li Z. Fosl1 promotes tumorigenesis in colorectal carcinoma by mediating the fbxl2/wnt/B-catenin axis via smurf1. *Pharmacol Res*. (2021) 165:105405. doi: 10.1016/j.phrs.2020.105405

frontiers | Frontiers in Endocrinology

TYPE Original Research
PUBLISHED 10 February 2025
DOI 10.3389/fendo.2025.1514264

OPEN ACCESS

EDITED BY
Francesca Coperchini,
University of Pavia, Italy

REVIEWED BY
Shioko Kimura,
National Institutes of Health (NIH), United States
Jing Pan,
Houston Methodist Research Institute, United States

*CORRESPONDENCE
Yufei Shi
yufei@kfshrc.edu.sa

RECEIVED 20 October 2024
ACCEPTED 24 January 2025
PUBLISHED 10 February 2025

CITATION
Zou M, Qattan A, Al-Alwan M, Ghebeh H, Binjumah N, Al-Haj L, Khabar KSA, Altaweel A, Almohanna F, Assiri AM, Aboussekhra A, Alzahrani AS and Shi Y (2025) Genome-wide transcriptome analysis and drug target discovery reveal key genes and pathways in thyroid cancer metastasis.
Front. Endocrinol. 16:1514264.
doi: 10.3389/fendo.2025.1514264

Genome-wide transcriptome analysis and drug target discovery reveal key genes and pathways in thyroid cancer metastasis

Minjing Zou[1], Amal Qattan[1], Monther Al-Alwan[2], Hazem Ghebeh[2], Naif Binjumah[1], Latifa Al-Haj[3], Khalid S. A. Khabar[3], Abdulmohsen Altaweel[1], Falah Almohanna[4], Abdullah M. Assiri[4], Abdelilah Aboussekhra[1], Ali S. Alzahrani[1,5] and Yufei Shi[1*]

[1]Department of Molecular Oncology, King Faisal Specialist Hospital and Research Centre, Riyadh, Saudi Arabia, [2]Department of Cell Therapy and Immunobiology, King Faisal Specialist Hospital and Research Centre, Riyadh, Saudi Arabia, [3]Department of Molecular Biomedicine, King Faisal Specialist Hospital and Research Centre, Riyadh, Saudi Arabia, [4]Department of Comparative Medicine, King Faisal Specialist Hospital and Research Centre, Riyadh, Saudi Arabia, [5]Department of Medicine, King Faisal Specialist Hospital and Research Centre, Riyadh, Saudi Arabia

Introduction: Metastasis is the major cause of thyroid cancer morbidity and mortality. However, the mechanisms are still poorly understood.

Methods: We performed genome-wide transcriptome analysis comparing gene expression profile of metastatic thyroid cancer cells (Met) with primary tumor cells established from transgenic mouse models of papillary thyroid cancer (PTC), follicular thyroid cancer (FTC), poorly differentiated thyroid cancer (PDTC), and anaplastic thyroid cancer (ATC).

Results: Genes involved in tumor microenvironment (TME), inflammation, and immune escape were significantly overexpressed in Met cells. Notably, IL-6-mediated inflammatory and PD-L1 pathways were highly active in Met cells with increased secretion of pro-inflammatory and pro-metastatic cytokines such as CCL2, CCL11, IL5, IL6, and CXCL5. Furthermore, Met cells showed robust overexpression of Tbxas1, a thromboxane A synthase 1 gene that catalyzes the conversion of prostaglandin H2 to thromboxane A2 (TXA2), a potent inducer of platelet aggregation. Application of aspirin, a TXA2 inhibitor, significantly reduced lung metastases. Mertk, a member of the TAM (Tyro, Axl, Mertk) family of RTKs, was also overexpressed in Met cells, which led to increased MAPK activation, epithelial–mesenchymal transition (EMT), and enrichment of cancer stem cells. Braf-mutant Met cells developed resistance to BRAFV600E inhibitor PLX4720, but remained sensitive to β-catenin inhibitor PKF118-310.

Conclusion: We have identified several overexpressed genes/pathways in thyroid cancer metastasis, making them attractive therapeutic targets. Given the complexity of metastasis involving multiple pathways (PD-L1, Mertk, IL6, COX-1/Tbxas1-TXA2), simultaneously targeting more than one of these pathways may be warranted to achieve better therapeutic effect for metastatic thyroid cancer.

KEYWORDS

CD274 (PD-L1), TBXAS1, MERTK, IL6, thyroid cancer metastasis

Introduction

Thyroid cancer is the most common malignancy in the endocrine system and its incidence have been rising in the past few decades with vast majority of this increase being ascribed to papillary thyroid carcinoma (PTC) (1–3). The rise in incidence seems to be due to over-diagnosis, but an actual increase in incidence and mortality cannot be completely ruled out (2, 4). The follicular cell-derived thyroid cancer can be histologically classified into papillary thyroid carcinoma (PTC), follicular thyroid carcinoma (FTC), poorly differentiated thyroid carcinoma (PDTC) and anaplastic thyroid carcinoma (ATC). Differentiated thyroid carcinoma (DTC) has excellent prognosis with a 10-year disease-specific survival of up to 90%, PDTC has poorer prognosis with a 5-year disease-specific survival at 66%. ATC is highly virulent with a mean survival of less than 8 months (5–7). PTC is the most common type of DTC, accounting for more than 85% of all thyroid cancer cases followed by FTC (5-10%), PDTC (4-7%) and ATC (about 2%) (7, 8).

The initiation and progression of thyroid cancer occur through gradual accumulation of multiple genetic alterations, leading to constitutive activation of two crucial signaling pathways: MAPK and PI3K/AKT (9). MAPK activation is considered to be crucial for PTC initiation, through point mutations of *BRAF* and *RAS* genes or chromosomal rearrangements of *RET/PTC* and neurotrophic tropomyosin receptor kinase (*NTRK*) gene. The $BRAF^{V600E}$ mutation is the most frequent genetic alteration in PTC with overall rate of 48.5% (10). PI3K/AKT activation is critical in FTC initiation and can be triggered by activating mutations in *RAS*, *PIK3CA*, and *AKT1* as well as by inactivation of *PTEN*. *RAS* (*HRAS*, *KRAS* and *NRAS*) mutations occur in 30–45% of FTC (11). The progression and dedifferentiation to PDTC and ATC are thought to arise from preexisting DTC as a result of acquiring additional genetic changes such as mutations in *TERT* promoter, *TP53*, *EIF1AX*, and *CDKN2A.TP53* mutations are present in 50–80% of ATC and is one of the pivotal molecular alterations discriminating ATC from PTC or FTC (12).

Distant metastasis is the leading cause of thyroid cancer mortality and morbidity (13, 14). The metastatic cascade represents a multi-step process which includes local tumor cell invasion of the basement membrane, intravasation into the vasculature, survival in the circulation, extravasation from the circulation, and final colonization by the circulating tumor cells at the distal sites (15). Distant metastasis occurs in about 10% of PTC and up to 25% FTC patients. The most common distant metastatic sites are lungs (~80%) and bones (~25%) (16, 17). The five-year survival rate dropped from 77.6% to 15.3% in patients with single organ and multi-organ distant metastasis, respectively (14).

Activation of metastatic reprogramming and survival of circulating tumor cells in the blood with eventual colonization at distant organs are critical steps for thyroid cancer metastasis. These steps are influenced by both tumor intrinsic (genetic mutations and epigenetic modifications) and extrinsic factors (tumor microenvironment or TME) (5, 16). However, detailed mechanisms contributing to thyroid cancer metastasis are still lacking. Understanding the underlying mechanisms would enable targeted intervention. The present study investigated the mechanisms that regulate circulating tumor cell survival in the blood circulation and colonization at lung by using cell lines derived from genetically engineered mouse models of PTC, FTC, PDTC, and ATC, representing the whole spectrum of thyroid carcinogenesis.

Materials and methods

Experimental animals

Athymic BALB/c-nu/nu (nude mice) were acquired from Jackson Laboratory. Mice were provided with autoclaved food and water ad libitum. The study was approved by the Animal Care and Use Committee of the institution and was conducted in compliance with the Public Health Service Guidelines for the Care and Use of Animals in Research (RAC#2230003).

Thyroid cancer cell lines

Four murine thyroid cancer cell lines derived from genetically engineered mouse models of PTC, FTC, PDTC, and ATC were established from primary tumors: PTC with $Braf^{V600E}$ mutation (BVE), FTC with $Kras^{G12D}$ mutation (KGD), PDTC with both $Kras^{G12D}$ and $Cdkn2a^{null}$ mutations (KGD^{Cdkn2a_null}), and ATC with both $Braf^{V600E}$ and $Trp53^{null}$ mutations (BVE^{Trp53_null}). The establishment of BVE, KGD, and BVE^{Trp53_null} strains were

described previously (18–21). KGD^{Cdkn2a_null} was established by cross-breeding among *Kras*^{G12D}, TPO-Cre, and *Cdkn2a*^{null} (strain 01XE4 obtained from The NCI Mouse Repository, (https://frederick.cancer.gov/resources/data-repositories/nci-mouse-repository) (79). PDTC was developed from a 13-month-old mouse with both *Kras*^{G12D} and *Cdkn2a*^{null} mutations. The KGD^{Cdkn2a_null} cell line was established from the tumor. Thyroid origin was confirmed by genotyping (Supplementary Figure 1). The cell lines were maintained in DMEM/F12 growth medium containing 10% fetal bovine serum, 100 units/ml penicillin, and 100 µg/ml streptomycin.

Metastatic thyroid cancer cell lines

To establish lung metastatic thyroid cancer cell lines, 1 x 10^6 BVE, KGD, KGD^{Cdkn2a_null} or BVE^{Trp53_null} cells were injected to tail vain of 5 nude mice for each group. Six weeks after injection, lung metastatic tumors were collected aseptically from the mice using blunt dissection, then mechanically dissociated by mincing and passing through a 40-µM mesh sterile screen, and suspended in DMEM/F12 growth medium for 3 months with a total of 6 passages to eliminate contaminated stromal fibroblasts, lymphocytes, and microphages present in the tumor cell culture. The primary culture were considered as permanent cell lines after six passages. The established metastatic cell lines were named as BVE-Met1, KGD-Met1, KGD^{Cdkn2a_null}-Met1, and BVE^{Trp53_null}-Met1, respectively. They were re-injected (1 x 10^6 cells) to a new group of nude mice (n=5 for each group) via tail vain for enrichment of cells with high metastatic potential. Three weeks following injection, lung metastatic tumors were harvested and propagated in DMEM/F12 growth medium for 3 month with at least 6 passages. The metastatic cell lines were named as BVE-Met2, KGD-Met2, KGD^{Cdkn2a_null}-Met2, and BVE^{Trp53_null}-Met2, respectively. The experimental procedures were summarized in Figure 1A and representative lung metastatic foci were presented in Figure 1B. The thyroid origin of these cell lines were confirmed by genotyping.

RNA sequencing analysis

RNA-Seq were used for quantification of differentially expressed genes (DEGs) between primary (BVE, KGD, KGD^{Cdkn2a_null}, and BVE^{Trp53_null}) and metastatic thyroid cancer cell lines: BVE-Met1, KGD-Met1, KGD^{Cdkn2a_null}-Met1, and BVE^{Trp53_null}-Met1, or BVE-Met2, KGD-Met2, KGD^{Cdkn2a_null}-Met2, and BVE^{Trp53_null}-Met2 cell lines. Total RNA from cell lines were isolated and libraries were constructed using an Illumina (San Diego, Ca, USA) TruSeq RNA Library Prep kit according to the manufacturer's procedure. Sequencing was performed on Illumina HiSeq 4000 with at least 20 million clean reads. The significant DEGs were selected based on the following criteria: Log2-fold change >2, false discovery rate (FDR) <0.001, and P-value from difference test<0.01. Gene list annotation and enrichment of biological pathways were performed using Metascape (https://metascape.org/gp/index.html#/main/step1).

The protein-protein interaction network construction and hub genes identification

Interactions among different proteins were performed using NetworkAnalyst (https://networkanalyst.ca/) to analyze an interactive relationship among DEGs. Genes with the degree of a node >10 (with more than 10 interacting genes) were considered as hub genes. The association of hub gene expression with disease-specific survival was performed by Kaplan–Meier analysis using TCGA-THCA mRNA expression dataset (n=498) and cBioPortal For Cancer Genomics (https://www.cbioportal.org/).

Quantitative real-time reverse transcriptase-PCR

qRT-PCR was used to validate DEGs as described previously (21). The cDNA mix was diluted 10-fold, and 2 µl of the dilution was used for qPCR analysis. The PCR conditions were 94°C for 30 sec followed by 30 cycles of amplification (94°C for 10 sec, 55°C for 5 sec, and 72°C for 10 sec). The PCR primers were listed below: Cd274-F, 5'-ACGGTGGTGCGGACTACAAG-3'(exon 3) and Cd274-R: 5'-TCCAGATTACCTCAGCTTCT-3' (exon4); Tbxas1-F, 5'-AGAGCCAATTGGAACTCCGAG-3' (exon 3), Tbxas1-R, 5'-ACCTGCTTGATCATGTCTGG-3' (exon4); Mertk-F, 5'-CAGCTGGCATTTCATGGTGGAA-3' (exon2), Mertk-R, 5'-TTCATCTTACAGAAGTACGAC-3' (exon 3). The resulting concentration of target PCR products was normalized by comparison with β-actin and was used to determine the relative mRNA level of DEGs in Met2 cells.

Cytokine/chemokine measurements

Tumor cells were cultured for 48h and the conditioned media were collected for cytokine and chemokine measurement using MILLIPLEX Mouse Cytokine/Chemokine panel coupled with the Luminex® xMAP® platform according to manufacturer's instruction (EMD Millipore Corporation, Billerica, MA). The following 32 cytokines and chemokines were measured simultaneously: Eotaxin (CCL11), G-CSF (CSF3), GM-CSF (CSF2), IFN-γ, IL-1α, IL-1β, IL-2, IL-3, IL-4, IL-5, IL-6, IL-7, IL-9, IL-10, IL-12 (p40), IL-12 (p70), IL-13, IL-15, IL-17, IP-10 (CCL10), KC (CXCL1), LIF(Leukemia inhibitory factor), LIX (CXCL5), MCP-1 (CCL-2), M-CSF (CSF1), MIG (CXCL9), MIP-1α (CCL3), MIP-1β (CCL4), MIP-2 (CXCL2), RANTES (CCL5), TNF-α, and VEGF.

Western blot analysis

Cell lysates were obtained by extraction in RIPA buffer (20mM Tris-HCl, pH7.4, 150mM NaCl, 5 mM EDTA, 1% NP-40)

10.3389/fendo.2025.1514264

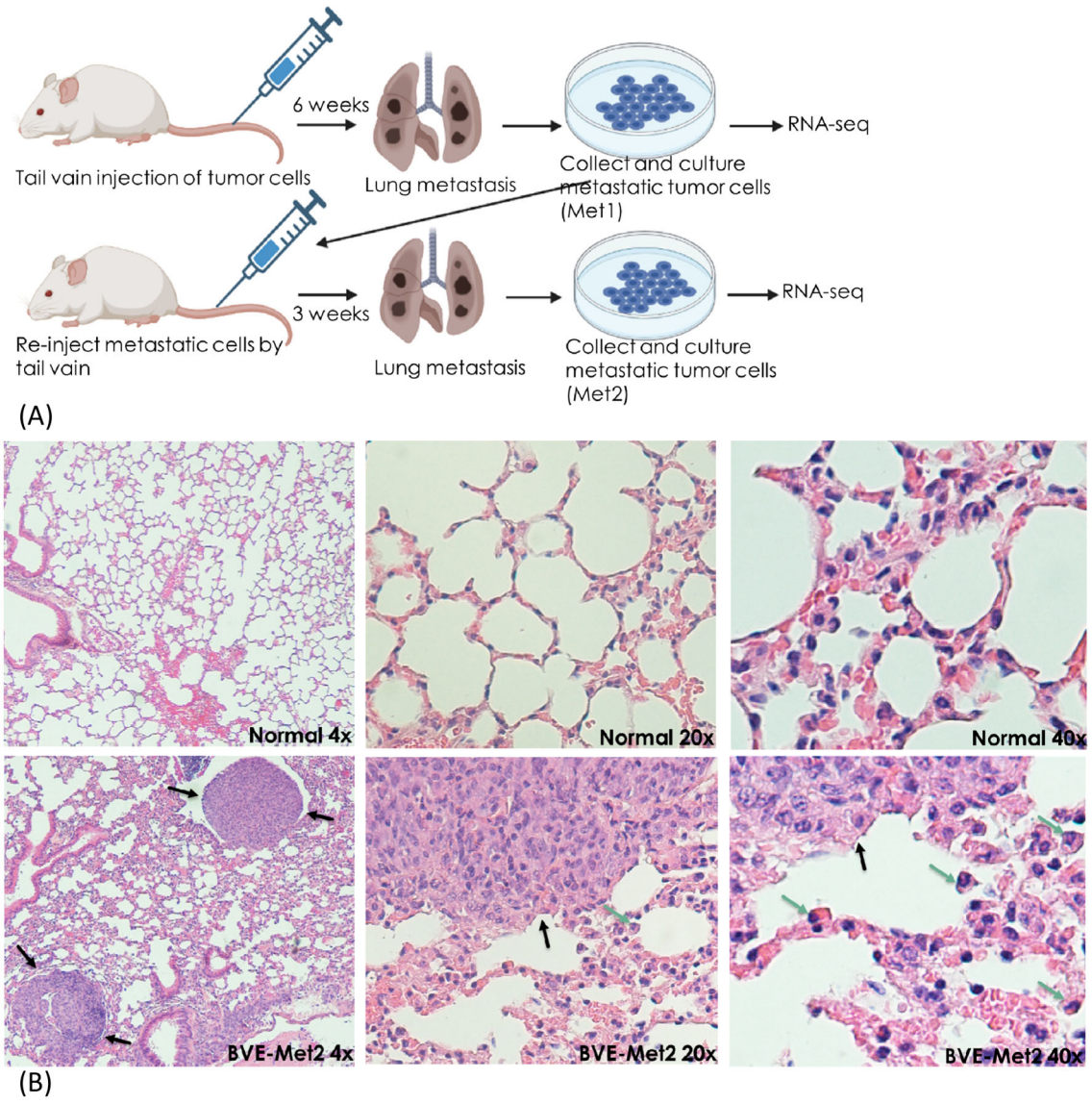

FIGURE 1
Experimental lung metastasis. **(A)** Schematic diagram summarizing experimental lung metastatic procedure. BVE, BVE^{Trp53null}, KGD, or KGD^{Cdkn2anull} cells (1 x 10^6 cells) were injected to tail vain of 5 nude mice for each group. Six weeks after injection, lung metastatic tumors were collected to establish Met1 cell lines. The established Met1 cells were re-injected (1 x 10^6 cells) to a new group of nude mice (n=5 for each group) via tail vain for enrichment of cells with high metastatic potential. Lung metastatic tumors were harvested three weeks following injection to establish Met2 cell lines. Met1, Met2 and primary tumor cells were subject to RNA sequencing to identify differentially expressed genes (DEGs). **(B)** Lung metastatic foci after tail vain injection of BVE thyroid cancer cells (H&E staining). Metastatic foci are indicated by black arrows and tumor infiltrating monocytes and macrophages are indicated by green arrows.

containing Pierce's Halt Protease Inhibitor Cocktail (Thermo Scientific, Rockford, IL). Proteins (40 µg) were loaded onto a 12% SDS-polyacrylamide gel and were transferred to a PVDF membrane. Western blot analysis was performed using antibodies (1:1000 dilution) from Cell Signaling Technology (Danvers, MA) against phospho-Erk (#4370, RRID: AB_2315112), phosphor-Akt (#4060, RRID: AB_2315049), E-Cadherin (#3195, RRID: AB_2291471), and Vimentin (#5741, RRID: AB_10695459), or antibodies against IL-6 (ab281935, RRID: AB_3661729), IL-6 receptor (ab300582, RRID: AB_300582), and PD-L1 (ab269674) from Abcam (Boston, MA). The experiments were repeated twice.

Flow cytometry analysis for cell surface markers and apoptosis

The expression of Ep-CAM, CD11b, CD24, and CD44 cell surface markers on tumor cells was analyzed by FACS

(fluorescence-activated cell sorting) flow cytometer (LSR I; Becton Dickinson, Mountain View, CA, USA) using anti-Ep-CAM-APC (Biolegend, San Diego, CA, USA, CAT#118214, RRID: AB_1134102), anti-CD11b (BD Biosciences, Heidelberg, Germany, CAT# 552850, RRID: AB_394491), anti-CD24-APC (Biolegend, CAT# 101814, RRID: AB_439716) and anti-CD44-PE-Cy7 (Biolegend, CAT#103030, RRID: AB_830787) labelled antibodies. The CSC-like cell subpopulation was identified by gating on $CD44^{high}/CD24^{low}$ cells, while differentiated-like cells were identified as $CD44^{low}/CD24^{high}$ cells (22). Ep-CAM was used to identify epithelial cells and epithelial cell-derived tumor cells, while CD11b was used to mark myeloid-lineage cells such as monocytes/macrophages, neutrophils cells. BVE and BVE-Met2 cells were cultured with different concentrations of PKF118-310, PLX4720, or both for 24h. The apoptosis was analyzed using the Vybrant apoptosis assay kit (Molecular Probes, Eugene, OR, USA).

Preparation and administration of aspirin to mice

The mouse dose equivalent to 100–150 mg/60kg human low dose aspirin was calculated as human equivalency dose (HED) = animal dose (mg/kg) × (animal km)/(human km), where mouse km factor is 3, and human km factor is 37. Aspirin (Chewable Aspirin 81 mg, Bayer) was prepared at 2.5 mg/mL in PBS to administer 10 µl/g body weight to deliver a dose of 25 mg/kg. Mice (n=10) were injected by tail vain of 1 x 10^6 BVE^{Trp53_null}-Met2 cells for lung metastasis. They were divided into 2 groups: group 1 (n=5) were given aspirin 3 times/week by oral gavage for 4 weeks while control mice (group 2) received the same volume of PBS.

Colony formation assay

The sensitivity of BVE and BVE-Met2 cells to $BRAF^{V600E}$ and β-catenin inhibitors were determined by colony formation assay. BVE and BVE-Met2 cells were plated into 6-well plates with different low cell seeding number (50 to 200 cells/well) for 14 days in the presence or absence of different concentrations of PLX4720, PKF118-310 or both. Cells were then fixed with methanol for 10 min and stained with 0.5% crystal violet dye in methanol:de-ionized water (1:5) for 10 min. After three washes with H2O to remove excess crystal violet dye, colonies containing more than 50 individual cells were counted using a microscope. Three separate experiments were performed and average were presented. Colony forming efficiency (CFE) was calculated using the formula: CFE = (number of colonies counted/number of cells plated) × 100.

Sphere formation assay

Tumor sphere assay was performed as described previously (23). Briefly, thyroid tumor cells (10000 cells/ml) were cultured in ultra-low attachment plates (Corning) in DMEM-F12 (Life Technologies) containing stem cell culture supplements (4% FBS, 1% antibiotics, 1% glutaMax, 2% B-27, 20 ng/ml EGF, 20 ng/ml bFGF, 500 ng/ml hydrocortisone, 5 µg/ml insulin, and 2 U/ml heparin). After 10 days in culture, spheres >50 µm were counted. Three separate experiments were performed and average were presented.

Statistical analysis

Student's *t*-test (two-tailed) was used to compare two groups and one-way ANOVA was used to compare multiple groups. A *P* value of 0.05 or less was considered significant.

Results

Genome-wide transcriptome analysis to identify critical genes in thyroid cancer metastases

To identify common genes and pathways driving thyroid cancer metastasis, we performed a comprehensive gene expression profile of primary and Met cell lines carrying single oncogenic driver mutations ($Braf^{V600E}$ or $Kras^{G12D}$) or in combination with inactivation of tumor suppressor genes ($Braf^{V600E}$ and $Trp53^{null}$ or $Kras^{G12D}$ and $Cdkn2a^{null}$). Many differentially expressed genes (DEGs) that were not detected in the Met1 cells appeared in the Met2 cells (Supplementary Figure 2). Additionally, Met2 cells formed lung metastases 3 weeks faster than Met1 cells (3 vs 6 weeks), indicating enrichment of tumor cells with high metastatic potential. Transcriptome analysis identified 88 up-regulated and 22 down-regulated genes (log2 fold-change >2) present in all four Met2 cell lines (Figure 2A; Supplementary Table 1). Gene ontology and pathway analysis showed that regulation of cytokine production, inflammatory and negative regulation of immune response, neutrophil migration and phagocytosis, and cytokine- or receptor-mediated pathways were the top enriched ontology clusters (Figure 2B). PPI network analysis by STRING identified 18 hub genes: *Tnf* (degree of node 47), *Fgfr1* (46), *Was* (30), *Itgb2* (27), *Ncf1* (25), *Fcer1g* (20), *C1qa* (19), *Inpp5d* (19), *Il2rg* (18), *Shank3* (15), *Nckap1* (13), *Nod1* (13), *Card11* (12), *Csf2rb* (12), *Cybb* (11), *Fcgr4* (11), *Nlrp3* (11), *Csf1r* (10) (Figure 2C). Consistent with STRING results, 5 were also identified as hub genes by InnateDB (innate immunity database): *Tnf* (degree of node 41), *Inpp5d* (28), *Csf1r* (20), *Was* (18), and *Nlrp3* (10) (Figure 2D). Intriguingly, *Irf8*, the most significant hub gene (with degree of node 272) was not identified by the STRING. The detailed function of these hub genes and their biological roles in cancer metastasis were listed in Supplementary Table 2. We next analyzed the association of these hub gene over-expression with disease-specific survival of PTC patients using thyroid carcinoma dataset (TCGA, PanCancer Atlas) (n=498). The over-expression of 4 hub genes (*Tnf*, *Nckap1*, *Nlrp3*, and *Card11*) was associated with poor disease-specific survival (Figure 2E). These 4 genes are involved in the inflammation and/or epithelial-mesenchymal transition (EMT) pathways, indicating the critical role of these pathways in thyroid

10.3389/fendo.2025.1514264

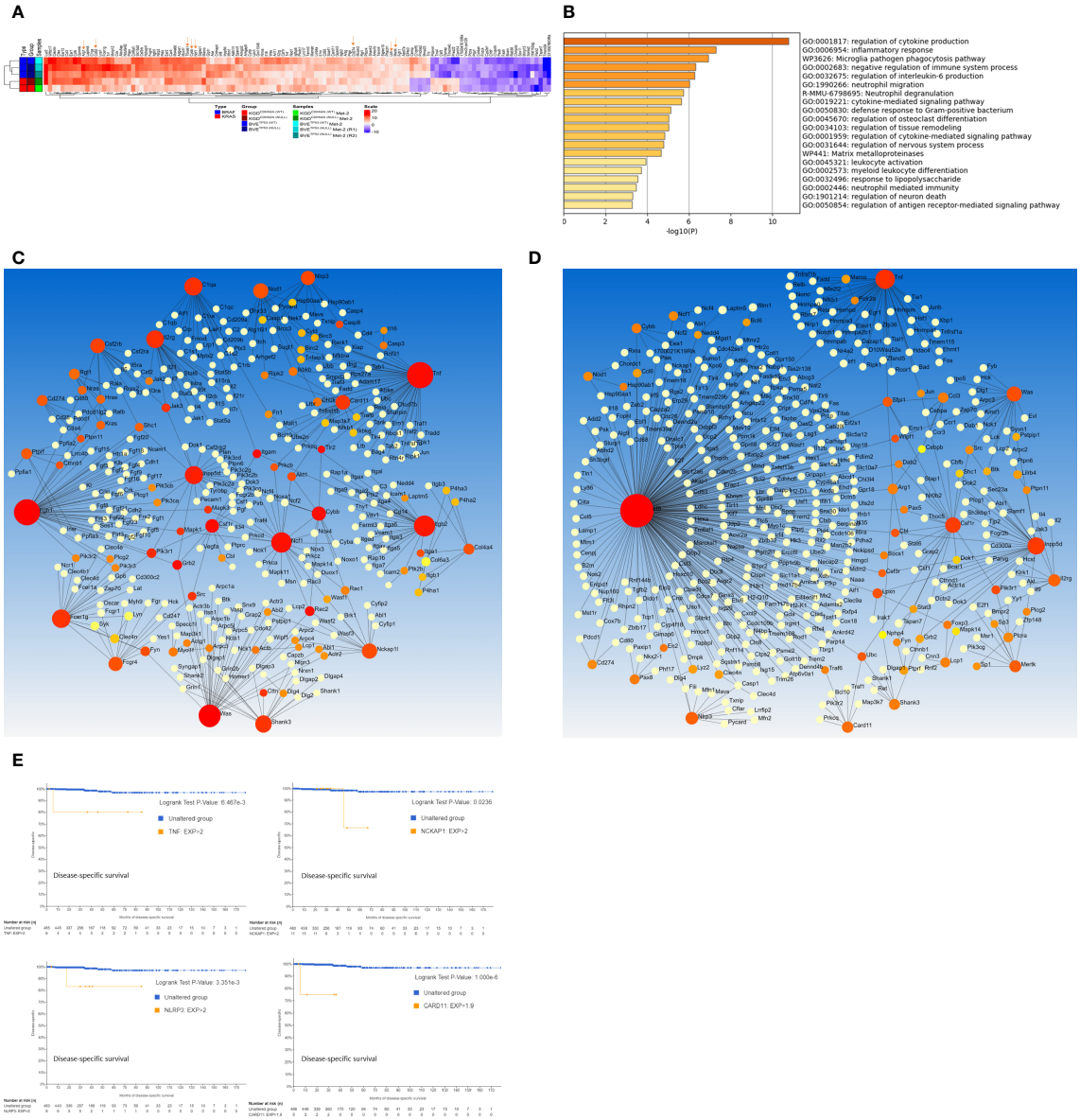

FIGURE 2
Genome-wide transcriptome analysis of DEGs in Met2 cells. **(A)** Heatmap of DEGs present in all 4 Met2 cells (BVE-Met2, BVE^{Trp53null}-Met2, KGD-Met2, and KGD^{Cdkn2a_null}-Met2). Several key genes involved in inflammation, immune checkpoint regulation and cancer stem cells are indicated by an arrow. **(B)** Top 20 Enriched ontology clusters of DEGs by Metascape analysis. Regulation of cytokine production, inflammatory response, phagocytosis pathway, negative regulation of immune system, and regulation of IL6 production are the top 5 enriched pathways. **(C)** PPI network and hub genes identification by NetworkAnalyst. STRING interactome with high confidence score of 900 (of maxium1000) was chosen for hub gene identification. Eighteen genes with the degree of a node >10 (bigger red nodes) were selected as hub genes **(D)** PPI network based on InnateDB. Six genes with the degree of a node >10 (bigger red nodes) were selected as hub genes. **(E)** Kaplan-Meier analyses of hub gene expression on disease-specific survival of PTC patients. Overexpression of 4 hub genes (Tnf, Nckap1, Nlrp3, and Card11) was associated with poor disease-specific survival. TCGA-THCA mRNA dataset (n=498) was used for Kaplan-Meier analysis.

cancer metastases, and may be useful biomarkers to predict disease prognosis.

Increased production of inflammatory cytokines by metastatic tumor cells

To assess whether over-expression of above genes in Met2 cells correlated with more inflammatory cytokine/chemokine production, we analyzed 32 cytokine and chemokine levels in the conditioned media of both primary and Met2 cells. As shown in Figure 3A, Met2 cells produced more inflammatory cytokines or chemokines such as CSF1 (colony stimulating factor 1 or macrophage colony-stimulating factor), CSF2 (colony-stimulating factor 2 or granulocyte-macrophage colony-stimulating factor), CSF3 (colony-stimulating factor 3 or granulocyte colony-stimulating factor), CCL2 (monocyte chemoattractant protein-1), CCL11 (eosinophil chemotactic protein), CXCL5 (epithelial-derived neutrophil-activating peptide 78, a chemotactic chemokine known to

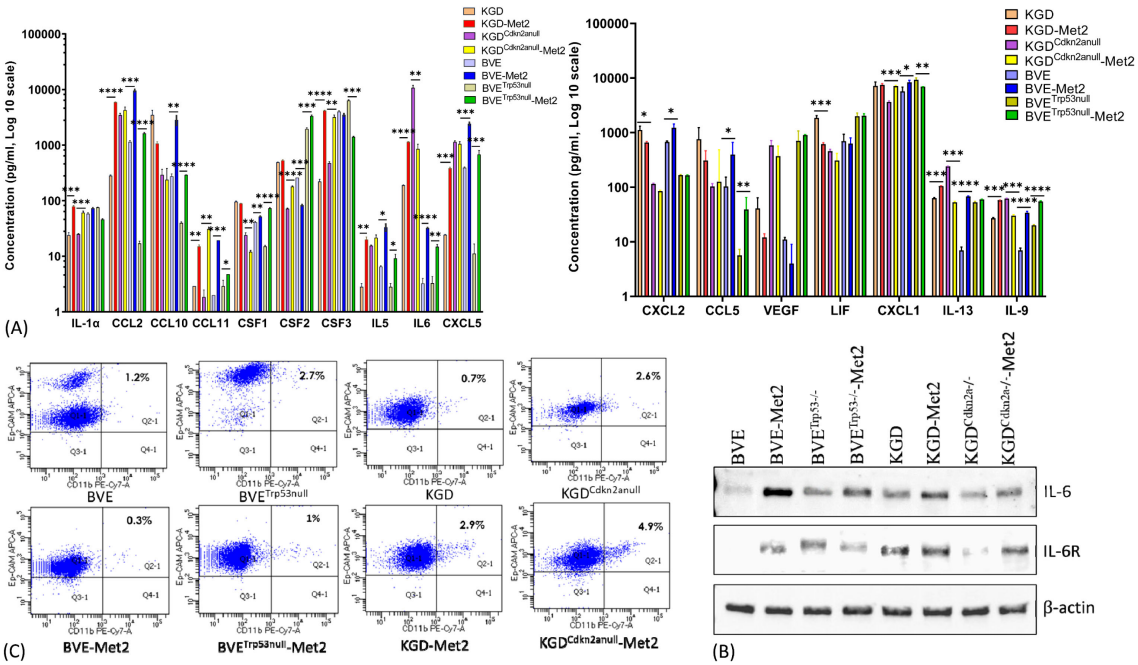

FIGURE 3
Cytokine/Chemokine production by Met2 cells. **(A)** Cytokine/Chemokine production was detected in conditioned media of both primary and Met2 cells using MILLIPLEX mouse ELISA assay. Increased production of inflammatory cytokines and chemokines were observed in Met2 cells. **(B)** Western blot analysis of IL-6 and IL-6 receptor expression in primary and Met2 cells. Increased IL-6 and IL-6 receptor expression were observed in Met2 cells. **(C)** FACS analysis of Ep-CAM and CD11b staining of both primary and Met2 cells. Ep-CAM is an epithelial cell marker, while CD11b is a myeloid cell marker highly expressed on the surface of innate immune cells, including macrophages and neutrophils. CD11b-positive cells were present in less than 5% of Met2 cell population *P<0.05, **P<0.01, ***P<0.001.

activate neutrophil during acute inflammatory responses), IL-1α and IL-6. We further confirmed increased expression of IL-6 and/or IL-6 receptor in Met2 cells by Western blot (Figure 3B). These cytokines/chemokines have been reported to promote tumor cell immune escape and metastasis by recruitment of tumor-associated macrophages (TAMs), myeloid-derived suppressor cells (MDSCs), tumor-associated neutrophils (TANs), and regulatory T (Treg) cells (24). Consistent with the reported roles of these cytokines/chemokines in mobilizing immunosuppressive inflammatory cells, there were increased monocyte and macrophage infiltration in TME (Figure 1B) and overexpression of Arg1 (arginase1), an immunosuppressive signal found predominantly on TAMs, in Met2 cells (Figure 2A; Supplementary Table 1). It has been shown that breast cancer-derived CSF2 regulates Arg1 to promote an immunosuppressive TME (25). Primary and Met2 cells were also analyzed by FACS for the expression of Ep-CAM (epithelial cell marker) and CD11b (myeloid cell marker highly expressed on the surface of monocytes/macrophages, and some CD8+ cytotoxic T cells) to rule out the possibility that increased inflammatory cytokine/chemokine production observed in the Met2 cells was due to contaminating monocytes, macrophages, and tumor-infiltrating lymphotyes. As shown in Figure 3C, majority of tumor cells were Ep-CAM$^+$ with minimal CD11b$^+$, indicating that Met2 cells were epithelial origin without significant contaminating monocytes/macrophages. The small fraction of CD11b$^+$ cells (<5%) may be due to increased EMT in Met2 cells.

Identification of druggable genes and pathways in metastatic tumor cells

The approach to identify common DEGs present in all 4 Met2 cell lines irrespective of their underlying genetic defects yielded encouraging results above. This strategy significantly reduced the number of DEGs to be analyzed from more than 2200 in each Met2 cell line to 110 (Figure 2A; Supplementary Figure 2), which increased the efficiency to identify drug targets and decreased false identification. We then focused on these genes to identify drug targets that could be applicable to all 4 tumor types. Tumor cell-induced platelet aggregation is a well-recognized mechanism for paraneoplastic thrombocytosis and a potential cause of reduced response to immune checkpoint inhibitors in hematogenous metastasis. Tbxas1, a thromboxane A synthase 1 gene which catalyzes the conversion of prostglandin H2 to thromboxane A2 (TXA2), was highly expressed in Met2 cells (Figures 2A, 4A). TXA2 is a potent inducer of platelet aggregation. The overexpression of Tbxas1 would trigger coagulation cascade and may explain the significant RBC infiltration observed in pre-metastatic niche of lung metastases (Figure 4C). Importantly, treatment with a low-dose of aspirin, an irreversible inhibitor of TXA2, significantly reduced the size and number (6.8 ± 1.5 vs 25 ± 3.4, p<0.01) of lung metastatic foci after intravenous injection of BVE^{Trp53_null}-Met2 cells to nude mice (n=5) (Figures 4D, E), thus, confirming the role of Tbxas1in

10.3389/fendo.2025.1514264

promoting platelet aggregation and metastatic niche formation. Moreover, Met2 cells over-expressed not only two immune checkpoint regulators, CD274 (PD-L1) (Figures 4A, B) and CD52 (Figure 2A, Supplementary Figure 2), but also Mertk, a member of the TAM (Tyro, Axl, Mertk) family of receptor tyrosine kinases (Figures 2A, 5A). Mertk has been reported to activate multiple signaling pathways (JAK/STAT, MAPK, PI3K/AKT, EMT, and PD-1/PD-L1) to promote tumor cell migration, immune escape, and cancer stem cell (CSC) transformation, and act as bypass mechanisms to EGFR blockade (26). Indeed, up-regulation of

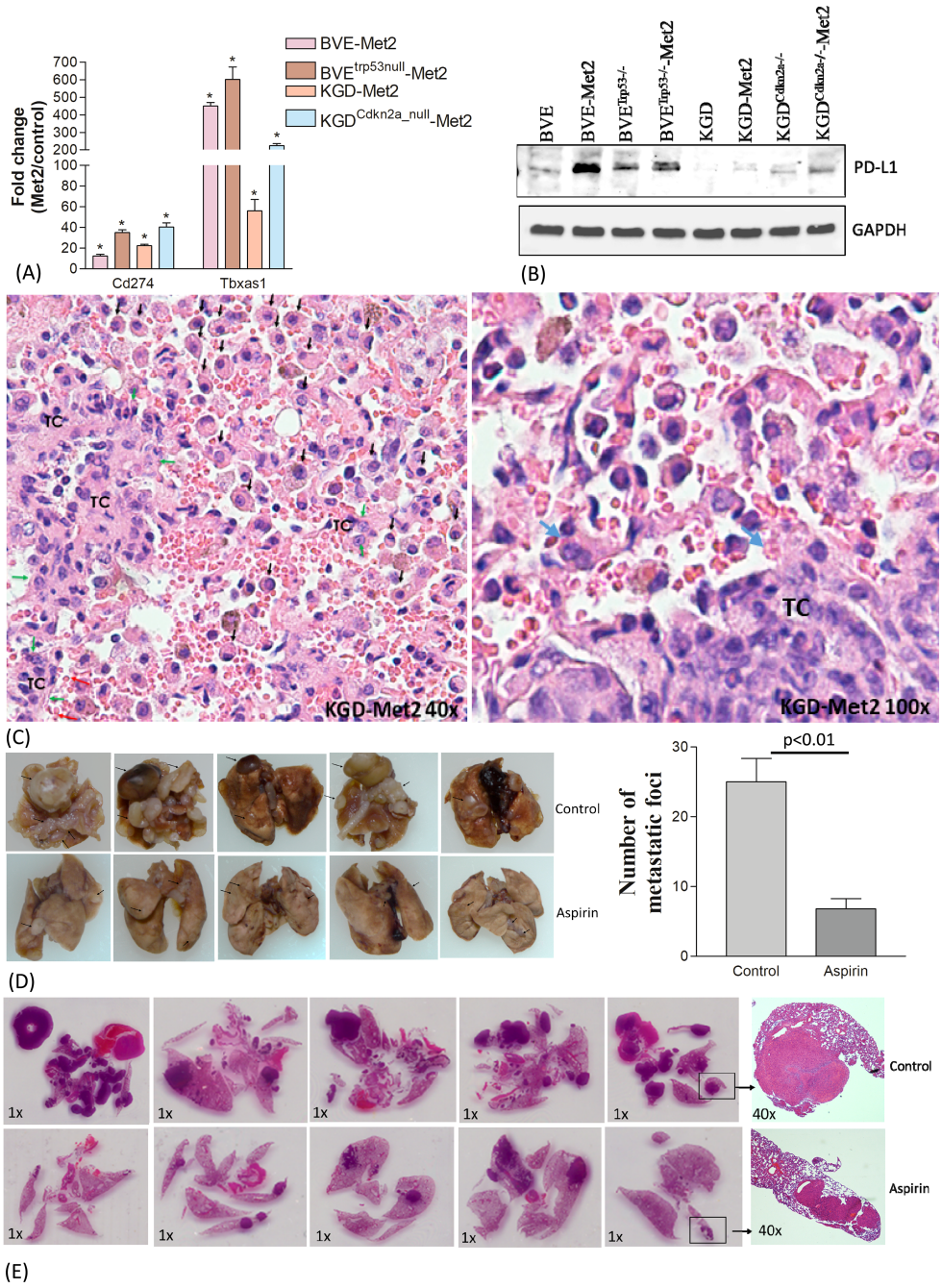

FIGURE 4
Contribution of Cd274 and Tbxas1 in pulmonary pre-metastatic niche formation. **(A)** Overexpression of Cd274 (PD-L1) and Tbxas1 mRNA in Met2 cells as compared to primary cells detected by qRT-PCR analysis.*p<0.01. **(B)** Western blot analysis of CD274 expression. Increased CD274 expression were observed in Met2 cells. **(C)** Microscopic metastatic foci of KGD-Met2 cells. Significant infiltration of RBCs, lymphocytes, and macrophages are noted at the interface between metastatic tumor foci and lung. Tumor cells are indicated by green arrows and marked as TC. Increased infiltration of monocytes and macrophages is indicated by black arrows. Increased RBC aggregation is noted and platelets aggregation on tumor cells is indicated by a blue arrow. **(D)** Lung metastasis of BVE^{Trp53null}-Met2 upon low dose aspirin treatment. The metastatic foci on the lung surface were counted and plotted as a bar graph. Significant reduction of lung metastatic foci was observed when mice were given aspirin (25 mg/kg) by oral gavage for 4 weeks. Data are presented as mean ± SEM. Representative metastatic foci are indicated by an arrow. **(E)** Histology (H&E staining) of lung metastases of thyroid tumor cells. The size and number of metastatic foci were reduced after aspirin treatment.

10.3389/fendo.2025.1514264

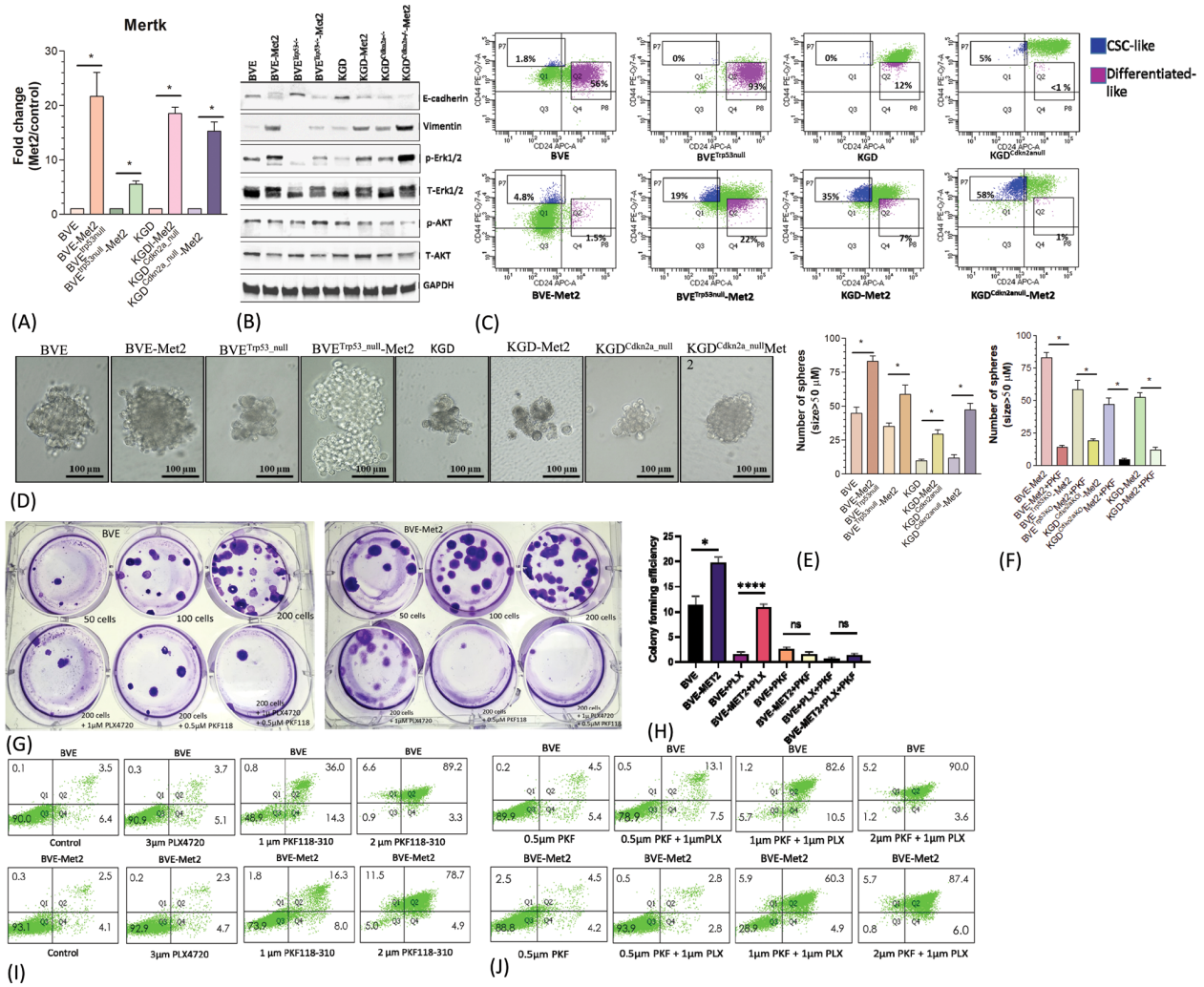

FIGURE 5
Up-regulation of MerTK-mediated signaling. **(A)** Mertk mRNA overexpression in Met2 cells detected by qRT-PCR analysis. *p<0.01. **(B)** Western blot analysis of E-cadherin, vimentin, p-Erk, and p-AKT expression in Met2 cell lines. Increased expression of vimentin and p-Erk and decreased expression of E-cadherin were demonstrated in all Met2 cells. Increased p-AKT expression was present only in the BVE^{trp53null}-Met2 cells. **(C)** FACS analysis of CD44/CD24 expression in Met2 cells. Increased CD24^{low}CD44^{high} staining was observed in Met2 cells. **(D)** Tumorspheres formation in ultralow attachment stem cells culture conditions. Representative tumorspheres are shown. **(E)** The number of spheres was counted and plotted as a bar graph. The number of tumorspheres was increased in Met2 cells, *p<0.01. **(F)** Inhibition of tumorspheres by PKF118-310. Significant reduction of tumorspheres was noted upon treatment with 1μM PKF118-310, *p<0.01. **(G)** Sensitivity of BVE-Met2 cells to BRAF^{V600E} and β-catenin inhibitors. BVE and BVE-Met2 cells were cultured in different low cell seeding numbers. A representative colony formation assay was shown. **(H)** The number of colonies was counted and plotted as a bar graph. Increased colony formation was observed in low seeding number of BVE-Met2 cells, which were resistant to BRAF^{V600E} inhibitor PLX4720 but remained sensitive to β-catenin inhibitor PKF118-310. *P<0.05, ****P<0.0001, NS, not statistically significant. **(I)** Flow cytometric analysis of apoptotic BVE and BVE-Met2 cells after treatment with BRAF^{V600E} or β-catenin inhibitors. **(J)** Flow cytometric analysis of apoptotic BVE and BVE-Met2 cells after combined treatment of BRAF^{V600E} and β-catenin inhibitors.

several down-stream signaling targets of Mertk was observed in Met2 cells such as increased expression of PD-L1 (Figure 4B), increased expression of vimentin and decreased expression of E-cadherin (EMT↑), and increased p-Erk (MAPK↑) (Figure 5B). Increased expression of p-AKT was found only in BVE^{Trp53null}-Met2 cells (Figure 5B). Taken together, these data strongly suggest the contribution of these genes/pathways to immune escape of metastatic tumor cells.

Metastatic tumor cells retain features of CSCs and resistance to monotherapy with BRAF^{V600E} inhibitor PLX4720

The role of WNT/μ-catenin pathway in thyroid cancer progression is well established (27). Met2 cells showed over-expression of Limb-Bud- and-Heart (LBH) (Figure 2A; Supplementary Table 1), a WNT/β-catenin target required for normal mammary stem cell self-renewal

10.3389/fendo.2025.1514264

(28) and an oncogene specifically expressed in tumor-initiating $CD24^{low}/CD44^{high}$ breast CSCs with high metastatic potential (29). Given Mertk is also involved in CSC transformation, we investigated CD44 and CD24 expression in Met2 cells. As shown in Figure 5C, increased CD44 and decreased CD24 expression was observed in Met2 cells, indicating either increased transformation to CSCs or enrichment of CSCs. Tumorsphere and colony formation are two *in vitro* stemness functional assays. Met2 cells showed more tumorsphere formation (Figures 5D, E) that was significantly reduced (more than 70% as compared to the control) after treatment with 1 μM β-catenin inhibitor PKF118-310 (Figure 5F). Only 10% reduction in tumorsphere formation was observed in BVE-Met2 and no reduction in $BVE^{Trp53null}$-Met2 cells upon treatment with 2 μM of $BRAF^{V600E}$ inhibitor PLX4720 (Supplementary Figure 4), indicating resistance to $BRAF^{V600E}$ inhibitor. In the colony formation assay, BVE-Met2 cells showed increased formation of colonies at low seeding numbers (19.7 ± 1.2 *vs* 11.3 ± 1.7, $p<0.05$) and resistance to 1 μM $BRAF^{V600E}$ inhibitor PLX4720 (10.8 ± 0.7 vs 1.5 ± 0.3 colonies, $p<0.01$) (Figures 5G, H). Both BVE and BVE-Met2 cells remained sensitive to 0.5 μM of β-catenin inhibitor PKF118-310 (11.3 ± 1.7 in BVE control vs 2.5 ± 0.3 colonies in BVE treatment, $p<0.01$; 19.7 ± 1.2 in BVE-Met2 control vs 1.5 ± 0.3 in BVE-Met2 treatment, $p<0.01$) (Figures 5G, H). Furthermore, as compared to 3 μM PLX4720 alone, PLX4720-induced apoptosis was significantly enhanced by combination of 1 μM PLX4720 and 1 μM PKF118-310: 8.8% vs 93.1% in BVE cells, and 7% vs 65.2% in BVE-Met2 cells (Figures 5I, J). Collectively, metastatic thyroid tumor cells expressed stemness features and became more resistance to $BRAF^{V600E}$ inhibitor PLX4720, but were still sensitive to β-catenin inhibitor PKF118-310. Combinational therapy with low doses of PLX4720 and PKF118-310 showed synergistic effect in BVE-Met2 cells.

Discussion

In the present study, we investigated the transcriptome landscape of metastatic tumor cells from 4 different thyroid cancer transgenic mouse models ranging from well-differentiated (PTC and FTC) to poorly-differentiated (PDTC) and anaplastic thyroid cancer (ATC). Despite different genetic mutations driving oncogenic transformation, we identified a group of metastatic genes and pathways shared by all four tumor types. The simultaneous activation of several key genes and pathways involved in endoplasmic reticulum (ER) stress and inflammation, platelet aggregation, negative immune regulation, and Mertk receptor tyrosine kinase provided insight into how metastatic cells evade immune elimination, survive in the circulation, and finally colonize at distant sites. The metastatic process and potential drug targets are illustrated in Figure 6.

Tail vein injection may not be the ideal method for studying metastasis mechanisms because it bypasses the first two steps of metastasis process (tumor cell invasion of the basement membrane and intravasation into the vasculature). Successful colonization of the secondary organ is the rate-limiting step in the metastatic process. However, since mouse models of thyroid cancer do not develop spontaneous metastases, we used tail-vein injection methods to interrogate key factors required for cancer cell colonization of secondary organs. This approach has been used for a high-throughput *in vivo* screening method in the mouse for identifying regulators of metastatic colonization (30) and is still valid for studying how tumor cells survive in the circulation, extravagate from the circulation, and colonize at the distal organs.

Currently, the main goal of anti-cancer therapies relies on the effective elimination of cancer cells by apoptosis (31). Paradoxically,

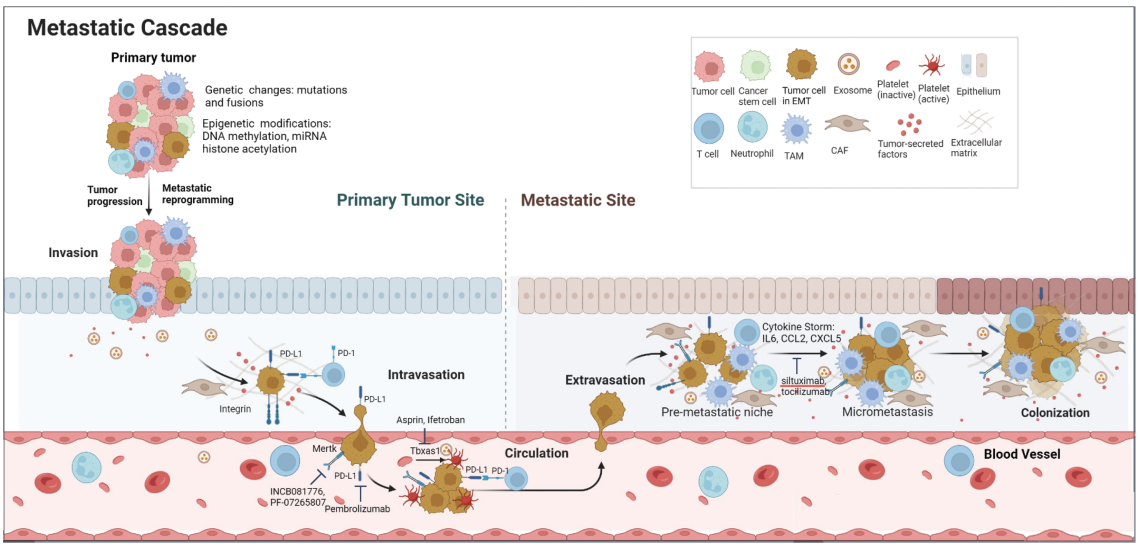

FIGURE 6
Schematic diagram of metastatic cascade of thyroid cancer cells and potential drug targets. Genetic changes and epigenetic modifications drive tumor progression and metastatic reprogramming. To evade immune elimination and survive in the blood circulation, metastatic cells express high levels of 'Don't eat me' signals such as Cd274 (PD-L1) and Cd52 as well as Tbxas1 and Mertk. At the metastatic site, the metastatic cells induce a cytokine storm by secreting a large amount of inflammatory cytokines and chemokines to help form a pre-metastatic niche and eventual colonization at the distant site.

cell-death-inducing therapies can enhance metastasis by inducing changes in TME triggered by a cell-death-driven cytokine storm and tumor-associated macrophages (32–36). Conod et al. have demonstrated that tumor cells that survive impending death become stable pro-metastatic tumor cells. These cells exhibit features such as metastatic reprogramming, stemness, cytokine storm, and ER stress, which could induce neighboring tumor cells to acquire pro-metastatic states and form distant metastases *in vivo* (37). Indeed, Met2 cells demonstrated these features such as stemness, increased inflammatory cytokine production, and ER stress. In a recent study of anaplastic transformation in thyroid cancer, Lu et al. uncovered the spectrum of ATC transformation: inflammatory PTC cells (iPTCs) → inflammatory ATC cells (iATCs) → mesenchymal ATC cells (mATCs), indicating inflammation plays an important role in ATC transformation (38). They further demonstrated that mATCs contributed to poor overall survival with aneuploid genomes, mesenchymal phenotypes, and overexpression of collagen genes (i.e., COL1A1, COL1A2, COL3A1, COL5A1, COL5A2) (38). Interestingly, Col6a3, a member of collagen family of genes, was over-expressed in Met2 cells and associated with poor disease-specific survival in PTC patients (TCGA-THCA dataset, Supplementary Figure 3).

NADPH oxidase isoform 2 (NOX2) is a multicomponent enzyme complex including 5 subunits: Cyba, Cybb, Ncf1, Ncf2, and Ncf4 and expressed almost solely in myeloid cells such as monocytes, macrophages and neutrophilic granulocytes. It generates reactive oxygen species (ROS) in defense against microbial pathogens. A recent study has showed it promotes melanoma pulmonary metastasis by inhibiting adjacent lung-infiltrating cytotoxic T and NK cells (39, 40). Two of NOX2 subunits (Ncf1 and Cybb) were highly expressed in Met2 cells, which may induce ER stress in TME and promote pulmonary metastatic colonization. The increased Ncf1 and Cybb expression in Met2 may reflect EMT and metastatic reprograming.

PD-L1 expression was elevated in all Met2 cells. Given nude mice has no functional T cells, the immune evasion is likely mediated by inhibition of NK cells. PD-1/PD-L1 blockade enhances anti-tumor efficacy of NK cells (41, 42). Various signaling pathways regulate PD-1/PD-L1 expression. PI3K/AKT, MAPK, JAK/STAT, Wnt/β-catenin, NF-κB, and Hedgehog pathways have all been reported to increase the expression of PD-1/PD-L1 axis (43). PD-L1 is highly glycosylated in tumor cells to maintain its stability via IL-6/JAK1-mediated phosphorylation and subsequent glycosylation (44). Since IL6 is a pro-inflammatory cytokine known to promote cancer metastasis and induces PD-1 expression in activated T cells, blocking IL6 pathway may reduce tumor immune escape in TME and enhance anticancer immunity (44). IL6 antibody siltuximab, IL6 receptor antibody tocilizumab, JAK1/2 kinase inhibitor ruxolitinib, and PD-L1 antibody (Atezolizumab, Avelumab, Durvalumab) have been approved by the FDA, simultaneously targeting both PD-1/PD-L1 and IL6/JAK1 may be more effective than single agent in cancer immunotherapy (45, 46).

Barkal et al. have recently identified CD24, a glycosylphosphatidylinositol (GPI)-anchored protein, as a novel 'don't eat me' signal expressed on tumor cells to evade macrophage-mediated phagocytosis by binding to Siglec10 inhibitory receptor expressed on tumour-associated macrophages (47). Although CD24 overexpression was not found in Met2 cells, another GPI-anchored protein CD52 was highly expressed in all Met2 cells, which binds to the same inhibitory receptor Siglec10 to suppress immune cell function (48, 49). The Siglec10 is widely expressed in immune cells, such as B cells, monocytes, dendritic cells, NK cells, and a subset of activated T cells. CD52 may function as a novel 'don't eat me' signal and potential drug target.

Tumor-secreted cytokines and chemokines play an important role in promoting cancer metastasis. CCL2, a potent chemokine in macrophage recruitment and polarization during inflammation was produced abundantly in Met2 cells. CCL2-secreting breast cancer cells have been shown to interact with CCR2+ macrophages to facilitate their metastasis to lung and bone (50). Similarly, CCL3 (macrophage inflammatory protein-1 α), a pro-inflammatory chemokine implicated in tumor metastasis, was highly expressed in Met2 cells. The CCL3-CCR5 axis regulates intratumoral trafficking of leukocytes and fibroblasts to promote angiogenesis and subsequent lung metastasis (51). IL6 production was elevated in Met2 cells (52). Tumor cell-secreted IL6 has been reported to induce CCL5 expression in lymphatic endothelial cells and accelerate metastasis in triple-negative breast cancer (53).

Platelets contribute to tumor metastasis via multiple mechanisms at different stages of metastatic cascades (54). Met2 cells expressed high levels of Tbxas1 for platelet activation. Activated platelets are involved in the formation of metastatic niche, which could be inhibited by aspirin (55). The benefit of aspirin in reducing cancer metastasis has been confirmed in clinical trials (56). The current study provides a mechanistic explanation for targeting COX-1/Tbxas1-TXA2 pathway against metastatic thyroid cancer. It has been reported that platelets could increase PD-L1 expression on tumor cells via NF-κB and TGFβ signaling (57). Furthermore, PD-L1 protein can be transferred from tumor cells to platelets to suppress anti-tumor immune response (58). The transfer of PD-L1 protein from tumor cells to platelets may explain the high levels of PD-L1 transcripts and subtle increase of PD-L1 protein in Met2 cells. The platelet aggregation and transfer of PD-L1 to platelets would create a physical and molecular shield to protect tumor cells. Thus, targeting COX-1/TXA2 signaling may improve the efficacy of PD-L1 immunotherapy by disrupting this protective shield. Given unwanted gastrointestinal side effects of aspirin, a potent and selective TXA2 receptor antagonist, Ifetroban, has been re-evaluated for the treatment of metastatic cancer and is currently under Phase II clinical trial (NCT03694249) (59).

One of the significant findings reported in this study was Mertk overexpression in Met2 cells. Mertk is known to activate multiple signaling pathways (MAPK, PI3K/AKT, JAK/STAT, and PD-1/PD-L1) in many types of cancer to promote immune tolerance, tumor progression and metastasis, and drug resistance (26, 60, 61). It likely plays a pivotal role in Met2 cell resistance to BRAF inhibitor and survival of NK cell-mediated immune elimination. Mertk signaling in tumor cells could increase PD-L1 expression to foster immune escape and survival (62). Paolino et al. have reported TAM inhibition enhances NK cell activity, leading to markedly reduction in murine mammary cancer and melanoma metastases (63). They have further showed that low-dose warfarin, which inhibits TAM receptor activity without affecting coagulation, exerts anti-metastatic activity in mice via

Cbl-b/TAM receptors on NK cells (63, 64). Several Axl/Mer inhibitors, such as INCB081776 (NCT03522142) and PF-07265807 (NCT04458259), are currently under Phase I clinical trial in patients with advanced or metastatic solid tumors (65).

In summary, we have uncovered several key genes and pathways driving thyroid cancer metastasis. They act in synchrony to promote inflammation, cytokine storm, platelet aggregation, and subsequently pre-metastatic niche formation. Given that cancer cells utilize multiple pathways to evade immune elimination and extensive cross-interactions among these pathways, combinational therapy against PD-L1, Tbsax1, and/or IL-6 may offer better therapeutic outcome.

Data availability statement

The datasets presented in this study can be found in online repositories. The names of the repository/repositories and accession number(s) can be found in the article/Supplementary Material.

Ethics statement

The animal studies were approved by The Animal Care and Use Committee of King Faisal Specialist Hospital and Research Centre. The studies were conducted in accordance with the local legislation and institutional requirements. Written informed consent was obtained from the owners for the participation of their animals in this study.

Author contributions

MZ: Data curation, Formal analysis, Investigation, Methodology, Validation, Visualization, Writing – original draft, Writing – review & editing, Resources. AQ: Formal analysis, Investigation, Methodology, Resources, Writing – review & editing, Software. MA: Formal analysis, Investigation, Methodology, Resources, Writing – review & editing, Data curation. HG: Data curation, Formal analysis, Investigation, Methodology, Resources, Writing – review & editing, Validation. NB: Data curation, Formal analysis, Investigation, Methodology, Writing – review & editing. LA: Data curation, Investigation, Methodology, Writing – review & editing. KK: Investigation, Writing – review & editing, Project administration, Resources, Supervision. AAl: Investigation, Resources, Writing – review & editing, Data curation, Software. FA: Data curation, Investigation, Writing – review & editing, Methodology. AMA: Investigation, Methodology, Writing – review & editing, Project administration, Resources. AAb: Investigation, Project administration, Resources, Writing – review & editing, Supervision. ASA: Investigation, Project administration, Resources, Supervision, Writing – review & editing. YS: Investigation, Project administration, Supervision, Writing – review & editing, Conceptualization, Data curation, Formal analysis, Funding acquisition, Methodology, Validation, Visualization, Writing – original draft.

Funding

The author(s) declare financial support was received for the research, authorship, and/or publication of this article. This study was supported by an institutional research fund RAC#2230003.

Acknowledgments

We would like to thank Ms. Huda BinEssa, Ms. Huda Alnasrallah, Ms. Bushra Alnwisser and Mr. Wilfredo Antiquera for excellent technical support; Drs. Shioko Kimura from National Cancer Institute and Catrin Pritchard from Leicester Cancer Research Centre at the University of Leicester for generous gifts of TPO-*Cre* and LSL-*Braf*^{V600E} mice, respectively; Dr. James A. Fagin from Memorial Sloan Kettering Cancer Center for helpful discussions. We dedicate this paper to the memory of Dr. Naif Binjumah, who tragically passed away while this study was in progress.

Conflict of interest

The authors declare that the research was conducted in the absence of any commercial or financial relationships that could be construed as a potential conflict of interest.

The author(s) declared that they were an editorial board member of Frontiers, at the time of submission. This had no impact on the peer review process and the final decision.

Generative AI statement

The author(s) declare that no Generative AI was used in the creation of this manuscript.

Publisher's note

Supplementary material

The Supplementary Material for this article can be found online at: https://www.frontiersin.org/articles/10.3389/fendo.2025.1514264/full#supplementary-material

References

1. La Vecchia C, Malvezzi M, Bosetti C, Garavello W, Bertuccio P, Levi F, et al. Thyroid cancer mortality and incidence: a global overview. *Int J Cancer*. (2015) 136:2187–95. doi: 10.1002/ijc.v136.9

2. Lim H, Devesa SS, Sosa JA, Check D, Kitahara CM. Trends in thyroid cancer incidence and mortality in the United States, 1974-2013. *Jama*. (2017) 317:1338–48. doi: 10.1001/jama.2017.2719

3. Kitahara CM, Sosa JA. The changing incidence of thyroid cancer. Nature reviews Endocrinology. *Nat Rev Endo*. (2016) 12:646–53. doi: 10.1038/nrendo.2016.110

4. Jung CK, Little MP, Lubin JH, Brenner AV, Wells SA Jr., Sigurdson AJ, et al. The increase in thyroid cancer incidence during the last four decades is accompanied by a high frequency of BRAF mutations and a sharp increase in RAS mutations. . *J Clin Endocrinol Metab*. (2014) 99:E276–285. doi: 10.1210/jc.2013-2503

5. Lang BH, Lo CY, Chan WF, Lam KY, Wan KY. Prognostic factors in papillary and follicular thyroid carcinoma: their implications for cancer staging. *Ann Surg Oncol*. (2007) 14:730–8. doi: 10.1245/s10434-006-9207-5

6. Hundahl SA, Fleming ID, Fremgen AM, Menck HR. A National Cancer Data Base report on 53,856 cases of thyroid carcinoma treated in the U.S., 1985-1995 [see commetns. *Cancer*. (1998) 83:2638–48. doi: 10.1002/(SICI)1097-0142(19981215)83:12<2638::AID-CNCR31>3.0.CO;2-1

7. Ibrahimpasic T, Ghossein R, Shah JP, Ganly I. Poorly differentiated carcinoma of the thyroid gland: current status and future prospects. *Thyroid: Off J Am Thyroid Assoc*. (2019) 29:311–21. doi: 10.1089/thy.2018.0509

8. Kakudo K, Bychkov A, Bai Y, Li Y, Liu Z, Jung CK. The new 4th edition World Health Organization classification for thyroid tumors, Asian perspectives. *Pathol Int*. (2018) 68:641–64. doi: 10.1111/pin.v68.12

9. Nikiforov YE, Nikiforova MN. Molecular genetics and diagnosis of thyroid cancer. *Nat Rev Endocrinol*. (2011) 7:569–80. doi: 10.1038/nrendo.2011.142

10. Xing M, Alzahrani AS, Carson KA, Shong YK, Kim TY, Viola D, et al. Association between BRAF V600E mutation and recurrence of papillary thyroid cancer. *J Clin oncology: Off J Am Soc Clin Oncol*. (2015) 33:42–50. doi: 10.1200/JCO.2014.56.8253

11. Xing M. Clinical utility of RAS mutations in thyroid cancer: a blurred picture now emerging clearer. *BMC Med*. (2016) 14:12. doi: 10.1186/s12916-016-0559-9

12. Singh A, Ham J, Po JW, Niles N, Roberts T, Lee CS. 2021 the genomic landscape of thyroid cancer tumourigenesis and implications for immunotherapy. *Cells*. (2021) 10:1082. doi: 10.3390/cells10051082

13. Zhang XY, Sun JW, Qiu ZL, Wang Y, Chen XY, Zhao JH, et al. Clinical outcomes and prognostic factors in patients with no less than three distant organ system metastases from differentiated thyroid carcinoma. *Endocrine*. (2019) 66:254–65. doi: 10.1007/s12020-019-01999-6

14. Wang LY, Palmer FL, Nixon IJ, Thomas D, Patel SG, Shaha AR, et al. Multi-organ distant metastases confer worse disease-specific survival in differentiated thyroid cancer. *Thyroid: Off J Am Thyroid Assoc*. (2014) 24:1594–9. doi: 10.1089/thy.2014.0173

15. Liu Q, Zhang H, Jiang X, Qian C, Liu Z, Luo D. Factors involved in cancer metastasis: a better understanding to "seed and soil" hypothesis. *Mol Cancer*. (2017) 16:176. doi: 10.1186/s12943-017-0742-4

16. Toraih EA, Hussein MH, Zerfaoui M, Attia AS, Marzouk Ellythy A, Mostafa A, et al. Site-specific metastasis and survival in papillary thyroid cancer: the importance of brain and multi-organ disease. *Cancers*. (2021) 13:1625. doi: 10.3390/cancers13071625

17. Hugen N, Sloot YJE, Netea-Maier RT, van de Water C, Smit JWA, Nagtegaal ID, et al. Divergent metastatic patterns between subtypes of thyroid carcinoma results from the nationwide dutch pathology registry. *J Clin Endocrinol Metab*. (2020) 105:e299–306. doi: 10.1210/clinem/dgz078

18. Parhar RS, Zou M, Al-Mohanna FA, Baitei EY, Assiri AM, Meyer BF, Shi Y. IL-12 immunotherapy of Braf(V600E)-induced papillary thyroid cancer in a mouse model. *Lab Invest*. (2016) 96:89–97. doi: 10.1038/labinvest.2015.126

19. Zou M, Baitei EY, Al-Rijjal RA, Parhar RS, Al-Mohanna FA, Kimura S, et al. KRAS(G12D)-mediated oncogenic transformation of thyroid follicular cells requires long-term TSH stimulation and is regulated by SPRY1. *Lab Invest*. (2015) 95:1269–77. doi: 10.1038/labinvest.2015.90

20. Zou M, Baitei EY, Al-Rijjal RA, Parhar RS, Al-Mohanna FA, Kimura S, et al. TSH overcomes Braf(V600E)-induced senescence to promote tumor progression via downregulation of p53 expression in papillary thyroid cancer. *Oncogene*. (2016) 35:1909–18. doi: 10.1038/onc.2015.253

21. Zou M, Baitei EY, BinEssa HA, Al-Mohanna FA, Parhar RS, St-Arnaud R, et al. cyp24a1 attenuation limits progression of braf(V600E) -induced papillary thyroid cancer cells and sensitizes them to BRAF(V600E) inhibitor PLX4720. *Cancer Res*. (2017) 77:2161–72. doi: 10.1158/0008-5472.CAN-16-2066

22. Mansour FA, Al-Mazrou A, Al-Mohanna F, Al-Alwan M, Ghebeh H. PD-L1 is overexpressed on breast cancer stem cells through notch3/mTOR axis. *Oncoimmunology*. (2020) 9:1729299. doi: 10.1080/2162402X.2020.1729299

23. Dontu G, Abdallah WM, Foley JM, Jackson KW, Clarke MF, Kawamura MJ, et al. *In vitro* propagation and transcriptional profiling of human mammary stem/progenitor cells. *Genes Dev*. (2003) 17:1253–70. doi: 10.1101/gad.1061803

24. Kohli K, Pillarisetty VG, Kim TS. Key chemokines direct migration of immune cells in solid tumors. *Cancer Gene Ther*. (2022) 29:10–21. doi: 10.1038/s41417-021-00303-x

25. Su X, Xu Y, Fox GC, Xiang J, Kwakwa KA, Davis JL, et al. Breast cancer-derived GM-CSF regulates arginase 1 in myeloid cells to promote an immunosuppressive microenvironment. *J Clin Invest*. (2021) 131:e145296. doi: 10.1172/JCI145296

26. Chen CJ, Liu YP. MERTK inhibition: potential as a treatment strategy in EGFR tyrosine kinase inhibitor-resistant non-small cell lung cancer. *Pharm (Basel Switzerland)*. (2021) 14:130. doi: 10.3390/ph14020130

27. Zou M, BinEssa HA, Al-Malki YH, Al-Yahya S, Al-Alwan M, Al-Jammaz I, et al. [amp]]beta;-catenin attenuation inhibits tumor growth and promotes differentiation in a BRAF(V600E)-driven thyroid cancer animal model. *Mol Cancer Ther*. (2021) 20:1603–13. doi: 10.1158/1535-7163.MCT-21-0037

28. Lindley LE, Curtis KM, Sanchez-Mejias A, Rieger ME, Robbins DJ, Briegel KJ. The WNT-controlled transcriptional regulator LBH is required for mammary stem cell expansion and maintenance of the basal lineage. *Dev (Cambridge England)*. (2015) 142:893–904. doi: 10.1242/dev.110403

29. Garikapati K, Ashad-Bishop K, Hong S, Qureshi R, Rieger ME, Lindley LE, et al. LBH is a cancer stem cell- and metastasis-promoting oncogene essential for WNT stem cell function in breast cancer. *bioRxiv*. (2021) 2001:2029.428659. doi: 10.1101/2021.01.29.428659

30. Speak AO, Swiatkowska A, Karp NA, Arends MJ, Adams DJ, van der Weyden L. A high-throughput *in vivo* screening method in the mouse for identifying regulators of metastatic colonization. *Nat Protoc*. (2017) 12:2465–77. doi: 10.1038/nprot.2017.118

31. Carneiro BA, El-Deiry WS. Targeting apoptosis in cancer therapy. *Nat Rev Clin Oncol*. (2020) 17:395–417. doi: 10.1038/s41571-020-0341-y

32. Karagiannis GS, Condeelis JS, Oktay MH. Chemotherapy-induced metastasis: molecular mechanisms, clinical manifestations, therapeutic interventions. *Cancer Res*. (2019) 79:4567–76. doi: 10.1158/0008-5472.CAN-19-1147

33. Poth KJ, Guminski AD, Thomas GP, Leo PJ, Jabbar IA, Saunders NA. Cisplatin treatment induces a transient increase in tumorigenic potential associated with high interleukin-6 expression in head and neck squamous cell carcinoma. *Mol Cancer Ther*. (2010) 9:2430–9. doi: 10.1158/1535-7163.MCT-10-0258

34. Vyas D, Laput G, Vyas AK. Chemotherapy-enhanced inflammation may lead to the failure of therapy and metastasis. *OncoTargets Ther*. (2014) 7:1015–23. doi: 10.2147/OTT.S60114

35. Liu G, Chen Y, Qi F, Jia L, Lu XA, He T, et al. Specific chemotherapeutic agents induce metastatic behaviour through stromal- and tumour-derived cytokine and angiogenic factor signalling. *J Pathol*. (2015) 237:190–202. doi: 10.1002/path.2015.237.issue-2

36. Middleton JD, Stover DG, Hai T. Chemotherapy-exacerbated breast cancer metastasis: A paradox explainable by dysregulated adaptive-response. *Int J Mol Sci*. (2018) 19:3333. doi: 10.3390/ijms19113333

37. Conod A, Silvano M, Ruiz IAA. On the origin of metastases: Induction of pro-metastatic states after impending cell death via ER stress, reprogramming, and a cytokine storm. *Cell Rep*. (2022) 38:110490. doi: 10.1016/j.celrep.2022.110490

38. Lu L, Wang JR, Henderson YC, Bai S, Yang J, Hu M, et al. Anaplastic transformation in thyroid cancer revealed by single-cell transcriptomics. *J Clin Invest*. (2023) 133:e169653. doi: 10.1172/JCI169653

39. van der Weyden L, Speak AO, Swiatkowska A, Clare S, Schejtman A, Santilli G, et al. Pulmonary metastatic colonisation and granulomas in NOX2-deficient mice. *J Pathol*. (2018) 246:300–10. doi: 10.1002/path.2018.246.issue-3

40. Martner A, Aydin E, Hellstrand K. NOX2 in autoimmunity, tumor growth and metastasis. *J Pathol*. (2019) 247:151–4. doi: 10.1002/path.2019.247.issue-2

41. Hsu J, Hodgins JJ, Marathe M, Nicolai CJ, Bourgeois-Daigneault MC, Trevino TN, et al. Contribution of NK cells to immunotherapy mediated by PD-1/PD-L1 blockade. *J Clin Invest*. (2018) 128:4654–68. doi: 10.1172/JCI99317

42. Oyer JL, Gitto SB, Altomare DA, Copik AJ. PD-L1 blockade enhances anti-tumor efficacy of NK cells. *Oncoimmunology*. (2018) 7:e1509819. doi: 10.1080/2162402X.2018.1509819

43. Han Y, Liu D, Li L. PD-1/PD-L1 pathway: current researches in cancer. *Am J Cancer Res*. (2020) 10:727–42.

44. Chan LC, Li CW, Xia W, Hsu JM, Lee HH, Cha JH, et al. IL-6/JAK1 pathway drives PD-L1 Y112 phosphorylation to promote cancer immune evasion. *J Clin Invest*. (2019) 129:3324–38. doi: 10.1172/JCI126022

45. Johnson DE, O'Keefe RA, Grandis JR. Targeting the IL-6/JAK/STAT3 signalling axis in cancer. *Nat Rev Clin Oncol*. (2018) 15:234–48. doi: 10.1038/nrclinonc.2018.8

46. Gong J, Chehrazi-Raffle A, Reddi S, Salgia R. Development of PD-1 and PD-L1 inhibitors as a form of cancer immunotherapy: a comprehensive review of registration trials and future considerations. *J immunotherapy Cancer*. (2018) 6:8. doi: 10.1186/s40425-018-0316-z

47. Barkal AA, Brewer RE, Markovic M, Kowarsky M, Barkal SA, Zaro BW, et al. CD24 signalling through macrophage Siglec-10 is a target for cancer immunotherapy. *Nature*. (2019) 572:392–6. doi: 10.1038/s41586-019-1456-0

48. Bandala-Sanchez E, Zhang Y, Reinwald S, Dromey JA, Lee BH, Qian J, et al. T cell regulation mediated by interaction of soluble CD52 with the inhibitory receptor Siglec-10. *Nat Immunol*. (2013) 14:741–8. doi: 10.1038/ni.2610

49. Bandala-Sanchez E, Gb N, Goddard-Borger ED, Ngui K, Naselli G, Stone NL, et al. CD52 glycan binds the proinflammatory B box of HMGB1 to engage the Siglec-10 receptor and suppress human T cell function. *Proc Natl Acad Sci United States America*. (2018) 115:7783–8. doi: 10.1073/pnas.1722056115

50. Lu X, Kang Y. Chemokine (C-C motif) ligand 2 engages CCR2+ stromal cells of monocytic origin to promote breast cancer metastasis to lung and bone. *J Biol Chem*. (2009) 284:29087–96. doi: 10.1074/jbc.M109.035899

51. Wu Y, Li YY, Matsushima K, Baba T, Mukaida N. CCL3-CCR5 axis regulates intratumoral accumulation of leukocytes and fibroblasts and promotes angiogenesis in murine lung metastasis process. *J Immunol (Baltimore Md: 1950)*. (2008) 181:6384–93. doi: 10.4049/jimmunol.181.9.6384

52. Rašková M, Lacina L, Kejík Z, Venhauerová A, Skaličková M, Kolář M, et al. The role of IL-6 in cancer cell invasiveness and metastasis-overview and therapeutic opportunities. *Cells*. (2022) 11:3698. doi: 10.3390/cells11223698

53. Lee E, Fertig EJ, Jin K, Sukumar S, Pandey NB, Popel AS. Breast cancer cells condition lymphatic endothelial cells within pre-metastatic niches to promote metastasis. *Nat Commun*. (2014) 5:4715. doi: 10.1038/ncomms5715

54. Gay LJ, Felding-Habermann B. Contribution of platelets to tumour metastasis. *Nat Rev Cancer*. (2011) 11:123–34. doi: 10.1038/nrc3004

55. Lucotti S, Cerutti C, Soyer M, Gil-Bernabé AM, Gomes AL, Allen PD, et al. Aspirin blocks formation of metastatic intravascular niches by inhibiting platelet-derived COX-1/thromboxane A2. *J Clin Invest*. (2019) 129:1845–62. doi: 10.1172/JCI121985

56. Rothwell PM, Wilson M, Price JF, Belch JF, Meade TW, Mehta Z. Effect of daily aspirin on risk of cancer metastasis: a study of incident cancers during randomised controlled trials. *Lancet (London England)*. (2012) 379:1591–601. doi: 10.1016/S0140-6736(12)60209-8

57. Cho MS, Lee H, Gonzalez-Delgado R, Li D, Sasano T, Carlos-Alcalde W, et al. Platelets increase the expression of PD-L1 in ovarian cancer. *Cancers*. (2022) 14:2498. doi: 10.3390/cancers14102498

58. Hinterleitner C, Strähle J, Malenke E, Hinterleitner M, Henning M, Seehawer M, et al. Platelet PD-L1 reflects collective intratumoral PD-L1 expression and predicts immunotherapy response in non-small cell lung cancer. *Nat Commun*. (2021) 12:7005. doi: 10.1038/s41467-021-27303-7

59. Werfel TA, Hicks DJ, Rahman B, Bendeman WE, Duvernay MT, Maeng JG, et al. Repurposing of a thromboxane receptor inhibitor based on a novel role in metastasis identified by phenome-wide association study. *Mol Cancer Ther*. (2020) 19:2454–64. doi: 10.1158/1535-7163.MCT-19-1106

60. Lahey KC, Gadiyar V, Hill A, Desind S, Wang Z, Davra V, et al. Mertk: An emerging target in cancer biology and immuno-oncology. *Int Rev Cell Mol Biol*. (2022) 368:35–59. doi: 10.1016/bs.ircmb.2022.04.004

61. Lin J, Xu A, Jin J, Zhang M, Lou J, Qian C, et al. MerTK-mediated efferocytosis promotes immune tolerance and tumor progression in osteosarcoma through enhancing M2 polarization and PD-L1 expression. *Oncoimmunology*. (2022) 11:2024941. doi: 10.1080/2162402X.2021.2024941

62. Kasikara C, Kumar S, Kimani S, Tsou WI, Geng K, Davra V, et al. Phosphatidylserine sensing by TAM receptors regulates AKT-dependent chemoresistance and PD-L1 expression. *Mol Cancer research: MCR*. (2017) 15:753–64. doi: 10.1158/1541-7786.MCR-16-0350

63. Paolino M, Choidas A, Wallner S, Pranjic B, Uribesalgo I, Loeser S, Penninger JM, et al. The E3 ligase Cbl-b and TAM receptors regulate cancer metastasis via natural killer cells. *Nature*. (2014) 507:508–12. doi: 10.1038/nature12998

64. Flemming A. Unleashing NK cell anti-metastatic activity. *Nat Rev Drug Discovery*. (2014) 13:257–7. doi: 10.1038/nrd4297

65. Rios-Doria J, Favata M, Lasky K, Feldman P, Lo Y, Yang G, et al. A potent and selective dual inhibitor of AXL and MERTK possesses both immunomodulatory and tumor-targeted activity. *Front Oncol*. (2020) 10:598477. doi: 10.3389/fonc.2020.598477

frontiers | Frontiers in Oncology

TYPE Case Report
PUBLISHED 11 February 2025
DOI 10.3389/fonc.2025.1467631

OPEN ACCESS

EDITED BY
Juan Pablo Nicola,
National University of Cordoba, Argentina

REVIEWED BY
An Wei,
Hunan Provincial People's Hospital, China
Fernando Di Fermo,
Sanatorio Otamendi, Argentina
Fernando Carrizo,
Instituto de Oncología Ángel H. Roffo, Argentina

*CORRESPONDENCE
Bo Xie
2913216904@qq.com
Juan Zhou
juanzhn@163.com

†These authors have contributed equally to this work

RECEIVED 20 July 2024
ACCEPTED 24 January 2025
PUBLISHED 11 February 2025

CITATION
Chen X, Xiong L, Liu H, Wang H, Cheng D, Wang W, He W, Xie B and Zhou J (2025) Diagnosis and treatment of thyroblastoma: a case report and review of literature. *Front. Oncol.* 15:1467631. doi: 10.3389/fonc.2025.1467631

Diagnosis and treatment of thyroblastoma: a case report and review of literature

Xiting Chen[1,2†], Lijuan Xiong[1,2†], Hongling Liu[2], Haoqiang Wang[2], Donghai Cheng[2], Wei Wang[3], Wenyuan He[3], Bo Xie[2*] and Juan Zhou[2*]

[1]Guangzhou University of Chinese Medicine, Guangzhou, Guangdong, China, [2]Department of Oncology, General Hospital of Southern Theater Command, Guangzhou, Guangdong, China, [3]Department of Pathology, General Hospital of Southern Theater Command, Guangzhou, Guangdong, China

Background and objective: The diagnosis of thyroblastoma initially identified as a thyroid malignant teratoma was subsequently classified as a distinct entity by the World Health Organization (WHO) in 2022. This classification was based on the observation that the tumor presents with independent primitive multilineage elements and is frequently associated with DICER1 hotspot mutations.The objective of this study was to explore and investigate the clinicopathologic characteristics, molecular features and treatment strategies of patients with thyroblastoma, followed by a review of the previous relevant literature.

Methods: The clinical manifestations, pathological characteristics, molecular features and treatment strategies of the initial case of thyroblastoma pathologically confirmed in China were analyzed.

Results: The tumor was revealed to have high invasive potential, rapid disease progression, and primitive multilineage elements of pathology, including immature thyroid epithelium, spindled mesenchymal proliferations, and neuroepithelial blastema. Next-generation sequencing (NGS) confirmed the presence of germline DICER1 heterozygous pathogenic mutation at p.G1784* in patient, accompanied by the somatic hotspot mutation at p.E1813D of the RNase IIIb domain. Despite local thyroid tumor resection, the disease continued to progress rapidly. However, chemotherapy with BEP led to a reduction in the tumor. The patient's progression-free survival (PFS) reached 15 months following the administration of BEP chemotherapy in conjunction with local radiotherapy. The patient ultimately died of cardiac arrest resulting from the progression of the cancer thrombus to the right atrium and right ventricle.

Conclusion: Although thyroblastoma has been treated as a separate entity with its distinctive morphologic and molecular characteristics, its clinicopathological features, diagnosis and treatment methods and prognosis remain poorly understood, which requires more accumulated clinical case data to provide basis for the correct diagnosis and treatment in the future.

KEYWORDS

DICER1, thyroblastoma, thyroid neoplasms, thyroid, diagnosis and treatment

1 Introduction

Thyroblastoma was formally recognized as a distinct tumor entity by the World Health Organization (WHO) in 2022. Previously frequently misdiagnosed as thyroid teratoma, the recent redefinition highlights its distinctive primitive characteristics. These include thyroid epithelium, spindle cells with rhabdomyoblastic differentiation, and immature neuroepithelium. It is often observed that this tumor presents with DICER1 hotspot mutations. Clinically, it differs significantly from other thyroid tumors. It is highly aggressive, progresses rapidly, and has a poor prognosis, with approximately 50% of patients succumbing to the disease. Globally, no more than 10 cases of thyroblastoma have been reported in medical literature to date, and no standardized treatment protocol currently exists. This article presents a comprehensive examination of the clinical and pathological characteristics, molecular basis, and the diagnostic and therapeutic trajectory of a newly diagnosed thyroblastoma with DICER1 mutation. The objective of this study is to integrate findings with existing literature and contribute valuable insights for future clinical practices in the diagnosis and management of this rare malignancy.

2 Case report

The patient is a 23-year-old unmarried male, visited our hospital on November 11, 2022 due to a thyroid mass that had been progressively enlarging for two months. The patient has no significant past medical history or family medical history. Upon admission, a physical examination revealed pronounced neck thickening, tracheal deviation towards the right, absence of jugular vein distension, and a palpable neck mass measuring approximately 8 cm × 6 cm. Bilateral thyroid enlargement (grade III) was observed, exhibiting a hard texture, uneven surface, absence of tenderness, and mobility with swallowing. Enlarged cervical lymph nodes were palpable, while thrill and vascular murmurs were absent. An ultrasound examination conducted at our institution on November 18, 2022, revealed the presence of multiple solid thyroid nodules, suggestive of thyroid cancer, and enlarged lymph nodes in regions II, III, IV, and VI of both neck (suggestive of metastasis) (Figures 1A, B). On November 23, 2022, a PET/CT scan indicated: 1. An irregular hypermetabolic mass was observed in the left lobe of the thyroid with calcification, suggestive of malignancy. This mass was found to be compressing the trachea, resulting in local tracheal stenosis and deviation to the right; 2. The presence of multiple hypermetabolic enlarged lymph nodes in the left neck (levels II-V) and mediastinum (map 1), is suggestive of metastasis; possible tumor thrombus and thrombosis in the superior vena cava and left brachiocephalic vein (Figures 2A, B).

On November 27, 2022, due to acute respiratory distress and upper airway obstruction, the patient required emergency tracheotomy and resection of the thyroid tumor. Intraoperatively, diffuse bilateral thyroid enlargement with a hard texture and adhesion to surrounding tissues was noted, along with tracheal compression causing rightward deviation. Partial resection of the thyroid isthmus tumor was performed, and a tracheotomy tube was inserted to relieve upper airway obstruction. Postoperative pathology report (Figure 3) indicated that the lesion was situated within the thyroid tissue. The tumor exhibited components of primitive multipotential origin, including thyroid epithelial, spindle stromal, and primitive neuroepithelial elements. The tumor tissue within the thyroid exhibited immature cells with a high nuclear-cytoplasmic ratio, forming daisy-shaped cluster structures, large nuclei with coarse chromatin, and frequent apoptosis and mitosis. The immunohistochemistry results indicated the following findings: Thyroid epithelial components exhibited the following characteristics: SALL4(+), TTF-1 partial (+), P16(+), PAX-8 weak (+), CD99 partial (+); Immature neuroepithelial components: Syn partial (+), NSE(+), Nestin(+) and CD56(+); Stromal rhabdomyoblastic components: vimentin (+), desmin(+) and myogenin (+); Other markers: TG(-), CT(-), CK7(-), CK19(-), CK20(-), MC(-), Galectin-3(-), BRAFV600E(-), CK(-), EMA(-), S-100(-), SOX10(-), H3K27Me3(-), SMA(-), CD117 weak (+), inhibin(-), CgA(-), WT-1 cytoplasmic (+), HMB45(-), Melan-A(-), INI-1 intact, Ki67 positive rate approximately 60%(+). The diagnosis of thyroblastoma was made on the basis of the tissue morphology and immunohistochemistry results. NGS gene mutation testing revealed a heterozygous germline pathogenic mutation in the DICER1 gene p.G1784* in peripheral blood leukocyte DNA. Furthermore, a somatic mutation

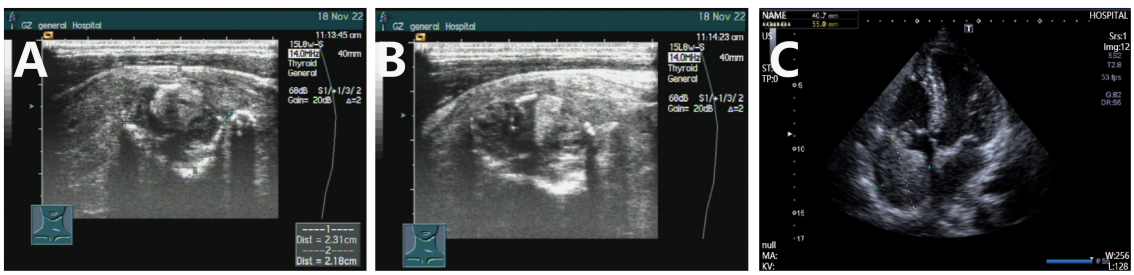

FIGURE 1
Color ultrasound examination of thyroblastoma. **(A, B)** Ultrasound results obtained on November 18 indicated an increased volume of both thyroid lobes, with heterogeneous internal echoes and multiple solid hypoechoic nodules, accompanied by calcification. **(C)** On May 20, 2024, cardiac ultrasound revealed the presence of a slightly hyperechoic mass within the right atrium, accompanied by enlargement of the right atrium and right ventricle.

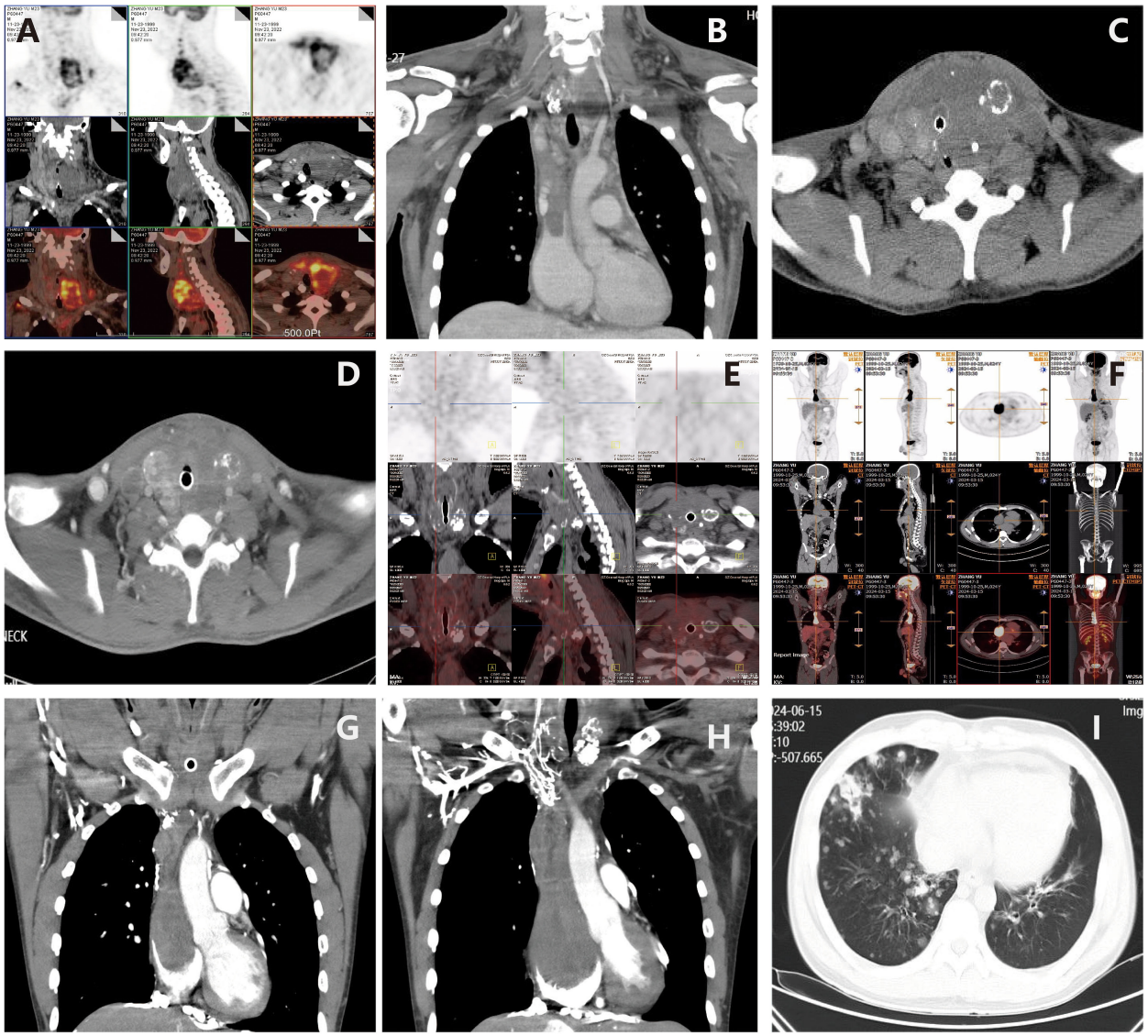

FIGURE 2
Imaging examination of thyroblastoma. **(A, B)** (November 23, 2022) PET/CT revealed irregular high-metabolic masses in the thyroid gland (more prominent in the left lobe) with calcification, compressing the trachea, causing local tracheal narrowing and rightward deviation; Multiple thromboses and cancerous thrombi were found in the superior vena cava, bilateral brachiocephalic veins, bilateral internal and external jugular veins, and the right subclavian vein. **(C)** (November 30, 2022) CT suggested rapid progression of thyroid tumor; **(D)** After two cycles of BEP regimen chemotherapy, enhanced CT (December 27, 2022) showed that the thyroid tumor had shrunk, the trachea was centered, and subcutaneous edema had decreased. **(E)** On August 25, 2023, follow-up PET/CT showed multiple low-density nodules with calcification in the thyroid, which were significantly smaller in volume than before, and metabolism had basically returned to normal, indicating that tumor activity was largely suppressed after treatment. The previously high-metabolic lesions in the superior vena cava and left brachiocephalic vein had returned to normal. **(F)** On March 15, 2024, PET/CT showed that the size of the thyroid lesion was unchanged and metabolism remained normal, suggesting suppressed tumor activity after treatment; however, new high-metabolic lesions in the superior vena cava and right atrium suggested cancer thrombi. **(G)** On March 19, 2024, CTA showed cancer thrombus formation in the lower lobe pulmonary arteries of both lungs, the right atrium, and the superior vena cava and its branches. **(H)** On June 12, 2024, CTA showed that cancerous thrombi had increased in size in the right atrium, right ventricle, superior vena cava, and left brachiocephalic vein. **(I)** On June 15, 2024, CT revealed multiple metastatic tumors in both lungs.

DICER1 gene p.E1813D was identified in plasma-free DNA, which is a hotspot mutation in the DICER1 gene RNase IIIb domain (Table 1).

Following surgery, the patient initially experienced temporary relief from respiratory distress for three days. However, subsequent CT indicated rapid progression of the thyroid tumor (Figure 2C). Fiberoptic bronchoscopy confirmed the growth of the tumor, which had compressed the airway, necessitating the placement of a tracheal stent. On December 6, 2022, the patient underwent emergency BEP chemotherapy (bleomycin, etoposide, cisplatin), resulting in the alleviation of respiratory distress symptoms post-treatment. A follow-up CT scan conducted on December 27, 2022, demonstrated a reduction in the size of the thyroid tumor (Figure 2D), prompting the continuation of the second course of BEP chemotherapy. From January 2023 to April 2023, the patient received four subsequent courses of BEP chemotherapy, achieving

10.3389/fonc.2025.1467631

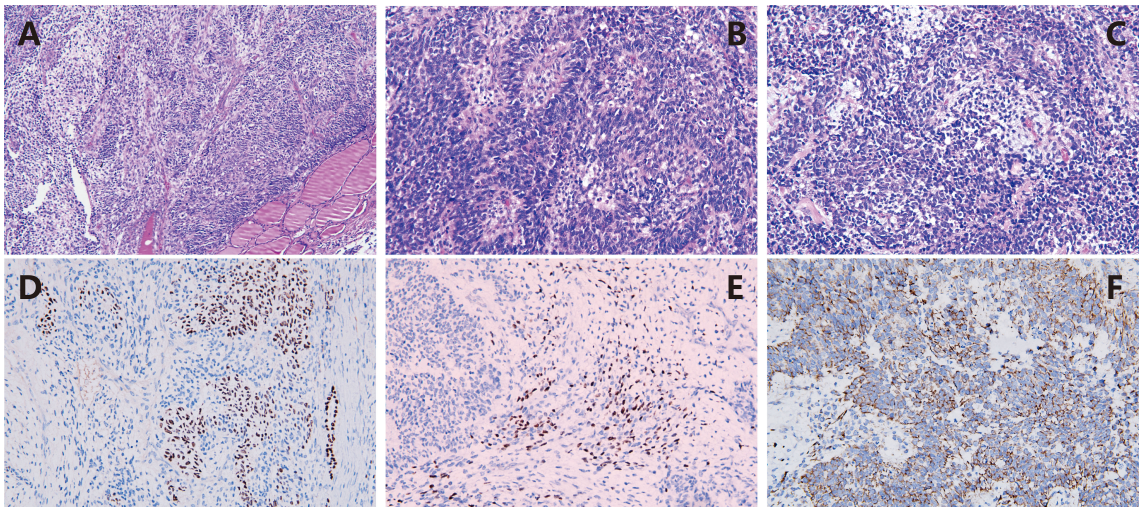

FIGURE 3
Pathological characteristics of thyroblastoma. **(A)** HE x100 The primitive tumor cells diffusely infiltrate between thyroid tissues; **(B)** HE x400 The immature cells with high nucleus-to-cytoplasm ratio are arranged in rosette-like structures; **(C)** HE x400 The tumor cells show evident apoptosis and mitotic figures, with local myogenic differentiation; **(D)** IHC x200 TTTF-1 is expressed in the primitive thyroid epithelial cells; **(E)** IHC x200 The area of rhabdomyoblastic differentiation shows immunoreactivity for Myogenin; **(F)** IHC x200 The primitive neuroepithelial components are positive for Nestin.

partial remission (PR) as the best response during this period. From April 12, 2023, to May 31, 2023, the thyroid tumor and cervical lymph node area were subjected to radiotherapy at a dose of 60Gy/30F. After radiotherapy, the tumor exhibited further reduction in size but did not achieve complete remission (CR).

After treatment, the patient was administered rivaroxaban for anticoagulation and underwent periodic follow-up examinations. The condition remained stable (Figure 2E). In March 2024, the patient presented to our department due to sudden syncope. The CT and PET/CT findings indicated multiple hypodense thyroid nodules with calcification, which was consistent with previous observations and indicative of essentially normal metabolism. These findings suggest inhibited tumor activity post-treatment. However, new hypermetabolic foci were detected in the superior vena cava and right atrium, suggesting the presence of a tumor thrombus. Computed tomography angiography (CTA) confirmed partial arterial involvement in the lower lobes of both lungs, right atrium, superior vena cava, bilateral brachiocephalic veins, internal and external jugular veins, and subclavian veins. Multiple collateral circulations were observed (Figures 2F, G). Cardiac ultrasound revealed the presence of slightly hyper-echoic masses within the right atrium, accompanied by enlargement of both the right atrium and right ventricle (Figure 1C). On March 24, 2024, and April 14, 2024, the patient received VIP chemotherapy (etoposide, ifosfamide, cisplatin). On May 13, 2024, the patient presented with a fever, cough, and respiratory distress, and was unable to assume a recumbent position. The follow-up CT scan indicated that the postoperative changes in the thyroid remained consistent, and the multiple tumor thrombi in the right atrium and superior vena cava were unchanged. The patient was treated for bilateral pneumonia with anti-infective agents, spasmolytics, and bronchodilators, resulting in clinical improvement and subsequent discharge. On June 12, 2024, the patient presented to the emergency department with sudden upper abdominal pain and vomiting. A CT scan revealed enlargement of tumor thrombi in the right atrium, right ventricle, superior vena cava, and left brachiocephalic vein, along with multiple pulmonary metastases (Figures 2H, I). After receiving anticoagulation and respiratory support, the patient's condition did not improve. Despite resuscitation efforts, the patient suffered a sudden cardiac arrest and died on June 15, 2024. A timeline chart has been created to illustrate the progression, diagnosis, and treatment of the patient's disease (Figure 4).

TABLE 1 NGS results of patient tissue specimens.

Gene	Chromosomal Coordinate	Exon	Nucleotide Change	Amino Acid Change	Zygosity	Frequency	Significance
DICER1	chr14:95557628	exon25	c.5439G>T	p.E1813D	Heterozygous	13.33%	Yes
DICER1	chr14:95560239	exon24	c.5350G>T	p.G1784*	Heterozygous	47.50%	Yes
ASXL1	chr20:31019399	exon9	c.896G>A	p.G299D	Heterozygous	48.80%	No
ERCC4	chr16:14042201	exon11	c.2748G>C	p.K916N	Heterozygous	49.80%	No

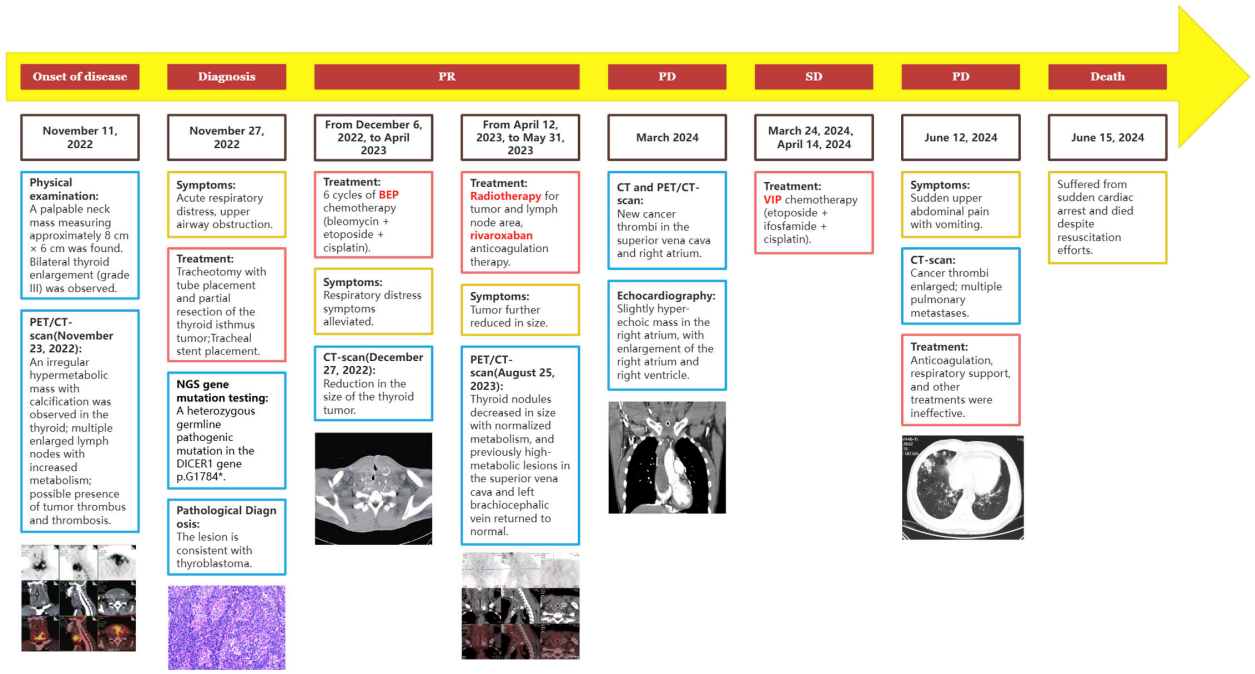

FIGURE 4
Timeline of the patient's disease progression, diagnosis, and treatment.

3 Discussion

According to the new classification in the 2022 WHO 5th edition of the "Classification of Endocrine and Neuroendocrine Tumors" (1), this case has been diagnosed as thyroblastoma. The literature on this particular tumor type is currently scarce, both within the domestic and international contexts. Previously classified as malignant thyroid teratoma, it is known that teratomas often occur in the reproductive system, while those occurring in the thyroid are very rare. Benign and immature teratomas mainly occur in infants, young children, and adolescents with a good prognosis, whereas malignant teratomas are more common in adults and have an aggressive course. The significant differences in clinical progression and prognosis suggest that benign/immature teratomas and malignant teratomas are completely independent solid tumors, rather than variations within a single tumor type. Thyroblastoma is primarily composed of primitive multipotential components. Thyroid follicles appear small and round, with scant cytoplasm and ovoid nuclei. Glial tissue is rare or absent, and some follicles may fuse, forming a microfollicular pattern. Spindle cell components typically exhibit a primitive undifferentiated state, with occasional short spindle and stellate shapes, often accompanied by significant mucinous degeneration and capillary proliferation. Some spindle cells exhibit rhabdomyoblastic differentiation (2–5). In contrast, benign/immature teratomas exhibit a broader spectrum of tissue components, including squamous epithelium with adnexal structures, respiratory epithelium, gastrointestinal epithelium, pancreatic parenchyma, hepatic parenchyma, pulmonary parenchyma, smooth muscle, skeletal muscle, cartilage, bone, and fibroadipose tissue. Immunohistochemistry resultsindicate the presence of immature neural elements, spindle cells exhibiting rhabdomyoblastic differentiation, and thyroid follicular-like epithelium in malignant teratomas (2, 6, 7). Typically, Pan-CK, TTF-1, and PAX8 are positive, with partial positivity for TG. Myogenic markers like Desmin and Myogenin are expressed in most spindle-shaped stromal cells, while S-100, CD99, TTF-1, and p63 may vary in expression. Primitive neuroepithelial components such as SALL4, NSE, Nestin and Syn are generally positive, with occasional positivity for Glypican-3 and TTF-1. In this case, the thyroid tissue lesion comprised multiple primitive multipotential components, including thyroid epithelial components, spindle stromal components, and primitive neuroepithelial components. Dual positivity for TTF1 and PAX8 suggests an origin from thyroid epithelium. Additionally, abundant undifferentiated spindle stromal cell components with rhabdomyoblastic differentiation were observed.Thyroblastoma needs to be differentiated from the following tumours: (1) Undifferentiated carcinoma of the thyroid (mesenchymal carcinoma): Undifferentiated carcinomas can show heterogeneous differentiation overlapping with that of thyroblastoma, including rhabdomyoblastoid cells or cartilaginous components. However, mesenchymal thyroid carcinomas occur in the elderly, usually show more pronounced cellular pleomorphism, and rarely have DICER1 mutations. Tumour cells are positive for CK, vimentin and PAX8, mutant p53 is often diffusely and strongly positive, TTF-1 is rarely positive, and neuroepithelial markers (Syn, CD56 and Nestin, etc.) are often negative (8); (2) Hypofractionated thyroid carcinoma (Insular carcinoma): Not only island-like, trabecular and microfollicular structures can be seen in poorly differentiated thyroid carcinoma, which overlap with immature fused follicles of thyroblastoma, but also some of poorly

differentiated thyroid carcinomas that occur in children or adolescents have DICER1 mutations, which need to be differentiated. Hypofractionated carcinomas lack the polyblastic component of thyroblastoma and are negative for neuroepithelial labelling by Syn and Nestin (9).

The defining molecular alteration in thyroblastoma is the acquired DICER1 hotspot mutation. The DICER1 gene, located on chromosome 14q32.13, encodes an RNase III family endoribonuclease, which is responsible for processing microRNA precursors into mature microRNAs. In thyroblastoma, mutations typically occur in specific codons of the RNase IIIb domain, such as E1705, D1709, G1809, D1810, and E1813 (10). These missense mutations disrupt normal microRNA synthesis and expression, thereby leading to tumorigenesis. DICER1 syndrome, a rare autosomal dominant familial tumor predisposition syndrome, that often manifests in infants and children under 30 years of age, is associated with heterozygous germline DICER1 mutations (11). The global incidence of DICER1 syndrome remains uncertain, characterized by diverse clinical manifestations where patients may develop one or multiple related tumors. Variability is notable even within families, with different members presenting different tumor types. Common DICER1-associated tumors include pleuropulmonary blastoma, ovarian Sertoli-Leydig cell tumor, and various thyroid diseases such as papillary, follicular, poorly differentiated carcinomas, and multinodular goiter. Less common tumors encompass nasal chondromesenchymal hamartoma, ciliary body medulloepithelioma, and pineoblastoma (12). DICER1 germline mutations outside hotspot regions, and a "second hit" - somatic mutations in the DICER1 RNase IIIb domain, contribute to the development of both benign and malignant tumors. Additionally, somatic DICER1 mutations can result in comparable tumour manifestations in patients lacking germline mutations (13). In recent years, advancements in molecular detection have led to the expanding scope of DICER1-related tumors. As of 2020, primary DICER1-related central nervous system sarcoma (14) and primitive sarcoma similar to pleuropulmonary blastoma and DICER1-related renal sarcoma (15) have been recognized. Now, thyroid blastoma has been newly classified among the DICER1-related malignant tumors. Rooper et al. (16) conducted next-generation sequencing (NGS) on 8 cases of thyroid teratoma (4 malignant, 3 benign, and 1 immature), revealing a DICER1 hotspot mutations in all 4 malignant cases, while no other clinically significant gene mutations were detected in the benign and immature cases. Study revealed that all 10 published cases meeting the genetic testing criteria for thyroid blastoma exhibited DICER1 hotspot mutations, including p.E1813Q (n=1, also had p.K868Ter), p.E1705K (n=3,one also had p.Y819fs), p.D1810H (n=1), p.E1813G (n=2), p.E1813K (n=1), p.G1809R (n=1), and p.D1709N (n=1) (6, 17). Among these, 4 cases had non-hotspot mutations that inactivated other DICER1 alleles, while 2 cases had TP53 mutations, 1 case had an NF1 mutation, and another 1 case had an ATM mutation. Notably, in one case confirmed via NGS, the patient was found to harbour a pathogenic heterozygous germline DICER1 gene mutation, p.G1784*, and a somatic mutation p.E1813D. This suggests that the inherited embryonic DICER1 mutation led to a secondary somatic cell mutation and subsequent development of thyroid blastoma. Heterozygous germline mutations at p.G1784* had not been previously reported.

As the range of tumors with DICER1 mutations expands, it is worth noting that despite their appearance in various anatomical locations, these tumors exhibit similar multi-germ layer components.These components include rhabdomyoblastic differentiation, primitive neuroepithelial components, immature cartilage or bone islands, and epithelial differentiation towards the organ of origin. The histological resemblance between the multi-germ layer components of thyroid blastoma and other DICER1-related malignancies suggests that the treatment approach for thyroid blastoma could be informed by DICER1-related malignancies. The treatment of tumours associated with DICER1 syndrome primarily relies on the tumor type and surgical pathology staging, with a combination of surgery and chemotherapy being the prevalent method. The International Pleuropulmonary Blastoma Registry recommends a chemotherapy regimen consisting of ifosfamide, doxorubicin, vincristine, and dactinomycin (18). For patients with pleuropulmonary blastoma who have residual disease post-surgery, recurrence, or metastasis, radiotherapy may also be employed. The primary treatment for DICER1 syndrome-related ovarian sex cord-stromal tumors is surgical resection, often followed by adjuvant chemotherapy, typically a platinum-based combination such as BEP or PEI (cisplatin, etoposide, and ifosfamide). Although the prognosis for malignant thyroid teratomas is generally poor, Ting et al. (19) reported successful treatment in 4 patients using surgery combined with chemotherapy. Regimens included CISCA (cyclophosphamide, doxorubicin, cisplatin), BEP, POMB (vincristine, methotrexate, bleomycin, and cisplatin), and ACE (dactinomycin-D, cyclophosphamide, and etoposide). A review of the published literature reveals that the primary treatment options for thyroid blastoma include total or subtotal thyroidectomy, combined with neoadjuvant chemotherapy, and adjuvant chemotherapy with or without adjuvant radiotherapy. The most commonly employed chemotherapy regimens include paclitaxel and carboplatin (4), PEI, and EVID (etoposide, vincristine, ifosfamide, and dactinomycin) (2), and so on. Reported survival times for patients range from 10 months to 125 months, yet the specific factors influencing survival prognosis remain unclear. The chemotherapeutic regimens previously reported in the literature for thyroblastoma include paclitaxel and carboplatin, PEI (cisplatin, etoposide, and ifosfamide), EVID (etoposide, vincristine, isocyclic aminophosphate, actinomycin), etc. Thyroblastoma was often diagnosed as teratoma, which was a type of germ cell tumour, and based on the above information, we chose the BEP(bleomycin, etoposide, cisplatin) regimen, which was a commonly used chemotherapeutic regimen for germ cell tumours, and was proved to be effective in this patient. The BEP regimen has become the 'gold standard' of chemotherapy for malignant germ cell tumours since 1994 (20), and after more than 30 years of clinical application, the efficacy of the BEP regimen has been widely verified by clinics, and it is the recommended regimen for the guidelines of the NCCN(National Comprehensive Cancer Network) and the CSCO(Chinese Society of Clinical Oncology) guidelines, the CR rate of germ cell tumour using BEP regimen is about 80%, and the 7-year OS rate is 69%. And side effects are manageable, with lower

haematological toxicity compared to VIP(cisplatin, etoposide, and ifosfamide) regimens (21). Following the diagnosis of this patient, due to the challenges of achieving complete surgical resection and the rapid tumor progression, we opted for the BEP regimen. This approach resulted in a significant reduction in the size of the thyroid tumor and improvement in respiratory function. The combination of chemotherapy with local radiotherapy resulted in a progression-free survival (PFS) of 15 months for the patient. However, significant thrombosis and cancer thrombus were present at the onset, which led to subsequent tumor progression, primarily manifesting as cancer thrombus progression. Despite effective control of the local thyroid tumors with chemotherapy and radiotherapy, the patient ultimately died of cardiac arrest caused by the cancer thrombus progression to the right atrium and right ventricle.

Thyroid blastoma is classified as a distinct solid tumor due to its distinctive morphological and molecular characteristics. Table 2 summarizes the clinical and pathological features of all 11 published cases of confirmed thyroid blastoma, along with our current case. This new classification provides clinicians with a more comprehensive understanding of these challenging tumours, facilitating more

TABLE 2 Published cases of thyroblastoma with morphologic and molecular characteristics.

Case	Sex	Age	Size (cm)	Presentation	Original Diagnosis	Treatment	Outcomes	Molecular	References
1	F	45	2.8	Neck mass	Carcinosarcoma	Total thyroidectomy, chemotherapy (taxol and carboplatin), and radiation	Lung metastasis, DOD at 11 mo	DICER1 p.E1705K	Yang et al. (4)
2	F	59	6.7	Rapidly progressing neck mass, hoarseness	Malignant teratoma	Neoadjuvant chemotherapy (primitive neuroectodermal tumor/ Ewing sarcoma protocol) and total thyroidectomy	NED at > 48 mo	DICER1 p.E1813G.TP53 p.R248Q,TP53 p.Y126_splice, NF1 p.N1054H	Rabinowits et al. (3)
3	F	65	1.9	Neck mass	Malignant teratoma	Total thyroidectomy and chemotherapy (unknown plan)	NED at 125 mo	DICER1 p.E1705K, DICER1 p.Y819fs	Rooper et al. (14)
4	F	29	10	Neck mass	Malignant teratoma	Total thyroidectomy, chemotherapy (unknown plan), and radiation	Para-aortic and clavicle metastases, DOD at 53 mo	DICER1 p.E1813G, DICER1 p.V448fs	Rooper et al. (14)
5	F	42	8	Neck mass	Malignant teratoma	Total thyroidectomy, chemotherapy (unknown plan), and radiation	NED at 64 mo	DICER1 p.E1813Q, DICER1 p.K868X	Rooper et al. (14)
6	M	60	1.7	Incidental on imaging	Malignant teratoma	Total thyroidectomy, adjuvant therapy deferred because of comorbidities	Widespread skeletal metastases, DOD at 10 mo	DICER1 p.D1810H	Rooper et al. (14)
7	M	17	8.2	Rapidly progressing neck mass	Malignant teratoma	Subtotal thyroidectomy with re-excision of tumor bed, chemotherapy (cisplatin, etoposide and ifosfamide), and radiation	NED at 8 mo	DICER1 p.D1709N, TP53 p.F134L	Agaimy et al. (2)
8	F	17	6.3	Rapidly progressing neck mass	Malignant teratoma	Total thyroidectomy and chemotherapy (etoposide, vincristine, ifosfamide and actinomycin; beomycin, etoposide and cisplatin)	Mediastinal progression, DOD at 12 mo	DICER1 p.G1809R	Agaimy et al. (2)
9	F	19	5.9	Neck mass	Malignant teratoma	Surgery, radioactive iodine, external-beam radiation therapy	NED	DICER1p.Glu1705Lys, ATM variant	Tikamporn et al. (5)
10	F	45	3	Neck mass	Malignant teratoma	Surgery, chemotherapy, external-beam radiation therapy,tyrosine kinase inhibitor	DOD	DICER1 p.Glu1813Lys	Tikamporn et al. (5)
11	M	23	15	Rapidly progressing neck mass	Thyroblastoma	Excision of thyroid isthmus tumor and chemotherapy (beomycin, etoposide and cisplatin)	Sudden cardiac arrest, DOD at 19 mo	DICER1 p.G1784*, DICER1 p.E1813D	Current

DOD, dead of disease; NED, no evidence of disease.

effective diagnosis and treatment. Nevertheless, additional clinical cases are required in order to enhance our comprehension of their clinical characteristics, treatment, and prognosis.

Data availability statement

The original contributions presented in the study are included in the article/supplementary material. Further inquiries can be directed to the corresponding authors.

Ethics statement

The studies involving humans were approved by Ethics Committee of General Hospital of Southern Theater Command, affiliated to General Hospital of Southern Theater Command. The studies were conducted in accordance with the local legislation and institutional requirements. The participants provided their written informed consent to participate in this study. Written informed consent was obtained from the individual(s) for the publication of any potentially identifiable images or data included in this article.

Author contributions

XC: Writing – original draft, Writing – review & editing. LX: Writing – original draft, Writing – review & editing. HL: Data curation, Resources, Writing – review & editing. HW: Conceptualization, Writing – review & editing. DC: Data curation, Writing – original draft. WW: Resources, Writing – original draft. WH: Resources, Writing – original draft. BX: Writing – review & editing. JZ: Writing – review & editing.

Funding

The author(s) declare that financial support was received for the research, authorship, and/or publication of this article. The present study was supported by Science and Technology Plan Project of Guangzhou (201904010018), Natural Science Foundation of Guangdong Province (NO.2021A1515220040).

Conflict of interest

The authors declare that the research was conducted in the absence of any commercial or financial relationships that could be construed as a potential conflict of interest.

Publisher's note

All claims expressed in this article are solely those of the authors and do not necessarily represent those of their affiliated organizations, or those of the publisher, the editors and the reviewers. Any product that may be evaluated in this article, or claim that may be made by its manufacturer, is not guaranteed or endorsed by the publisher.

References

1. Baloch ZW, Asa SL, Barletta JA, Ghossein RA, Juhlin CC, Jung CK, et al. Overview of the 2022 WHO classification of thyroid neoplasms. *Endocr Pathol.* (2022) 33:27–63. doi: 10.1007/s12022-022-09707-3

2. Agaimy A, Witkowski L, Stoehr R, Cuenca JCC, González-Muller CA, Brütting A, et al. Malignant teratoid tumor of the thyroid gland: an aggressive primitive multiphenotypic Malignancy showing organotypical elements and frequent DICER1 alterations-is the term "thyroblastoma" more appropriate? *Virchows Arch.* (2020) 477:787–98. doi: 10.1007/s00428-020-02853-1

3. Rabinowits G, Barletta J, Sholl LM, Reche E, Lorch J, Goguen L. Successful management of a patient with Malignant thyroid teratoma. *Thyroid.* (2017) 27:125–8. doi: 10.1089/thy.2016.0201

4. Yang J, Sarita-Reyes C, Kindelberger D, Zhao Q. A rare Malignant thyroid carcinosarcoma with aggressive behavior and DICER1 gene mutation: a case report with literature review. *Thyroid Res.* (2018) 11:11. doi: 10.1186/s13044-018-0055-8

5. Jitpasutham T, Faquin WC, Torous VF, Nosé V. Thyroblastoma: A DICER1-associated embryonal neoplasm and fine needle aspiration diagnostic criteria. *Diagn Cytopathol.* (2023) 51:E142–8. doi: 10.1002/dc.25105

6. Guilmette J, Dias-Santagata D, Lennerz J, Selig M, Sadow PM, Hill DA, et al. Primary thyroid neoplasm with fetal morphology associated with *DICER1* mutations: expanding the diagnostic profile of thyroblastoma. *Thyroid.* (2022) 32:1423–8. doi: 10.1089/thy.2022.0060

7. Rooper LM. From Malignant thyroid teratoma to thyroblastoma: evolution of a newly-recognized DICER1 -associated Malignancy. *Adv Anat Pathol.* (2023) 30:136–45. doi: 10.1097/PAP.0000000000000364

8. Oliveira G, Polónia A, Cameselle-Teijeiro JM, Leitão D, Sapia S, Sobrinho-Simões M, et al. EWSR1 rearrangement is a frequent event in papillary thyroid carcinoma and in carcinoma of the thyroid with Ewing family tumor elements (CEFTE). *Virchows Archiv: An Int J Pathol.* (2017) 470:517–25:5. doi: 10.1007/s00428-017-2095-1

9. Chernock RD, Rivera B, Borrelli N, Hill DA, Fahiminiya S, Shah T, et al. Poorly differentiated thyroid carcinoma of childhood and adolescence: a distinct entity characterized by DICER1 mutations. *Modern Pathol: An Off J United States Can Acad Pathol Inc.* (2020) 33:1264–74. doi: 10.1038/s41379-020-0458-7

10. Robertson JC, Jorcyk CL, Oxford JT. DICER1 syndrome: DICER1 mutations in rare cancers. *Cancers (Basel).* (2018) 10:143. doi: 10.3390/cancers10050143

11. González IA, Stewart DR, Schultz KAP, Field AP, Hill DA, Dehner LP. DICER1 tumor predisposition syndrome: an evolving story initiated with the pleuropulmonary blastoma. *Mod Pathol.* (2022) 35:4–22. doi: 10.1038/s41379-021-00905-8

12. Zhang L, Ye H, Duan. H. Research progress of DICER1 syndrome related tumors. *Chin J Obstetrics Gynecolog.* (2020) 55:498–502.

13. Foulkes WD, Priest JR, Duchaine TF. DICER1: mutations, microRNAs and mechanisms. *Nat Rev Cancer.* (2014) 14:662–72. doi: 10.1038/nrc3802

14. Kamihara J, Paulson V, Breen MA, Laetsch TW, Rakheja D, Shulman DS, et al. DICER1-associated central nervous system sarcoma in children: comprehensive clinicopathologic and genetic analysis of a newly described rare tumor. *Mod Pathol.* (2020) 33:1910–21. doi: 10.1038/s41379-020-0516-1

15. Schultz KAP, Nelson A, Harris AK, Finch M, Field A, Jarzembowski JA, et al. Pleuropulmonary blastoma-like peritoneal sarcoma: a newly described Malignancy associated with biallelic DICER1 pathogenic variation. *Mod Pathol.* (2020) 33:1922–9. doi: 10.1038/s41379-020-0558-4

16. Rooper LM, Bynum JP, Miller KP, Lin MT, Gagan J, Thompson LDR, et al. Recurrent DICER1 hotspot mutations in Malignant thyroid gland teratomas: molecular characterization and proposal for a separate classification. *Am J Surg Pathol.* (2020) 44:826–33. doi: 10.1097/PAS.0000000000001430

17. Erickson LA, Rivera M, Guo R, Torres-Mora J, Gupta S. Thyroblastoma-a primitive multilineage thyroid neoplasm with somatic DICER1 alteration. *Endocr Pathol*. (2023) 34:159–60. doi: 10.1007/s12022-023-09750-8

18. Zhang X, Zeng Q, Zhang N, Chen C, Yu J. Diagnosis and treatment of pediatric pleuropulmonary blastoma: a report of 38 cases. *J Clin Pediatr Surgery*. (2020) 19:63–8.

19. Ting J, Bell D, Ahmed S, Ying A, Waguespack SG, Tu SM, et al. Primary Malignant thyroid teratoma: an institutional experience. *Thyroid*. (2019) 29:229–36. doi: 10.1089/thy.2018.0206

20. Williams S, Blessing JA, Liao SY, Ball H, Hanjani P. Adjuvant therapy of ovarian germ cell tumors with cisplatin, etoposide, and bleomycin: a trial of the Gynecologic Oncology Group. *J Clin Oncol: Off J Am Soc Clin Oncol*. (1994) 12:701–6. doi: 10.1200/JCO.1994.12.4.701

21. Hinton S, Catalano PJ, Einhorn LH, Nichols CR, David Crawford E, Vogelzang N, et al. Cisplatin, etoposide and either bleomycin or ifosfamide in the treatment of disseminated germ cell tumors: final analysis of an intergroup trial. *Cancer*. (2003) 97:1869–75. doi: 10.1002/cncr.11271

frontiers | Frontiers in Oncology

TYPE Original Research
PUBLISHED 15 April 2025
DOI 10.3389/fonc.2025.1536063

OPEN ACCESS

EDITED BY
Juan Pablo Nicola,
National University of Cordoba, Argentina

REVIEWED BY
Young-Suk Jo,
Yonsei University, Republic of Korea
Chang Deng,
Chongqing Seventh People's Hospital, China

*CORRESPONDENCE
JianMin Li
wzyxyljmin@163.com

RECEIVED 28 November 2024
ACCEPTED 26 March 2025
PUBLISHED 15 April 2025

CITATION
Hu L, Lin Y, Zheng J, Wan L, Zhao R, Ma Y and Li J (2025) Transcriptome sequencing revealed that lymph node metastasis of papillary thyroid microcarcinoma is associated with high THBS4 expression and PDGFRA+ cancer-associated fibroblasts. *Front. Oncol.* 15:1536063. doi: 10.3389/fonc.2025.1536063

Transcriptome sequencing revealed that lymph node metastasis of papillary thyroid microcarcinoma is associated with high THBS4 expression and PDGFRA+ cancer-associated fibroblasts

LeYin Hu[1], Yi Lin[2], JingYu Zheng[1], Li Wan[1], Rui Zhao[3], Yi Ma[2] and JianMin Li[1]*

[1]Department of Pathology, Wenzhou Medical University First Affiliated Hospital, Wenzhou, Zhejiang, China, [2]Department of Pathology, Sanmen People's Hospital, Taizhou, Zhejiang, China, [3]Department of Gastroenterology, Wenzhou Medical University First Affiliated Hospital, Wenzhou, Zhejiang, China

Background: Cervical lymph node metastasis is a major factor influencing recurrence after surgery for papillary thyroid cancer. Molecular markers that can predict the presence of lymph node metastasis and assess the aggressiveness of papillary thyroid microcarcinoma (PTMC) remain poorly understood. The research question addressed whether specific genes, such as thrombospondin-4 (THBS4), could serve as predictive biomarkers for guiding surgical strategies, particularly in cases where current imaging modalities fail to detect LNM in the central region, and the decision for prophylactic central neck dissection remains controversial.

Methods: Transcriptome sequencing was employed to screen for differentially expressed genes and perform enrichment analysis. The study defined two groups of PTMC patients: LNM(n=50) and NLNM(n=50). 10 samples from each group were used for transcriptome sequencing. The expression of THBS4 was evaluated in both groups. Additionally, the correlation between THBS4 expression and cancer-associated fibroblasts (CAFs), specifically the PDGFRA+ inflammatory CAFs, was investigated to understand the stromal regulatory protein's role in PTMC aggressiveness.

Results: The analysis of sequencing data revealed that THBS4 expression was significantly higher in LNM PTMC compared to the NLNM group (Fold Change > 1.6 and $P < 0.05$). LNM PTMCs were also associated with a higher presence of PDGFRA+ inflammatory CAFs ($P < 0.05$), while no significant difference in the quantity of SMA+ myofibroblastic CAFs was observed between the two groups ($P>0.05$). Immunohistochemical analysis demonstrated increased THBS4($P < 0.01$) and PDGFRA($P < 0.001$) expression in LNM groups, while SMA staining showed no significant intergroup differences($P>0.05$).

Conclusion: This study's findings indicate that THBS4 could be a potential biomarker for predicting the risk of lymph node metastasis in papillary thyroid microcarcinoma, thus potentially guiding more personalized surgical interventions. Further validation in larger patient cohorts and the interactions between THBS4 and CAFs are necessary.

KEYWORDS

papillary thyroid microcarcinoma, tumor immune microenvironment, thrombospondin-4, lymph node metastasis, cancer-associated fibroblasts subsets

1 Introduction

Thyroid cancer (TC) is the most prevalent endocrine malignancy and has seen a striking rise in global incidence rates (1). Within TC, differentiated thyroid cancer (DTC) constitutes the majority of cases, with papillary thyroid cancer (PTC) being the most frequent subtype (2). Papillary thyroid carcinoma is prone to cervical lymph node metastasis, and extensive cervical lymph node metastasis also occur in papillary thyroid microcarcinoma (PTMC, traditionally defined as PTCs ≤ 1.0 cm in size), especially in some high-risk histologic subtypes (3). Rationally standardized cervical lymph node dissection is the primary treatment modality for these patients. However, Current imaging techniques, such as ultrasound, lack the sensitivity to reliably detect LNM, particularly in zone VI or in small lymph nodes (4, 5). This limitation hinders clinicians' ability to effectively identify metastatic lymph nodes. The need for prophylactic lymph node dissection, especially central neck dissection (CND), in these patients in whom no lymph node metastasis is detected at preoperative examination is still controversial in various guidelines (6–9). The benefits of preventive CND remain unclear. Therefore, effective identification of cervical lymph node metastasis is an urgent issue to be explored. Nonetheless, a subset of PTMCs presents with adverse pathologic features and aggressive clinical behaviors, including lymph node metastasis, distant metastasis, and structural recurrence following surgery (10–13). In severe instances, these tumors can be fatal, with progression to high-grade carcinoma often observed in metastatic lymph nodes (14, 15).

To address these diagnostic challenges, molecular diagnostic techniques are increasingly used to complement radiographic examinations. Although BRAFV600E is the most common mutation in papillary thyroid cancer, its role as a reliable risk factor for lymph node metastasis is yet to be determined (16, 17). Hence, there is a pressing need to identify new molecular markers that can predict the likelihood of lymph node metastasis.

Advances in high-throughput sequencing technology have facilitated the discovery of molecular markers for PTMCs. Despite recent advances (18–21), the genomic differences between PTMC with and without lymph node metastasis remain underexplored. In this study, we employed transcriptome sequencing to investigate the genomic characteristics of PTMC, identifying genomic features that diverge from previous reports. After performing further screening we found that thrombospondin-4 (THBS4) and its corresponding proteins were associated with whether PTMC developed lymph node metastasis or not. AS an extracellular matrix protein, THBS4 is usually considered to play a key role in tissue growth and remodeling under physiological conditions (22–24). In the context of tumor biology, THBS4 may contribute to tumor growth, proliferation, and migration, thereby promoting aggressive tumor behavior (25–27). Notably, THBS4 expression in some tumors is not directly secreted by tumor cells but rather by cancer-associated fibroblasts (CAF) (27–29). For this reason, we further explored the correlation between THBS4 and CAF in PTMC. Our results suggest THBS4 may serve as a molecular marker for predicting lymph node metastasis in PTMC.

2 Materials and methods

2.1 Biospecimen collection, pathological assessment, and public data processing

This retrospective study was approved by local ethical committees (The First Hospital of Wenzhou Medical University), and written informed consents were obtained from all patients. FFPE tissue samples (stored within six months) and corresponding haematoxylin-eosin stained slides from 100 PTMC patients were obtained from the Department of Pathology, First Affiliated Hospital, Wenzhou Medical University, and 20 of these were used for RNA sequencing. We performed simple random sampling using R (v4.0.3) with the command set.seed(); selected_LNM<-sample (1:50, size=10, replace=FALSE), selected_NLNM<- sample(51:100, size=10, replace=FALSE).Two pathologists independently performed histopathological review of the tumor sections. TNM stage of the disease was defined by pathologists according to the 8th AJCC/UICC staging system. All enrolled patients with thyroid carcinoma met the following inclusion criteria (1): Primary tumor;(2) Maximum tumor diameter ≤1 cm;(3) Histologically confirmed papillary thyroid carcinoma;(4) At least central neck dissection performed during surgery;(5) Surgical excision of

suspicious regional lymph nodes identified during preoperative evaluation;(6) Absence of distant metastasis (M0). RNA-sequencing counts, and clinical data of 48 PTC and normal thyroid tissue were acquired from The Cancer Genome Atlas Program (https://portal.gdc.cancer.gov/projects/TCGA-THCA). Use ComBat and ComBat_seq from the SVA package to correct for batch effects.

2.2 Nucleic acid extraction and library construction

Total RNA from FFPE samples was extracted using miRNeasy FFPE kit (QIAGEN). Ribosomal RNA was depleted using KAPA Stranded RNA-seq Kit with RiboErase (HMR) (KAPA Biosystems). Library preparations were performed with KAPA Stranded RNA-seq Library Preparation Kit (Roche). Library concentration was determined by KAPA Library Quantification Kit (KAPA Biosystems), and library quality was accessed by Agilent High Sensitivity DNA kit on Bioanalyzer 2100 (Agilent Technologies), which was then sequenced on Illumina Novaseq6000 NGS platforms (Illumina).

2.3 Gene expression analysis and sequent analysis

Base calling was performed on bcl2fastq v2.16.0.10 (Illumina, Inc.) to generate sequence reads in FASTQ format (Illumina 1.8+ encoding). Quality control (QC) was performed with Trimmomatic (version 0.33) (30). STAR (version 2.5.3a) (31) is used for transcriptome mapping followed by isoform and gene level quantification performed by RSEM (version 1.3.0) (32). Differential expression analysis was conducted by R packages DESeq2 (version 1.16.1) (33) and edgeR (version 3.18.1) (34). Differentially expressed genes of cohort were selected by Fold Change > 1.6 and P value < 0.05. Data from one of the samples was removed as an outlier. Differentially expressed genes of TCGA dataset were selected by Fold Change > 2 and P value < 0.05. Corresponding volcano plots and heatmaps were generated by in-house R scripts. GO and KEGG enrichment analysis were performed by ClusterProfiler (version 3.6.4) (35). Gene set enrichment analyses (GSEA) were performed using the GSEA software. The NMF package was used to perform an NMF clustering. K-M survival curves coupled with Logrank test were performed using the R packages "survival" (v.3.4–0) and "survminer" (v.0.4.9). The relative abundance of immune cell populations was then calculated using the R package "immunedeconv" (v.2.0.4) (36), which allows the community to perform integrated deconvolution using seven approaches including xCell (37) (Detailed data are provided in the Supplementary Material). Receiver operating characteristics (ROC) analysis was performed using the R package pROC (version 1.17.0.1) to obtain AUC.

2.4 Survival analysis

We downloaded the harmonized and standardized pan-cancer dataset from the UCSC (https://xenabrowser.net/) database and the previously published TCGA prognostic study in Cell (38). Prognostic dataset from UCSC (https://xenabrowser.net/datapages/), and TARGET follow-up data from UCSC (https://xenabrowser.net/datapages/) As a supplement, samples with expression level of 0 were filtered and samples with follow-up shorter than 30 days were excluded, and a log2(x+0.001) transformation was performed for each expression value to exclude cancers with less than 10 samples in a single cancer type. We calculated the optimal cut-off value of ENSG00000113296 (THBS4) using the R package maxstat, and set the minimum number of group samples to be greater than 25% and the maximum number of group samples to be less than 75% to finally obtain the optimal cut-off value, based on which the patients were divided into high and low groups, and further analyzed the prognostic difference between the two groups using the survfit function of the R package survival, and the significance of the prognostic difference between the samples of different groups was assessed using the logrank test method. The prognostic differences between the two groups were further analyzed using the survfit function of the R package survival, and the significance of the prognostic differences between the samples of different groups was assessed using the logrank test method.

2.5 Immunohistochemistry staining and quantification

Immunohistochemistry was performed. Briefly, sections were dewaxed and rehydrated. Antigen retrieval was performed by pretreating the slides in citrate buffer (pH 6.0; Thrombospondin 4) in a pressure cooker for 1 minute or EDTA (pH 8.0; PDGFRA and SMA) boiling for 20 minutes at 95°C. The slides were incubated with PBS containing 3% hydrogen peroxide for 10 min and subsequently incubate in the primary antibody (dilution ratios 1:150, Thrombospondin 4 antibody, catalog number orb1289935, biorbyt; dilution ratios 1:50, PDGFRA antibody, catalog number ZA-0377, ZSGB-BIO; dilution ratios 1:200, SMA antibody, catalog number ZM-0003, ZSGB-BIO) at 40°C for 1 hour. The slides were then probed with horseradish peroxidase conjugated secondary antibody for 20 mins at 40°C, followed by reaction with diaminobenzidine and counterstaining with Mayer's hematoxylin. Immunohistochemistry sections were digitally scanned using a whole slide image scanner. FIJI software was utilized for the quantitative assessment of average density within the region of interest.

2.6 Statistical analysis

All analyses were performed using R software v4.0.3 (https://cran.r-project.org/). T test was used to compare the distributions of continuous variable. Then chi-square test was performed to compare

the composition differences of categorical variable. Correlation was obtained with Spearman correlation test. Unless otherwise noted, a p-value < 0.05 was considered statistically significant.

3 Result

3.1 Research process and clinicopathologic features

The process of this study is shown in Figure 1. We defined PTMC as two groups; those with pathologically confirmed at least one regional lymph node metastasis, which we termed the LNM group, and those without, termed the NLNM group. There were no significant differences in baseline characteristics between the two groups (Table 1).

3.2 Differential gene expression analysis between LNM and NLNM PTMC

Transcriptome sequencing revealed 61 differentially expressed genes (DEGs) between the two groups. 55 of these were long non-coding RNAs and 6 were messenger RNAs (Figure 2A, Supplementary Table S2). Subsequently, Gene Set Enrichment Analysis (GSEA) was conducted on all expressed genes, revealing significant enrichment in 13 pathways. Notably, these pathways encompass focal adhesion, the PI3K-Akt signaling pathway, proteoglycans in cancer, and regulation of the actin cytoskeleton (Figure 2B). ROC analysis showed good differentiation of the two tumor groups by expression level of GP6 and THBS4 (Figure 3). To further screen for genes of interest, we obtained RNA sequencing data and clinical information from the TCGA-THCA dataset for PTC, selecting 48 cases each of tumor samples and normal thyroid samples. Using the normal thyroid tissue transcriptome from TCGA as a control, we identified DEGs between tumor and normal tissues separately. Our cohort data revealed 7348 DEGs and TCGA 4458 DEGs. Among the 3105 overlapping genes, 1746 were simultaneously upregulated and 1078 were simultaneously downregulated in both cohorts (Figures 2C, D). These DEGs were then subjected to Gene Ontology (GO) and Kyoto Encyclopedia of Genes and Genomes (KEGG) analysis (Figures 4A, B), which highlighted significant effects on extracellular matrix organization and ligand-receptor interactions, including extracellular matrix (ECM)-receptor interaction. Non-negative Matrix Factorization (NMF) clustering grouped the 20 samples into three clusters, with clusters 1 exhibiting a higher proportion of LNM tumors (Figure 2D). Next, we performed an enrichment analysis of cluster 1 and showed that pathways such as PI3K-Akt signaling pathway and ECM-receptor interaction were up-regulated (Figure 4C). We analyzed the impact of THBS4 on the

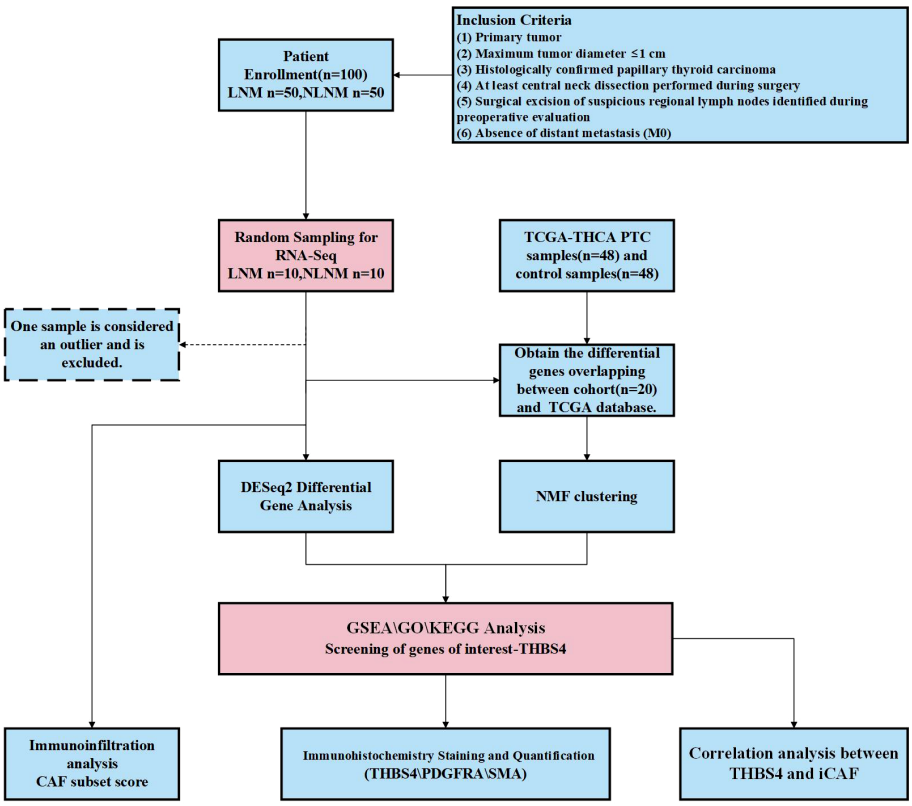

FIGURE 1
The flowchart of this study. PTC, papillary thyroid carcinoma; LNM. lymph node metastasis; NLNM, non-lymph node metastasis; THBS4, thrombospondin-4; CAF, cancer-associated fibroblasts; iCAF inflammatory CAF.

TABLE 1 Patients' clinicopathologic features.

Variable	NLNM (n=50)	LNM (n=50)	*P*-value
Age(n)			0.288
≥55 years	19	14	
<55 years	31	36	
Gender(n)			0.317
Male	27	22	
Female	23	28	
Maximum diameter of nodule (mm)	0.640 ± 0.176	0.680 ± 0.173	0.256
T stage(n)			1.000
T1a	50	50	
Minimal Extrathyroid Extension			0.110
No	47	42	
Yes	3	8	
BRAF mutation(n)			0.487*
Yes	44	47	
No	6	3	
Subtype(n)			0.827
Classic	27	26	
Infiltrative follicular	18	17	
Tall cell	5	7	

Statistical analysis was performed using chi-square test or Fisher's exact test* for categorical variable and t test for continuous variable

prognosis of patients with THCA and several other tumors using the TCGA database. Kaplan-Meier survival analyses showed that the higher THBS4 expression group typically had worse overall survival (Figure 5). These results suggest that tumor impact on the mesenchyme may significantly influence the probability of biological behavior of tumors including lymph node metastasis. We therefore selected THBS4, a gene involved in PI3K-Akt signaling pathway and associated with mesenchymal components, for further exploration. Additionally, we compared the abundance of immune cells in the microenvironment of both groups using seven common algorithms. In our cohort, the two groups did not differ significantly in the composition of the immune microenvironment, with only differences observed in the abundance of NK cells (Figure 6).

3.3 THBS4 is highly expressed in LNM PTMC

THBS4, one of the genes we identified, is involved in the focal adhesion and PI3K-Akt signaling pathways and is highly expressed in the LNM group. According to recent studies, the origin of THBS4 varies in different tumors, either from tumor cells or mesenchymal stromal cells, suggesting heterogeneity of THBS4 expression among tumors (29, 39). Immunohistochemical analysis of THBS4 expression in LNM and NLNM PTMC tissues revealed more positive staining in the tumor cytoplasm of the former, while fibroblasts in the tumor mesenchyme were barely stained (Figures 7A, B).

3.4 Increased abundance of PDGFRA+CAFs in LNM PTMC

In some studies, THBS4 regulates tumor biological behavior by affecting CAF (27), whereas a similar process has not been intensively investigated in papillary thyroid carcinoma. CAF is usually the most abundant mesenchymal cell component and may play a number of important biological functions in papillary thyroid carcinoma. Through single-cell sequencing, several studies have identified more functional subsets of CAF in various tumors (40–42). As with papillary thyroid carcinoma, CAFs have been broadly categorized into myofibroblastic CAFs (myoCAFs) and inflammatory subset (iCAFs) (43, 44). So, we next assessed the abundance of both CAFs in our cohort.

We assessed the abundance of both CAF subsets in our cohort, using marker gene expression averages derived from single-cell sequencing, as in previous studies (45) (Supplementary Table S1). We found that myoCAF scores did not differ between the two groups, whereas iCAF scores were higher in the LNM tumors, suggesting an increased presence of iCAFs in these cases (Figure 8A). Considering that there is no exclusive marker for either subset, after referring to previous studies (44), we used SMA and PDGFRA to label myoCAF and iCAF, respectively, and immunohistochemical staining showed an abundant presence of myoCAFs in both groups, while iCAFs were relatively scarce and primarily located at the infiltrating leading edge of the tumor in LNM PTMC (Figure 8B). Also, A significant positive correlation was observed between THBS4 expression and iCAF scores (Supplementary Figure S1. R=0.738, p<0.001, Spearman rank correlation).

4 Discussion

In our study, we investigated the genomic disparities between PTMC with and without LNM, yielding new insights through transcriptome sequencing. Though the six mRNAs (TRABD2B, GP6, THBS4, ESM1, HOXC6, EMX2) lack direct experimental evidence of interaction in our study, emerging literature suggests their potential convergence in metastatic progression. THBS4 and ESM1 may cooperatively modulate TGF-β bioavailability—a known EMT inducer—and endothelial activation (23, 46). EMX2 has been implicated in epithelial plasticity regulation via epigenetically silenced (47, 48). As a platelet-specific collagen receptor, GP6 is known to mediate platelet adhesion and activation, which may indirectly influence tumor progression through platelet-tumor microenvironment crosstalk (49). Intriguingly, HOXC6 might

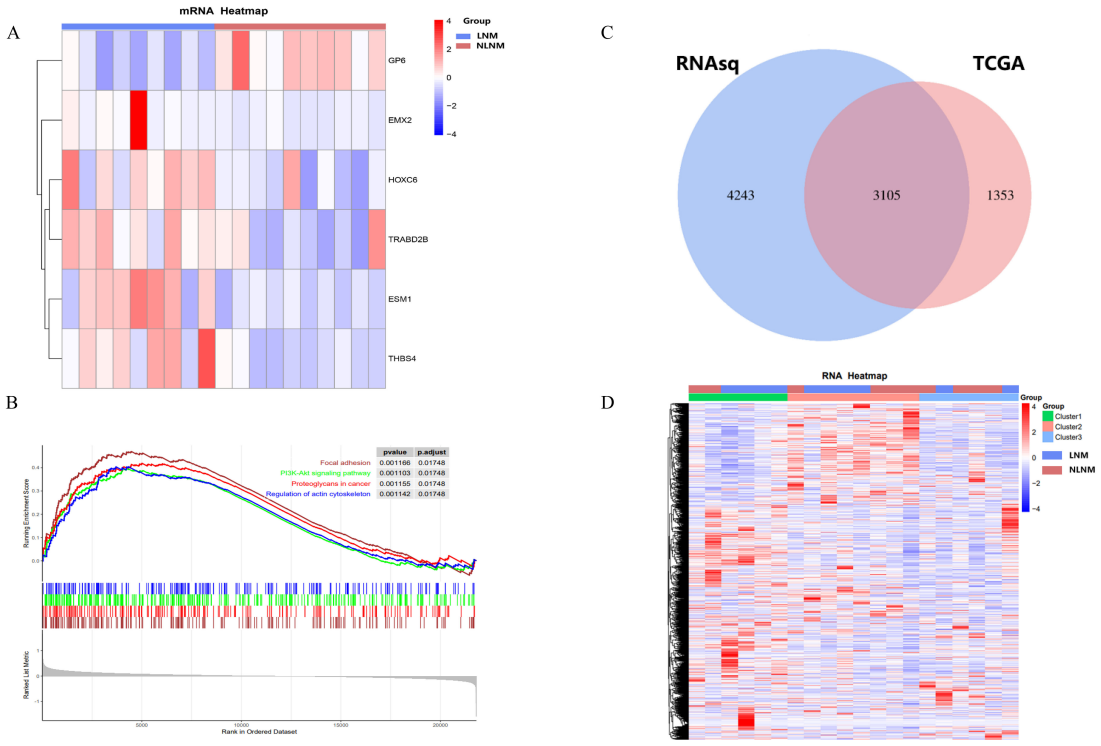

FIGURE 2
(A) Heatmap of differentially expressed genes encoding messenger RNAs. **(B)** The Gene Set Enrichment Analysis (GSEA) of all DEGs. **(C)** DEGs in the two cohorts and **(D)** NMF clustering of differentially expressed genes.

participate in stromal reprogramming (50) and stem cell identity maintenance (51). While this hypothetical framework requires experimental validation, the genes' collective enrichment in "extracellular matrix organization" and "ECM-receptor interaction" implies a plausible biological synergy warranting further investigation.

From the DEGs identified in our discovery cohort, THBS4 emerged as the prime candidate for three synergistic reasons (1): Its expression exhibited superior diagnostic accuracy in distinguishing LNM from NLNM tumors (AUC=0.9), outperforming other candidates; (2) Functional triangulation through GSEA, TCGA cohort validation, and NMF clustering convergently implicated PI3K-Akt signaling and ECM remodeling – pathways directly modulated by THBS4; (3) Pan-cancer survival analysis revealed that THBS4 overexpression universally predicted poor prognosis, suggesting its conserved role in metastatic progression. We therefore propose THBS4 as a promising marker gene for predicting lymph node metastasis and for guiding surgical strategies, yet the precise mechanisms by which it influences PTMC behavior remain unclear. We hypothesized that THBS4 may alter the composition of CAF subsets in the PTMC mesenchyme, and our findings support the notion of increased iCAF presence in LNM group. These discoveries enhance our comprehension of PTMC.

Previous studies have provided some characterization of PTMC transcriptome features. Fan Yang et al. identified nine core genes that may be used to predict the development of PTMC (18). A group of genes, including collagen type I alpha 1 (COL1A1), fibronectin 1 (FN1), laminin subunit gamma 2 (LAMC2), periostin (POSTN), transforming growth factor beta induced (TGFBI), are involved in extracellular mesenchymal organization and affect tumor behavior, akin to our findings. However, the impact of these genes on lymph node metastasis was not investigated. Other studies compared the transcriptome characteristics of patients with or without lateral lymph node metastasis. Consistent with our study, the differences in genetic characteristics between the two groups were relatively modest (19). Dilmi Perera et al. identified several DEGs, but they do not share a common molecular pathway or a single gene expression profile, making it difficult to explain the underlying physiological processes that the occurrence of LNM (20). The role of epithelial-mesenchymal transition and cancer stem cell-like properties in extensive lymph node spread of PTMC has been noted, as have the associations of lncRNA and circRNA with LNM (52–54). Overall, these studies have primarily focused on tumor parenchymal cells in search of markers predicting adverse behavior. A recent large sample study categorized PTMC into PTMC-proliferation (PTMC-Pro) and PTMC-inflammatory (PTMC-Inf) types based on their respective marker genes (55). PTMC- Inf was related with activated immune cell signaling and interferon-γ response and had a lower 5-year PFS rate than PTMC-pro. In contrast to our study, there were more differences in immune cell abundance between PTMC-Pro and PTMC-Inf. This suggests that in addition to clinical features, PTMC are heterogeneous

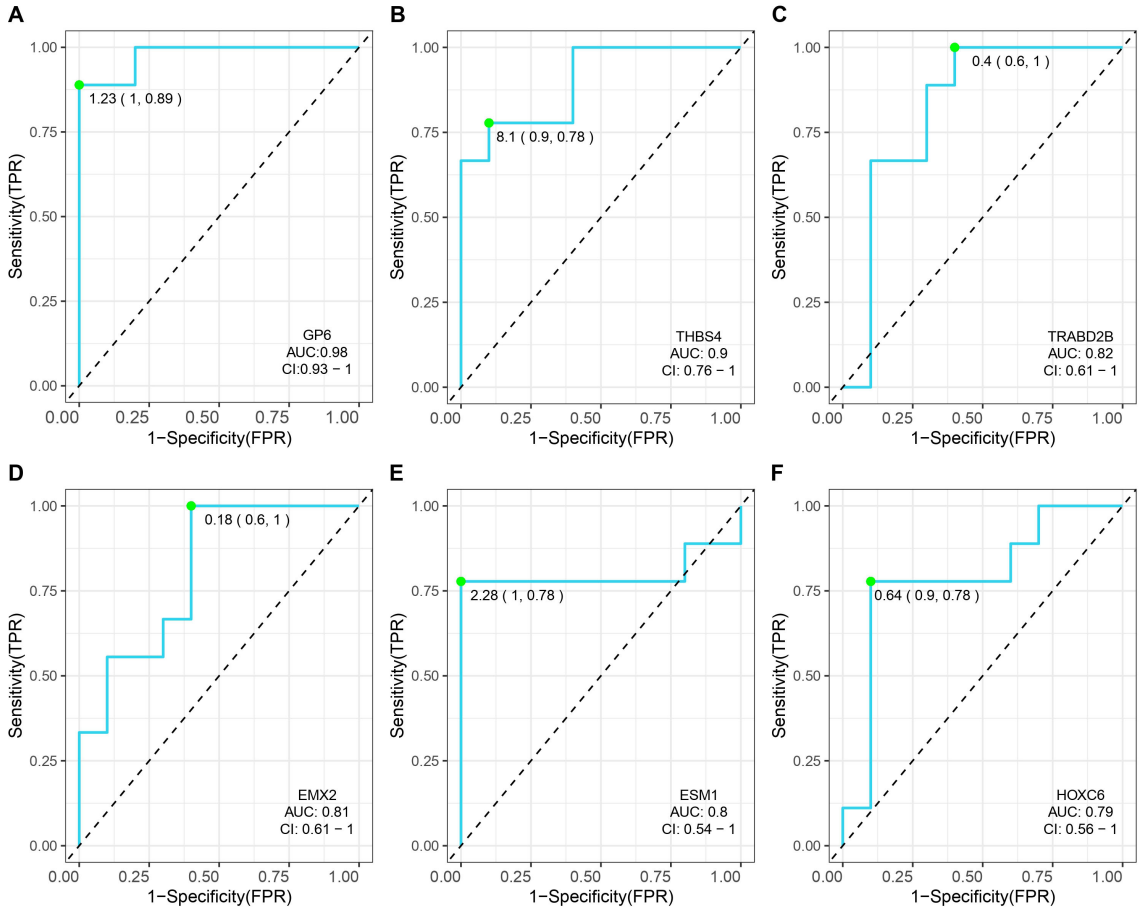

FIGURE 3
Receiver operating characteristic (ROC) curves and the associated areas under curves (AUCs) of six gene for the PTMC cohort. **(A)** GP6,glycoprotein VI platelet; **(B)** THBS4,thrombospondin 4; **(C)** TRABD2B,TraB domain containing 2B; **(D)** EMX2,empty spiracles homeobox 2 **(E)** ESM1,endothelial cell specific molecule 1; **(F)** HOXC6,homeobox C6;

in immune microenvironment, potentially leading to early-stage extensive lymph node metastasis. Our study, therefore, centered on tumor-microenvironment interactions, particularly the roles of THBS4 and CAFs.

Thrombospondin-4 (THBS-4) is a member of the thrombospondin protein family, which consists of five highly homologous members. In human tissues, THBS4 is abundantly expressed in cardiovascular, skeletal muscle, tendon and nerve tissues, with roles in cardiovascular and skeletal muscle being the most extensively studied. In the healthy heart, THBS4 prevents interstitial ECM deposition and cardiac hypertrophy (56, 57). And in skeletal muscle, THBS4 is important for proper motor unit assembly and function, and both muscle and tendon require THBS4 for attachment (58). *In vitro*, experiments have confirmed that THBS4 inhibits collagen synthesis in human fibroblasts and endothelial cells. All of these functions may be related to the regulation of ECM by THBS4, and THBS4 deficiency results in cardiac interstitial ECM deposition and skeletal muscle ECM deficiency.

Recently, high expression of THBS4 was found in several tumors. Interestingly, in most tumors, THBS4 promoted tumor progression. Similar to our findings in PTMC, in hepatocellular carcinoma, bladder cancer and prostate cancer, high expression of THBS4 in tumor cells promoted tumor growth, proliferation and invasion (25, 26, 59). In contrast, in colon cancer, the THBS4 gene is methylated and silenced, while increased expression of THBS4 in colon cancer colonies significantly inhibits tumor growth (60). The role of THBS4 on tumors is not only complex, but also varies in its origin in tumors. A typical example is gastric adenocarcinoma where, in contrast to PTMC, THBS4 is derived from tumor-associated fibroblasts in diffuse gastric adenocarcinoma, whereas THBS4 expression is not detectable in tumor cells (28, 29, 61). Another study in gallbladder cancer found that THBS4 is secreted by a variety of cells, but its main source is also CAF (27); in addition to CAF, the abundance of tumor-associated macrophages can also be regulated by THBS4 and play a role in tumor invasiveness (62). The specific regulatory mechanism of THBS4 in both normal and

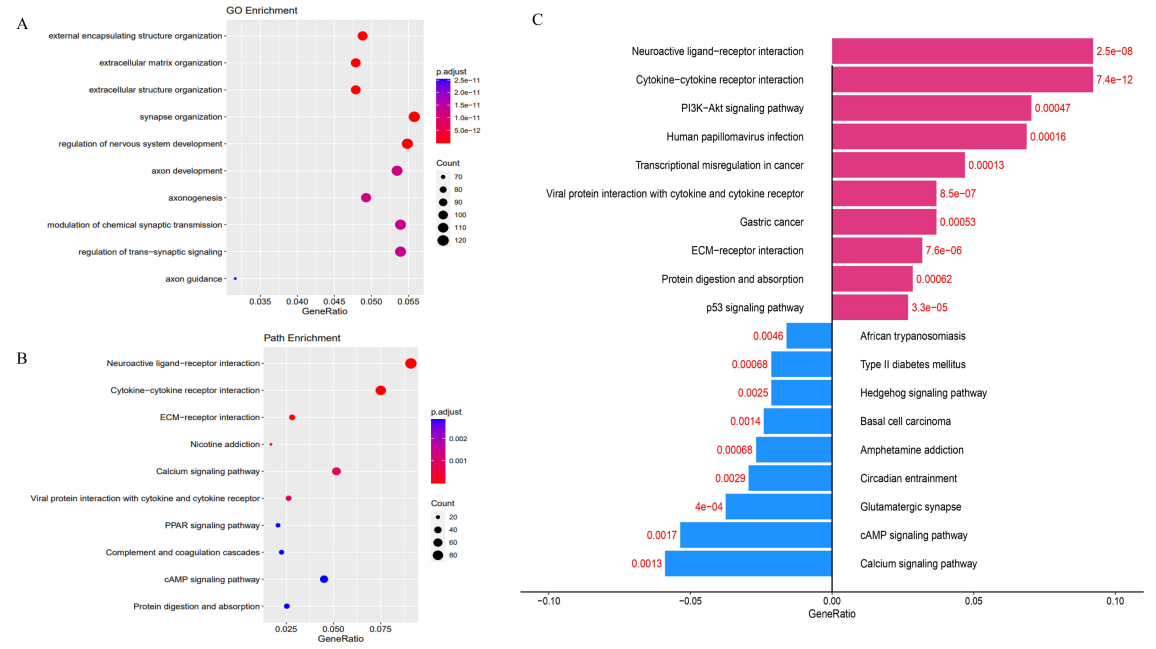

FIGURE 4
(A) Gene Ontology (GO) and **(B)** KEGG analysis of DEGs in two cohorts. **(C)** Gene Ontology analysis of DEGs in cluster 1.

tumor tissues is not well understood, among which transforming growth factor β (TGF-β) signaling has been shown to be closely related, and it has been reported that SMAD3 is involved in the regulation of THBS4 by TGF-β (23).

The tumor microenvironment (TME) is a concept that has emerged in recent years and is defined as the surrounding microenvironment in which tumor cells exist, including peripheral blood vessels, immune cells, fibroblasts, myeloid-

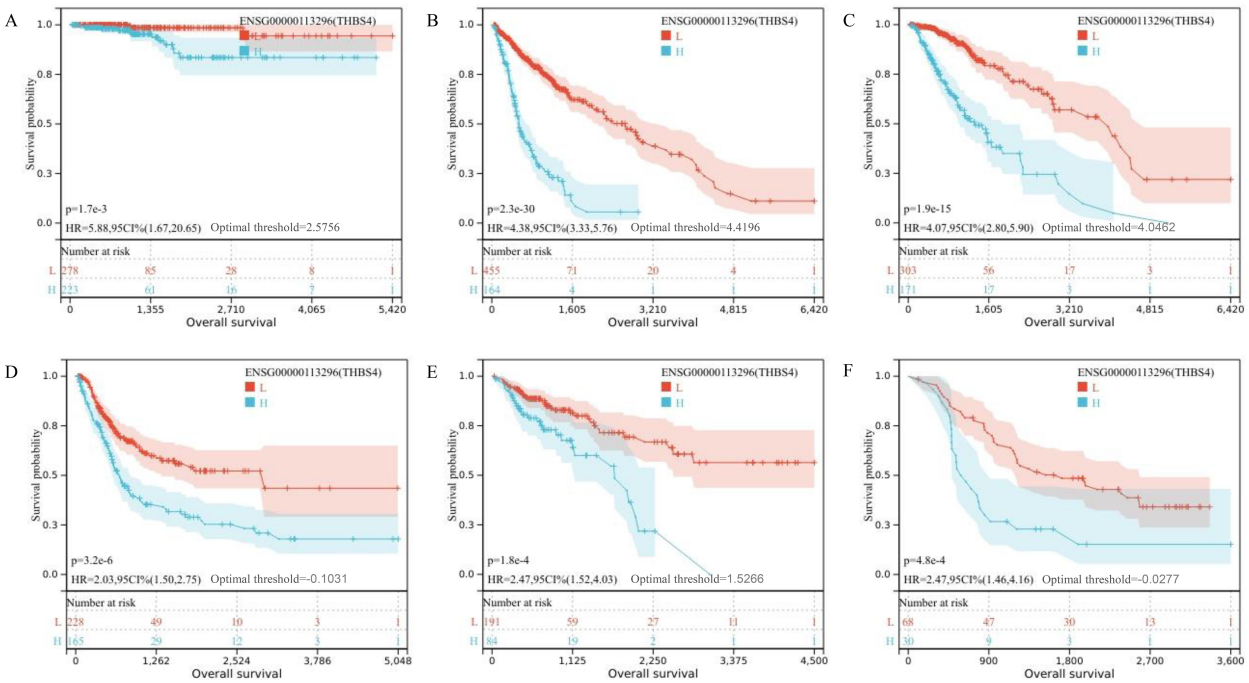

FIGURE 5
(A–F) Kaplan-Meier survival analysis showing overall survival for TCGA-THCA, TCGA-GBMLGG, TCGA-LGG, TCGA-BLCA, TCGA-COAD and TCGA-ALL-R.

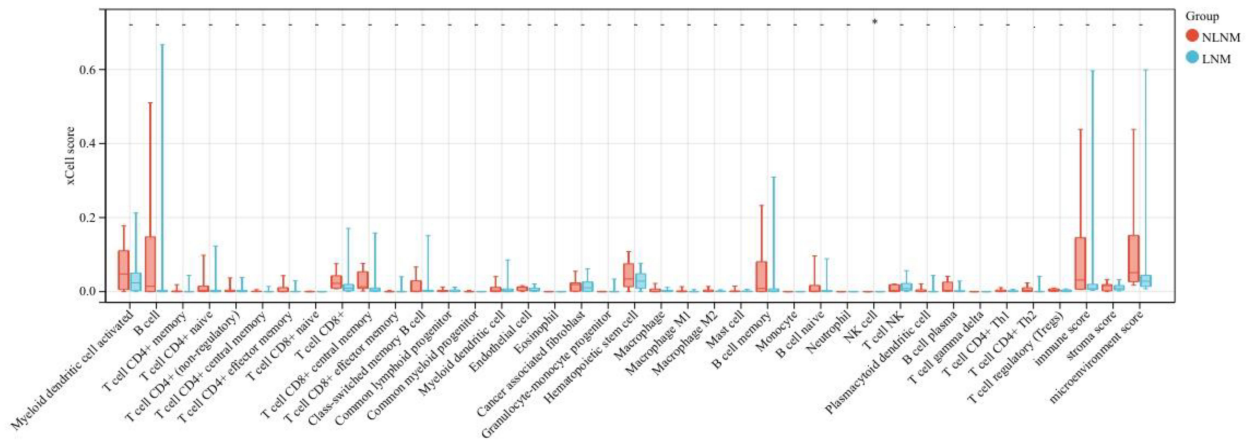

FIGURE 6
Differences in infiltrating immune cells between LNM and NLNM groups.

derived inflammatory cells, a variety of signaling molecules, and extracellular matrix (ECM). In current studies, CAF is typically one of the most abundant components of the TME (63). Some studies have shown that CAF is associated with LNM, upregulation of immune checkpoints, enrichment of immune cells, and tumor-associated macrophage polarization in PTCs (64). However, the heterogeneity of CAF in TME was not well recognized in PTMC until the widespread use of single-cell sequencing technology. Previous studies of PTC have used only SMA-labeled CAF, leaving the impact of CAF subsets on tumors poorly understood (65). A recent multi-sample single-cell sequencing study revealed distinct subsets of CAF in PTC (44). One subset is associated with cell motility, contraction, and extracellular matrix, and the other subset is associated with an abundance of immunomodulatory molecules and chemokines. iCAF is often hypothesized to carry out intercellular communication to influence the biological behavior of tumors, which may consequently undergo adverse pathologic features (66–68). Another single-cell sequencing of a single sample yielded similar results (43). In other tumors, CAF isoforms exert immunomodulatory functions through the expression of various cytokines, a typical molecule being interleukin-6 (69, 70). However, the situation in PTC is somewhat different. Weilin Pu et al. hypothesized through bioinformatics analysis that myoCAF tends to exert mechanical and chemical influences on tumor progression, whereas iCAF exerts immunomodulatory functions by recruiting and crosstalking various immune cells through chemokines such as CCL5, CCL3L3 and other chemotactic factors in the TME (44).

To our knowledge, no biological validation of the CAF subset in PTMC has been performed. Here, we compared data from samples from our center with previous studies, similar to iCAF with less cellular abundance than myoCAF, only iCAF differed between

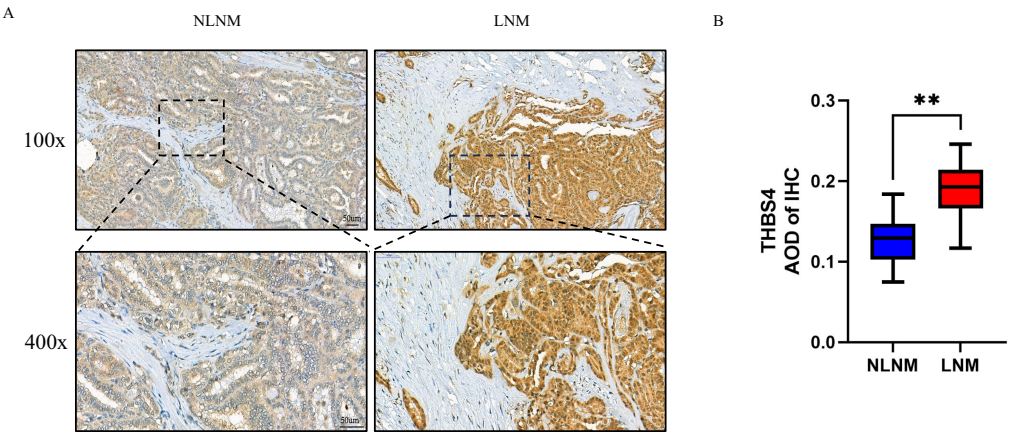

FIGURE 7
(A) Representative image of the immunohistochemistry of THBS4. **(B)** Average optical density (AOD) of immunohistochemical staining image. **P < 0.01 by Wilcoxon rank-sum test.

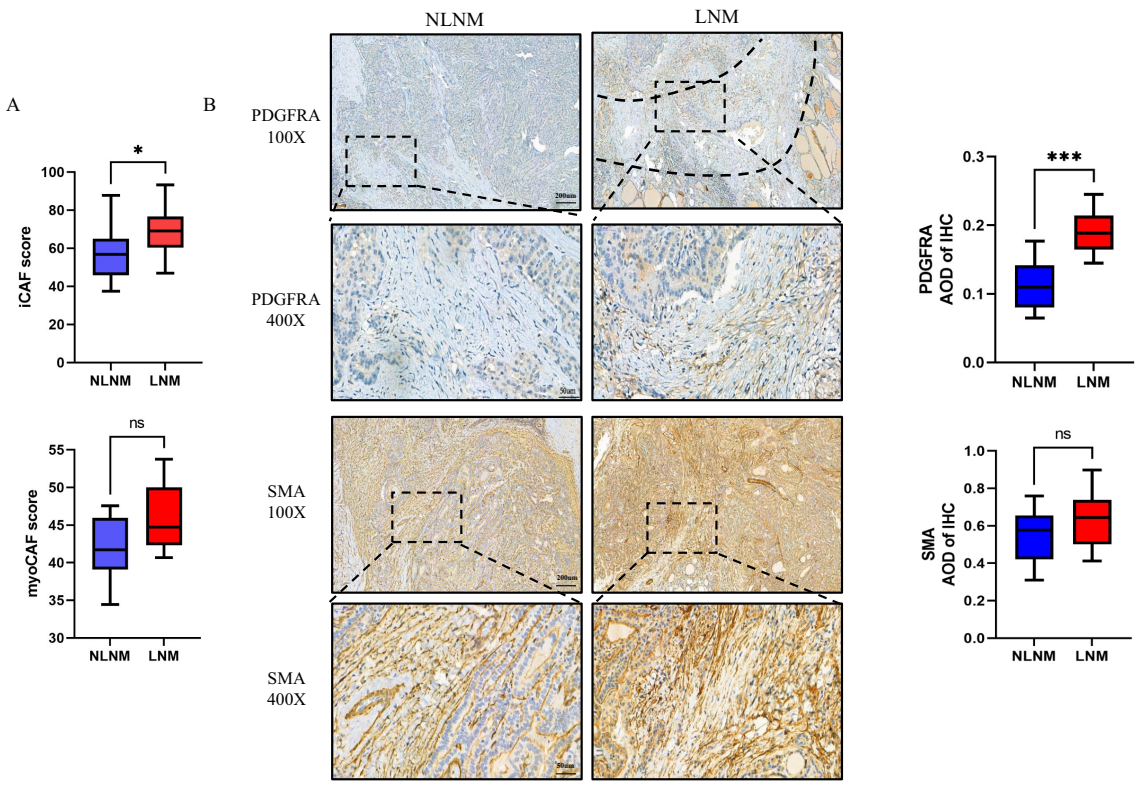

FIGURE 8
(A) Marker gene scores for CAF subsets in the LNM and NLNM groups. p=0.0433 or p=0.0753 by Wilcoxon rank-sum test. **(B)** Representative image of immunohistochemistry of PDGFRA and SMA, and corresponding average optical density (AOD). The dotted line shows the fibrous band between the tumor and normal tissue *P < 0.05 or ***P < 0.001 by Wilcoxon rank-sum test. ns, no significance.

LNM and NLNM PTMC, and the expression level of THBS4 was positively correlated with the iCAF score. Based on previous studies and our results, we speculate that tumor cells and CAF in PTMC may be involved in bidirectional regulation through THBS4 and TGF-β signaling pathways, which needs to be further confirmed in *in vitro* and *in vivo* experiments. In addition, in the available bulk RNA sequencing study, CAF did not show an effect on the biological behavior of PTC, probably because iCAF accounted for a small proportion of the total CAF (55).

Our study demonstrates the potential clinical utility of using THBS4 and PDGFRA as biomarkers to predict PTMC lymph node metastasis. Regrettably, there are several limitations to this study. First, this is a single-center study, and the generalizability of its results needs to be validated by a larger cohort. Second, we did not analyze the prognosis of patients in this cohort because of the short follow-up time. Thirdly, although no significant differences were observed in baseline patient characteristics, certain selection biases existed in the histological subtype selection of our cohort. This limitation was primarily attributable to the exclusion of rare histological subtypes from our study population, and secondly, to the inherent propensity of certain subtypes to exhibit higher rates of lymph node metastasis (3). Furthermore, in the AJCC 8th edition, extrathyroid extension that is only visible microscopically does not increase the T stage because it does not affect the patient's prognosis (71). However, tumor invasion of the vasculature or nerves in the soft tissue can sometimes be seen. Although it is unclear whether this leads to enhanced metastatic potential, this pathological categorization may nevertheless introduce potential confounding factors. In addition, we did not distinguish the pattern of lymph node metastases in detail, which may have introduced confounding bias. Whether different metastatic patterns represent different underlying mechanisms remains to be investigated in larger samples and cohorts. Finally, we did not investigate the causal relationship between THBS4 expression and iCAF abundance in tumors. We were unable to provide evidence of a direct association between THBS4 and iCAF. Further mechanistic studies are essential to elucidate the exact interaction between THBS4 and iCAF and to identify potential therapeutic targets.

In conclusion, our study integrated transcriptome sequencing and TCGA RNA sequencing data and identified THBS4 as a potential biomarker for predicting lymph node metastasis in papillary thyroid microcarcinoma (PTMC). Our findings suggest that THBS4 expression levels may influence the composition of CAF subsets in the tumor microenvironment. Despite these promising results, our study has limitations, including its single-center design and the need for further

studies on the interaction between THBS4 and iCAFs. Future studies should validate these findings in larger cohorts and explore the predictive value of THBS4 and PDGFRA as biomarkers of PTMC lymph node metastasis.

Data availability statement

The datasets generated in this study are available through the GSA for Human in the Genome Sequence Archive (GSA), BioProject ID: PRJCA038155, accession ID: HRA011009. The data of the public database can be accessed through the above-mentioned URLs.

Ethics statement

The studies involving humans were approved by Wenzhou Medical University First Affiliated Hospital ethical committees. The studies were conducted in accordance with the local legislation and institutional requirements. The participants provided their written informed consent to participate in this study.

Author contributions

LH: Formal analysis, Investigation, Resources, Visualization, Writing – original draft, Writing – review & editing. YL: Conceptualization, Methodology, Writing – original draft, Writing – review & editing. JZ: Conceptualization, Methodology, Writing – review & editing. LW: Investigation, Resources, Writing – review & editing. RZ: Formal analysis, Visualization, Writing – review & editing. YM: Formal analysis, Visualization, Writing – review & editing. JL: Conceptualization, Methodology, Writing – review & editing.

Funding

The author(s) declare that no financial support was received for the research and/or publication of this article.

Acknowledgments

This study was performed with the technical support of department of pathology, Wenzhou Medical University First Affiliated Hospital.

Conflict of interest

The authors declare that the research was conducted in the absence of any commercial or financial relationships that could be construed as a potential conflict of interest.

Generative AI statement

The author(s) declare that no Generative AI was used in the creation of this manuscript.

Publisher's note

Supplementary material

The Supplementary Material for this article can be found online at: https://www.frontiersin.org/articles/10.3389/fonc.2025.1536063/full#supplementary-material

SUPPLEMENTARY FIGURE 1
Correlation analysis of expression of THBS4 and iCAF scores, R=0.738, p<0.001, Spearman rank correlation

References

1. Sung H, Ferlay J, Siegel RL, Laversanne M, Soerjomataram I, Jemal A, et al. Global cancer statistics 2020: GLOBOCAN estimates of incidence and mortality worldwide for 36 cancers in 185 countries. *CA A Cancer J Clin*. (2021) 71:209–49. doi: 10.3322/caac.21660

2. Schmidbauer B, Menhart K, Hellwig D, Grosse J. Differentiated thyroid cancer—Treatment: state of the art. *IJMS*. (2017) 18:1292. doi: 10.3390/ijms18061292

3. Baloch ZW, Asa SL, Barletta JA, Ghossein RA, Juhlin CC, Jung CK, et al. Overview of the 2022 WHO classification of thyroid neoplasms. *Endocr Pathol*. (2022) 33:27–63. doi: 10.1007/s12022-022-09707-3

4. Zhang Y, Lu Yy, Li W, Zhao Jh, Zhang Y, He Hy, et al. Lymphatic contrast-enhanced US to improve the diagnosis of cervical lymph node metastasis from thyroid cancer. *Radiology*. (2023) 307:e221265. doi: 10.1148/radiol.221265

5. Kim SK, Woo JW, Park I, Lee JH, Choe JH, Kim JH, et al. Computed tomography-detected central lymph node metastasis in ultrasonography node-negative papillary thyroid carcinoma: is it really significant? *Ann Surg Oncol*. (2017) 24:442–9. doi: 10.1245/s10434-016-5552-1

6. Ito Y, Masuoka H, Fukushima M, Inoue H, Kihara M, Tomoda C, et al. Excellent prognosis of patients with solitary T1N0M0 papillary thyroid carcinoma who underwent thyroidectomy and elective lymph node dissection without radioiodine therapy. *World J Surg*. (2010) 34:1285–90. doi: 10.1007/s00268-009-0356-0

7. Viola D, Materazzi G, Valerio L, Molinaro E, Agate L, Faviana P, et al. Prophylactic central compartment lymph node dissection in papillary thyroid carcinoma: clinical implications derived from the first prospective randomized controlled single institution study. *J Clin Endocrinol Metab*. (2015) 100:1316–24. doi: 10.1210/jc.2014-3825

8. Ito Y, Higashiyama T, Takamura Y, Miya A, Kobayashi K, Matsuzuka F, et al. Risk factors for recurrence to the lymph node in papillary thyroid carcinoma patients without preoperatively detectable lateral node metastasis: validity of prophylactic modified radical neck dissection. *World J Surg*. (2007) 31:2085–91. doi: 10.1007/s00268-007-9224-y

9. jun ZW, Luo H, mei ZY, yu DW, qiang ZJ. Evaluating the effectiveness of prophylactic central neck dissection with total thyroidectomy for cN0 papillary thyroid

carcinoma: An updated meta-analysis. *Eur J Surg Oncol*. (2017) 43:1989–2000. doi: 10.1016/j.ejso.2017.07.008

10. Yang F, Zhong Q, Huang Z, Lian M, Fang J. Survival in papillary thyroid microcarcinoma: A comparative analysis between the 7th and 8th versions of the AJCC/UICC staging system based on the SEER database. *Front Endocrinol*. (2019) 10:10. doi: 10.3389/fendo.2019.00010

11. Jin WX, Ye DR, Sun YH, Zhou XF, Wang OC, Zhang XH, et al. Prediction of central lymph node metastasis in papillary thyroid microcarcinoma according to clinicopathologic factors and thyroid nodule sonographic features: a case-control study. *CMAR*. (2018) 10:3237–43. doi: 10.2147/CMAR.S169741

12. Arora N, Turbendian HK, Kato MA, Moo TA, Zarnegar R, Fahey TJ. Papillary thyroid carcinoma and microcarcinoma: is there a need to distinguish the two? *Thyroid*. (2009) 19:473–7. doi: 10.1089/thy.2008.0185

13. Park YJ, Kim YA, Lee YJ, Kim SH, Park SY, Kim KW, et al. Papillary microcarcinoma in comparison with larger papillary thyroid carcinoma in BRAF ^{V600E} mutation, clinicopathological features, and immunohistochemical findings. *Head Neck*. (2010) 32:38–45. doi: 10.1002/hed.21142

14. Ghossein R, Ganly I, Biagini A, Robenshtok E, Rivera M, Tuttle RM. Prognostic factors in papillary microcarcinoma with emphasis on histologic subtyping: A clinicopathologic study of 148 cases. *Thyroid*. (2014) 24:245–53. doi: 10.1089/thy.2012.0645

15. Piana S, Ragazzi M, Tallini G, De Biase D, Ciarrocchi A, Frasoldati A, et al. Papillary thyroid microcarcinoma with fatal outcome: evidence of tumor progression in lymph node metastases. *Hum Pathology*. (2013) 44:556–65. doi: 10.1016/j.humpath.2012.06.019

16. Li F, Chen G, Sheng C, Gusdon AM, Huang Y, Lv Z, et al. BRAFV600E mutation in papillary thyroid microcarcinoma: a meta-analysis. *Endocrine-Related Cancer*. (2015) 22:159–68. doi: 10.1530/ERC-14-0531

17. Barbaro D, Incensati RM, Materazzi G, Boni G, Grosso M, Panicucci E, et al. The BRAF V600E mutation in papillary thyroid cancer with positive or suspected pre-surgical cytological finding is not associated with advanced stages or worse prognosis. *Endocrine*. (2014) 45:462–8. doi: 10.1007/s12020-013-0029-5

18. Yang F, Lian M, Ma H, Feng L, Shen X, Chen J, et al. Identification of key genes associated with papillary thyroid microcarcinoma characteristics by integrating transcriptome sequencing and weighted gene co-expression network analysis. *Gene*. (2022) 811:146086. doi: 10.1016/j.gene.2021.146086

19. Kim M, Kwon CH, Jang MH, Kim JM, Kim EH, Jeon YK, et al. Whole-exome sequencing in papillary microcarcinoma: potential early biomarkers of lateral lymph node metastasis. *Endocrinol Metab*. (2021) 36:1086–94. doi: 10.3803/EnM.2021.1132

20. Perera D, Ghossein R, Camacho N, Senbabaoglu Y, Seshan V, Li J, et al. Genomic and transcriptomic characterization of papillary microcarcinomas with lateral neck lymph node metastases. *J Clin Endocrinol Metab*. (2019) 104:4889–99. doi: 10.1210/jc.2019-00431

21. Song YS, Kang BH, Lee S, Yoo SK, Choi YS, Park J, et al. Genomic and transcriptomic characteristics according to size of papillary thyroid microcarcinoma. *Cancers*. (2020) 12:1345. doi: 10.3390/cancers12051345

22. Stenina-Adognravi O, Plow EF. Thrombospondin-4 in tissue remodeling. *Matrix Biol*. (2019) 75–76:300–13. doi: 10.1016/j.matbio.2017.11.006

23. Muppala S, Xiao R, Krukovets I, Verbovetsky D, Yendamuri R, Habib N, et al. Thrombospondin-4 mediates TGF-β-induced angiogenesis. *Oncogene*. (2017) 36:5189–98. doi: 10.1038/onc.2017.140

24. Frolova EG, Sopko N, Blech L, Popović ZB, Li J, Vasanji A, et al. Thrombospondin-4 regulates fibrosis and remodeling of the myocardium in response to pressure overload. *FASEB J*. (2012) 26:2363–73. doi: 10.1096/fj.11-190728

25. Chou K, Chang A, Ho C, Tsai T, Chen H, Chen P, et al. Thrombospondin-4 promotes bladder cancer cell migration and invasion via MMP2 production. *J Cell Mol Med*. (2021) 25:6046–55. doi: 10.1111/jcmm.v25.13

26. Guo D, Zhang D, Ren M, Lu G, Zhang X, He S, et al. THBS4 promotes HCC progression by regulating ITGB1 via FAK/PI3K/AKT pathway. *FASEB J*. (2020) 34:10668–81. doi: 10.1096/fj.202000043R

27. Shi Y, Sun L, Zhang R, Hu Y, Wu Y, Dong X, et al. Thrombospondin 4/integrin α2/HSF1 axis promotes proliferation and cancer stem-like traits of gallbladder cancer by enhancing reciprocal crosstalk between cancer-associated fibroblasts and tumor cells. *J Exp Clin Cancer Res*. (2021) 40:14. doi: 10.1186/s13046-020-01812-7

28. Chen X, Huang Y, Wang Y, Wu Q, Hong S, Huang Z. THBS4 predicts poor outcomes and promotes proliferation and metastasis in gastric cancer. *J Physiol Biochem*. (2019) 75:117–23. doi: 10.1007/s13105-019-00665-9

29. Förster S, Gretschel S, Jöns T, Yashiro M, Kemmner W. THBS4, a novel stromal molecule of diffuse-type gastric adenocarcinomas, identified by transcriptome-wide expression profiling. *Modern Pathology*. (2011) 24:1390–403. doi: 10.1038/modpathol.2011.99

30. Bolger AM, Lohse M, Usadel B. Trimmomatic: a flexible trimmer for Illumina sequence data. *Bioinformatics*. (2014) 30(15):2114–20. doi: 10.1093/bioinformatics/btu170

31. Dobin A, Davis CA, Schlesinger F, Drenkow J, Zaleski C, Jha S, et al. STAR: ultrafast universal RNA-seq aligner. *Bioinformatics*. (2013) 29(1):15–21. doi: 10.1093/bioinformatics/bts635

32. Li B, Dewey CN. RSEM: accurate transcript quantification from RNA-Seq data with or without a reference genome. *BMC Bioinf*. (2011) 12:323. doi: 10.1186/1471-2105-12-323

33. Love MI, Huber W, Anders S. Moderated estimation of fold change and dispersion for RNA-seq data with DESeq2. *Genome Biol*. (2014) 15:550. doi: 10.1186/s13059-014-0550-8

34. Robinson MD, McCarthy DJ, Smyth GK. edgeR: a Bioconductor package for differential expression analysis of digital gene expression data. *Bioinformatics*. (2010) 26:139–40. doi: 10.1093/bioinformatics/btp616

35. Yu G, Wang LG, Han Y, He QY. clusterProfiler: an R package for comparing biological themes among gene clusters. *OMICS: A J Integr Biol*. (2012) 16:284–7. doi: 10.1089/omi.2011.0118

36. Sturm G, Finotello F, List M. Immunedeconv: an R package for unified access to computational methods for estimating immune cell fractions from bulk RNA-sequencing data, in: *Bioinformatics for cancer immunotherapy* (2020). New York, NY: Springer US (Accessed May 2, 2024). Methods in Molecular Biology; vol. 2120.

37. Aran D, Hu Z, Butte AJ. xCell: digitally portraying the tissue cellular heterogeneity landscape. *Genome Biol*. (2017) 18:220. doi: 10.1186/s13059-017-1349-1

38. Liu J, Lichtenberg T, Hoadley KA, Poisson LM, Lazar AJ, Cherniack AD, et al. An integrated TCGA pan-cancer clinical data resource to drive high-quality survival outcome analytics. *Cell*. (2018) 173:400–416.e11. doi: 10.1016/j.cell.2018.02.052

39. Kim MS, Choi HS, Wu M, Myung J, Kim EJ, Kim YS, et al. Potential role of PDGFRβ-associated THBS4 in colorectal cancer development. *Cancers*. (2020) 12:2533. doi: 10.3390/cancers12092533

40. Kennel KB, Bozlar M, De Valk AF, Greten FR. Cancer-associated fibroblasts in inflammation and antitumor immunity. *Clin Cancer Res*. (2023) 29:1009–16. doi: 10.1158/1078-0432.CCR-22-1031

41. Chen Z, Zhou L, Liu L, Hou Y, Xiong M, Yang Y, et al. Single-cell RNA sequencing highlights the role of inflammatory cancer-associated fibroblasts in bladder urothelial carcinoma. *Nat Commun*. (2020) 11:5077. doi: 10.1038/s41467-020-18916-5

42. Li X, Sun Z, Peng G, Xiao Y, Guo J, Wu B, et al. Single-cell RNA sequencing reveals a pro-invasive cancer-associated fibroblast subgroup associated with poor clinical outcomes in patients with gastric cancer. *Theranostics*. (2022) 12:620–38. doi: 10.7150/thno.60540

43. Yan T, Qiu W, Weng H, Fan Y, Zhou G, Yang Z. Single-cell transcriptomic analysis of ecosystems in papillary thyroid carcinoma progression. *Front Endocrinol*. (2021) 12:729565. doi: 10.3389/fendo.2021.729565

44. Pu W, Shi X, Yu P, Zhang M, Liu Z, Tan L, et al. Single-cell transcriptomic analysis of the tumor ecosystems underlying initiation and progression of papillary thyroid carcinoma. *Nat Commun*. (2021) 12:6058. doi: 10.1038/s41467-021-26343-3

45. Isella C, Terrasi A, Bellomo SE, Petti C, Galatola G, Muratore A, et al. Stromal contribution to the colorectal cancer transcriptome. *Nat Genet*. (2015) 47:312–9. doi: 10.1038/ng.3224

46. Chen Q, Liu Y, Jeong HW, Stehling M, Dinh VV, Zhou B, et al. Apelin+ Endothelial niche cells control hematopoiesis and mediate vascular regeneration after myeloablative injury. *Cell Stem Cell*. (2019) 25:768–783.e6. doi: 10.1016/j.stem.2019.10.006

47. Okamoto J, Hirata T, Chen Z, Zhou HM, Mikami I, Li H, et al. EMX2 is epigenetically silenced and suppresses growth in human lung cancer. *Oncogene*. (2010) 29:5969–75. doi: 10.1038/onc.2010.330

48. Wang L, Jin J, Zhou Y, Tian Z, He B, Huang Y, et al. EMX2 is epigenetically silenced and suppresses epithelial–mesenchymal transition in human esophageal adenocarcinoma. *Oncol Rep*. (2019) 29(44):5969–75. doi: 10.3892/or.2019.7284

49. Zhan K, Yang X, Li S, Bai Y. Correlation of endoplasmic reticulum stress patterns with the immune microenvironment in hepatocellular carcinoma: a prognostic signature analysis. *Front Immunol*. (2023) 14:1270774. doi: 10.3389/fimmu.2023.1270774

50. Qi L, Chen J, Zhou B, Xu K, Wang K, Fang Z, et al. HomeoboxC6 promotes metastasis by orchestrating the DKK1/Wnt/β-catenin axis in right-sided colon cancer. *Cell Death Dis*. (2021) 12:337. doi: 10.1038/s41419-021-03630-x

51. Ren S, Wu D, Shen X, Wu Q, Li C, Xiong H, et al. Deciphering the role of extrachromosomal circular DNA in adipose stem cells from old and young donors. *Stem Cell Res Ther*. (2023) 14:341. doi: 10.1186/s13287-023-03575-2

52. He S, Arikin A, Chen J, Huang T, Wu Z, Wang L, et al. Transcriptome analysis identified 2 new lncRNAs associated with the metastasis of papillary thyroid carcinoma. *ORL*. (2022) 84:247–54. doi: 10.1159/000518085

53. Yang W, Bai C, Zhang L, Li Z, Tian Y, Yang Z, et al. Correlation between serum circRNA and thyroid micropapillary carcinoma with cervical lymph node metastasis. *Medicine*. (2020) 99:e23255. doi: 10.1097/MD.0000000000023255

54. Lee S, Bae JS, Jung CK, Chung WY. Extensive lymphatic spread of papillary thyroid microcarcinoma is associated with an increase in expression of genes involved in epithelial-mesenchymal transition and cancer stem cell-like properties. *Cancer Med*. (2019) 8:6528–37. doi: 10.1002/cam4.v8.15

55. Li Q, Feng T, Zhu T, Zhang W, Qian Y, Zhang H, et al. Multi-omics profiling of papillary thyroid microcarcinoma reveals different somatic mutations and a unique transcriptomic signature. *J Transl Med*. (2023) 21:206. doi: 10.1186/s12967-023-04045-2

56. Frolova EG, Drazba J, Krukovets I, Kostenko V, Blech L, Harry C, et al. Control of organization and function of muscle and tendon by thrombospondin-4. *Matrix Biol.* (2014) 37:35–48. doi: 10.1016/j.matbio.2014.02.003

57. Gabrielsen A, Lawler PR, Yongzhong W, Steinbrüchel D, Blagoja D, Paulsson-Berne G, et al. Gene expression signals involved in ischemic injury, extracellular matrix composition and fibrosis defined by global mRNA profiling of the human left ventricular myocardium. *J Mol Cell Cardiol.* (2007) 42:870–83. doi: 10.1016/j.yjmcc.2006.12.016

58. Vanhoutte D, Schips TG, Kwong JQ, Davis J, Tjondrokoesoemo A, Brody MJ, et al. Thrombospondin expression in myofibers stabilizes muscle membranes. *eLife.* (2016) 5:e17589. doi: 10.7554/eLife.17589

59. Liu J, Cheng G, Yang H, Deng X, Qin C, Hua L, et al. Reciprocal regulation of long noncoding RNAs THBS4-003 and THBS4 control migration and invasion in prostate cancer cell lines. *Mol Med Rep.* (2016) 14:1451–8. doi: 10.3892/mmr.2016.5443

60. Greco SA, Chia J, Inglis KJ, Cozzi SJ, Ramsnes I, Buttenshaw RL, et al. Thrombospondin-4 is a putative tumour-suppressor gene in colorectal cancer that exhibits age-related methylation. *BMC Cancer.* (2010) 10:494. doi: 10.1186/1471-2407-10-494

61. Fuyuhiro Y, Yashiro M, Noda S, Kashiwagi S, Matsuoka J, Doi Y, et al. Upregulation of cancer-associated myofibroblasts by TGF-β from scirrhous gastric carcinoma cells. *Br J Cancer.* (2011) 105:996–1001. doi: 10.1038/bjc.2011.330

62. Muppala S, Xiao R, Gajeton J, Krukovets I, Verbovetskiy D, Stenina-Adognravi O. Thrombospondin-4 mediates hyperglycemia- and TGF -beta-induced inflammation in breast cancer. *Int J Cancer.* (2021) 148:2010–22. doi: 10.1002/ijc.33439

63. Bagaev A, Kotlov N, Nomie K, Svekolkin V, Gafurov A, Isaeva O, et al. Conserved pan-cancer microenvironment subtypes predict response to immunotherapy. *Cancer Cell.* (2021) 39:845–865.e7. doi: 10.1016/j.ccell.2021.04.014

64. Yang Z, Wei X, Pan Y, Xu J, Si Y, Min Z, et al. A new risk factor indicator for papillary thyroid cancer based on immune infiltration. *Cell Death Dis.* (2021) 12:51. doi: 10.1038/s41419-020-03294-z

65. Minna E, Brich S, Todoerti K, Pilotti S, Collini P, Bonaldi E, et al. Cancer associated fibroblasts and senescent thyroid cells in the invasive front of thyroid carcinoma. *Cancers.* (2020) 12:112. doi: 10.3390/cancers12010112

66. Tsoumakidou M. The advent of immune stimulating CAFs in cancer. *Nat Rev Cancer.* (2023) 23:258–69. doi: 10.1038/s41568-023-00549-7

67. Chen Y, McAndrews KM, Kalluri R. Clinical and therapeutic relevance of cancer-associated fibroblasts. *Nat Rev Clin Oncol.* (2021) 18:792–804. doi: 10.1038/s41571-021-00546-5

68. Chen X, Song E. Turning foes to friends: targeting cancer-associated fibroblasts. *Nat Rev Drug Discovery.* (2019) 18:99–115. doi: 10.1038/s41573-018-0004-1

69. Hanahan D. Hallmarks of cancer: new dimensions. *Cancer Discovery.* (2022) 12:31–46. doi: 10.1158/2159-8290.CD-21-1059

70. Sahai E, Astsaturov I, Cukierman E, DeNardo DG, Egeblad M, Evans RM, et al. A framework for advancing our understanding of cancer-associated fibroblasts. *Nat Rev Cancer.* (2020) 20:174–86. doi: 10.1038/s41568-019-0238-1

71. Woo CG, Sung CO, Choi YM, Kim WG, Kim TY, Shong YK, et al. Clinicopathological significance of minimal extrathyroid extension in solitary papillary thyroid carcinomas. *Ann Surg Oncol.* (2015) 22:728–33. doi: 10.1245/s10434-015-4659-0

frontiers | Frontiers in Oncology

TYPE Original Research
PUBLISHED 04 June 2025
DOI 10.3389/fonc.2025.1535966

OPEN ACCESS

EDITED BY
Cesar Seigi Fuziwara,
University of São Paulo, Brazil

REVIEWED BY
Vladimir A. Saenko,
Nagasaki University, Japan
Fernando Di Fermo,
Sanatorio Otamendi, Argentina
Fernando Carrizo,
Instituto de Oncología Ángel H. Roffo, Argentina

*CORRESPONDENCE
Cheng Xiang
chengxiang@zju.edu.cn

RECEIVED 28 November 2024
ACCEPTED 20 May 2025
PUBLISHED 04 June 2025

CITATION
Liu X, Zhu Q-l, He Z-y, Shu J-d and Xiang C (2025) Identification of risk factors for high-risk dedifferentiation in papillary thyroid carcinoma and construction of discriminative model. *Front. Oncol.* 15:1535966. doi: 10.3389/fonc.2025.1535966

Identification of risk factors for high-risk dedifferentiation in papillary thyroid carcinoma and construction of discriminative model

Xiang Liu[1], Qiao-li Zhu[1], Zi-yi He[1], Jing-de Shu[1] and Cheng Xiang[2]*

[1]Department of Breast and Thyroid Surgery, The Quzhou Affiliated Hospital of Wenzhou Medical University, Quzhou People's Hospital, Quzhou, Zhejiang, China, [2]Department of Thyroid Surgery, The Second Affiliated Hospital of Zhejiang University College of Medicine, Hangzhou, Zhejiang, China

Objective: We initially found that the thyroid differentiation score (TDS) was associated with the prognosis of papillary thyroid carcinoma (PTC) patients. Therefore, this study aimed to investigate the influencing factors and construct a discriminative model of high-risk dedifferentiation, and to explore the possible mechanisms.

Methods: Data were sourced from the TCGA database. The influences of the TDS, tumor mutation burden, and immune score on the progression-free interval (PFI) were assessed by the Kaplan-Meier method and multivariable Cox regression. Then, logistic regression analyses were utilized to explore the factors of dedifferentiation and a nomogram model was conducted. Additionally, differentially expressed genes (DEGs) were identified using *RNA* sequencing data, while their regulatory pathways were determined by the Kyoto Encyclopedia of Genes and Genomes (KEGG) analysis. Finally, the differential expression of key genes of major pathways was explored.

Results: This study included 391 PTC patients. After analyzing the influences of the three indicators on survival, only TDS showed an association with PFI. Multivariable logistic analysis revealed that the disease duration and PTC subtypes influenced dedifferentiation. The nomogram model based on these two variables showed improved discriminative capability. The study identified 17 overlapping DEGs associated with the dedifferentiation and three primary enrichment pathways, with complement and coagulation cascade pathways being the most significant ($P<0.001$). The central gene was *CD55*, which showed high expression in high-risk dedifferentiated and tall cell PTC, and the expression level increased as the disease progressed.

Conclusion: This research may contribute to promising identifying high-risk dedifferentiated PTC and also provide a potential therapeutic target.

KEYWORDS

thyroid differentiation score, papillary thyroid carcinoma, dedifferentiation, differentially expressed genes, CD55

1 Introduction

Thyroid cancer (THCA) is the most prevalent endocrine system malignancy, with 821,000 new cases worldwide in 2022, accounting for 4.1% of all new cancer cases globally and ranking 7th among malignant tumors (1, 2). Papillary thyroid carcinoma (PTC) is the most common subtype of THCA, accounting for approximately 80%-90% of all cases (3). PTC originates from follicular epithelium (4). It includes more than ten subtypes, such as classical/usual PTC, infiltrating follicular PTC, tall cell PTC (TCPTC), and columnar cell PTC (5). PTC is highly differentiated and prone to regional lymph node metastasis at an early stage, with low local infiltration and recurrence rate, resulting in a better prognosis. The 5-year survival rates of PTC range from 83% to 98%, while well-differentiated classic PTC has a 10-year survival rate of up to 97% (6, 7). However, some PTC subtypes may undergo dedifferentiation, making the tumor cells more aggressive and losing iodide uptake capacity, then leading to increased disease progression and mortality (8–10). Compared to identifying dedifferentiation through histopathology alone, the thyroid differentiation score (TDS) integrates the *mRNA* expression levels of 16 genes associated with thyroid metabolism and function, providing a more consistent method for identifying dedifferentiation (11, 12).

With the advancements in immuno-oncology, immune checkpoint inhibitor (ICI) therapies have revolutionized cancer treatment. However, these groundbreaking therapies also have side effects (13). Tumor mutation burden (TMB), as an emerging biomarker, is considered to be a promising predictor of response to ICI therapy (14). Research has demonstrated that elevated TMB is associated with the response to ICI in several types of tumors. For example, in non-small cell lung cancer, high TMB is linked to significantly improved progression-free interval (PFI) in patients receiving combined Nivolumab and Ipilimumab treatment (15). Similarly, increased TMB is associated with improved survival rates in head and neck cancer and bladder cancer patients undergoing ICI therapy (16).

The tumor immune microenvironment (TIME) plays a crucial role in cancer progression and influences treatment outcomes and prognosis (17). In TIME, the key cluster cells that are most likely to influence clinical outcomes of THCA may be immune cells (18). Currently, immune scores can be obtained using multiple computer algorithms such as Cibersort, Timer, and ImmuCellAI, which can assess immune cell infiltration by *RNA-seq* expression data (19–21). PTC immune infiltrating cells such as dendritic cells, biased M2 phenotype tumor-associated macrophages, and mast cells are associated with tumor differentiation or anti-tumor immune responses (22–24). Several studies have investigated the relationship between known differentially expressed genes (DEGs) in PTC, TIME, and prognosis (25–27). However, these studies did not include currently unproven immune-related genes or prognostic genes that were not differentially expressed in the analysis. In addition, models that incorporate multiple genes limit the feasibility of their clinical application. To address these limitations, this study employed the ESTIMATE algorithm to calculate immune scores for PTC cases.

Dedifferentiation, gene mutation, and immune microenvironment significantly impact the biological behavior and clinical prognosis of PTC. In this study, we initially explored the effects of these three markers on PFI in PTC patients, revealing that only TDS influenced prognosis. Subsequently, the influencing factors and mechanisms were explored for TDS to guide intervention strategies.

2 Materials and methods

2.1 Data acquisition and preprocessing

The transcriptome data and clinical information data of the PTC patients were from the Cancer Genome Atlas (TCGA) genome database (https://portal.gdc.cancer.gov/). PTC samples in the TCGA database were collected and sequenced primarily between 2010 and 2015. We obtained 507 PTC patients' data, and 391 of them with complete TDS, TMB, and immune scores data were analyzed. Perl version 5.24.3 software was utilized to transform original *RNA* sequencing data into an RNA expression matrix.

2.2 Calculation of immune score, TDS, and TMB in PTC patients

ESTIMATE, a computerized algorithm, can infer the level of stromal and immune cell infiltration in tumor tissue based on expression profiles (28). The immune score of the immune microenvironment in PTC patients was calculated by the ESTIMATE algorithm.

TDS encompasses the expression levels of 16 thyroid metabolic and functional *mRNAs* (12). The $\log_2$ normalized RSEM values were first centered on the median of each sample to derive the $\log_2$ (fold-change) (FC), and then the TDS of each tumor tissue was obtained by summing the 16 genes of each sample. The calculation formula was as follows: TDS = $\log_2$ (FC) average of 16 genes (29, 30). The genes involved were *DIO1*, *DIO2*, *DUOX1*, *DUOX2*, *FOXE1*, *GLIS3*, *NKX2-1*, *PAX8*, *SLC26A4*, *SLC5A5*, *SLC5A8*, *TG*, *THRA*, *THRB*, *TPO*, and *TSHR*.

TMB was defined as the number of somatic, coding, base substitution, and insertion-deletion variants per megabase (Mb) of the examined target genomic region (14). The formula was calculated as follows: sample TMB = number of mutations/exon region size (31). The TMB distribution for patients was directly acquired from the TCGA database.

2.3 Key indicators identification

We first explored the influence of immune score, TDS, and TMB on the survival outcome of PTC patients by Kaplan-Meier (KM) method and log-rank test. Due to the long overall survival and tumor-specific survival of PTC patients, this study collected limited mortality data. PFI was used as the survival indicator. PFI is defined as the time interval between the date of diagnosis of the disease and the occurrence of a new tumor event, including disease progression, local recurrence, distant metastasis, the new primary tumor, or death from a tumor (32). In the KM analysis, all the patients were divided into high and low groups according to the optimal cut-off value and median of TDS, TMB, and immune scores. The optimal cut-off value is the minimum *P*-value cut-off for univariable Cox analysis when PFI is the primary endpoint and is obtained from the R software package "survminer". We then performed a Cox regression analysis to assess their association with PFI. The factor of PFI was regarded as the key indicator.

2.4 Definition of high/low-risk dedifferentiation

In this study, only TDS showed an association with PFI, thus becoming the research topic in the subsequent analysis. The 391 PTC patients were grouped by the optimal cut-off value (-0.303) of the TDS score. The low-differentiation score group (TDS≤-0.303) was defined as high-risk dedifferentiation, while the high-differentiation score group (TDS>-0.303) was designated as low-risk dedifferentiation. We then compared the baseline data between high and low-risk dedifferentiation groups.

2.5 Collected baseline variables

Relevant variables collected in this study were related to: demographic characteristics (age, sex, race), tumor-related clinical variables (disease duration, tumor size, TNM stage, PTC subtypes, stage, site, and focus type of primary lesions, lymph node preoperative assessment diagnostic imaging type, medical history of the thyroid gland disorder, radiation therapy and response to therapy, postoperative tumor residue after resection) and follow-up (follow-up after radiation treatment, PTC status after initial treatment).

The disease duration was defined as the time interval between initial diagnosis and completion of the TCGA program. Tumors with ≥99% of follicular structures were considered to be follicular variant PTC, and those with tall cells content ≥50% were defined as TCPTC. It has been noted that stage 1 and 2 tumors remain confined to the thyroid gland and have not yet spread to the central compartment of the lymph nodes; in stages 3 and 4, the cancer spreads to the lymph nodes, including other organs (33). Therefore, we combined stage 1 and 2 samples as early-stage samples and stage 3 and 4 samples as advanced-stage samples. Preoperative lymph node imaging was categorized as ultrasound-only or other. The other included computed tomography (CT)-only, magnetic resonance imaging (MRI)-only, or combinations. Response to radiotherapy was classified as complete response or other, with other conditions including partial response, stable disease, and radiographic progressive disease. Residual tumors after resection were categorized as absent or present. Complete resection of the tumor was defined as no tumor residue, resection with residue under a microscope and residue visible to the naked eye was classified as having residue. In the follow-up results, the status of PTC after initial treatment included both no imaging evidence of disease and disease persistence. Disease persistence included persistent locoregional disease and persistent distant metastases. In spite some samples had missing data, which are clinically valuable and worth analyzing, they were retained for baseline and/or subsequent analyses.

2.6 Influencing factors and model construction of high-risk dedifferentiation

After baseline comparison, we conducted a logistic regression analysis to explore the key factors and established a nomogram model for predicting the high-risk dedifferentiation. The performance of the nomogram model was then evaluated by several analyses. The detailed information is shown in the following Statistical analysis section.

2.7 Potential mechanism exploration associated with dedifferentiation

The *RNA-seq* expression data of PTC patients were normalized using the $\log_2$ (X+1) method. Supplementary Table S1 displays the normalized data of 16 TDS-related genes and CD55. The "Limma" package in R software was used to detect the differentially expressed genes (DEGs) between the high-risk dedifferentiation group and the low-risk differentiation group (DEG1), as well as high and low nomogram score groups (DEG2), based on the threshold of

adjusted *P*-value < 0.05 and $|\log_2 (FC)| > 1$. Gene expression volcano plots were created with Graphpad Prism 8. Overlapping genes between DEG1 and DEG2 were identified using Venn diagrams (bioinformatics.psb.ugent.be/webtools/Venn/). Kyoto Encyclopedia of Genes and Genomes (KEGG) enrichment analysis was performed to determine the pathways associated with the overlapping genes and identify genes in major pathways. Finally, the expression levels of key genes involved in the major pathways were analyzed for differences between PTC subtypes and dedifferentiation risk groups, and the correlation between gene expression level and disease duration was also assessed.

2.8 Statistical analysis

Continuous variables with non-normal distribution were characterized by medians and quartiles (P25, P75), and the differences between high and low-risk dedifferentiation groups were compared using the Wilcoxon-Mann-Whitney test. Categorical variables were presented as frequencies (n) and proportions (%) and then compared by the Chi-square test/Fisher exact test. Variables that were statistically different from baseline comparisons were included in logistic regression analyses to explore the factors influencing high-risk dedifferentiation in PTC patients. Collinearity analysis was performed due to the joint confirmation of tumor staging by T, N, and M staging indicators, and the potential for interactions among other indicators. Collinearity was considered present when the variance inflation factor (VIF) exceeded 10.

Based on the results of multivariable logistic regression, a model for high-risk dedifferentiation was constructed using the nomogram method. Receiver operating characteristic analysis (ROC) was used to evaluate the performance of the key factors in predicting high-risk dedifferentiation using "pROC" packages, while decision curve analysis (DCA) based on "rmda" packages was used to assess the net clinical benefit of the model. In addition, based on the "dplyr" and "Hmisc" packages in the R software, integrated discrimination improvement (IDI) analysis and net reclassification improvement (NRI) analysis were conducted to explore the improvement in the performance of the models compared to the individual influences. Restricted cubic spline (RCS) analysis via "rms" packages was utilized to explore the association of nomogram score and dedifferentiation. These analyses were performed using R software (version 4.4.1), with statistical significance set at $P < 0.05$.

3 Results

3.1 The influence of three biomarkers on PFI

The influence of three tumor biomarkers including TDS, TMB, and immune scores on PFI was analyzed in 391 PTC patients. All patients were divided into high and low-score groups according to the optimal cut-off value and median of TDS, TMB, and immune scores. For the TDS score, the high-differentiated group had a better prognosis compared to the low-differentiated group ($P<0.05$) (Figures 1A, B). Regarding TMB, groups with high mutation burden showed worse prognosis compared to the low mutation burden group ($P<0.001$) (Figures 1C, D). Immune score showed no significant influence on prognosis ($P>0.05$) (Figures 1E, F). The results of multivariable Cox regression analysis revealed that on both continuous and dichotomous TDS, TMB, and immune scores categorized by the optimal cut-off value, only TDS remained an influencing factor of PFI after adjusted age, sex, and race (Table 1). Due to the association between TDS and PFI, therefore the differentiation status of PTC patients became the topic of our next analysis.

3.2 Baseline characteristics of high/low-risk dedifferentiation groups

Table 2 demonstrates the differences in baseline data between the high/low-risk dedifferentiation groups. The median age of 391 PTC patients was 46.000 (34.000,58.000). The majority were non-Hispanic (90.064%), with a lower proportion in the high-risk group compared to the low-risk group (86.250% vs. 94.079%, $P=0.021$). Among the continuous variables, disease duration, tumor length, tumor width, number of examined lymph nodes, and number of positive lymph nodes were higher in the high-risk group than the low-risk group (all $P<0.05$). Among the categorical variables, 28.302% of patients in the high-risk group had a medical history of thyroid gland disorder, lower than the low-risk group (44.643%) ($P=0.006$). The percentage of patients with classic/usual PTC was higher in the high-risk group than in the low-risk group (82.065% vs 60.099%) ($P<0.001$). T3 stage, T4 stage, N1 stage, advanced stage, follow-up after radiation treatment, and residual tumor were more prevalent in the high-risk group than in the low-risk group (all $P<0.05$).

3.3 The influencing factors of high-risk dedifferentiation

Collinearity analysis of the 13 significantly different variables revealed no collinearity (all VIF<10) (Supplementary Table S2). The 13 variables were included in the logistic regression analysis. The results of univariable logistic regression showed that except for the number of examined lymph nodes, the other 12 variables were related to dedifferentiation (all $P<0.05$). Further multivariable logistic analysis containing all variables showed that only disease duration and PTC subtypes were influential factors for high-risk dedifferentiated PTC. Follicular variant PTC was a protective factor for high-risk dedifferentiation (OR=0.207, 95%CI: 0.035-0.872) and tall cell PTC was a risk factor for it (OR=8.035, 95%CI: 1.389-72.04). Longer disease duration increased the likelihood of dedifferentiation (OR=1.192, 95%CI: 1.018-1.427) (all $P<0.05$) (Table 3). Further analysis revealed that TCPTC had the lowest TDS, and TDS decreased with increasing disease duration (Figures 2A, B).

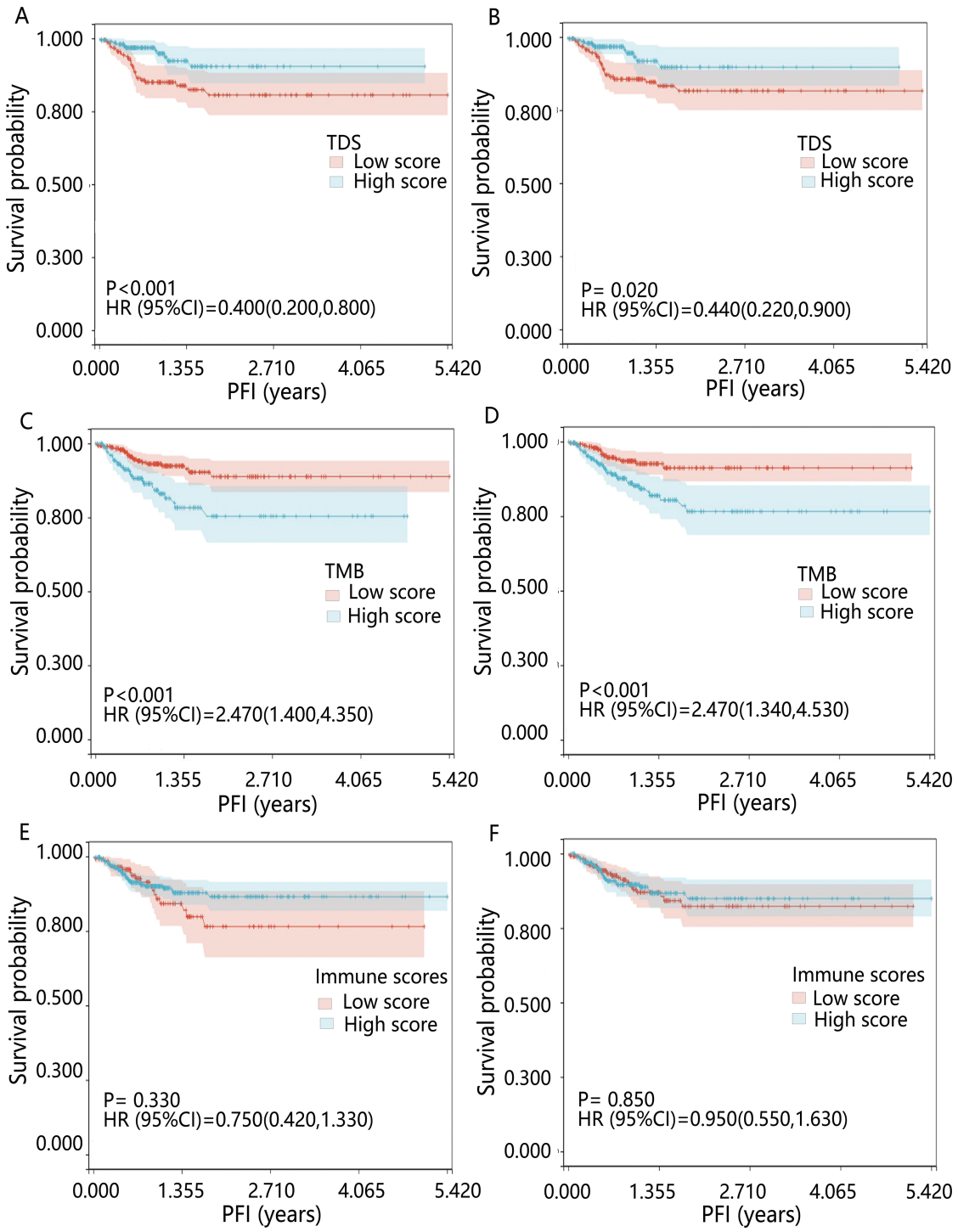

FIGURE 1
Kaplan-Meier survival curves for PFI across various biomarkers. Patients were grouped by **(A)** optimal cut-off value of TDS; **(B)** median TDS; **(C)** optimal cut-off value of TMB; **(D)** median TMB; **(E)** optimal cut-off value of immune scores; **(F)** median immune scores. HR was derived from the results of the univariable Cox regression analysis.

3.4 Nomogram model construction and performance evaluation

Based on the multivariable logistic regression results, the nomogram model was constructed based on disease duration and PTC subtypes. Meanwhile, the calibration curve of the nomogram model was plotted, demonstrating good calibration (Figures 3A, B). The performance of disease duration and PTC subtypes as well as the nomogram model in predicting high-risk dedifferentiation was further evaluated by ROC analysis (Table 4, Figure 3C). Results indicated that PTC subtypes had the highest specificity (0.821), while the nomogram model exhibited the highest AUC (0.740),

TABLE 1 Results of multivariable Cox analysis of the influences of TDS, TMB and immune scores on PFI in PTC patients.

Variables	HR	95%CI	*P*-value
COX model 1			
Age	1.018	0.997-1.039	0.093
Gender	0.770	0.372-1.594	0.481
Race	0.644	0.190-2.183	0.480
TDS as continuous variable	0.691	0.506-0.945	0.021
TMB as continuous variable	1.285	0.875-1.888	0.201
Immune score as continuous variable	1.000	1.000-1.000	0.179
COX model 2			
Age	1.012	0.989,1.035	0.314
Gender	0.763	0.370,1.573	0.463
Race	0.636	0.191,2.117	0.461
TDS as dichotomized variable	2.480	1.186,5.185	0.016
TMB as dichotomized variable	1.615	0.779,3.344	0.197
Immune score as dichotomized variable	0.533	0.264,1.076	0.079

HR, Hazard ratio; CI, Confidence interval; TDS, Thyroid differentiation score; TMB, Tumor mutation burden.

sensitivity (0.957), Youden index (0.328), and accuracy (0.524). The Delong test revealed that the AUC value of the nomogram model was significantly higher than the AUC values for disease duration alone and PTC subtypes alone (all $P<0.001$). DCA confirmed that the nomogram model could provide a net clinical benefit, with a risk interval of 0.40-0.76 (Figure 3D). IDI analysis showed that the performance of the nomogram model was improved by 15.3% compared to single disease duration (IDI=0.153, 95%CI: 0.118-0.188, $P<0.001$) and 18.8% improvement compared to PTC subtypes (IDI=0.188, 95%CI: 0.149-0.228, $P<0.001$). NRI analysis suggested that nomogram model discriminative performance improved by 25.8% and 5.7% compared to PTC subtypes (NRI=0.258, 95%CI: 0.180-0.337) and disease duration (NRI=0.057, 95%CI: -0.039-0.169), respectively. These results indicated that the constructed nomogram model possessed good discriminative capability.

3.5 Potential mechanism associated with dedifferentiation

We next explored the potential mechanism associated with the PTC dedifferentiation. RCS analysis initially indicated a linear positive relationship between nomogram score and dedifferentiation risk (*P* for

TABLE 2 The baseline information of participants grouped by the risk of dedifferentiation.

Variables	Total (n=391)	Low risk (n=205)	High risk (n=186)	*P*-value
Age, years	391(100.000)	46.000(34.000,58.000)	47.000(34.000,58.000)	0.904
Tumor depth, cm	319(81.586)	1.500(1.000,2.000)	1.600(1.000,2.500)	0.240
Tumor length, cm	369(94.373)	2.400(1.500,3.500)	2.800(1.800,4.000)	0.016
Tumor width, cm	334(85.422)	1.900(1.200,2.700)	2.200(1.500,3.000)	0.015
Number of examined lymph nodes	297(75.959)	4.000(2.000,10.000)	7.000(3.000,17.000)	0.014
Number of positive lymph nodes	294(75.192)	0.000(0.000,3.000)	2.000(0.000,6.000)	<0.001
I-131 doses, mCi	184(47.059)	100.000(75.200,125.000)	101.000(94.600,150.000)	0.268
Disease duration, years	390(99.744)	1.000(1.000,3.000)	2.000(1.000,5.000)	<0.001
Gender, n(%)				0.715
Male	100(25.575)	54(26.341)	46(24.731)	
Female	291(74.425)	151(73.659)	140(75.269)	
Race, n(%)				0.021
Non-Hispanic	281(90.064)	143(94.079)	138(86.250)	
Hispanic	31(9.936)	9(5.921)	22(13.750)	
PTC subtypes, n(%)				<0.001
Classical/usual	273(70.543)	122(60.099)	151(82.065)	
Follicular	85(21.964)	76(37.438)	9(4.891)	
Tall cell	29(7.494)	5(2.463)	24(13.043)	
Stage, n(%)				0.002

(Continued)

TABLE 2 Continued

Variables	Total (n=391)	Low risk (n=205)	High risk (n=186)	*P*-value
Early	268(68.895)	155(75.980)	113(61.081)	
Advanced	121(31.105)	49(24.020)	72(38.919)	
T stage, n(%)				<0.001
T1	114(29.306)	73(35.784)	41(22.162)	
T2	131(33.676)	78(38.235)	53(28.649)	
T3	129(33.162)	52(25.490)	77(41.622)	
T4	15(3.856)	1(0.490)	14(7.568)	
N stage, n(%)				<0.001
N0	186(47.570)	119(58.049)	67(36.022)	
N1	205(52.430)	86(41.951)	119(63.978)	
M stage, n(%)				0.358
M0	217(55.641)	109(53.431)	108(58.065)	
M1	173(44.359)	95(46.569)	78(41.935)	
PTC status after initial treatment, n(%)				0.083
Tumor free	233(91.016)	135(93.750)	98(87.500)	
Persistent	23(8.984)	9(6.250)	14(12.500)	
Follow-up after radiation treatment, n(%)				0.010
No	136(39.306)	84(45.652)	52(32.099)	
Yes	210(60.694)	100(54.348)	110(67.901)	
Lymph node preoperative assessment diagnostic imaging type, n(%)				0.830
Ultrasound	225(78.947)	116(79.452)	109(78.417)	
Other	60(21.053)	30(20.548)	30(21.583)	
Medical history of thyroid gland disorder, n(%)				0.006
Normal	207(63.303)	93(55.357)	114(71.698)	
Nodular hyperplasia	57(17.431)	38(22.619)	19(11.950)	
Lymphocytic thyroiditis	63(19.266)	37(22.024)	26(16.352)	
Primary neoplasm focus type, n(%)				0.569
Unifocal	206(53.927)	104(52.525)	102(55.435)	
Multifocal	176(46.073)	94(47.475)	82(44.565)	
Primary site, n(%)				0.106
Left lobe	140(36.269)	68(33.333)	72(39.560)	
Right lobe	166(43.005)	98(48.039)	68(37.363)	
Bilateral and isthmus	80(20.725)	38(18.627)	42(23.077)	
Radiation, n(%)				0.057
No	55(35.714)	31(43.662)	24(28.916)	
Yes	99(64.286)	40(56.338)	59(71.084)	
Radiation response, n(%)				0.511
Complete	120(85.106)	55(87.302)	65(83.333)	

(Continued)

TABLE 2 Continued

Variables	Total (n=391)	Low risk (n=205)	High risk (n=186)	*P*-value
Other	21(14.894)	8(12.698)	13(16.667)	
Residual tumor, n(%)				0.023
Absent	306(88.696)	169(92.350)	137(84.568)	
Present	39(11.304)	14(7.650)	25(15.432)	

PTC, Papillary thyroid carcinoma.

TABLE 3 Results of logistic regression analysis of factors associating with high-risk of dedifferentiation.

Variables	Univariable analysis	Multivariable analysis
	OR(95%CI)	OR(95%CI)
Tumor length	1.168(1.025-1.332)**	0.752(0.356-1.531)
Tumor width	1.230(1.023-1.477)**	2.131(0.828-5.920)
Number of examined lymph nodes	1.011(0.996-1.027)	0.976(0.932-1.020)
Number of positive lymph nodes	1.048(1.003-1.096)**	1.071(0.940-1.242)
Disease duration, years	1.136(1.065-1.212)***	1.192(1.018-1.427)**
Race		
Non- Hispanic	Reference	Reference
Hispanic	2.533(1.127-5.694)**	2.398(0.614-11.466)
PTC subtypes		
Classical/usual	Reference	Reference
Follicular	0.096(0.046-0.199)***	0.207(0.035-0.872)**
Tall cell	3.878(1.437-10.464)**	8.035(1.389-72.04)**
T stage		
T1	Reference	Reference
T2	1.210(0.721-2.030)	0.592(0.162-2.027)
T3	2.636(1.568-4.433)***	1.511(0.368-6.093)
T4	24.927(3.163-196.456)**	3.94(0.182-146.565)
N stage		
N0	Reference	Reference
N1	2.458(1.634-3.696)***	2.199(0.749-6.585)
Stage		
Early	Reference	Reference
Advanced	2.016(1.303-3.119)**	0.381(0.099-1.309)
Follow-up after radiation treatment		
No	Reference	Reference
Yes	1.777(1.145-2.757)**	0.948(0.346-2.534)
Medical history of thyroid gland disorder		
Normal	Reference	Reference
Nodular hyperplasia	0.408(0.221-0.754)**	1.556(0.394-6.212)
Lymphocytic thyroiditis	0.573(0.324-1.015)	0.819(0.283-2.355)

(Continued)

TABLE 3 Continued

Variables	Univariable analysis	Multivariable analysis
	OR(95%CI)	OR(95%CI)
Residual tumor		
Absent	Reference	Reference
Present	2.203(1.103-4.400)**	2.158(0.403-14.145)

* : $P<0.05$,**; $P<0.001$,***.
OR, Odds ratio; CI, Confidence interval; PTC, Papillary thyroid carcinoma.

overall<0.001, *P* for nonlinear=0.841), suggesting the involvement of common biomarkers between them (Figure 4A). Therefore, we then explored the DEGs between high and low-risk dedifferentiation groups, as well as between high and low-nomogram score groups who were divided by their optimal cut-off value. According to the criteria of $|\log_2 FC)|>1$ and adjusted *P*-value<0.05 (Figures 4B, C), there were 290 DEGs obtained in the different dedifferentiation groups (Supplementary Table S3) and 32 DEGs obtained in the different nomogram score groups (Supplementary Table S4), with 17 overlapping genes between the two groups (Supplementary Table S5; Figure 4D). Among the 17 overlapping genes, we found 11 up-regulated genes and 6 down-regulated genes. KEGG enrichment analysis revealed three significant pathways: complement and coagulation cascades, proteoglycans in cancer, and aldosterone-regulated sodium reabsorption (all $P<0.05$) (Figure 5A). Among these, the complement and the coagulation cascades pathway were the main pathway, with *CD55* identified as a key factor (Figure 5B).

We further analyzed the expression level of *CD55* between groups with different PTC subtypes, disease duration, and dedifferentiation (Figures 6A–C). The results showed significant upregulation of *CD55* expression in the high-risk dedifferentiation group. Tall cell PTC exhibited higher *CD55* expression levels compared to follicular PTC. Additionally, *CD55* expression levels demonstrated an increasing trend with prolonged disease duration.

4 Discussion

Clinical treatment response and prognosis in PTC patients can be evaluated using dedifferentiation, TMB, and immune scores. Our research utilized high-throughput sequencing data from the TCGA database to calculate TDS, TMB, and immune scores for PTC tumor samples. The influences of the three tumor biomarkers on PFI in PTC patients were further examined. Multivariable Cox analysis revealed that only TDS was an influence factor of PFI, highlighting the crucial role of cellular differentiation levels in patient prognosis. Therefore, investigating the high-risk clinical features and molecular mechanisms of high-risk dedifferentiated populations could facilitate early detection, enabling appropriate therapeutic interventions and potentially improving patient outcomes.

Multivariable logistic regression analysis of high-risk dedifferentiation indicated that PTC subtypes and disease duration were significant risk factors for dedifferentiation. The nomogram model combining PTC subtypes and disease duration

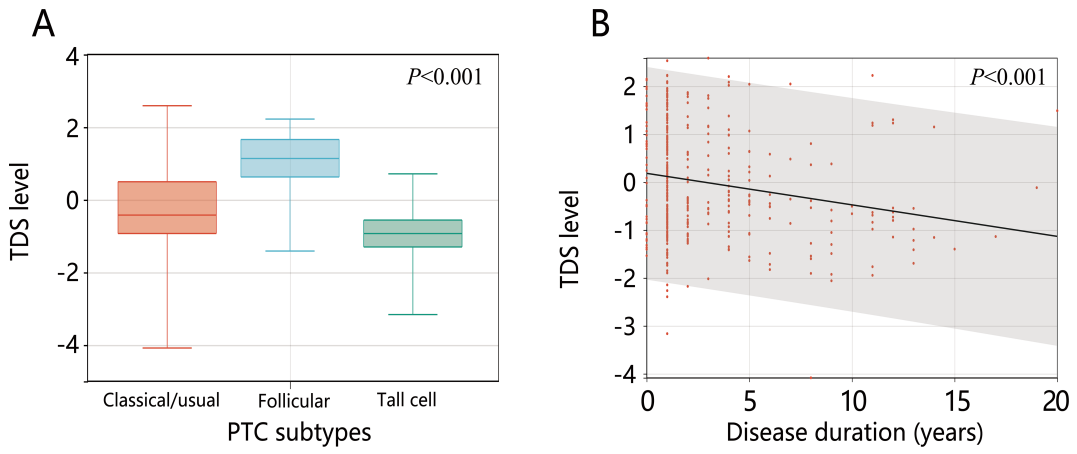

FIGURE 2
The levels of TDS in **(A)** different PTC subtypes and **(B)** disease duration.

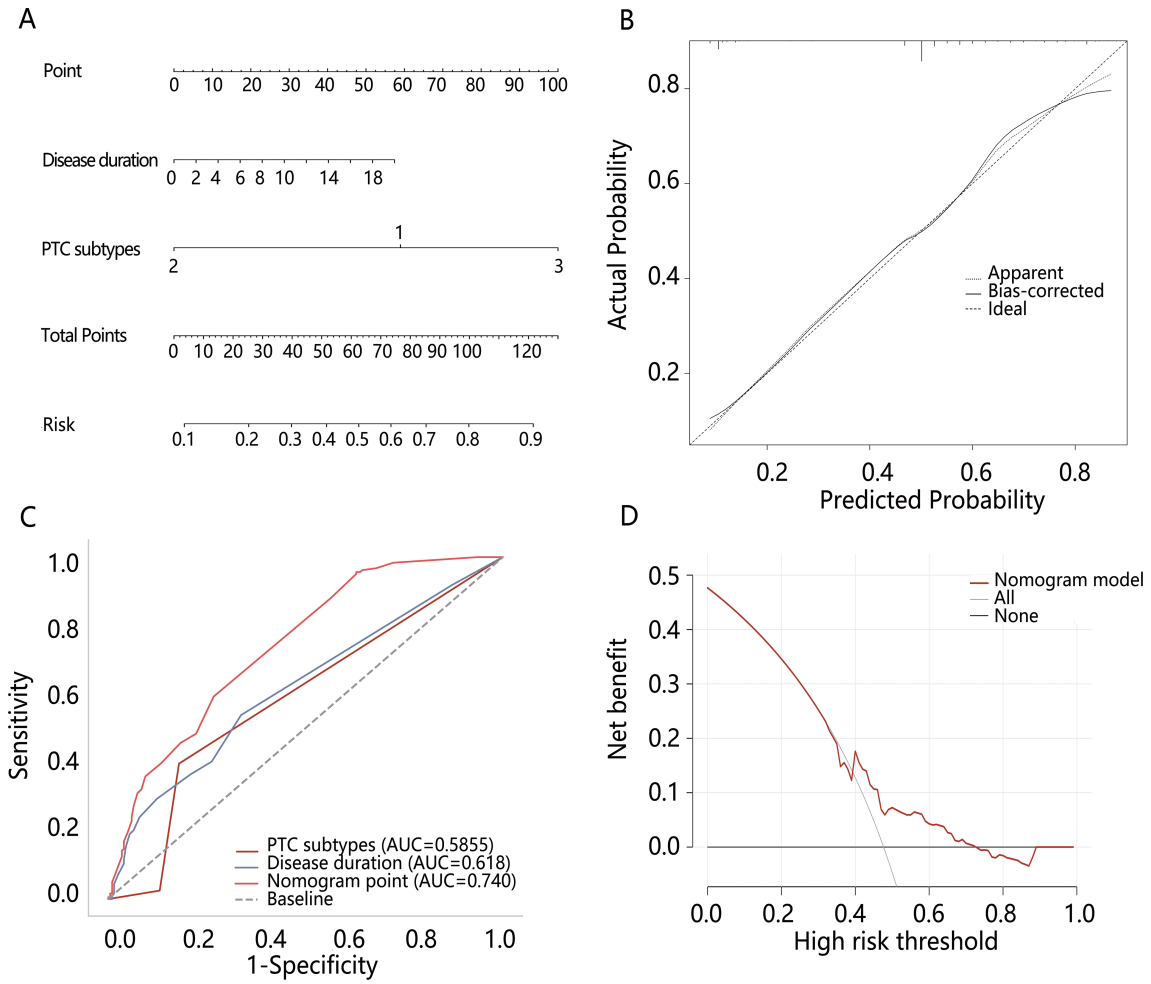

FIGURE 3
The construction and evaluation of the nomogram model. **(A)** The nomogram model of high-risk dedifferentiation; **(B)** The calibration curve of the nomogram model; **(C)** Comparison of ROC between the nomogram model and different variables; **(D)** The DCA of the nomogram model.

demonstrated good discriminative ability and can be clinically beneficial. PTC exhibits various variant subtypes (34). The American Thyroid Association classifies PTC subtypes such as tall cell, diffuse sclerosing, and hobnail as intermediate risk based on their aggressiveness, with TCPTC being the most common aggressive PTC subtype. These subtypes are less differentiated than classic PTC (35–37). Our results also revealed that TCPTC had the highest risk of dedifferentiation compared with classic/usual PTC and follicular variant PTC. In KEGG pathway analysis, we found that *FN1* as a marker of epithelial-mesenchymal transition

TABLE 4 The results of ROC analysis of factors associated with high-risk dedifferentiation.

Variables	PTC subtypes	Disease duration	Nomogram Point
AUC	0.585(0.534-0.620)	0.618(0.572-0.667)	0.740(0.696-0.792)
Sensitivity	0.396(0.338-0.458)	0.538(0.239-0.606)	0.957(0.575-0.987)
Specificity	0.821(0.754-0.860)	0.663(0.617-0.927)	0.371(0.323-0.781)
Youden index	0.217(0.133-0.288)	0.201(0.149-0.286)	0.328(0.268-0.426)
Accuracy	0.476(0.410-0.535)	0.523(0.468-0.578)	0.524(0.480-0.574)
Best cutoff	2.000(2.000-2.000)	2.000(2.000-6.000)	37.338(14.361-64.719)
Delong test	$P<0.001$	$P<0.001$	/

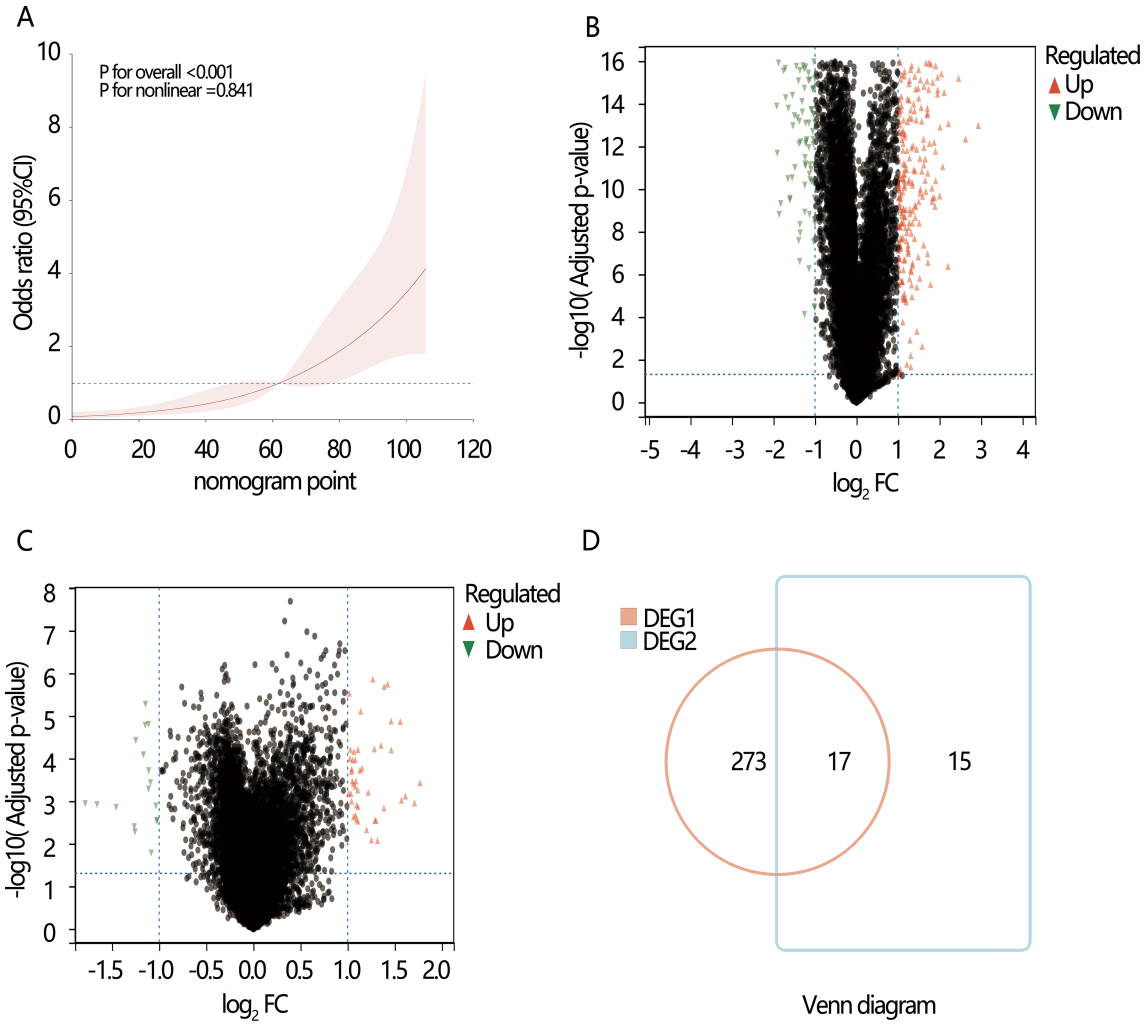

FIGURE 4
The potential genes and pathways exploration associated with the dedifferentiation. Volcano plots show the differentially expressed genes (DEGs). **(A)** The restricted cubic spline (RCS) analysis between nomogram point and dedifferentiation; **(B)** DGE1: DEGs between the high and low-risk dedifferentiation samples; **(C)** DGE2: DEGs between the high and low nomogram point samples; **(D)** Venn diagram shows the overlapping DEGs in DGE1 and DGE2.

(EMT) was involved in PTC dedifferentiation. EMT plays a key role in PTC invasion and anaplastic transformation (38, 39). It has been suggested that as the disease progresses, some PTCs may undergo dedifferentiation, transforming into anaplastic thyroid cancer (ATC) and poorly differentiated thyroid cancer, accompanied by more aggressive pathological and clinical behaviors (8). A median disease duration transforming PTC into ATC has been reported as 6 years (40). Furthermore, in terms of molecular classification, PTC can be categorized into *BRAF*-like and *RAS*-like PTC (41). Different oncogenic drivers may cause PTC to exhibit different degrees of differentiation (or TDS) (42). TDS is a comprehensive indicator related to the expression and function of genes involved in iodine metabolism (43). Low TDS may cause patients to develop radioactive iodine resistance, leading to poor prognosis and high mortality (44).

Further, our study identified 17 genes associated with PTC dedifferentiation. Enrichment analysis of these DEGs revealed core pathways and hub genes, potentially offering new insights into dedifferentiation mechanisms. KEGG analysis demonstrated that the *PLAUR* gene was involved in the proteoglycans in cancer. Research has shown that the *PLAUR* gene plays a role in PTC differentiation and *HER2*-positive breast cancer metastasis (45, 46). Evidence suggests that the *PLAUR* gene activates the urokinase fibrinogen activator receptor (uPAR). uPAR promotes the

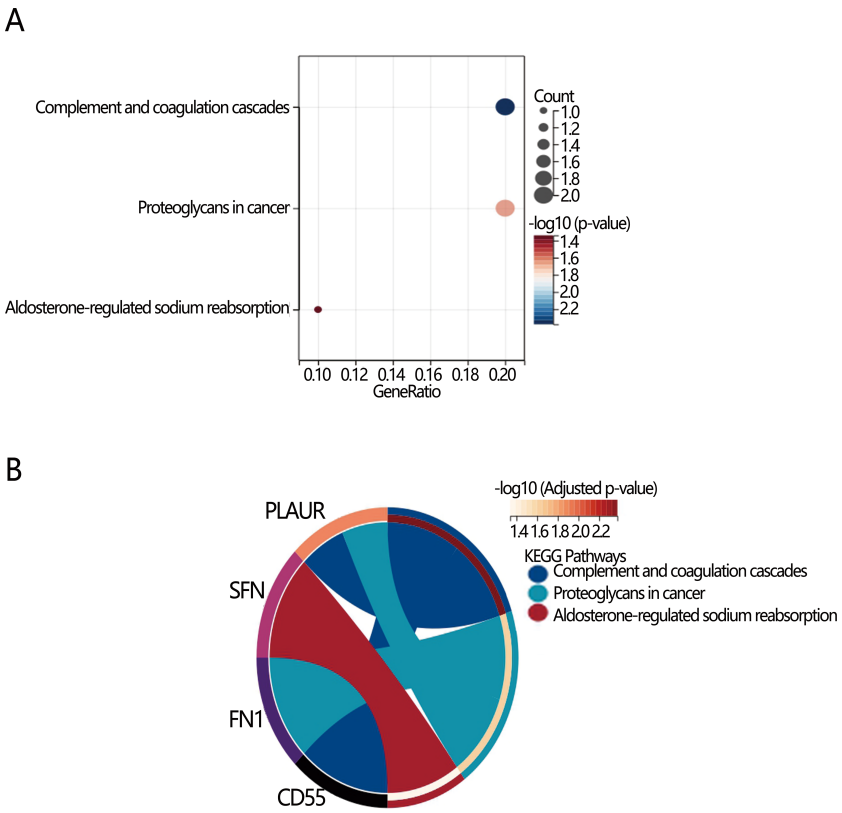

FIGURE 5
Visualization of KEGG enrichment analysis of 17 overlapping DEGs differential pathways. **(A)** Bubble diagram; **(B)** Chord diagram.

activation of fibrinogen, which breaks down the peri-tumor stroma and basement membrane (e.g., fibronectin, proteoglycans), creating conditions for tumor invasion and metastasis (47).

Our analysis revealed that the most important pathways in the KEGG enrichment analysis were the complement and coagulation cascades. The complement system is crucial for eliminating foreign microorganisms and regulating both innate and adaptive immunity (48). Research has demonstrated that the coagulation and complement cascade pathway has multiple positive and negative effects on the incidence, progression, and prognosis of tumors, as well as influencing tumor microenvironment components (49–51). Activation of the complement pathway leads to the formation of membrane attack complexes that induce cellular activity under target cell lysis or shedding. Inappropriate complement activation or altered expression of complement regulatory proteins inhibits the elimination of tumor cells by immune cells, which is associated with a variety of tumors (52, 53) Coagulation begins after complement activation, subsequently triggering platelet activity (54). Activated platelets can influence immune cell function, leading to inflammation (55). The previous study has confirmed thrombocytosis accompanying inflammation-related colorectal cancer and highlighted the crucial role of interleukin-6 (IL-6) in this process (56). Research has shown that IL-6, activin-A, and granulocyte colony-stimulating factor (G-CSF) in the tumor microenvironment promote the dedifferentiation of hepatocellular carcinoma cells as well as thyroid cancer cells (57, 58). In the present study, *CD55* was identified as a key gene in the coagulation and complement cascade pathway. Known as a complement decay accelerator, *CD55* is involved in tumor dedifferentiation, proliferation, invasion, and migration and its upregulation may be associated with tumor progression (59–61). Previous studies have shown that the complement system is activated in PTC and regulated through *CD46*, *CD55*, and *CD59* (62). *CD55* protects thyroid cancer cells from complement-mediated attack and promotes carcinogenesis by allowing tumor cells to escape from cytolysis (63). The results of our analysis suggested that *CD55* expression in patients was up-regulated with increasing disease duration (or in TCPTC), potentially activating complement and coagulation cascade pathway, thus promoting cancer cell dedifferentiation. Based on these results we propose the following clinical recommendations: first, *CD55* can be used as a potential prognostic marker for identifying patients at high risk of dedifferentiation, and it is recommended that *CD55* immunohistochemical evaluation can be added to postoperative pathology testing and follow-up monitoring should be intensified

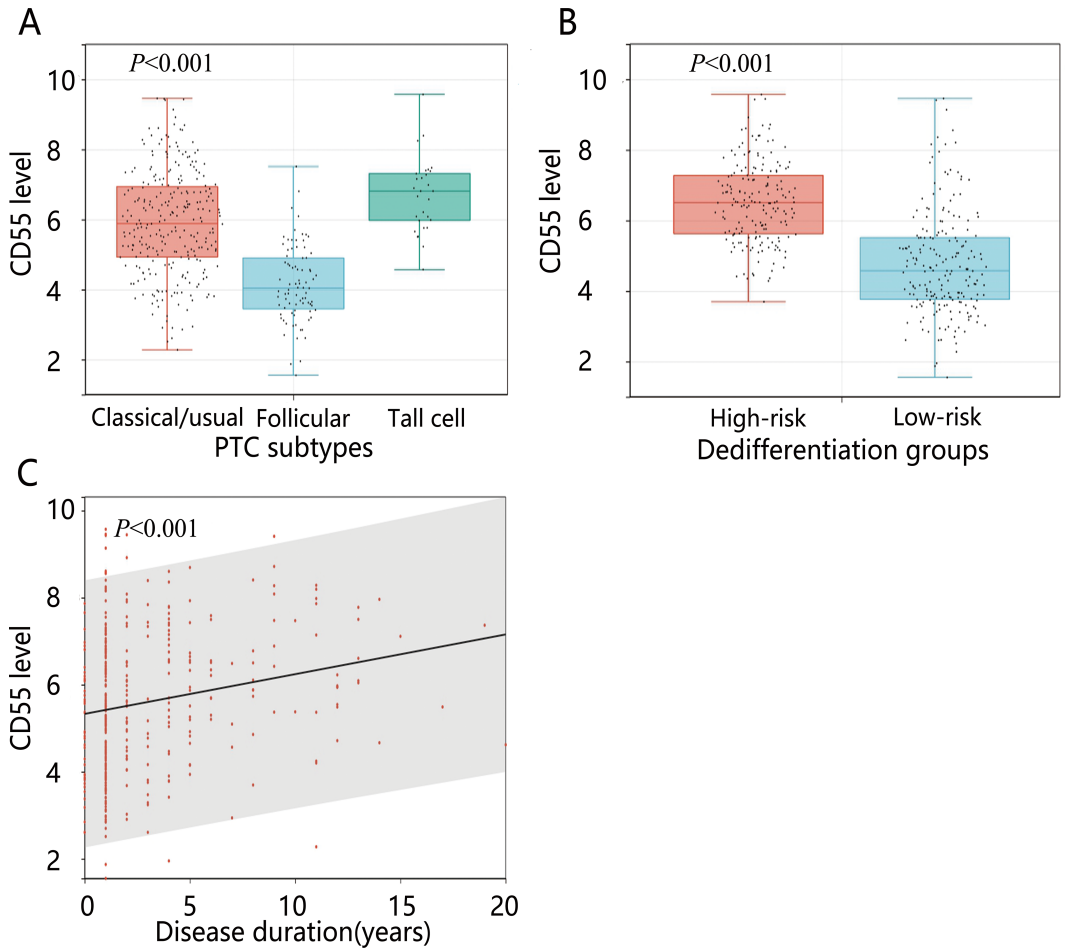

FIGURE 6
The expression levels of *CD55* in different variables. **(A)** PTC subtypes; **(B)** Dedifferentiation; **(C)** Disease duration.

(e.g., by shortening the interval between follow-ups or by increasing the number of imaging studies) for patients at high risk. Second, more aggressive treatment strategies should be considered for patients with high *CD55* expression, such as expanding the extent of surgery or consideration of adjuvant therapies targeting *CD55*-related pathways (e.g., complement signaling or EMT pathway). In addition, future studies should further validate the predictive value of *CD55* and explore its molecular mechanisms to develop possible targeted interventions, such as immunotherapy combined with complement-modulating therapies. Ultimately, the clinical application of *CD55* needs to be optimized through multicenter prospective studies to optimize detection criteria and integrate other molecular markers to improve the accuracy of risk stratification.

The innovation of this study is to combine clinical and genetic data to achieve individualized prognostic assessment of PTC patients, providing a more accurate tool for clinical practice and facilitating personalized treatment and management of PTC patients. Nevertheless, there are some limitations of this study: (1) No external validation was performed; (2) There were no clear boundaries for TDS subgroups. In this study, TDS was grouped by the optimal cut-off value, while some studies were grouped by median or 0 (43, 64). Therefore, future research should investigate optimal TDS grouping thresholds; (3) Data were only obtained from the TGCA database, which limited the extrapolation of results due to the influences of region and ethnicity.

5 Conclusion

In terms of clinical features, our findings revealed that disease duration and PTC subtypes were risk factors for high-risk dedifferentiation. At the molecular level, we identified 17 DEGs linked to high-risk dedifferentiation, potentially playing crucial roles in regulating PTC dedifferentiation. The complement coagulation cascade pathway may play a dominant role in PTC dedifferentiation, and the *CD55* could be the critical gene for PTC dedifferentiation, but further studies are needed to validate the results of these findings.

Data availability statement

The raw data supporting the conclusions of this article will be made available by the authors, without undue reservation.

Ethics statement

Ethical approval was not required for the study involving humans in accordance with the local legislation and institutional requirements. Written informed consent to participate in this study was not required from the participants or the participants' legal guardians/next of kin in accordance with the national legislation and the institutional requirements.

Author contributions

XL: Conceptualization, Data curation, Writing – original draft. QZ: Formal Analysis, Writing – original draft. ZH: Methodology, Writing – original draft. JS: Investigation, Writing – original draft. CX: Conceptualization, Data curation, Supervision, Writing – original draft.

Funding

The author(s) declare that no financial support was received for the research and/or publication of this article.

Conflict of interest

The authors declare that the research was conducted in the absence of any commercial or financial relationships that could be construed as a potential conflict of interest.

Generative AI statement

The author(s) declare that no Generative AI was used in the creation of this manuscript.

Publisher's note

Supplementary material

The Supplementary Material for this article can be found online at: https://www.frontiersin.org/articles/10.3389/fonc.2025.1535966/full#supplementary-material

References

1. Carling T, Udelsman R. Thyroid cancer. *Annu Rev Med*. (2014) 65:125–37. doi: 10.1146/annurev-med-061512-105739

2. Bray F, Laversanne M, Sung H, Ferlay J, Siegel RL, Soerjomataram I, et al. Global cancer statistics 2022: GLOBOCAN estimates of incidence and mortality worldwide for 36 cancers in 185 countries. *CA Cancer J Clin*. (2024) 74:229–63. doi: 10.3322/caac.21834

3. Laetitia G, Sven S, Fabrice J. Combinatorial therapies in thyroid cancer: an overview of preclinical and clinical progresses. *Cells*. (2020) 9:830. doi: 10.3390/cells9040830

4. Xing M. Molecular pathogenesis and mechanisms of thyroid cancer. *Nat Rev Cancer*. (2013) 13:184–99. doi: 10.1038/nrc3431

5. Rindi G, Mete O, Uccella S, Basturk O, La Rosa S, Brosens LAA, et al. Overview of the 2022 WHO classification of neuroendocrine neoplasms. *Endocr Pathol*. (2022) 33:115–54. doi: 10.1007/s12022-022-09708-2

6. Axelsson TA, Hrafnkelsson J, Olafsdottir EJ, Jonasson JG. Tall cell variant of papillary thyroid carcinoma: a population-based study in Iceland. *Thyroid*. (2015) 25:216–20. doi: 10.1089/thy.2014.0075

7. Ito Y, Miyauchi A, Kihara M, Fukushima M, Higashiyama T, Miya A. Overall survival of papillary thyroid carcinoma patients: A single-institution long-term follow-up of 5897 patients. *World J Surg*. (2018) 42:615–22. doi: 10.1007/s00268-018-4479-z

8. Volante M, Lam AK, Papotti M, Tallini G. Molecular pathology of poorly differentiated and anaplastic thyroid cancer: what do pathologists need to know? *Endocr Pathol*. (2021) 32:63–76. doi: 10.1007/s12022-021-09665-2

9. Fagin JA, Wells SA Jr. Biologic and clinical perspectives on thyroid cancer. *N Engl J Med*. (2016) 375:1054–67. doi: 10.1056/NEJMra1501993

10. Antonelli A, Fallahi P, Ferrari SM, Carpi A, Berti P, Materazzi G, et al. Dedifferentiated thyroid cancer: a therapeutic challenge. *BioMed Pharmacother*. (2008) 62:559–63. doi: 10.1016/j.biopha.2008.07.056

11. Papp S, Asa SL. When thyroid carcinoma goes bad: a morphological and molecular analysis. *Head Neck Pathol*. (2015) 9:16–23. doi: 10.1007/s12105-015-0619-z

12. Cancer Genome Atlas Research N. Integrated genomic characterization of papillary thyroid carcinoma. *Cell*. (2014) 159:676–90. doi: 10.1016/j.cell.2014.09.050

13. Ritterhouse LL. Tumor mutational burden. *Cancer Cytopathol*. (2019) 127:735–6. doi: 10.1002/cncy.22174

14. Chalmers ZR, Connelly CF, Fabrizio D, Gay L, Ali SM, Ennis R, et al. Analysis of 100,000 human cancer genomes reveals the landscape of tumor mutational burden. *Genome Med*. (2017) 9:34. doi: 10.1186/s13073-017-0424-2

15. Hellmann MD, Ciuleanu TE, Pluzanski A, Lee JS, Otterson GA, Audigier-Valette C, et al. Nivolumab plus ipilimumab in lung cancer with a high tumor mutational burden. *N Engl J Med*. (2018) 378:2093–104. doi: 10.1056/NEJMoa1801946

16. Samstein RM, Lee CH, Shoushtari AN, Hellmann MD, Shen R, Janjigian YY, et al. Tumor mutational load predicts survival after immunotherapy across multiple cancer types. *Nat Genet*. (2019) 51:202–6. doi: 10.1038/s41588-018-0312-8

17. Nieto P, Elosua-Bayes M, Trincado JL, Marchese D, Massoni-Badosa R, Salvany M, et al. A single-cell tumor immune atlas for precision oncology. *Genome Res*. (2021) 31:1913–26. doi: 10.1101/gr.273300.120

18. Ferrari SM, Fallahi P, Galdiero MR, Ruffilli I, Elia G, Ragusa F, et al. Immune and inflammatory cells in thyroid cancer microenvironment. *Int J Mol Sci*. (2019) 20:4413. doi: 10.3390/ijms20184413

19. Newman AM, Liu CL, Green MR, Gentles AJ, Feng W, Xu Y, et al. Robust enumeration of cell subsets from tissue expression profiles. *Nat Methods*. (2015) 12:453–7. doi: 10.1038/nmeth.3337

20. Li T, Fan J, Wang B, Traugh N, Chen Q, Liu JS, et al. TIMER: A web server for comprehensive analysis of tumor-infiltrating immune cells. *Cancer Res*. (2017) 77:e108–e10. doi: 10.1158/0008-5472.CAN-17-0307

21. Miao YR, Zhang Q, Lei Q, Luo M, Xie GY, Wang H, et al. ImmuCellAI: A unique method for comprehensive T-cell subsets abundance prediction and its application in cancer immunotherapy. *Adv Sci (Weinh)*. (2020) 7:1902880. doi: 10.1002/advs.201902880

22. Na KJ, Choi H. Immune landscape of papillary thyroid cancer and immunotherapeutic implications. *Endocr Relat Cancer*. (2018) 25:523–31. doi: 10.1530/ERC-17-0532

23. Caillou B, Talbot M, Weyemi U, Pioche-Durieu C, Al Ghuzlan A, Bidart JM, et al. Tumor-associated macrophages (TAMs) form an interconnected cellular supportive network in anaplastic thyroid carcinoma. *PloS One*. (2011) 6:e22567. doi: 10.1371/journal.pone.0022567

24. Melillo RM, Guarino V, Avilla E, Galdiero MR, Liotti F, Prevete N, et al. Mast cells have a protumorigenic role in human thyroid cancer. *Oncogene*. (2010) 29:6203–15. doi: 10.1038/onc.2010.348

25. He W, Sun Y, Ge J, Wang X, Lin B, Yu S, et al. STRA6 regulates tumor immune microenvironment and is a prognostic marker in BRAF-mutant papillary thyroid carcinoma. *Front Endocrinol (Lausanne)*. (2023) 14:1076640. doi: 10.3389/fendo.2023.1076640

26. Su Y, Xu B, Li J, Shen Q, Lei Z, Ma M, et al. Identification of m6A-associated LncRNAs as predict factors for the immune infiltration and prognosis of thyroid cancer. *Ann Med*. (2023) 55:1298–316. doi: 10.1080/07853890.2023.2192049

27. Wang L, Yao B, Yang J, Tian Z, He J. Construction of a novel cuproptosis-related gene signature for predicting prognosis and estimating tumor immune microenvironment status in papillary thyroid carcinoma. *BMC Cancer*. (2022) 22:1131. doi: 10.1186/s12885-022-10175-5

28. Yoshihara K, Shahmoradgoli M, Martinez E, Vegesna R, Kim H, Torres-Garcia W, et al. Inferring tumour purity and stromal and immune cell admixture from expression data. *Nat Commun*. (2013) 4:2612. doi: 10.1038/ncomms3612

29. Liu Y, Wang X, Sun X, Li H, Wang L. Nomogram for predicting the risk of cervical lymph node metastases and recurrence in papillary thyroid carcinoma based on the thyroid differentiation score system and clinical characteristics. *BMC Endocr Disord*. (2025) 25:39. doi: 10.1186/s12902-025-01867-7

30. Zhang QY, Wang Y, Zhang Q, Huo DW, Li Y, Gao D, et al. Construction of thyroid cancer classification and iodine metabolism related diagnostic model using thyroid differentiation score and bioinformation. *Med (Baltimore)*. (2024) 103:e39464. doi: 10.1097/MD.0000000000039464

31. Wang Y, He Y, Cao L, Peng X, Gu Z, Yan J. Exploring the correlation analysis of immune microenvironment, mutation burden and prognosis of papillary thyroid carcinoma based on Estimate algorithm. *Gland Surg*. (2022) 11:860–7. doi: 10.21037/gs-22-211

32. Lin B, Wang K, Yuan Y, Wang Y, Liu Q, Wang Y, et al. A novel approach to the analysis of Overall Survival (OS) as response with Progression-Free Interval (PFI) as condition based on the RNA-seq expression data in The Cancer Genome Atlas (TCGA). *BMC Bioinf*. (2024) 25:300. doi: 10.1186/s12859-024-05897-1

33. Bhalla S, Kaur H, Kaur R, Sharma S, Raghava GPS. Expression based biomarkers and models to classify early and late-stage samples of Papillary Thyroid Carcinoma. *PloS One*. (2020) 15:e0231629. doi: 10.1371/journal.pone.0231629

34. Sak SD. Variants of Papillary Thyroid Carcinoma: Multiple Faces of a Familiar Tumor. *Turk Patoloji Derg*. (2015) 31(Suppl 1):34–47. doi: 10.5146/tjpath.2015.01313

35. Haugen BR, Alexander EK, Bible KC, Doherty GM, Mandel SJ, Nikiforov YE, et al. 2015 American thyroid association management guidelines for adult patients with thyroid nodules and differentiated thyroid cancer: the american thyroid association guidelines task force on thyroid nodules and differentiated thyroid cancer. *Thyroid*. (2016) 26:1–133. doi: 10.1089/thy.2015.0020

36. Ghossein R, Livolsi VA. Papillary thyroid carcinoma tall cell variant. *Thyroid*. (2008) 18:1179–81. doi: 10.1089/thy.2008.0164

37. Haddad RI, Nasr C, Bischoff L, Busaidy NL, Byrd D, Callender G, et al. NCCN guidelines insights: thyroid carcinoma, version 2.2018. *J Natl Compr Canc Netw*. (2018) 16:1429–40. doi: 10.6004/jnccn.2018.0089

38. Liao Y, Hua Y, Li Y, Zhang C, Yu W, Guo P, et al. CRSP8 promotes thyroid cancer progression by antagonizing IKKalpha-induced cell differentiation. *Cell Death Differ*. (2021) 28:1347–63. doi: 10.1038/s41418-020-00656-0

39. Zhou Q, Chen J, Feng J, Xu Y, Zheng W, Wang J. SOSTDC1 inhibits follicular thyroid cancer cell proliferation, migration, and EMT via suppressing PI3K/Akt and MAPK/Erk signaling pathways. *Mol Cell Biochem*. (2017) 435:87–95. doi: 10.1007/s11010-017-3059-0

40. Yau T, Lo CY, Epstein RJ, Lam AK, Wan KY, Lang BH. Treatment outcomes in anaplastic thyroid carcinoma: survival improvement in young patients with localized disease treated by combination of surgery and radiotherapy. *Ann Surg Oncol*. (2008) 15:2500–5. doi: 10.1245/s10434-008-0005-0

41. Baloch ZW, Asa SL, Barletta JA, Ghossein RA, Juhlin CC, Jung CK, et al. Overview of the 2022 WHO classification of thyroid neoplasms. *Endocr Pathol*. (2022) 33:27–63. doi: 10.1007/s12022-022-09707-3

42. Landa I, Ibrahimpasic T, Boucai L, Sinha R, Knauf JA, Shah RH, et al. Genomic and transcriptomic hallmarks of poorly differentiated and anaplastic thyroid cancers. *J Clin Invest*. (2016) 126:1052–66. doi: 10.1172/JCI85271

43. Boucai L, Seshan V, Williams M, Knauf JA, Saqcena M, Ghossein RA, et al. Characterization of subtypes of BRAF-mutant papillary thyroid cancer defined by their thyroid differentiation score. *J Clin Endocrinol Metab*. (2022) 107:1030–9. doi: 10.1210/clinem/dgab851

44. Syed AR, Gorana A, Nohr E, Yuan XK, Amin MP, Ghaznavi S, et al. Predictors of radioiodine (RAI)-avidity restoration for NTRK fusion-positive RAI-resistant metastatic thyroid cancers. *Eur Thyroid J*. (2024) 13:e230227. doi: 10.1530/ETJ-23-0227

45. Li CW, Shi X, Ma B, Wang YL, Lu ZW, Liao T, et al. A 4 gene-based immune signature predicts dedifferentiation and immune exhaustion in thyroid cancer. *J Clin Endocrinol Metab*. (2021) 106:e3208–e20. doi: 10.1210/clinem/dgab132

46. Indira Chandran V, Eppenberger-Castori S, Venkatesh T, Vine KL, Ranson M. HER2 and uPAR cooperativity contribute to metastatic phenotype of HER2-positive breast cancer. *Oncoscience*. (2015) 2:207–24. doi: 10.18632/oncoscience.146

47. Schmitt M, Janicke F, Moniwa N, Chucholowski N, Pache L, Graeff H. Tumor-associated urokinase-type plasminogen activator: biological and clinical significance. *Biol Chem Hoppe Seyler*. (1992) 373:611–22. doi: 10.1515/bchm3.1992.373.2.611

48. Defendi F, Thielens NM, Clavarino G, Cesbron JY, Dumestre-Perard C. The immunopathology of complement proteins and innate immunity in autoimmune disease. *Clin Rev Allergy Immunol*. (2020) 58:229–51. doi: 10.1007/s12016-019-08774-5

49. Gong Z, He Y, Mi X, Li C, Sun X, Wang G, et al. Complement and coagulation cascades pathway-related signature as a predictor of immunotherapy in metastatic urothelial cancer. *Aging (Albany NY)*. (2023) 15:9479–98. doi: 10.18632/aging.205022

50. Su H, Chen Y, Wang W. Novel prognostic model of complement and coagulation cascade-related genes correlates with immune environment and drug sensitivity in hepatocellular carcinoma. *Heliyon*. (2024) 10:e38230. doi: 10.1016/j.heliyon.2024.e38230

51. Liu Y, Xiong S, Liu S, Chen J, Yang H, Liu G, et al. Analysis of gene expression in bladder cancer: possible involvement of mitosis and complement and coagulation cascades signaling pathway. *J Comput Biol*. (2020) 27:987–98. doi: 10.1089/cmb.2019.0237

52. Revel M, Daugan MV, Sautes-Fridman C, Fridman WH, Roumenina LT. Complement system: promoter or suppressor of cancer progression? *Antibodies (Basel)*. (2020) 9:57. doi: 10.3390/antib9040057

53. Noris M, Remuzzi G. Overview of complement activation and regulation. *Semin Nephrol*. (2013) 33:479–92. doi: 10.1016/j.semnephrol.2013.08.001

54. Heemskerk JW, Bevers EM, Lindhout T. Platelet activation and blood coagulation. *Thromb Haemost*. (2002) 88:186–93. doi: 10.1055/s-0037-1613209

55. Schlesinger M. Role of platelets and platelet receptors in cancer metastasis. *J Hematol Oncol*. (2018) 11:125. doi: 10.1186/s13045-018-0669-2

56. Josa V, Ferenczi S, Szalai R, Fuder E, Kuti D, Horvath K, et al. Thrombocytosis and effects of IL-6 knock-out in a colitis-associated cancer model. *Int J Mol Sci*. (2020) 21:6218. doi: 10.3390/ijms21176218

57. Rodrigues CFD, Serrano E, Patricio MI, Val MM, Albuquerque P, Fonseca J, et al. Stroma-derived IL-6, G-CSF and Activin-A mediated dedifferentiation of lung carcinoma cells into cancer stem cells. *Sci Rep*. (2018) 8:11573. doi: 10.1038/s41598-018-29947-w

58. Zhang L, Xu S, Cheng X, Wu J, Wang Y, Gao W, et al. Inflammatory tumor microenvironment of thyroid cancer promotes cellular dedifferentiation and silencing of iodide-handling genes expression. *Pathol Res Pract*. (2023) 246:154495. doi: 10.1016/j.prp.2023.154495

59. Yin X, Shen C, Yin Y, Cai Z, Wang J, Zhao Z, et al. Overexpression of CD55 correlates with tumor progression and poor prognosis in gastric stromal tumors. *Onco Targets Ther*. (2019) 12:4703–12. doi: 10.2147/OTT.S195182

60. Chan CKF, Gulati GS, Sinha R, Tompkins JV, Lopez M, Carter AC, et al. Identification of the human skeletal stem cell. *Cell*. (2018) 175:43–56 e21. doi: 10.1016/j.cell.2018.07.029

61. Dho SH, Cho EH, Lee JY, Lee SY, Jung SH, Kim LK, et al. A novel therapeutic anti–CD55 monoclonal antibody inhibits the proliferation and metastasis of colorectal cancer cells. *Oncol Rep*. (2019) 42:2686–93. doi: 10.3892/or.2019.7337

62. Yamakawa M, Yamada K, Tsuge T, Ohrui H, Ogata T, Dobashi M, et al. Protection of thyroid cancer cells by complement-regulatory factors. *Cancer*. (1994) 73:2808–17. doi: 10.1002/1097-0142(19940601)73:11<2808::aid-cncr2820731125>3.0.co;2-p

63. Lucas SD, Karlsson-Parra A, Nilsson B, Grimelius L, Akerstrom G, Rastad J, et al. Tumor-specific deposition of immunoglobulin G and complement in papillary thyroid carcinoma. *Hum Pathol*. (1996) 27:1329–35. doi: 10.1016/s0046-8177(96)90346-9

64. Wang JR, Zafereo ME, Cabanillas ME, Wu CC, Xu L, Dai Y, et al. The association between thyroid differentiation score and survival outcomes in papillary thyroid carcinoma. *J Clin Endocrinol Metab*. (2025) 110:356–63. doi: 10.1210/clinem/dgae532

Frontiers in Endocrinology

Explores the endocrine system to find new therapies for key health issues

The second most-cited endocrinology and metabolism journal, which advances our understanding of the endocrine system. It uncovers new therapies for prevalent health issues such as obesity, diabetes, reproduction, and aging.

Discover the latest Research Topics

See more →

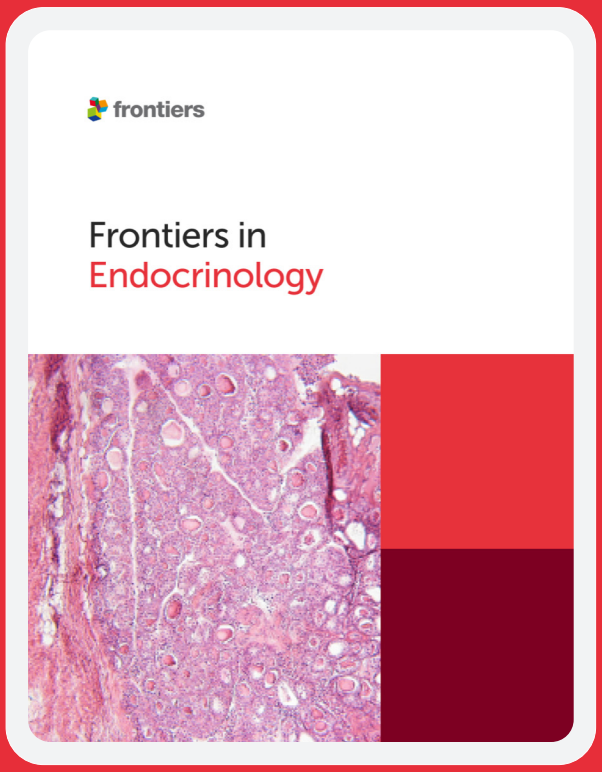

Frontiers

Avenue du Tribunal-Fédéral 34
1005 Lausanne, Switzerland
frontiersin.org

Contact us

+41 (0)21 510 17 00
frontiersin.org/about/contact